

Variation Conscious Assembly Fixturing Methodologies for the Preliminary Weld Processes of Segmented Ring Structures

Stewart Lowth

BSc MSc

Thesis submitted to the University of Nottingham for the degree of Doctor of Philosophy

Department of Mechanical, Materials, and Manufacturing Engineering

July 2016

Abstract

This project was sponsored by Rolls-Royce, who had an interest in using scientific principles to improve the geometric accuracy (circularity) of large welded annular structures. This project therefore critically examines and models the mechanisms by which manufacturing variation in wedges components stack and propagate to influence the final assembly geometry. The Trent 900 (T900) Front Bearing Housing (FBH) Ring of Vanes (RoV), was used as an illustrative test-piece, so that the typical sources of variation in large annular assemblies could identified. Also examined was the interplay between assembly gaps created by component variation played and the thermal-mechanical distortions of the Preliminary Welding Process (PWP).

Based on the fundamental sight gained form the illustrative test-piece a number of novel Variation Conscious Assembly Fixturing (VCAF) methodologies are proposed. The VCAF methodologies: the Circumscribed Geometric (CG), Inscribed Geometric (IG) and Translation Build (TB) are based on mathematical models of the wedge component and their assembly. The VCAF approaches generate in-fixture build conditions that are idealised for circularity by correcting the positions of the assembly locators in response to component variations. To experimentally validate the proposed VCAF fixturing methodologies, a ring assembly comprising of ten wedge-shaped components was designed and manufactured. In addition to the ten nominal assembly components (containing only implicit

manufacturing variation), a number of explicitly oversized and undersized assembly components were also produced. Furthermore, a flexible test-bench fixture was also designed and built, its flexibility allowed it to utilise any of the proposed VCAF build methods, while also accommodating traditional fixed location diameter builds. This allowed each of the proposed and established fixturing methodologies to be tested in the same fixture, keeping fixturing errors consistent. Additionally, as the assembly input variation of the components could be controlled; so by purposely inducing an error into the assembly, and measuring the resultant circularity, the response of each build method to the input variation could be assessed. Working in this way the new CG method was shown to be the most effective at controlling circularity of annular assemblies, showing a 5x circularity improvement over the traditional fixed build diameter location approaches.

The relationship between manufacturing variation and thermo-mechanical weld distortion is also presented in this research. Using a series of fixtured and free-state plate assemblies, the influence of inter-component gaps on PWP distortion has been experimentally studied and evaluated. The knowledge generated during these tests was then used to augment a Finite Element (FE) simulation of the welding process. Once the nature of the gap/weld interdependence was identified, a series of ring structures were welded. These ring assemblies demonstrated that with an understanding of the gap/weld interdependence PWP distortion could be substantially reduced.

"*The most difficult thing is a decision to act, the rest is merely tenacity*"

- Amelia Earhart

Publications originating from the thesis

Journal publications

S. Lowth & D. Axinte, "An assessment of 'variation conscious' precision fixturing methodologies for the control of circularity within large multi-segment annular assemblies." *Precision Engineering*. Vol. 38, no. 2, pp. 379-390, April 2014

Conference papers

S. Lowth & D. Axinte & W. Sun. "An investigation into the influence of inter-component assembly gaps upon the geometry of tack welded annular structures*". CIRP Annals - Manufacturing Technology. Vol. 64,* 2015.

Patents

S. Lowth**,** "A device for the clamping circular components within a large range of diametric variation", Filed by Rolls-Royce 2013.

Acknowledgments

First and foremost I would like to offer thanks to my supervisor Professor Dragos Axinte, whose tireless passion for research and drive to excel has been an inspiration throughout this project. Dragos' constant inquisitiveness and questioning has challenged me to be the best researcher I can be. I would also like to thank my other supervisor Professor Wei Sun, whose wise words and calming influence kept me focused. My gratitude also goes my external examiner Professor Paul Maropoulos, and my internal examiner Doctor Joel Segal for their time in reviewing my work and challenging me to improve it. For his support throughout the project I would also like to thank Peter Winton from Rolls-Royce.

I would like to acknowledge the support of my family and their encouragement through the ups and downs of research. I would especially like to thank my wife and principal proofreader Lorna, who has been patient, understanding and shown (or at time feigned) interest in my work. Indeed, without Lorna's belief in me and caring support I would have never had the courage to undertake a PhD; it has been a journey together.

Finally, I would like to thank my brothers and sister in arms…. the other University of Nottingham Rolls-Royce UTC PhD students, especially: Christopher Herbert, Kiran Kolluru, David Palmer, Xin Dong, Moritz Stoesslein, Alfonso Garcia and Oliver Craig; all of whom helped make my PhD experience fun and rewarding – even for an old timer like me.

Glossary of terms

Active fixturing: A fixture that responds in real-time to the stresses or dynamic conditions created during a manufacturing process. An active fixture responds to these conditions by intelligently manipulating the applied clamping forces and/or locator positions.

Chewing Gum Elements: A specialized element type used in the modelling of welding processes. A chewing gum element, starts a simulation with a modulus of elasticity of $1x10^{-5}$ that of the base material. However, once heated above the base material's liquidus temperature, the element reverts to the base materials usual modulus of elasticity.

Circularity: or roundness is a measure of how closely a manufactured item adheres to an idealised circular profile. It is generally expressed using Minimum Zone circle (MZC), which is the difference in radius between an inscribed and circumscribed circle fitted around the measured profile.

Fixture: A production tool used to deterministically locate and hold a work-piece during a manufacturing operation.

FK Point: A vane datum point, located on the trailing edge of the upper platform. This point acts as the origin for the vanes local coordinate system.

GTAW welding: Gas Tungsten Arc welding a fusion welding process (also known as TIG), which uses an electrical plasma arc in localised inert gas

atmosphere to fuse components together. GTAW welding uses permanent electrodes and a separate filler material.

Key Characteristic: Given a complex assemblages of components, it is impossible and/or expensive to control every single dimension with the system. The concept of Key characteristics (KCs) highlights only the dimensions that are functional important to a product's function or its safe use. Moreover, other dimension within the system can be allowed to vary (as they have little impact on the products use /perceived quality) as long as the KCs of the product are maintained. This focuses manufacturing effort on maintaining only those features that influence the functional quality of the product – saving wasted effort on less important product dimensions.

Six Sigma: A total quality management tool developed by Motorola, which aims to minimise defect in a system. The aim is to have ±6 standard deviations (or σ) of manufactured features made without defects, or put another way, a maximum of 3.4 defects per million items produced.

Seam weld: A weld used to permanently join an assembly's components. This weld type can be either continuous or a chain of intermittent welds; it typically runs the length of the joint between two or more components.

Tack weld: A point weld used to temporally stabilise the components of an assembly prior to the final seam welding process.

TIG welding: Tungsten Inert Gas welding, see GTAW welding

Variation conscious assembly fixturing: A fixturing methodology that responses to the manufacturing variation of the input components. The variation conscious approach enhances the locator set-up before the components are loaded. Not to be confused with an active fixture.

Wash weld: A wide shallow finishing weld used to improve a joint's fatigue-life and cosmetic appearance.

Weldment: A fusion welded assembly structure.

Weldpool: A puddle of molten material generated by a welding process. This molten puddle is generated from the base material of the components to being joined (and filler, if used). Convection currents then mix the pool and it is then the solidification of this mixed material that then creates the bond between the components.

Abbreviations

AWc	Absolute Worst-case
CG	Circumscribed Geometric build
CMM	Coordinate Measurement Machine
CoS	Condition of Supply
DCEN	Direct Current Electrode Negative
DFC	Datum Flow Chains
DIC	Dual Image Correlation
DMAIC	Define, Measure, Analyse, Improve and Control
DoF	Degrees of Freedom
EB	Electron Beam
EC	Eccentric Cam
FBH	Front Bearing Housing
FE	Finite Element
FEA	Finite Element Analysis
FEM	Finite Element Method
FRL	Fixed Ring Linkage

GD&T	Geometric Dimensioning and Tolerancing
GPS	Geometric Product Specification
GTAW	Gas Tungsten Arc Welding
IG	Inscribed Geometric build
IMZCI	Inner Minimum Zone reference CIrcle
KC	Key Characteristics
LaCCU	Locate and Clamp Carriage Units
LCS	Local Coordinate System
LWC	Local Weld Conditions
MAA	Metrology (or Measurement) Assisted Assembly
MMP	Multi-station Manufacturing Process
MZC	Minimum Zone Circle
OMZCI	Outer Minimum Zone reference Circle
PD	Product Development
PPM	Parts Per Million
PT	Parametric Tolerancing
PWP	Preliminary Weld Process (i.e. tack welding)

RBM	Rigid Body Motion
RoV	Ring of Vanes
SDT	Small Displacement Torsor
SiQ	Summation in Quadrature
SL	Scissor Linkage
SoV	Stream of Variance
SoVA	Stream of Variance Analysis
T900	Trent 900
TB	Translational Build
TIG	Tungsten Inert Gas
TTRS	Topologically and Technologically Related Surfaces
UKPO	United Kingdom Patent Office
VCAF	Variation Conscious Assembly Fixturing

Nomenclature

Symbol	Description	Units
AR_i	Assembly radial position for component *i*	Metres
C	Chord length	Metres
EIC_i	Effective inner chord length for component *i*	Metres
FL_i	Radial position of fixture locators for component *i*	Metres
IC_i	Inner chord length for component *i*	Metres
IC_i'	Adjusted inner chord length for component *i*	Metres
ΔIC_a	Change of inner chord at face "a" due to parallelism errors	Metres
ΔIC_b	Change of inner chord at face "b" due to parallelism errors	Metres
IR_i	Measured inner radius for component *i*	Metres
IS_i	Sagitta height of inner arc for component *i*	Metres
$I\theta_i$	Measured inner angle for component *i*	Radians
L	Length of side for regular polygon	Metres
LD	Locator pin diameter	Metres
n	Number of faces	N/a
OC_i	Outer chord length for component *i*	Metres
OS_i	Sagitta height of outer arc for component *i*	Metres
OR_i	Measured outer radius for component *i*	Metres
$O\theta_i$	Measured outer angle for component *i*	Radians
P_a	Face "a" parallelism error	Metres
P_b	Face "b" parallelism error	Metres
R	Arc radius	Metres
Rb	Fixture build diameter (position of locators)	Metres
Rb_i	Fixture build diameter (position of locators) for component *i*	Metres

R_{cir}	Theoretical build radius for CG build methodology	Metres
R_{ins}	Theoretical build radius for IG build methodology	Metres
T_i	Length along polygon side to inscribed tangent	Metres
α	Angular position of fixture locators	Radians
β_i	Angle of component *i* chord relative to assembly center	Radians
γ_i	True arc angle for component *i*	Radians
φ_i	Angle of angular breaking error for component *i*	Radians
ε_i	lobed non-circularities for component *i*	Metres
ε_{max}	The largest lobed non-circularity within an assembly	Meters
θ	Angle of arc	Radians
ρ_i	Stepped non-circularity for component *i*	Metres
ρ_{max}	An assembly's largest absolute value of stepped non-circularity	Metres

Table of contents

ABSTRACT **1**

PUBLICATIONS ORIGINATING FROM THE THESIS **4**

ACKNOWLEDGMENTS **5**

GLOSSARY OF TERMS **6**

ABBREVIATIONS **9**

NOMENCLATURE **12**

TABLE OF CONTENTS **14**

LIST OF FIGURES **19**

LIST OF TABLES **25**

1 INTRODUCTION **26**

1.1 BACKGROUND 26

1.1 MOTIVATION 29

1.2 AIM AND OBJECTIVES 33

1.3 ACADEMIC AND INDUSTRIAL BENEFITS 36

1.4 THESIS STRUCTURE 39

2 LITERATURE SURVEY **41**

2.1 INTRODUCTION 41

2.2 DEFINING FUNCTIONAL REQUIREMENTS: KEY CHARACTERISTICS 42

2.3 PRODUCT SPECIFICATION: DEFINING ALLOWABLE VARIANCE 45

2.3.1 Geometric Product Specification (GPS) *46*

2.3.2 Approaches for the assignment of tolerances *50*

2.3.3 Tolerance specification *51*

2.3.3.1 Methods for defining tolerance 52

2.3.3.2 Parametric tolerance (PT) 53

2.3.3.3 Geometric Dimensioning and Tolerancing (GD&T) 54

2.3.3.3.1 Flatness 59

2.3.3.3.2 Roundness / Circularity 59

2.3.3.3.3 Circular Run-out 61

2.3.4 Tolerance analysis *62*

2.3.4.1 Traditional approaches to tolerance stack-up 63

2.3.4.1.1 Arithmetic worst-case (AWc) 65
2.3.4.1.2 Linear Statistical propagation 66
2.3.4.1.3 Non-linear propagation 68
2.3.4.2 Geometric approaches to tolerance propagation 69
2.3.4.2.1 Vector loop 70
2.3.4.2.2 Variational approach 74
2.3.4.2.3 Matrix approaches 79
2.3.4.2.4 Jacobian method 81
2.3.4.3 Small displacement torsors 83
2.3.4.3.1 Summary of tolerance analysis approaches 84
2.3.4.4 Computer Aided Tolerancing (CAT) 85
2.3.5 Tolerance synthesis approaches 87
2.4 MANUFACTURING PROCESS VARIABILITY AND QUALITY 90
2.4.1 Six Sigma 92
2.4.2 Six Sigma measurement/analysis methods 94
2.5 ASSEMBLY AND VARIATION MANAGEMENT IN THE CONTEXT OF FIXTURING 98
2.5.1 Weld fixturing 101
2.5.2 Stream of Variation Analysis (SOVA) 102
2.5.3 Metrology Assisted Assembly (MAA) 107
2.6 METROLOGY AND VERIFICATION 112
2.6.1 Measurement Uncertainty 112
2.6.2 Uncertainty and the implication for tolerances 117
2.6.3 Coordinate Measurement Machine (CMM) 119
2.6.4 Photogrammetry 123
2.6.4.1 Speckled Dual Image Coloration (DIC) 125
2.6.4.2 Structured light photogrammetry 126
2.7 THE INFLUENCE OF WELDING IN ASSEMBLY VARIATION 128
2.7.1 The gas tungsten arc welding process 129
2.7.2 The impact of assembly gaps on welding 130
2.7.3 Tack welding 131
2.8 CONCLUSIONS AND IDENTIFIED RESEARCH GAPS 133
2.9 IDENTIFIED RESEARCH GAPS 139
3 METHODOLOGY 141
3.1 INTRODUCTION 141

3.2 THE OVERARCHING APPROACH 141
3.3 PHASE 1 - IDENTIFY KEY MANUFACTURING VARIATIONS 143
3.4 PHASE 2 - MODEL VARIATION AND VCAF DEFINITION 144
3.5 PHASE 3 - PWP MODELLING 148
3.6 CONCLUSION 151

4 IDENTIFYING KEY MANUFACTURING VARIATIONS: CRITICAL ANALYSIS OF AN EXISTING ANNULAR WELDMENT ASSEMBLY SYSTEM 154

4.1 INTRODUCTION 154
4.2 THE ILLUSTRATIVE ANNULAR TEST-PIECE ASSEMBLY 156
4.2.1 Assembly Key Characteristics 157
4.2.2 Vane datums 159
4.2.3 Overview of the annular assembly manufacturing process 160
4.3 ANALYSIS OF ILLUSTRATIVE ANNULAR ASSEMBLY PRODUCTION DATA 162
4.3.1 Approximate circular run-out findings 163
4.3.2 Flatness measurement findings 165
4.4 ANALYSIS OF THE ILLUSTRATIVE ANNULAR ASSEMBLY'S COMPONENTS 168
4.4.1 Interrogation of vane scan data 171
4.4.2 Further investigation of component mono-directional twist 174
4.5 APPRAISAL OF ILLUSTRATIVE ANNULAR ASSEMBLY FIXTURING 174
4.6 SURVEY OF ILLUSTRATIVE ANNULAR ASSEMBLY PWP 177
4.7 CONCLUSIONS 179

5 A MODEL OF COMPONENT AND ASSEMBLY VARIATION 183

5.1 INTRODUCTION 183
5.1.1 Assumptions 183
5.2 A MODEL OF MANUFACTURING VARIATION WITHIN WEDGE SHAPED ASSEMBLY COMPONENTS. 185
5.2.1 True wedge angle 187
5.2.2 Out-of-plane error 189
5.3 DEFINITION OF VCAF ASSEMBLY METHODOLOGIES 191
5.4 THE GEOMETRIC ASSEMBLY METHODS 192
5.4.1 The circumscribed geometric methodology 194
5.1.1.1 Precise Calculation of the theoretical build diameter 195
5.1.1.2 Estimated calculation of the theoretical build diameter 197
5.1.1.3 The locators angular position 199
5.4.2 The inscribed geometric methodology 201

5.1.1.4 The calculation for the theoretical build diameter 202
5.1.1.5 The locators angular position 204
5.4.3 Angular breaking errors 209
5.5 THE TRANSLATIONAL BUILD METHOD 213
5.6 INTRINSIC NON-CIRCULARITIES 217
5.6.1 Lobed non-circularities 218
5.6.2 Stepped non-circularities 219
5.7 CONCLUSIONS 222
6 VALIDATION OF VCAF BUILD APPROACHES 226
6.1 INTRODUCTION 226
6.2 THE GENERIC TEST-BENCH ASSEMBLY 227
6.2.1 The design 228
6.2.2 Validation of manufactured geometry 229
6.3 DESIGN EXPERIENTIAL TEST-BENCH FIXTURING 232
6.3.1 Requirements of the design 232
6.3.2 The design concepts 234
6.3.2.1 The EC design 235
6.3.2.2 The FRL design 235
6.3.2.3 The SL design 236
6.3.2.4 Stacked designs 237
6.3.3 The flexible fixture's final design 238
6.3.3.1 The LaCCU's make-up 240
6.3.4 Validation of manufactured accuracy of the flexible fixture 242
6.4 EXPERIMENTAL VALIDATION; THE EVALUATION OF BUILD ERROR 243
6.4.1 The build sets 244
6.4.2 The testing procedure 246
6.4.3 The results and discussion 249
6.4.3.1 Results analysis; the inner diameter 253
6.4.3.2 Result analysis; circularity 256
6.4.3.3 Result analysis; angular breaking errors 259
6.5 EXPERIMENTAL VALIDATION; NON-CIRCULARITY DRIVERS 262
6.5.1 The testing procedure 262
6.5.2 The results and discussion 264
6.5.2.1 Result analysis; lobed non-circularities 264

6.5.2.2 Result analysis; stepped non-circularities 265
6.6 CONCLUSIONS 267
7 INVESTIGATIONS INTO THE INTERACTION BETWEEN PWP AND ANGULAR BREAKING ERROR WITHIN WELD RING ASSEMBLIES 271
7.1 INTRODUCTION 271
7.1.1 Chapter outline 272
7.2 WELDED PLATES EXPERIMENTATION 273
7.2.1 Free-state welding 273
7.2.1.1 Experimental testing 274
7.2.1.2 Experimental testing results 276
7.2.1.3 FE modelling of 0.5mm assembly 279
7.2.1.4 Modelling results 282
7.2.2 Constrained state welding 284
7.2.2.1 The weld fixture and components 284
7.2.2.2 The testing 286
7.2.2.3 The results 288
7.3 WELD RINGS EXPERIMENTATION 293
7.3.1 Fundamental distortion shapes 294
7.3.2 Physical weld trials 297
7.3.3 FE Modelling 305
7.4 CONCLUSIONS 311
8 CONCLUSIONS 318
8.1 INTRODUCTION 318
8.1.1 Summary of approach 318
8.2 KEY ACADEMIC OUTCOMES 320
8.2.1 Industrial relevance 325
9 FUTURE WORK 326
REFERENCES 330
APPENDIX 1 – ENGINEERING DRAWINGS 344
APPENDIX 2 – CMM UNCERTAINTY CALCULATIONS 370

List of Figures

FIGURE 1-1: THE TRENT 900 GAS TURBINE AERO-ENGINE [4] 27

FIGURE 1-2: FUTURE PREDICTION OF AIR-TRAFFIC [6].....29

FIGURE 1-3: HISTORIC PLOT OF KEY AIRCRAFT CAPACITY FACTORS [6].....29

FIGURE 1-4: THE T900 FBH ROV ASSEMBLY. 32

FIGURE 2-1 : UBIQUITOUS ROLE OF TOLERANCES IN A PRODUCT LIFE CYCLE [22].....46

FIGURE 2-2 : THE UNCERTAINTY CREATED THOUGH POOR FEATURE DEFINITION [24].
.....47

FIGURE 2-3 : INTERRELATIONSHIP OF THE GEOMETRICAL FEATURE DEFINITIONS [25]
.....48

FIGURE 2-4 : EXPRESSING PARAMETRIC TOLERANCES ON LINEAR DIMENSIONS. 54

FIGURE 2-5 : EXPLANATION OF THE FUNDAMENTS OF GEOMETRIC TOLERANCING.....55

FIGURE 2-6 : USING GD&T A) EXAMPLE DRAWING, B) THE TOLERANCE FRAME, C)
DATUM CALL OUT. 58

FIGURE 2-7 : DEFINITION OF FLATNESS EXTRACTED FROM ISO 12781-1:2011 [40].
.....59

FIGURE 2-8 : THE MEASUREMENT OF CIRCULARITY 60

FIGURE 2-9 : AN EXAMPLE OF THE TOLERANCE ALLOCATION METHOD 63

FIGURE 2-10 : CYLINDRICAL TOLERANCE ZONE.....80

FIGURE 2-11 : THE VIRTUAL JOINTS OF THE JACOBIAN METHOD, A) THE NOMINAL
MODEL, B) WITH SMALL DISPLACEMENTS TO REPRESENT POSSIBLE VARIANCE [87].
.....82

FIGURE 2-12 : EXAMPLE OF STATISTICAL OUTPUT OF TYPICAL CAT SYSTEM [98] 86

FIGURE 2-13 : THE 3-2-1 APPROACH WHEN FIXTURING ASSEMBLIES..... 100

FIGURE 2-14 : TYPICAL MMP SHOWING SPACE STATE MODEL INPUTS [153]..... 104

FIGURE 2-15 : ASSEMBLY/PART/FIXTURE VARIANCE BEING ACCOMMODATED BY FLANGE WIDTH [158] 105

FIGURE 2-16 : MAA SYSTEM DIAGRAMMATIC OVERVIEW [175]..... 108

FIGURE 2-17 : A TYPICAL DISTRIBUTION OF A MEASUREMENT DUE TO UNCERTAINTY 113

FIGURE 2-18 : IMPLICATIONS OF UNCERTAINTY IN THE VALIDATION OF TOLERANCES 119

FIGURE 2-19 : TYPICAL GANTRY TYPE CMM WITH CONTACT PROBE 120

FIGURE 2-20 : A TYPICAL DUAL IMAGE CORRELATION SYSTEM [215]..... 126

FIGURE 2-21 : A TYPICAL STRUCTURED LIGHT PHOTOGRAMMETRY SCANNER [218]. 127

FIGURE 2-22 : THE GTAW WELDING PROCESS [50] 130

FIGURE 3-1: THE OVERARCHING RESEACH METHODOLOGY..... 141

FIGURE 3-2: THE PROJECT PHASE 1 METHODOLOGY..... 143

FIGURE 3-3: THE PROJECT PHASE 2 METHODOLOGY..... 145

FIGURE 3-4: THE PROJECT PHASE 3 METHODOLOGY..... 149

FIGURE 3-5: COMPLETE PROJECT METHODOLOGY FLOWCHART 152

FIGURE 4-1: THE ILLUSTRATIVE ANNULAR ASSEMBLY..... 154

FIGURE 4-2: THE DISTIRBUTON OF STANDARD AND SERVICE VANES WITHIN ROV. ... 157

FIGURE 4-3: OVERALL DIMENSION OF THE ILLUSTRATIVE ANNULAR ASSEMBLY. 158

FIGURE 4-4: VANE DATUM SCHEMES: (A) MANUFACTURE, (B) ASSEMBLY. 160

FIGURE 4-5: APPROXIMATED RUN-OUT FOR THE ILLUSTRATIVE ANNULAR ASSEMBLY. 163
FIGURE 4-6: RADIAL FK POINT VALUES FOR ALL DATASETS. 164
FIGURE 4-7: RADAR PLOT OF FK POINT MEAN RADIAL POSITION 165
FIGURE 4-8: OUT-OF-PLANE VALUES FOR ILLUSTRATIVE ANNULAR ASSEMBLIES. 166
FIGURE 4-9: VARIANCE IN OUT-OF-PLANE MEASUREMENT PER VANE. 166
FIGURE 4-10: POSITIONAL DEVIATION OF "A" FACE FROM DESIGNED NOMINAL. 167
FIGURE 4-11: COMPARATIVE PLOT OF FK POSITION AND DEVIATION IN "A" FACE 167
FIGURE 4-12: SCANNING THE VANES OF THE ROV 169
FIGURE 4-13: CONVERTING POINT-CLOUD MEASUREMENT TO SURFACE MODEL 170
FIGURE 4-14: TYPICAL SCAN RESULT WITH MONO-DIRECTIONAL TWIST 171
FIGURE 4-15: ANGULAR OF VANE SCAN DATA (ALL ±4.2X10-4° AT 95% CONFIDENCE) 172
FIGURE 4-16: VANE UPPER PLATFORM DISPLACEMENT *(±0.0111 AT 95% CONFIDENCE)* 172
FIGURE 4-17: THE LIKELY POSITION OF VANE BASED ON CHORD WIDTH 173
FIGURE 4-18: SEGMENTED BUILD APPROACH OF ILLUSTRATIVE ANNULAR ASSEMBLY 176
FIGURE 4-19: BUILD SEGMENT BREAKS AGAINST APPROXIMATE RUN-OUT 177
FIGURE 5-1 : ASSUMED TYPICAL STYLE OF COMPONENT GEOMETRY 185
FIGURE 5-2 : DEFINITION OF CHORDAL LENGTH 186
FIGURE 5-3 : THE EFFECT OF MANUFACTURING VARIATION WITHIN THE UPPER AND LOWER PLATFORMS UPON COMPONENT WIDTH 187
FIGURE 5-4 : THE WEDGE COMPONENTS TRUE ANGLE 188

FIGURE 5-5 : THE INFLUENCE OF OUT-OF-PLANE ERROR ON THE EFFECTIVE CHORD. 190

FIGURE 5-6 : GEOMETRIC BUILD METHODS; (A) CIRCUMSCRIBE, (B) INSCRIBED 194

FIGURE 5-7 : THE CG BUILD METHODOLOGY 195

FIGURE 5-8 : TYPICAL CAD SKETCHES USED IN VERIFIED OF CG SET-UP MODEL 196

FIGURE 5-9 : COMPARISON OF AVERAGING METHODS VERIFIED AGAINST CAD NOMINAL 199

FIGURE 5-10 : ASSEMBLY ANGLE IN RESPECT TO CHORD'S RADIAL POSITION. 200

FIGURE 5-11 : THE IG BUILD METHODOLOGY 202

FIGURE 5-12 : COMPARISON OF AVERAGING METHODS AGAINST CAD NOMINAL 204

FIGURE 5-13 : THE INFLUENCE OF LINE LENGTH UPON TANGENCY POINT 205

FIGURE 5-14 : A TYPICAL CAD SKETCH, USED AS VERIFIED OF IG SET-UP MODEL 208

FIGURE 5-15 : THE INTERNAL ANGLES OF A POLYGON 209

FIGURE 5-16 : UNDERSIZED (A) AND OVERSIZED (B) ASSEMBLED WEDGE ANGLES ... 210

FIGURE 5-17 : THE TB METHODOLOGY 213

FIGURE 5-18 : TRANSLATION OF THE CHORAL LINE' EIC_i TO CORRECT B_i 215

FIGURE 5-19 : A) LOBED GEOMETRY B) STEPPED GEOMETRY 218

FIGURE 5-20 : LOBED NON-CIRCULARITY TYPE 218

FIGURE 5-21 : STEPPED NON-CIRCULARITIES 220

FIGURE 6-1 : DRAWING OF GENERIC TEST-BENCH ASSEMBLY 229

FIGURE 6-2: THE BUILD METHODS VALIDATED: A) CG, B) TB, C) FDI AND D) FDC 233

FIGURE 6-3 : A) EC PROTOTYPE CLOSED, B) CAM DETAIL, C) EC PROTOTYPE OPEN 235

FIGURE 6-4 : A) FRL DESIGN IN CLOSED, AND B) UNFURLED POSITIONS 236

FIGURE 6-5 : SL PROTOTYPE (30MM RANGE) INSIDE Ø420MM COMPONENT 237

FIGURE 6-6 : A SINGLE SL FIXTURE CLAMPING Ø380MM AND Ø520MM CYLINDERS. .. 237

FIGURE 6-7 : A) STACKED SL FIXTURES, B) PROFILES CAPABLE OF BEING CLAMPED 238

FIGURE 6-8 : THE FINAL FLEXIBLE FIXTURE DESIGN FOR THE TEST-BENCH ASSEMBLY. 239

FIGURE 6-9 : THE FLEXIBLE FIXTURE'S OPERATING PRINCIPLE 240

FIGURE 6-10 : GENERAL ASSEMBLY OF FIXTURE AND CLAMPING UNITS..... 241

FIGURE 6-11 : DATUM JIG-PLATE FOR SETTING THE NOMINL POSTION OF LACCU 242

FIGURE 6-12 : FLOW CHART OF EXPERIMENTAL PROCESS 246

FIGURE 6-13 : POSITIONING A LACCU USING THE CALLIPER GUIDE COMPONENT 249

FIGURE 6-14 : A GRAPHIC REPRESEANTATION OF THE BUILD RESULTS..... 253

FIGURE 6-15 : MEASURED INNER DIAMETER AGAINST BUILD-SET 254

FIGURE 6-16 : MZC MEASUREMENTS AGAINST BUILD-SET..... 257

FIGURE 6-17 : GRAPHS OF THE AVERAGED BUILD-SET RESULTS..... 259

FIGURE 6-18 : GAPS OBSERVED IN DIAMETRICALLY UNDERSIZED BUILDS WHEN USING FDI METHOD. 261

FIGURE 6-19 : PROCEDURE FOR VALIDATING NON-CIRCULARITY DRIVER MODEL..... 264

FIGURE 6-20 : A TYPICAL STEPPED TYPE NON-CIRCUALARTIES..... 267

FIGURE 7-1 : EXPERIMENTAL PRE-WELD SET-UP PROCEDURE 276

FIGURE 7-2 : A GAP CLOSURE RESULT OF THE FREE-STATE WELDING TRIALS..... 278

FIGURE 7-3: PLOT OF DIC CAMERA GAP SIZE RESULTS..... 279

FIGURE 7-4 : TYPICAL PWP WELD AND CROSSS-SECTION 281

FIGURE 7-5 : DISPLACEMENT RESULTS OF FREE-STATE WELD SIMUALTION..... 283

FIGURE 7-6 : THE PLATES AND FIXTURE FOR THE CONSTAINED PLATE WELD TRIAL. 285

FIGURE 7-7 : THE CONSTAINED PLATE FIXTURE OPERATION SEQUENCE. 286

FIGURE 7-8 : THE CONSTRAINED WELDING TRIAL SET-UP..... 288

FIGURE 7-9 : PLATE MOVMENT ALONG JOINT – SINGLE STAGE WELD PROCESSES..... 291

FIGURE 7-10: PLATE MOVMENT ALONG JOINT – SINGLE STAGE WELD PROCESSES 291

FIGURE 7-11 : TYPICAL STRUCTURES QUANTISED A) CONIC, AND B) SADDLE 295

FIGURE 7-12 : EXPERIMENTAL TEST RING ASSEMBLY AND FIXTURE 298

FIGURE 7-13 : TYPICAL SCAN OF WELDED RING, WITH 2MM SLICE RESOLULTION..... 302

FIGURE 7-14 : RESULTS OF CMM CONTACT SCANNING..... 302

FIGURE 7-15 : WELDED RING JOINTS OBSERVED WITH 50X OPTICAL MIRCOSCOPE ... 305

FIGURE 7-16 : SET-UP FOR WELD SIMULATION 307

FIGURE 7-17 : THE EFFECT OF MELTING CONTACT ON GAP-END OF THE JOINT. 311

List of tables

TABLE 2-1: CATEGORIES OF GEOMETRIC TOLERANCE [37] 57

TABLE 2-2 : PROCESS CAPABILITY (CPK) IMPLICATIONS [138] 97

TABLE 2-3 : COMPARATIVE OVERVIEW TABLE OF VARIATIONAL MANAGEMENT APPROACHES 134

TABLE 6-1 : COMPONENT MEASUREMENTS 230

TABLE 6-2 : CALCULATED COMPONENT DATA 231

TABLE 6-3 : CMM RESULTS OF FIXTURE ACCURACY AND REPEATABILITY TESTING 243

TABLE 6-4 : THE BUILD-SET DEFINITIONS ARRANGED BY DISTRIBUTION CATEGORY 245

TABLE 6-5 : RESULTS OF EXPERIMENTAL BUILD TRIALS (UNCERTAINTIES FOR DIAMETRIC MEASUREMENTS ±0.0099 AT 95% CONFIDENCE – SEE APPENDIX) 251

TABLE 6-6 : OBSERVED ASSEMBLY GAPS WITHIN ASSEMBLED STRUCTURES 260

TABLE 6-7 : RESULTS FOR LOBED NON-CIRCUALIRTIES BUILD TRIALS 265

TABLE 6-8 : RESULTS FOR STEPPED NON-CIRCUALIRTIES BUILD TRIALS 266

TABLE 7-1 RESULT OF FREE-STATE WELDING TRIALS 277

TABLE 7-2 : RESULT OF CONSTRAINED WELDING TRIAL 290

TABLE 7-3 : GAP CLOUSRE ASSEMBLIES INDUCED ERRORS 294

TABLE 7-4 : OUT-OF-PLANE ERROR IN ASSEMBLED RING GEOMETRY 296

TABLE 7-5 : PRE-WELD ASSEMBLY MEASUREMENTS 299

TABLE 7-6 : POST-WELD ASSEMBLY MEASUREMENTS 300

TABLE 7-7 : FEA WELD SIMULATION RESULTS 308

1 Introduction

1.1 Background

It is common practice, where the production of repeatable components is required, that jigs and fixtures are used to aid the process of manufacture. These manufacturing aides deterministically locate and securely clamp single or multiple work-pieces, permitting one or more stages of manufacture to be performed. They offer a beneficial impact on the manufacturing process in terms of productivity, cost-per-part and quality [1]. However, designing and manufacturing a fixturing system for a specific task can be both time consuming and expensive, with their creation constituting 10-20% of the total set-up cost of a manufacturing process [2]. Moreover, a poorly realised fixture concept can lead to manufacturing errors and low process repeatability, through: inadequate location; flexing of the fixture/workpiece; or general geometric inaccuracy in the fixture [3].

Large metal annular structures are a family of manufactured components that require substantial amounts of fixturing during their production. These structures are of great significance to a number of economically important heavy industries, such as gas turbines, power generation, and heavy plant. These high precision rings are frequently manufactured using a stock material or a near-net-shape blank, on to which various conventional or non-conventional machining processes are employed until the final geometry is achieved. However, as size and/or the complexity of such rings

grow it becomes technically and financially less effective to produce these geometries in a single piece. It is therefore, common practice that large ring structures are assembled from smaller segmented components and then joined via fusion welding. However, creating a ring in this manner adds new sources of potential variation into the production process, via; manufacturing variance in component geometry, positional assembly errors, and weld distortion.



Figure 1-1: The Trent 900 gas turbine aero-engine [4]

The gas-turbine aero-engine industry in particular has a vested interest in the creation of large high accuracy ring structures. This is because gas turbine aero-engines (as shown in Figure 1-1) typically require a number of large geometrically complex annular components, which must be produced a very high level of precision. This need for precision is twofold;

firstly, it enables in-service efficiency and reliability, as demanded by airlines and the various governmental agencies which regulate the industry. Secondly, manufacturing a component at near net-shape saves waste and time as fewer finishing operations are required.

A future trends report by Airbus expects passenger numbers to double in the next fifteen years (Figure 1-2) and predicts a 4.7% year-on-year growth in passenger numbers. Boeing in their own report, make a similar 5.0% year-on-year growth prediction [5]. As a consequence of these predictions, and with an eye to reducing the environmental impact of this extra traffic, the trend for the airframe builders has been to design larger aircraft (shown on Figure 1-3). However, these larger aircrafts also require a new generation of larger, more powerful, more efficient and cleaner burning gas turbine engines. Unfortunately though, as engine sizes increase, so too do the component parts, but with an increase in part size, so it becomes more difficult to manufacture these components at the required accuracy. This makes scalability a major future challenge for the aero-engine industry, as their customers make more explicit demands upon their product line.

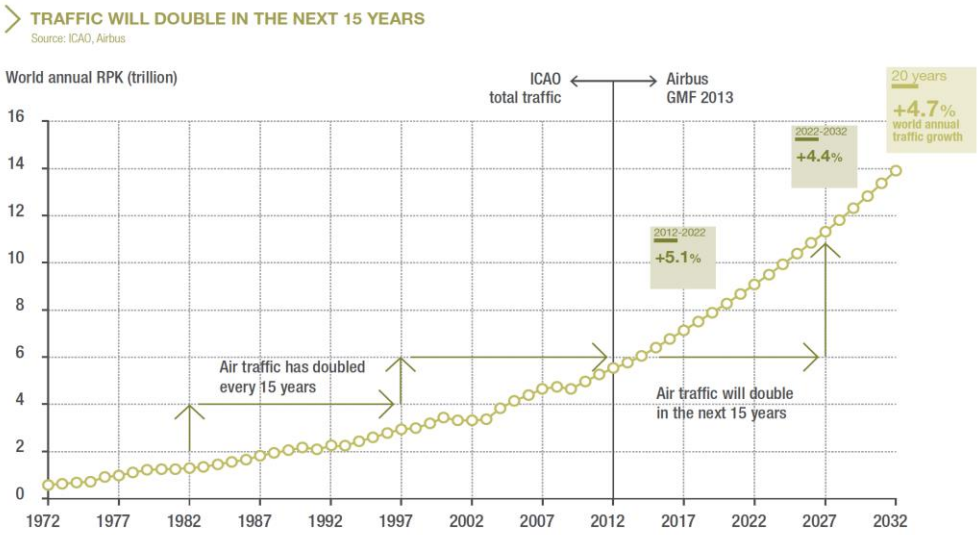


Figure 1-2: Future prediction of air-traffic [6]

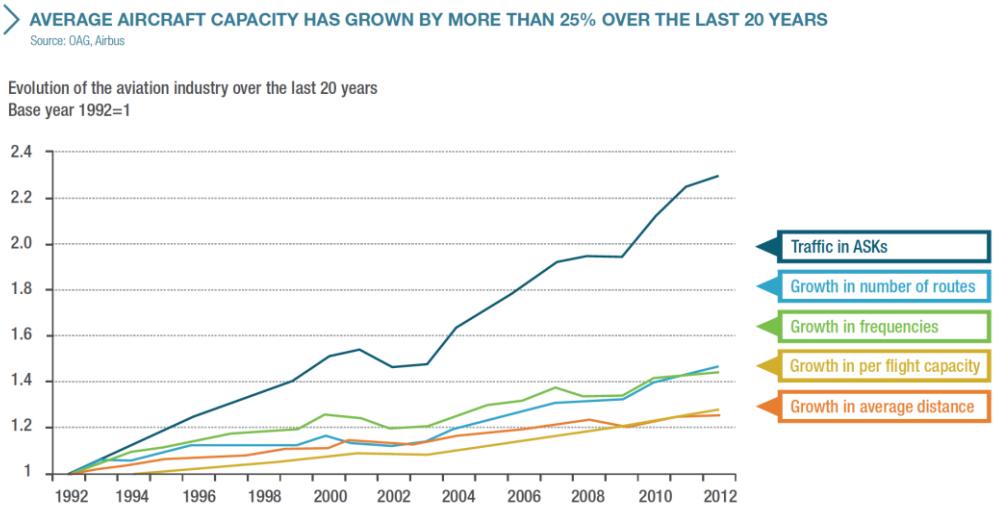


Figure 1-3: Historic plot of key aircraft capacity factors [6]

1.1 Motivation

This project was initiated by Rolls-Royce; who were interested in research to improve the construction approaches for large welded annular structures. Across their product range, Rolls-Royce manufactures engines of various sizes; from small military jet engines to large turbofans for

commercial airliners. This makes Rolls-Royce acutely aware of the challenges of producing increasing large welded annular structures. This project was therefore in response to Rolls-Royce's discordant future requirements of needing to manufacture increasingly large annular assemblies, while increasing their geometric quality and accuracy.

In order to address these requirements, the need for a fundamental scientific understanding of the propagation of component manufacturing variation within these structures was realised. This would lead to a greater comprehension of how these uncertainties "stack" to influence the final assembly geometry. Understanding this propagation will enable the intelligent adjustment of less important geometric parameters, allowing a manufacturer to focus its efforts on maintaining only those component tolerances that have relevance to the assembly quality.

A further benefit of understanding the stacking variation of the assembly is that; the fixturing can be enhanced to maximise build quality. Improving the fixturing in this way will offer a number of benefits within a manufacturing environment, as it will: decrease assembly time (as the components will fit together with greater ease); increase geometric repeatability; improve geometric predictability; reduce the need for finishing and clean-up operations. These improvements will also be felt further downstream, as subsequent production/assembly operations become easier to perform with the more consistent geometry.

Circularity is a key quality metric when designing and manufacturing these annular structures, as good circularity will make subsequent assembly operations easier. By way of example; a circular hub can easily be turned to fit an annular structure if the mating assembly also has a good degree of circularity. However, if a hub is fitted to an assembly with poor circularity, it would be difficult to correctly manufacture the hub to satisfactorily fit the mating assembly. Moreover, in situations of poor circularity, poor axial alignment between the hub and the ring assembly is also likely to occur. This could lead to substandard balancing, or increased bearing wear, or a multitude of other issues. Obviously, these issues will also proliferate further into the production process.

In addition to circularity errors, an important consideration in the quality of an assembled ring structure is the influence of the jointing process on the structure's final geometry. This concern is also especially relevant when using a fusion welding jointing process, as it is well known to induce thermal-mechanical distortions in assembly geometry. Furthermore, the fusion welding of an assembly is normally a two-stage, consisting of; a Preliminary Welding Process (PWP) and final seam weld. However, because the PWP (colloquially known as a tack weld) is used to fix the initial positions of the component parts in-fixture prior to the seam weld, it this process that will be of most interest when considering assembly geometry. The PWP consists of a series of shallow, low penetration point welds, used to pre-join and stabilise an assembly's geometry before it is removed from its assembly fixture. Stabilising the geometry in this way reduces the

amount of clamping required in the any later seam weld fixture. This is important, as over-constraining (clamping) the assembly during the seam welding process increases the post weld residual stresses in the final structure. However, the small size of the PWP leads to a very steep but fleeting thermal gradient during the welding cycle. This short weld cycle makes the PWP thermal-mechanical stresses (and thus distortion) very different from those of the slower seam welds. However, in terms of previous scientific research, the wider scientific community has a good understanding of the seam welding process, while there has been little previous interest in the PWP.

Responding to the technical needs described above, is a complex multifaceted academic challenge. The modelling of component manufacturing variations, the development of a variation stacking model for closed ring assemblies, and the development of circularity improved fixturing methodologies are all substantial challenges in their own right. However, the further requirement for an understanding of the weld conditions and their interactions with the identified manufacturing uncertainties made for a challenging research project.

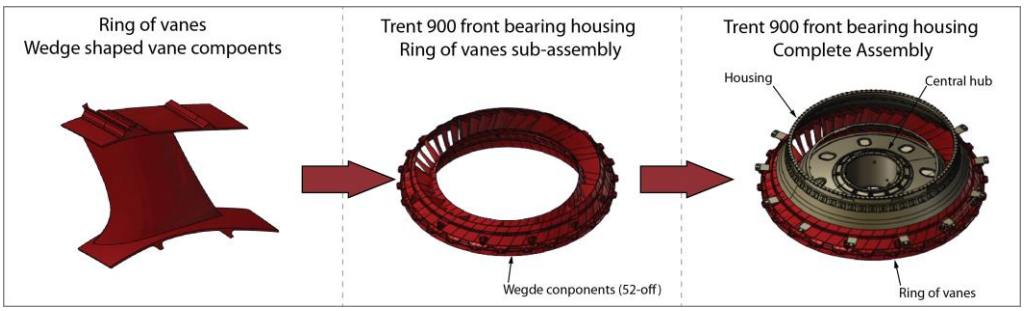


Figure 1-4: The T900 FBH RoV assembly.

In order to meet their research needs Rolls-Royce offered the Trent 900 (T900) Front Bearing Housing (FBH) Ring of Vanes, as an exploratory assembly for observing the key geometric parameters essential to assembly circularity. The 1.7m inner and 2.2m of diameters of T900 FBH RoV (shown in Figure 1-4) make it one of the largest welded ring assemblies produced by the company and an excellent illustrative test-piece. The T900 FBH RoV is assembled from 52 forged titanium wedge shaped components. These components are initially joined via a Gas Tungsten Arc Welding (GTAW) PWP, prior to a full-seam Electron Beam (EB) weld.

1.2 Aim and Objectives

The aim of this research is to define new concepts and models to improve the circular quality of large tack welded annular structure though the creation "variation conscious" fixturing methodologies. That is, by intelligently positioning a fixture's datum locators in harmony with the in-coming component variances, the circularity of the final structure can be improved. This a totally novel way to approach such problem as is opposed to traditional fixturing approaches which try to fit the assembled parts to fixed nominal location scheme with no appreciation of the component variances.

To achieve the project's aim a number of objectives must be realised:

1. The mapping of a typical welded ring structure production system as used by a high-value manufacturer. This refers to the

investigation of an industrial assembly and fixturing system to generate a “root-cause roadmap” of likely sources of process/part variance encountered during the manufacture of an exemplar segmented ring structure. The “root-cause roadmap” addresses the academic challenge of understanding generic variance in the assembled structure originating from such sources as: component manufacture, assembly error, fixture location and the tack welding process.

2. In-depth analysis of the relationships between key characteristics of the final annular structure and the key characteristics of the assembly’s components. This is in response to a need in understanding of the important system input parameters (i.e. component and fixture geometry) in the context of the key output parameters (i.e. ability of the assembly to fulfil functional requirements).
3. The development of a robust single part key characteristics variance model to describe a typical wedge-faced component as used within the assembly of weld annular structures; addressing the challenge of capturing and describing the components so that they can be utilised within an assembly system variance model.
4. A novel model for predicting the propagation of the stacked single component variance within a looped assembly, so that the final geometric form of the assembled structure can be predicated. This model pay particular attention to the circularity key characteristic

of the assembled structure via a novel “inverse” fixturing approach, i.e. varying the position of the locators to accommodate the variances of the parts for minimizing circularity error of the assembly.

5. Develop the new concept of “Variation Conscious” Assembly Fixturing (VCAF), whose foundation is the derived component and assembly models. This focuses on the challenge of producing an intelligently designed fixturing systems that works symbiotically with the implicit system variances to improve the output circularity of an annual assembly.
6. An explicative single joint model of assembly imperfection (i.e. gaps and steps) and their impact upon thermal-mechanical weld distortions of the highly localized preliminary weld process. This seeks an understanding of the influence of the local “per-joint” weld conditions on the final geometry of a single welded joint.
7. The development of a framework which combines the “per-joint” weld distortion predictions in to system-wide forecast of the thermal-mechanical distortion induced by the complete preliminary weld process. Moreover, this addresses the research challenge of predicting the final geometric shape of the assembled annular structure at the end of is assembly process (i.e. as it leaves the fixture).

1.3 Academic and Industrial benefits

Achieving the stated aims and objectives of this project will generate a number of benefits to the wider scientific and academic communities, new knowledge generated from this project will be;

1. The creation of new approaches for the stacking of manufacturing variation within a closed loop assembly system. These differ substantially from previous studies which have generally focused on the linear stacking of component variation. The presented approaches may have applications beyond circular ring structures and could potentially be extended to other closed loop geometries, such as regular and irregular polygonal structures.
2. The novel variation conscious assembly fixture approaches, along with the benefits of an assembly fixturing system that responds to component manufacturing variation is demonstrated and explained.
3. A better understanding of the preliminary weld process (tack welding) process, filling a substantial gap in current welding knowledge. The preliminary weld process has been somewhat overlooked by the scientific community in preference of seam welding, this is despite it being an industrially ubiquitous production approach when fusion welding.
4. A better understanding of the influence of component variation on the thermal-mechanical distortions of the fusion welding process. This is needed as in reality it is inevitable that the assembly will be

subject to component variation. However, the majority of welding FEA and experimental studies make the assumption that all the components are manufactured and assembled perfectly. This is partially due to the idealised perfection of the FEA modelling environment and the difficulty in understanding the nature of the components which contain manufacturing variation.

Although the primary focus of the project is the creation of large annular structures, the findings can also be cross-fed in to smaller annular assemblies. Applying the research findings to these smaller structures will extend the impact and benefit of the project, and would also see; an increase in the assembled circularity, an increase in ease of assembly, and a reduction in weld distortion for these smaller structures. Therefore, the industrial community at large will see a number of benefits from this project, namely;

1. The technical ability to manufacture larger engine assemblies at increased levels of geometric quality, while also improving the quality of smaller existing products. This will allow the company to respond to the future demands and requirements of their customers and regulatory bodies.
2. Producing these assemblies closer to the final net-shape will reduce the number and severity of finishing operations, saving production time, cost and waste.

3. As the assembly's components will fit together better there will be an improved consistency in the build process and a reduction in assembly errors. This will generate a "right-first-time" production ethos, increasing production speeds and reducing the need for post-process error correction operations.
4. The ability to fully understand a component's tolerances during the design process. This will focus effort during manufacture in maintaining only parameters key to the assembly's circularity, rather than wasting resources and effort on maintaining less critical dimensions.
5. The creation of enhanced fixturing methodologies for annular assemblies will allow the most circular build possible for a given set of components. Furthermore, improving the fixturing will intrinsically increase build quality, even if the components are not tailored specifically to improve overall assembly circularity.
6. A reduction in preliminary weld process thermal-mechanical distortion will result in the conjoined ring geometry being less ambiguous when it is re-fixtured for later manufacturing processes. This will make any re-fixturing both more accurate and of greater repeatability.
7. As the preliminary weld process distortion is lowered, so the subsequent electron beam weld distortion will be applied to a less misshapen initial assembly. This will lessen the severity of the

stacked weld distortions and result in the production of a final structure with greater geometric accuracy.

1.4 Thesis Structure

Chapter 1 – Introduction: An introduction to the presented research and a description of its motivation and aims.

Chapter 2 - Literature survey: A literature survey of current scientific thinking in areas related to the project, such as; the fixturing and location of components, the stacking of component variations, and welding (specifically tack welding) and its simulation through FEA.

Chapter 3 – Project methodology: An overview and description of the methodology used during the project.

Chapter 4 – Identifying key manufacturing variations; a critical analysis of an existing annular weldment assembly system: The geometric analysis of a large-scale industrial ring assembly (T900 FBH RoV). This illustrative test-piece will be then used to identify the key drivers of variation within annular assemblies.

Chapter 5 – A model of component and assembly variation: This chapter describes a manufacturing variation model for the assembly's components, and explains the influence of this variation upon the assembly's final geometry. A mathematical description of the proposed VCAF methodologies is presented.

Chapter 6 - Validation of VCAF build approaches: A description of the experimentation performed with the flexible test-bed fixture to validate the proposed VCAF methods.

Chapter 7 – Investigations into the interaction between PWP and angular breaking error within ring assemblies: A description of the plate welding FEA and experimental trials used to examine the impact of assembly inaccuracy on the preliminary weld process. A series of ring weld trials is also narrated, along with their corresponding FEA simulations.

Chapter 8 – Conclusions: A discussion around the conclusions of the presented research.

Chapter 9 – Future Work: Future research directions are discussed.

2 Literature survey

2.1 Introduction

During Product Development (PD) a designer will have a number of functional requirements which their design is expected to fulfil. Consequently, it is the design's ability to satisfy these requirements that determines the ultimate quality of the manufactured product. What is more, most manufactured of products are assemblages of components, whose interactions determine the functions and abilities of the final product [7]. Moreover, these interactions between components are themselves determined by the geometric features (i.e. faces, holes, shafts and so on) that constitute each assembled part [8]; how closely the dimeter of a shaft feature on one component matches the diameter of a hole feature in a second component for example, determines how freely the two parts rotate relative to each other. In an ideal world the product imagined by the designer during PD would be manufactured perfectly, creating a precise embodiment of designer's vision. However, in reality every manufactured feature and assembly stage used to embody a product contains at least some degree of implicit variance due to uncertainties within the production process. Therefore, to ensure a product still meets its functional requirements this inherit variance must be accounted for during the PD cycle [8]. To do this the designer must define the acceptable bounds of deviation (or tolerances) within which a manufactured component will still

fully embody the design intent and functional requirements of the product. Although, the designer may define a very narrow band of acceptable manufacturing deviation, such an approach may not be acceptable as higher precision manufacturing processes are generally more expensive, inflating the cost of the manufactured product considerably [9]. Furthermore, a tolerance may not be technically feasible given a specified manufacturing process, leading to an increased number of reject or "out-of-tolerance" components being produced and scrapped. The designer must therefore strike a balance between the functional quality of the product and the cost of manufacture [10]. Determining an acceptable tolerance scheme which achieves the right cost/quality/capability balance for a given product, assembly or component is not a trivial task and as such has been a long standing area of scientific interest. Nonetheless, tolerancing for manufacturing variation is still a problematic area, despite many computer aided and manual systems being available to the designer [11, 12].

2.2 Defining functional requirements: Key Characteristics

An important step in design is to capture and understand the functional requirements of the product under development [13]. For modern PD this begins with a high-level description of measurable properties required by the final assembly in terms performance, function, safety or quality. These high-level parameters are essential to the effective functioning of the product and are referred to as its Key Characteristics (KCs) [14]. KC's can be any parameter of the product that can be quantified and measured. They

can be a physical property (i.e. geometric size, weight or density), a dynamic property (i.e. rotate at a given speed), a chemical property (i.e. a given material or tolerant to an operational environment), an electrical property (i.e., operate within a safe voltage range or output power), a financial requirement (i.e. cost, or production volume), a defined aesthetic or even a social need (i.e. made from recycled material or made from a locally sourced materials). KCs are defined by many large companies in ways relating to their customer; Rolls-Royce for example define KCs as: *"Key Characteristics (KCs) are product characteristics or process input / output variables that are designated by Rolls-Royce or the supplier, whose variation has the greatest impact upon customer requirements / expectations."* [15].

Within assembled products KC requirements are considered hierarchic, with a systematic flow that aligns with the "Product ⇒ Sub-assembly ⇒ Part" structure that constitutes a product and is referred in literature as "flow-down" [16]. That is to say that, the ability of the product at the top level to achieve KC requirements is dependent upon (or put at risk by) the combine quality and features of the lower-level assemblies and component parts. It is worth noting that, each component and sub-assembly will also be subject to its own KCs which would include interfacing or assembly requirement. Interestingly, Witney [17] highlights that as fixtures are assembled to the product and influence the geometry, they too are subject to, and influenced by, the KC's of the product and assembled components (as well as the parts having their own).

The hierarchic nature of KC's has led to suggestions for further categorisation of the KCs into more specific groups [18], such as: Manufacturing KC's (MKCs), Assembly KC's (AKCs), and Control KC's (CKCs). While, the aerospace industry in the US and Europe has created a separate definitions for Critical Characteristics (CCs) and general KCs, to enforce their importance within safety critical aerospace items [19].

The primary benefit of the KCs to modern industry is that they focus the manufacturer's efforts into the areas of most importance to the product's function. Given that many modern complex products (such as automobiles, aircraft, rolling stock or gas turbines) contain many thousands of components, it would be too time-consuming and too technically challenging to ensure every feature of every component was manufactured perfectly. Further adding to the difficulty, many of these high complexity products are frequently produced by large global organisations who utilise geographically dispersed subsidiaries or sub-contracting to manufacturer many of their components and sub-assemblies [20]. Using the KCs "top-down" approach to define the most important functional parameters of a product, assembly or part, reduces the total number of parameters that must be controlled during production; efforts can then be focused on ensuring that the most important functional parameters are met, even if detrimental to other less essential component or assembly features. Reducing the number of important parameter also reduces the inspection and conformance checks required when sub-contracted parts and sub-

assemblies are then introduced into the production process for final assembly.

The drawback of KCs is the problem of choosing the correct parameters or set of parameters to define as a KCs. Choose too few KCs for a given product, assembly or part and the design intent may not be fully captured by the during manufacture. However capture too many KCs and either the design becomes difficult to embody with repeatability or the focus on the true key parameters becomes lost. To address the problem Thornton [21] proposed a quantitative KC model to identify the KCs base on an effectiveness measure. The paper's approach is a blunt cost/benefit method that takes no account of other important factors such as safety. A final issue with the KC approach is its hierarchic flow-down. Indeed, it can be difficult following the features which influence the top-level KCs down through the assembly and into the individual component features. To assist with assembly fit-up issues in aerospace assemblies Mantripragada and Whitney [16] proposed Datum Flow Chains (DFC). A modelling approach that captures underlying assembly intent and logic, so that assembly KCs transfer between hierarchy stages maintaining the integrity of the design intent .

2.3 Product specification: defining allowable variance

A persistent issue when specifying allowable manufacturing variance is the dependence on the designer. It is required that the designer understands: the functional requirements of the product and how that relates to the interaction of component features; the limitations and optimal cost/quality

relationship for the manufacturing process being used; the tolerancing methodologies for the various geometric features as defined in the standards; and how the variance propagates through each level of the products construction. As Hong and Chang [22] show (Figure 2-1) the choices made when specifying tolerances during PD impacts the entire product life cycle.

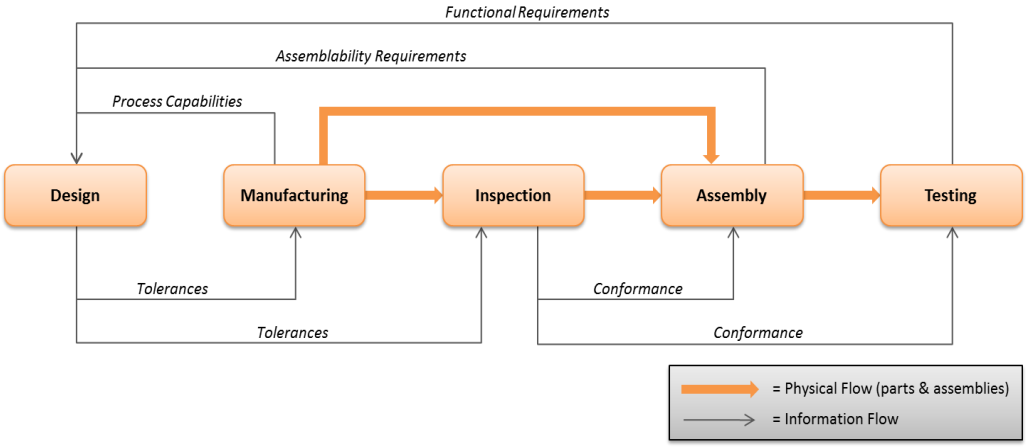


Figure 2-1 : Ubiquitous role of tolerances in a product life cycle [22].

2.3.1 Geometric Product Specification (GPS)

The tolerance(s) chosen during PD have a wide reaching impact across the product lifecycle; creating a special relationship between the definition of tolerances (the specification procedure) and the verification of the product (the measurement procedure). As Figure 2-2 shows, it is the differences between the specification operator of a features design and the measurement procedure for a feature that generates ambiguity and uncertainty, leading to difficulties in assessing conformance (an effect referred to as the "*duality principle*"). In a bid to remove uncertainty from

the definition and interruption of geometric features between the design and measurement communities, the ISO has developed the Geometric Product Specifications (GPS) standards. The GPS standards are an overlapping hierarchic family of standards which act as the foundation for: unambiguous drawing specification; programming of measurement instrumentation; and the estimation of measurement uncertainties [23].

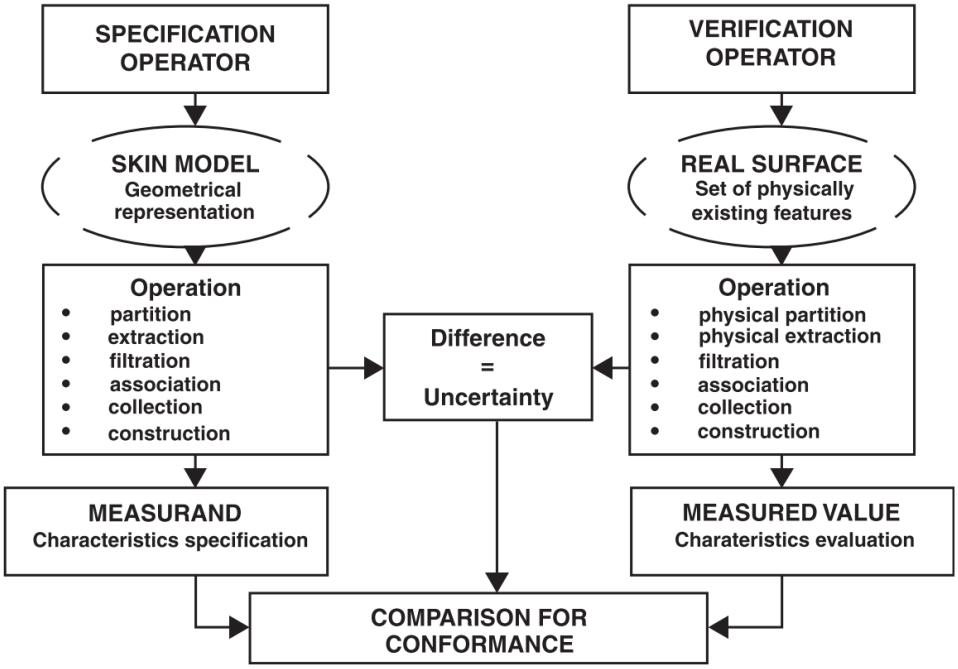


Figure 2-2 : The uncertainty created though poor feature definition [24].

At the most fundamental level ISO 14660:2000 defines the features with respect to design, manufacture, metrology and compliance. As shows Figure 2-3, ISO 14660:2000 defines design feature definitions as nominal features, manufactured features as real features, measured features as extracted, and conformance features as associated [25].

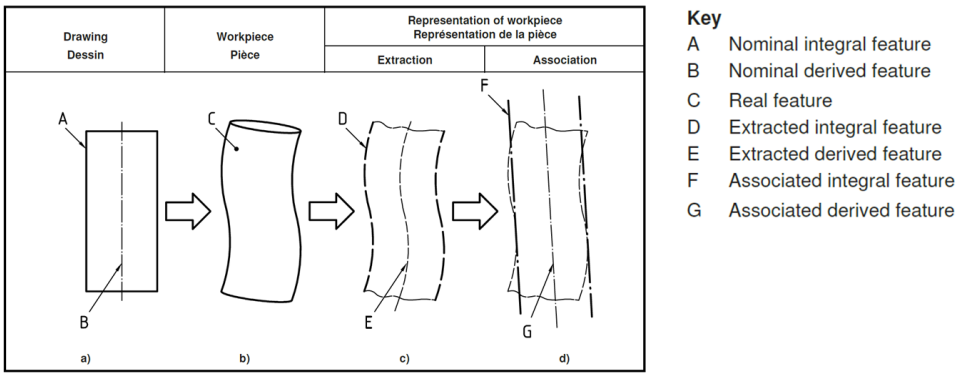


Figure 2-3 : Interrelationship of the geometrical feature definitions [25]

ISO 17450-1:2011 describes and defines the basis for the principle of duality, the full definition is another standard (ISO 8015). The ISO 17450-1:2011 standard also defines the "*ideal nominal model*" as expressing designer generated design intent and "*non-ideal surface model*" extracted from the workpiece as being used for part verification [26]. The standard explains the difference between these two models as the geometric uncertainty of the design. Furthermore, ISO 17450-1:2011 defines measurement workflow "*operators*" from design intent through to conformance verification, with the main process steps being:

- *Partitioning* – The identification of fundamental geometric features (i.e. planes, cylinders, points, and so on) for measurement.
- *Extraction* – A non-ideal is model generated though the measurement of the partitioned features using a finite number of discrete measurement points.
- *Filtering* – The smoothing of measurement data due to the resolution of the measurement process (i.e. the size of the CMM probe).

- *Association* – The alignment of the measured geometry with an ideal form (as per the required standard), including the required tolerance zones.
- *Collection* – collecting data between several associated features for comparison (i.e., check parallelism between two planes).
- *Construction* – build extrapolated and constructed ideal datum features from associated and/or collected features.
- *Evaluation* – Determine the deviation of the measurements from the design nominal feature and tolerances.

ISO 8015 is also the other key fundamental GPS standard, explaining the tolerancing assumptions such as: defining functional and tolerancing limits; stating the absolute nature of the tolerancing (i.e., the workpiece functions 100% within the defined tolerance and 0% outside); the "*definite drawing principle*" (i.e. the drawing defines the enforceable specification in its entirety); and the "*invocation principle*" (i.e. the idea of "unless otherwise state" refer to the corresponding ISO standard) [27]. ISO 8015 is also more specific in defining the duality principle; stating that the GPS design specification on a drawing is independent of the measurement procedure, while the measurement process is independent of the design specification – but should mirror its intent.

The hierarchic nature of the ISO GPS definition has resulted in its sprawl across a large number of standards. To help the reader of any single standard understand both the scope and context of the standard being

consulted the ISO has developed a matrix layout system, which maps out a standard's sphere influence. Broadly though, the GPS standards fall into the categories of: fundamental, global, general and complimentary within the hierarchy [27].

2.3.2 Approaches for the assignment of tolerances

Given the importance of tolerances (as KCs) on the functional performance, cost and manufacturability of a product, much previous research has been conducted in approaches to assist the designer in assigning a tollerancing scheme. Broadly, these approaches fall into three categories, namely [28]:

Tolerance specification: Looking at a component/assembly, the functionally important features are identified as datums for tolerancing. Each of these datum features then have tolerances chosen which limits the geometric variation relative to the nominal geometry. This is typically performed at a part/feature level

Tolerance analysis: Based on the functional requirements of the product, measurable mechanical feature/requirements of the product such gaps, angles and play are determined. The tolerances on the functional requirements are then calculated based the deviations in feature geometry. This is typically performed at the assembly level.

Tolerance synthesis: Initial empirical "best guess" tolerances are assigned to the components based on its required function; these are then refined, adjusted or optimised based on the functional performance and/or cost of

manufactured products. This is normally performed at the part/assembly level.

These approaches to tolerancing assist the designer to ensure the integrity of the design intent is maintained across all levels of the product structure. Furthermore, maintaining the design intent across the product structure is vital for ensuring conformance of the product to the high-level KC. However, as to be expected, each of these approaches has its own benefits and shortcomings; which will be discussed in greater depth in the following sections.

2.3.3 Tolerance specification

The tolerance specification methods of tolerancing that operates primarily at the feature level. The approach takes the features of a component and defines allowable "values" of deviation from the nominal design geometry so that the individual feature can perform its required function. Working in this manner the designer would usually choose a few datum features (normally based of the relational structure within the assembly) and allocates tolerances to them to limit their variation [29]. Once the datum features are defined the remaining features are then dimensioned from these datum features. The tolerance specification method is therefore a bottom-up approach to the tolerance system, which builds up through the feature chain to determine top-level functional performance of the product.

Tolerance specification is typically applied to Topologically and Technologically Related Surface (TTRS) [30]; Which are the faces and features that contain some functional relationship within the same component part. Beyond the TTRS, tolerance specification can be used at the assembly and sub-assembly level but that is a smaller proportion of its use.

2.3.3.1 *Methods for defining tolerance*

When specifying the functionally allowable manufacturing variance of features within a manufactured product a designer has two main tools at their disposal:

- *Parametric Tolerancing (PT)* – Places linear limits of allowable deviation upon dimensions key to the function of the component or product.
- *Geometric Dimensioning and Tolerancing (GD&T)* – Defines the allowable deviation of a geometric feature, without reference to the size of their base feature.

Currently, both approaches are widely used industrially, either individually or in combination. This coexistence is likely to continue for some time to come as both systems have their short comings. PT is an overly simplistic for complex geometries leaving ambiguity within the geometries, while GD&T is complex to interpret and lacks a fully coherent definition across the various bodies (ISO, ANSI, DIN BS and so on) or within individual companies [23].

Under the ISO, ASME and DIN standards all specified tolerances (be they PT or GD&T) are absolute allowable limits unless specified as "statistical" (via a special drawing symbol - which is yet to be agreed internationally) [23]. When a statistical value is used the designer must also defines a spread (i.e. ±0.1 over 50% of the parts manufactured). This approach therefore permits oversized and under sized features, so long as the majority of the manufacture features fall within the tolerance zone and product function is not hampered.

2.3.3.2 *Parametric tolerance (PT)*

Parametric tolerancing is the eldest of all tolerancing techniques, appearing on engineering drawings in the early 1900's driven by the advent of mass production [31]. Using this method the designer simply places allowable limit of manufacturing variation on to a linear or angular dimension. As Figure 2-4 shows, there are a number of ways this limit can be expressed [32]. A PT can be expressed on a drawing as a symmetrical (Figure 2-4a) or asymmetrical (Figure 2-4b) deviation about a nominal value; an absolute upper and lower value (Figure 2-4c); or even as an ISO limit and fit denomination (Figure 2-4d) where the tolerance is specified through a ISO standard look-up table. It should be noted that even on dimensions that do not explicitly express a tolerance allowance (Figure 2-4e & Figure 2-4f) most drawing standards inforce an implied parametric tolerance to them [33]; frequently via a "catch-all" note on the drawing or a system where the number of decimal places determines the inferred

tolerance. These decimal place methods are normally specific to a given industry or company; consequently the tolerance values denoted for a given number of digits can vary considerably between companies. An ISO and British Standards compliant catch-all tolerancing system is also defined, were a general parametric tolerance can be denoted via a signifying letter (i.e. f, m, c of v) adjacent to the dimension's value [34].

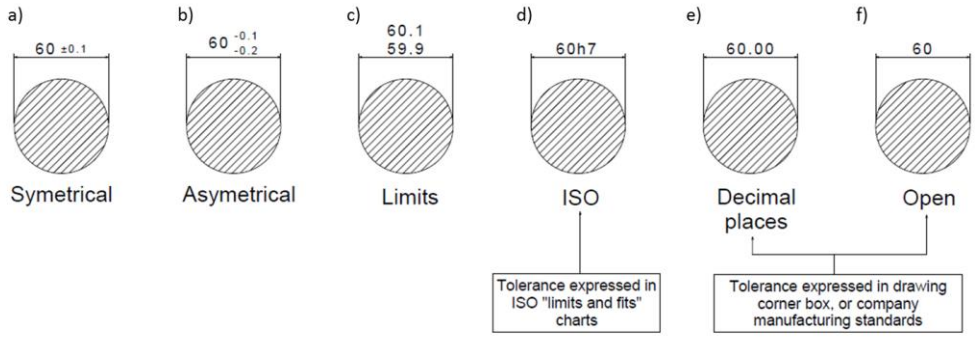


Figure 2-4 : Expressing parametric tolerances on linear dimensions.

Although PT is easy to apply, it is in effect only controlling the envelope sizes of a component features, and expressing nothing about the geometric character of the underlying geometry or how to measure it [35].

2.3.3.3 *Geometric Dimensioning and Tolerancing (GD&T)*

The geometric tolerancing of features was born of assembly ambiguities within military hardware during the World War II [36]. The American war effort saw the creation of a distributed production systems to allow the high volume production of complex sub-assemblies, many of which were safety and function critical. However, the large assemblies became difficult to assembly reliably after shipping to the assembly plant. Realising the

problem a committee consisting of government, academic and industrial representatives was established to examine the issue; the result being the creation of a tolerancing system based on geometric quality of manufactured features.

The aim of GD&T is to define the geometric variance of a manufactured feature by comparing it to a virtual reference geometry. An off-set envelope of allowable variance - the "tolerance zone" - is defined symmetrically around the reference geometry and it is this envelope the manufactured part is then compared against. Take Figure 2-5 for example, here an idealised reference plane has been visualised and an allowable tolerance zone of variation defined by two symmetrically offset planes; if the sample part is manufactured within tolerance the entirety of its manufacture surface must fall within the tolerance zone envelope. Since the underlying idealised reference geometry is perfectly flat, comparison to the manufactured face gives an indication of the "flatness" of the manufactured feature. However, although this method geometrically characterises the flatness requirement of the surface, it generates no indication of its size, position or orientation of the surface itself; only its deviation.

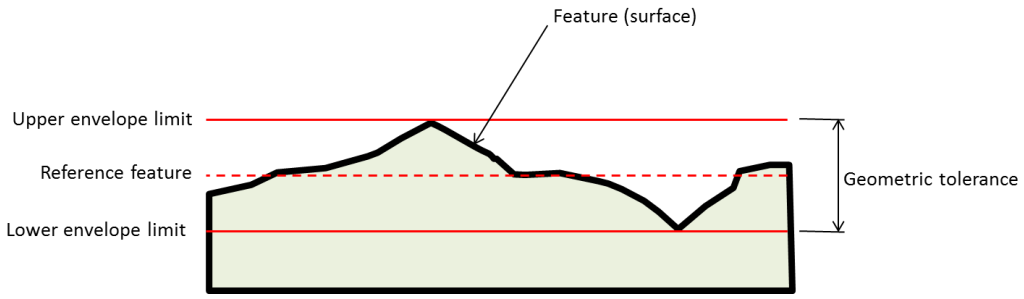


Figure 2-5 : Explanation of the fundaments of geometric tolerancing

Current GD&T tolerancing standards [37, 38] enable the definition of many geometric qualities through the application of: point, 2D, and 3D reference geometries and envelopes. This allows geometric qualities such as roundness or conformance to a free-form CAD modelled surface to be quantified. Furthermore, these standards also permit other manufactured features of a component to be used as a reference, enabling the quantification of geometric qualities such as: perpendicularity or angularity between two faces; concentricity between axial features; and the asymmetry of two or more features.

Table 2-1 shows the geometric tolerances defined by the ISO 1101:2004 and the symbol used to define the geometric tolerance on an engineering drawing. It should be noted that while the ASME standards share the same symbols and tolerances, the definition of the tolerance zones are subtlety different [23] – this thesis will focus primarily on the ISO standard as it is most widely (globally) applicable. The table also shows categorisation ISO 1101:2012 uses to group tolerances: form, orientation, location and run-out.

Tolerances	Characteristics	Symbol	Datum needed
Form	Straightness	—	no
	Flatness	▱	no
	Roundness	○	no
	Cylindricity	⌭	no
	Profile any line	⌒	no
	Profile any surface	⌓	no
Orientation	Parallelism	//	yes
	Perpendicularity	⊥	yes
	Angularity	∠	yes
	Profile any line	⌒	yes
	Profile any surface	⌓	yes
Location	Position	⌖	yes or no
	Concentricity (for centre points)	◎	yes
	Coaxiality (for axes)	◎	yes
	Symmetry	⌯	yes
	Profile any line	⌒	yes
	Profile any surface	⌓	yes
Run-out	Circular run-out	↗	yes
	Total run-out	⌰	yes

Table 2-1: Categories of geometric tolerance [37]

An example of how geometric tolerancing operates in practice is shown in Figure 2-6a. In this drawing a number of holes have their positions defined via GD&T using a positional tolerance. To define the positional parameters a tolerance frame call-out is utilised. Figure 2-6b shows a typical tolerance frame which states the tolerance type as a symbol; the size of the tolerance zone is stated along with the reference datums to be used (the number of datums can vary from none to three, depending on the tolerance type requirement). It should be noted that ISO 2768-2:1989 defines a number of standard bands of tolerances (denoted H, K and V) for the various geometric tolerance types, so a numeric value may not always be present in the tolerance frame [39]. Figure 2-6c shows how the datum features are identified. A final feature of note in Figure 2-6 are the boxed dimensions (in

Figure 2-6a), these define the position of the idealised reference features and as these dimensions are to an imaginary/virtual point, so they are error-free.

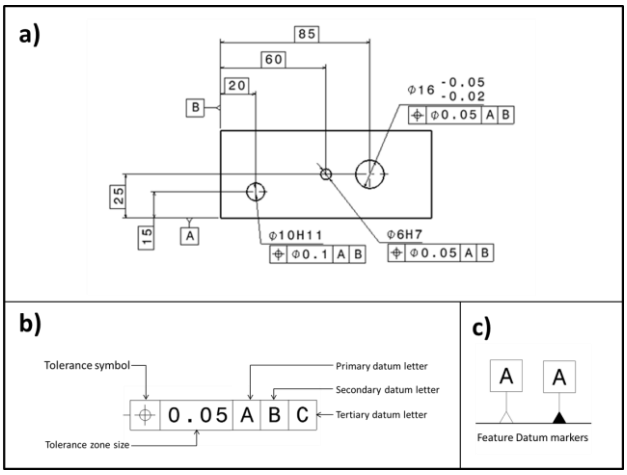


Figure 2-6 : Using GD&T a) example drawing, b) the tolerance frame, c) datum call out.

Although geometric tolerancing is a powerful tool it can be a confusing system to use effectively in practice. This is due to an overlap between tolerance types and the lack of consistency between international standards. For example a designer could specify the flatness of a given planar feature in a number of ways: using a parallelism, angularity or perpendicularity to a datum feature; using a profile tolerance to a flat profile; or via an actual flatness tolerance. Adding to the confusion further, each tolerance type generally has a 2D and 3D variant which the designer must also choose.

For the geometry examined in this thesis Rolls-Royce defined flatness and circularity (roundness) as the assembly KCs. Therefore, these two

geometric tolerance types will be examined in the sections below to understand their geometric implications in greater detail.

2.3.3.3.1 Flatness

Flatness is defined as the minimum separation between an inner and outer minimum zone reference plane placed symmetrically about a mean zone reference plane [40]. In practise, to measure a planar feature an average reference plane is determined using a least squares deviation measure between the peaks and valleys of the surface. The peaks and valleys of the measured surface must then be entirely bound within the two symmetric (inner and outer) reference planes; the distance between the planes being the flatness tolerance zone

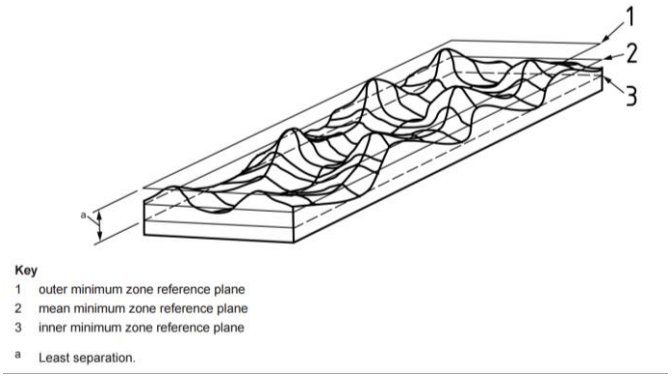


Figure 2-7 : Definition of flatness extracted from ISO 12781-1:2011 [40].

2.3.3.3.2 Roundness / Circularity

Figure 2-8 shows, the ISO 12181-1:2011 (the specific circularity standard) [41] definition of circularity (also referred to as roundness). It defines circularity as the minimum distance between an inscribed Inner Minimum Zone reference CIrcle (IMZCI) and a circumscribed Outer Minimum Zone

reference CIrcle (OMZCI); referring to the radial distance between them as the Minimum Zone Circle (MZC). The IMZCI and OMZCI are considered to be perfectly concentric, and fitted to the geometry so that the MZC is as small as possible, ignoring any functional axial requirement of the geometry. Finding the smallest possible MZC referred to in literature as the min/max criterion [42]. There is a small amount of ambiguity surrounding how the MZC is found from the point data generated by a Coordinate Measurement Machine (CMM). Indeed a number of researcher have suggested approaches to solve this including: linear simultaneous equations [43, 44], equi-distant (Voronoi) techniques [45], Cheby-shev Criterion [46], least squared circle [47], and simplex search [48]. However, ISO 12181-1:2011 recommends a root mean square roundness method based on a least square reference circle should be used if no other approach is specified.

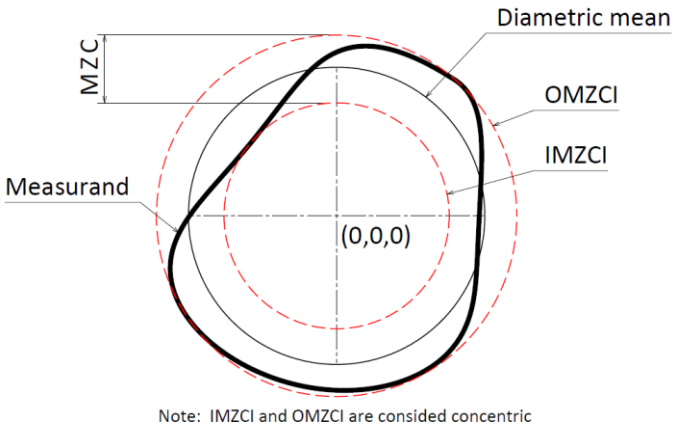


Figure 2-8 : The measurement of circularity

2.3.3.3.3 Circular Run-out

Circular run-out and circularity are frequently confused, as they both express geometric deviation from a circular nominal geometry, but in subtlety different ways. Currently, circular run-out has no individual ISO standard so its definition is capture within ISO 1101:2012. The standard defines circular run-out as "*The tolerance zone is limited within an cross-section perpendicular to the datum axis by two concentric circles with a difference in radii of t, the centers of which coincide with the datum*"[37]. Fundamentally, circular run-out ties the reference circles to the functional axis of the component, rather than fitting the circles generated to the smallest area of deviation possible; as we see in circularity's definition. Determining the axial position from measurement uncertainties is defined mathematically by ISO 14660-2:1999 [49].

In summary, tolerance specification deals purely with defining allowable deviation of individual features from their nominal sizes. Two tools to achieve this are available to the designer: parametric tolerancing to define the size of features (but not its geometric integrity); and geometric tolerances to define geometric quality (but making no reference to the size of the features). Indeed, to fully define the functionally allowable variance within a manufactured design the designer must use both systems to ensure design intent is retained throughout the production process.

2.3.4 Tolerance analysis

Tolerance analysis differs from tolerance specification as it operates in top-down manner rather than bottom-up. Tolerance analysis looks for measurable functional requirements at the product level (i.e. the size of gaps, opening angles or play) and works back through the product hierarchy calculating the tolerances needed at each level to produce the defined functional output. Consequently, as the tolerance analysis approach examines how the hierarchy of tolerances interact so it is commonly referred to as "tolerance stack-up analysis" within literature and industry [50]. Figure 2-9 shows an example of this approach, where the designer is interested in dimensionally controlling the gap B. Functionally the gap B needs to be manufactured to be within a given size range for the product to function properly. However, each component within the assembly will be subject to manufacturing variance in their width (A1-A4). Therefore, if a design is to achieve the required variance range in the value of B, the designer must work backward and determine the allowable variance values for A1 to A4 in order ensure the functional requirement for B is met when the product is manufactured.

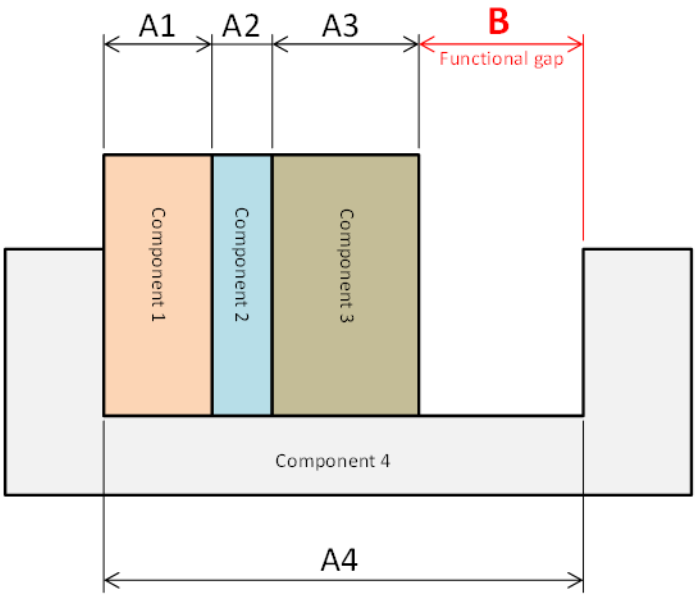


Figure 2-9 : An example of the tolerance allocation method

2.3.4.1 *Traditional approaches to tolerance stack-up*

Eq. 1, shows the generalised expression of the unidirectional manufacturing variation for a given feature relative to a measurement datum or reference feature [51];

$$Y = f(X_1 \dots X_n) \qquad \textit{Eq. 1}$$

Where, Y is the output dimension dependent on a function f, comprised of independent random scalar input variables $X_1 \dots X_n$ derived from dimension of the features. The function (f), is referred to in literature as the "tolerancing equations" and it defines the cause-effect relationship between the input variables and the output value and its definition is considered a key stage of any tolerance analysis process [52].

Assuming the function input variables $X_1 \dots X_n$ are subject to a defined range of variation (i.e. the tolerance), inputting all the minimum values for each X variable ($X_{1min} \dots X_{nmin}$) into the function f will generate the smallest possible value for Y, or Y_{min}. While, inputting the largest possible values for each X variable ($X_{1max} \dots X_{nmax}$) into the function f will generate the largest possible value for Y, or Y_{max} . Therefore, as Eq. 2 shows subtracting Y_{min} from the Y_{max} value, allows calculation of ΔY or the total variance within Y based in the variance range of inputs (X variables).

$$\Delta Y = |Y_{max} - Y_{min}| \qquad \textit{Eq. 2}$$

Based on this thinking the total variance range within each X parameter (ΔX_i) can also be expressed but subtraction of the smallest allowable value from the largest; as Eq. 3 shows.

$$\Delta X_i = |X_{imax} - X_{imin}| \qquad \textit{Eq. 3}$$

Therefore, combining Eq. 2 and Eq. 3, the total variance in Y (ΔY) can also be determined by passing the total variance of each X (ΔX_i) parameter through Eq. 4

$$\Delta Y = f(\Delta X_1 \dots \Delta X_n) \qquad \textit{Eq. 4}$$

A number of the techniques used to express the possible "stacking" of manufacturing variation within an assembly system, require the variability in scalar variables ($X_1 \dots X_n$) to be expressed as a symmetric (±) range about the nominal value of X_i. Working in this symmetric (±) manner, the ΔY

output from the function shown in Eq. 4 will also generate an output symmetric about the nominal value of *Y*.

The traditional (and industrially most common) functions for consolidating assembly variations are; the Arithmetic Worse-case (AWc) and Summation in Quadrature (SiQ) methods; both extremely well documented linear approaches [23, 31, 53]. These approaches will be discussed in the following section.

2.3.4.1.1 Arithmetic worst-case (AWc)

In a simple linear assembly such as a stack of rigid parallelepiped blocks on a tabletop, the variance in overall height of the assembled pile is simply the sum of all the variance in the system, as expressed via Eq. 5. Where: ΔY is the possible range of variation within the tolerance system under consideration, (e.g. the total height of the stack of blocks) expressed as a symmetrical (±) range; and ΔX_i is the symmetric variation in the component parts of ΔY (e.g. the variation in the individual block's height).

$$\Delta Y = \sum_{i=1}^{n} |\Delta X_i| \qquad Eq.\ 5$$

This approach is will generally produce an overly pessimistic output, especially as the number of components or features in the system increases. For tolerance chains longer than a few features, the AWc approach will suggest a higher/tighter tolerance than is likely to be seen in the manufactured real-world component or assembly. The cause of this

overestimation is based on the assumption of a uniform distribution from the production process for each feature where a more centrally weighted distribution occurs in practice. For example, a designer specifies a single feature which requires a variance of say ±0.1mm; a Bayesian assumption supposes that the ±0.1mm total variance zone approximates to 6σ (6x standard deviation) in a Gaussian distributed manufacturing process. However, based on the center weighted statistical distribution, the majority of the manufactured features would be produced at smaller levels of variation than the required ±0.1mm. Consequently, 99.7% of the features would be produced at greater accuracy than ±0.1mm, while 68% of the produced parts would have a variance of ±0.033mm – assuming an idealised distribution [31]. Moreover, as more components / features are added in to the tolerance system (i.e. assembly or part), so the statistical weighting to the manufacturing process has greater influence; making the variance suggested by the AWc increasing unrealistic.

However, the AWc approach is easy to calculate, and perfectly suited to simple components or small assemblies. Most importantly the AWc method offers an absolute and thus "safe" answer, so the method persists especially in industry [54].

2.3.4.1.2 Linear Statistical propagation

The SiQ (also called Root Sum of the Squares (RSS)), statistical-fit or variance law model) method assumes that the manufacturing variability within parameters $X_1 \dots X_n$ are mutually independent and normally

distributed at an interval of 6σ [31]. Based on this assertion the Central Limit Theory (CLT) dictates that; when combining the $X_1 \ldots X_n$ parameters in the function, the statistical probability of the combined parameters producing the worse-case diminishes as the number of parameters increases. However, that is not to say that the worse-case will not or cannot happen, it is just statistically unlikely. The calculation for combining error through the SiQ is shown in Eq. 6.

$$\Delta Y = \sqrt{\sum_{i=1}^{n} \Delta X_i{}^2} \qquad \textit{Eq. 6}$$

It should be noted that there are also issues with the SiQ approach. Firstly, the SiQ method underestimates the amount of variation in an assembly. This is because of the Bayesian assumption that the input variables are normally distributed and independent. However, given that a normal distribution is an idealised mathematical construct all manufacturing processes will exhibit some form of skew and/or kurtosis; causing a misalignment between the calculated SiQ prediction and real-world results [55]. Therefore, Nigam and Turner [51] recommend when using the SiQ method that the first four moments of the distribution (mean, variance, skew and kurtosis respectively) should be known for the input variables.

A number of researchers have attempted to address the underestimation problem of the statistical SiQ approach. Bender [56] and Gladman [57] proposed a simple inflation factor based on empirical knowledge. While,

Shen and Duffie [58] and Spotts [59] looked to combine both the AWc and SiQ approaches, in the hope of creating a middle ground between the over and underestimation of the two methods. The results in both these combination studies, showed an underestimation in the calculated variation.

2.3.4.1.3 Non-linear propagation

Weak non-linear problems can be approximated using partial derivatives of the tolerancing equations, (the function $f(X_1 \dots X_n)$) to create approximations of the proportional contribution from each parameter [31]. Once the partial derivatives are calculated they can then be combined using either an arithmetic or summation in quadrature approach. Eq. 7, shows the Derivative Worse-case (DWc) method is based on the simple summation of the manufacturing variation (ie AWc). While Eq. 8, shows the Derivative Summation in Quadrature (DSiQ), based on the linear SiQ method.

$$\Delta Y \approx \sum_{i=1}^{n} \left| \frac{\partial f}{\partial X_i} \right| \cdot \Delta X_i \qquad \textit{Eq. 7}$$

$$\Delta Y \approx \sqrt{\sum_{i=1}^{n} \left(\frac{\partial f}{\partial X_i} \right)^2 \cdot \Delta {X_i}^2} \qquad \textit{Eq. 8}$$

The partial derivative methods allow the designer to see the sensitivity coefficient (weighting) for each of the parameters (X_i) upon the total error (ΔY) leading to better appreciation of individual manufacturing tolerances

and their impact systemically. However, in situations of strong non-linearity in both DWc and DSiQ , a Taylor series expansion may be used to more accurately predict the resultant effect of the sensitivity coefficient [60].

Both partial derivative methods also suffer the same issues as their linear counterparts; DWc method generally pessimistically overestimates the amount of error in the system, while the DSIQ method optimistically underestimates.

2.3.4.2 *Geometric approaches to tolerance propagation*

The traditional tolerance analysis techniques are only truly suited to simple linear and nonlinear 1D problems, as the definition of the tolerancing equations becomes overly difficult for complex 2D and 3D assemblies [61]. The traditional techniques in particular struggle to capture the subtlety of GD&T tolerancing. Consequently, more recent research [62] has moved away from simple numeric tolerance analysis methods using discrete mathematics. To address the complexities of GD&T a number of geometric tolerancing approaches have been developed, the most prevalent being: vector loop, variation modelling, matrix, Jacobian and Small Displacement Torsor (SDT) methods [63]. Most of these approaches still calculate the worst case and/or summation in quadrature to determine the total range of system deviation likely.

2.3.4.2.1 Vector loop

Initially proposed in the late 1960's [64], the vector loop method defines the tolerance system using a series of 2D or 3D vectors whose magnitude and direction map the relevant dimensions. Once the system is mapped the vector's magnitude can be lengthened and shorten to represent the systemic variance. It should be noted the although the approach is generally referred to in literature as vector loop, the tolerance system under analysis is not forced to be a loop; the approach is also capable of resolving open-ended tolerance chains (i.e. tolerancing a gap). In their seminal work, Chase *et al.* further developed the vector loop method proposing the Direct Linearization Method (DLM) [65]. DLM creates matrices of not only parametric dimensional vectors, but also kinematic and geometric variance vectors to give a description of the assembly and it mechanical interactions.

The kinematics portion of the DLM defines the allowable translations and rotations of the system's components (in either 2D or 3D), defining the joint/interfaces between each components of the assembly. Rigid, prismatic, cylindrical (co-axial), revolute (pin), parallel cylinders, spherical, planar slider, cylindrical slider, edge slider, point slider, and crossed cylinders kinematic interactions can all be modelled using this technique. In addition to the allowable motion, the DLM approach also allows changes in a mechanisms velocities and accelerations (via first and second derivatives of the Jacobian matrix) due to variance in a mechanisms components to be determined [66].

Possible GD&T geometric variances are captured in a matrix form when using DLM [67]. To describe the GD&T tolerances in a usable matrix form the ISO/ASME geometric tolerances are deconstructed into their rotational and translation deviations (much like the kinematics).

As Eq. 9 shows [68], a concatenated homogenous transformation matrix is used to express a vector loop tolerancing model.

$$\boldsymbol{R}_1 \cdot \boldsymbol{T}_1 \cdot \ldots \cdot \boldsymbol{R}_i \cdot \boldsymbol{T}_i \cdot \ldots \cdot \boldsymbol{R}_n \cdot \boldsymbol{T}_n \cdot \boldsymbol{R}_f = \boldsymbol{H} \qquad \text{Eq. 9}$$

Where, $\boldsymbol{R}_i$is the rotational matrix about the X origin (for a 2D analysis) and $\boldsymbol{T}_i$ is the translational matrix of the node at position i (with 1 and n denoting the first and last nodes respectively). $\boldsymbol{R}_f$ is the final closing rotational matrix and $\boldsymbol{H}$ is the resultant matrix. $\boldsymbol{H}$ will be either the identity matrix of a closed vector loop or the magnitude and direction of a gap or clearance when examining an open-loop assembly. Eq. 9 shows only systemic variance due to parametrical (i.e. non-geometric) tolerancing, but without accounting for geometric variation, therefore to included geometric qualities such as flatness Eq. 10 must be used [69].

$$\boldsymbol{R}_1 \cdot \boldsymbol{T}_1 \cdot \ldots \cdot \left[\boldsymbol{R}_{ig} \cdot \boldsymbol{T}_{ig}\right] \cdot \boldsymbol{R}_i \cdot \boldsymbol{T}_i \cdot \ldots \cdot \boldsymbol{R}_n \cdot \boldsymbol{T}_n \cdot \boldsymbol{R}_f = \boldsymbol{H} \qquad \text{Eq. 10}$$

Where, $\left[\boldsymbol{R}_{ig} \cdot \boldsymbol{T}_{ig}\right]$ are the corresponding rotational and translation adjustments required to capture the effect of geometric deviation at node *i*. As DLM can be used for 2D and 3D tolerance analysis the structure of the matrices $\boldsymbol{R}_1$and $\boldsymbol{T}_1$ will vary, but for brevity just 2D will be examined here. The 2D rotation and translation matrices are shown in Eq. 11.

$$\boldsymbol{R}_i = \begin{bmatrix} \cos\phi_i & \sin\phi_i & 0 \\ \sin\phi_i & \cos\phi_i & 0 \\ 0 & 0 & 1 \end{bmatrix} \qquad \boldsymbol{T}_i = \begin{bmatrix} 1 & 0 & L_i \\ 0 & 1 & 0 \\ 0 & 0 & 1 \end{bmatrix} \qquad \text{Eq. 11}$$

Where, ϕ_i is the inter-vector angle at node i and the magnitude of the vector at node i is L_i. The solving of Eq. 9 and Eq. 10 is often not a trivial matter as they are non-linear equations, however due to the small nature of the variations with a manufactured system a linearized Taylor expansion will generate a suitable approximation. Eq. 12 shows the first order Taylor series expansion of a closed tolerance loop, while Eq. 13 shows the open loop (i.e. clearance gap) expansion.

$$\Delta\boldsymbol{H_c} = \boldsymbol{A} \cdot \Delta\boldsymbol{X} + \boldsymbol{B} \cdot \Delta\boldsymbol{U} + \boldsymbol{F} \cdot \Delta\boldsymbol{\alpha} = [0] \qquad \text{Eq. 12}$$

$$\Delta\boldsymbol{H_o} = \boldsymbol{C} \cdot \Delta\boldsymbol{X} + \boldsymbol{D} \cdot \Delta\boldsymbol{U} + \boldsymbol{G} \cdot \Delta\boldsymbol{\alpha} \qquad \text{Eq. 13}$$

Where, $\Delta\boldsymbol{H_c}$ is the vector of variance for a closed loop and $\Delta\boldsymbol{H_o}$ is the vector of variance for the open clearance gap; $\Delta\boldsymbol{X}$ is variation within the dimensions of the manufactured features; $\Delta\boldsymbol{U}$ the variance vector for the assembly dimensions; $\Delta\boldsymbol{\alpha}$ is the vector of variance due to geometric (i.e. GD&T) variance of the system; $\boldsymbol{A}$ and $\boldsymbol{C}$ are the partial derivatives for the open and closed loop manufactured part features respectively; $\boldsymbol{B}$ and $\boldsymbol{D}$ are the partial derivatives for the open and closed loop assembly features respectively; $\boldsymbol{F}$ and $\boldsymbol{G}$ are the partial derivatives for the geometric component of the open and closed loop respectively.

As input to Eq. 12 and Eq. 13 $\Delta\boldsymbol{U}$ is required, for a closed loop system $\Delta\boldsymbol{U}$ is obtain from Eq. 14 if $\boldsymbol{B}$ is a full-ranked matrix and Eq. 15 if $\boldsymbol{B}$ is a singular

matrix. While for an open-loop system Eq. 16 and Eq. 17 can be used for ranked and singular matrices respectively.

$$\Delta \boldsymbol{U} = -\boldsymbol{B}^{-1} \cdot \boldsymbol{A} \cdot \Delta \boldsymbol{X} - \boldsymbol{B}^{-1} \cdot \boldsymbol{F} \cdot \Delta \boldsymbol{\alpha} \quad \text{Eq. 14}$$

$$\Delta \boldsymbol{U} = -(\boldsymbol{B}^{T} \cdot \boldsymbol{B})^{-1} \cdot \boldsymbol{B}^{T} \cdot \boldsymbol{A} \cdot \Delta \boldsymbol{X} - (\boldsymbol{B}^{T} \cdot \boldsymbol{B})^{-1} \cdot \boldsymbol{B}^{T} \cdot \boldsymbol{F} \cdot \Delta \boldsymbol{\alpha} \quad \text{Eq. 15}$$

$$\Delta \boldsymbol{U} = (\boldsymbol{C} - \boldsymbol{D} \cdot \boldsymbol{B}^{T} \cdot \boldsymbol{A}) \cdot \Delta \boldsymbol{X} + (\boldsymbol{G} - \boldsymbol{D} \cdot \boldsymbol{B}^{-1} \cdot \boldsymbol{F}) \cdot \Delta \boldsymbol{\alpha} \quad \text{Eq. 16}$$

$$\Delta \boldsymbol{U} = (\boldsymbol{C} - \boldsymbol{D} \cdot (\boldsymbol{B}^{T} \cdot \boldsymbol{B})^{-1} \cdot \boldsymbol{B}^{T} \cdot \boldsymbol{A}) \cdot \Delta \boldsymbol{X} + (\boldsymbol{G} - \boldsymbol{D} \cdot (\boldsymbol{B}^{T} \cdot \boldsymbol{B})^{-1} \cdot \boldsymbol{B}^{T} \cdot \boldsymbol{F}) \cdot \Delta \boldsymbol{\alpha} \quad \text{Eq. 17}$$

At this point the worst case (T_{wc}) and SiQ (T_{SiQ}) propagation of variance for the system can be calculated (Eq. 18 and Eq. 19 respectively) using the sensitivity matrices of the dimensional and geometric variables.

$$T_{wc} = \sum_{j=1}^{m} \left| S_{ij}^{d} \right| \cdot T_{ij}^{d} + \sum_{j=1}^{n} \left| S_{ij}^{\alpha} \right| \cdot T_{ij}^{\alpha} \quad \text{Eq. 18}$$

$$T_{SiQ} = \sqrt{\left(\sum_{j=1}^{m} \left| S_{ij}^{d} \right| \cdot T_{ij}^{d} \right)^{2} + \left(\sum_{j=1}^{n} \left| S_{ij}^{\alpha} \right| \cdot T_{ij}^{\alpha} \right)^{2}} \quad \text{Eq. 19}$$

Where: S_{ij}^{d} is the sensitivity matrix of the parametric dimensional variables; S_{ij}^{α} is the sensitivity matrix of the geometric variables; *m* and *n* are the total number of geometric and dimensional parameters. In summary, calculating $\Delta \boldsymbol{H_c}$ or $\Delta \boldsymbol{H_o}$ gives vector (magnitude and angle) of functional parameter, while T_{wc} and T_{SiQ} estimates the possible variance (i.e. the propagated tolerance) within the parameter.

Although a long standing method of tolerance analysis vector-loop / DLM has a number of issues surrounding its use in practice. Firstly, its uses of a Taylor series expansion so will generate only and approximation of the true answer. Clancy and Chase [70] did proposed a further improvement for the estimation accuracy of DLM, via the incorporation of Monte Carlo study data and a second order Taylor series expansion. The Second issue, with DLM is that it's representation of the geometric tolerances are not strictly aligned with the ISO or ASME definitions. Thirdly, that the method poorly describes functional clearances (i.e. "limits and fits") between components. Finally, the DLM method will not allow tolerance independence or the envelope rules to be applied to tolerances on the same part (as required by the standards) [71, 72].

2.3.4.2.2 Variational approach

The foundation of this approach dates back to the 1970 's, and early work looking at the parametric modelling of components for use in CAD systems [73]. The power of parametric models comes from describing the geometry of a component or assembly mathematically. The size, position and orientation of a component feature can easily be altered; making it easier for a designer to explore the embodiment of the design intent. Due to the ease and adaptability of a parametric model, it became apparent that this method could be used to model or simulate manufacturing variance of a component or assembly. By taking a nominal geometric feature and resizing it to represent the maximum and minimum material conditions, and

performing other mathematical offset operations (such as a prediction of the influence of geometric tolerances) a geometric representation of allowable manufacturing variance can be defined in either 2D [74] or 3D [74, 75] space. The approach can then be further extended by assembling these component representations together, generating a representation of the impact of manufacturing variance within an assembly system.

Mathematically the variation approach uses homogeneous transformation matrices to define the nominal base geometry and variations due to tolerances [76]. Each hierarchic level of the nominal parametric model for an assembly contains its own coordinate reference frame (i.e. one per feature, component and one for the final assembly), the $\boldsymbol{TN}$ matrix contains the roto-translational information needed to pass from one level of coordinate reference frame to the next [77]. The tolerance variances are then represented with a second homogeneous transformation matrix called $\boldsymbol{DT}$. Furthermore, $\boldsymbol{DT}$ contains the translational and rotational displacements require to offset the nominal geometric features to the tolerance zone limit, without altering the form of the nominal geometry – just displacing it. Eq. 20 shows, by moving from the coordinate reference frame of the part *i*, $\boldsymbol{R}i$; to the reference frame of feature *j*, $\boldsymbol{R}ij$, all that is required is a multiplication of the matrices.

$$\boldsymbol{T}_{\boldsymbol{R}i\rightarrow\boldsymbol{R}ij} = \boldsymbol{TN}_{\boldsymbol{R}i\rightarrow\boldsymbol{R}ij} \cdot \boldsymbol{DT}_{\boldsymbol{R}ij} \qquad \text{Eq. 20}$$

Where: $\boldsymbol{T}_{\boldsymbol{R}i\rightarrow\boldsymbol{R}ij}$ is the total transformation matrix to move from the coordinate reference frame of part *i* to feature *j*; $\boldsymbol{TN}_{\boldsymbol{R}i\rightarrow\boldsymbol{R}ij}$ is the

transformation matrix for the nominal geometry from feature *j*, to the part coordinate frame; and $\boldsymbol{DT_{Rij}}$ is the transformation matrix for the displaced geometry *j* (i.e. with tolerance variance) to the part *i*.

After adjusting the part's feature to represent the allowable variance in each part of an assembly they can then be assembled, via a differential homogenous transformation. However this differential assembly matrix, (referred to as $\boldsymbol{DA}$), is complex to evaluate as it must consolidate mating part tolerances, feature contact and assembly conditions while defining each part's shifted position [78]. Eq. 21 shows the transformation to pass from two components in the assembly.

$$\boldsymbol{A_{Ri\rightarrow Rij} = AN_{Ri\rightarrow Rl} \cdot DA_{Ri\rightarrow Rl}} \qquad \text{Eq. 21}$$

Where: $\boldsymbol{A_{Ri\rightarrow Rij}}$ is the transform matrix to move between part *i* and part *l*; and $\boldsymbol{AN_{Ri\rightarrow Rl}}$ is the matrix of transformation between the nominal positions of part *i* to part *l*; and $\boldsymbol{AN_{Ri\rightarrow Rl}}$ is the matrix of transformation between the displaced positions of part *i* to part *l*. The expanded form of this is shown in Eq. 22

$$\boldsymbol{A_{Ri\rightarrow Rij} = TN_{Ri\rightarrow Rij} \cdot DT_{Rij} \cdot DA_{Rij\rightarrow Rlk} \cdot DT_{Rlk}^{-1} \cdot TN_{Rl\rightarrow Rlk}^{-1}} \qquad \textit{Eq. 22}$$

Where: $\boldsymbol{TN_{Ri\rightarrow Rij}}$ is the nominal transformation matrix between part *i* coordinate frame and feature *j* coordinated frame; $\boldsymbol{DT_{Rij}}$ is the differential matrix between feature *j* (on part *i*) in its nominal and variance positions relative to the part coordinate frame; $\boldsymbol{DA_{Rij\rightarrow Rlk}}$ is the deformational

transformation matrix between feature *j* of part *i* and feature *k* of part *l* in the assembly coordinate frame; $\boldsymbol{DT}_{\boldsymbol{R}lk}$ is the differential matrix between feature k (on part l) in its nominal and variance positions relative to the part coordinate frame; and $\boldsymbol{TN}_{\boldsymbol{R}l\rightarrow\boldsymbol{R}lk}$ is the nominal transformation matrix between part *l* coordinate frame and feature *k* coordinated frame.

Having defined the assembly conditions and consolidated the effects of the geometric component variation, all features can be transferred into the global (i.e. assembly) coordinates frame. Using Eq. 23, the movement in a given feature X_{ik} can be calculated as a vector relative to it nominal assembly position x_k.

$$X_{ik} = \boldsymbol{AN}_{\boldsymbol{R}i\rightarrow\boldsymbol{R}l} \cdot \boldsymbol{DA}_{\boldsymbol{R}i\rightarrow\boldsymbol{R}l} \cdot \boldsymbol{TN}_{\boldsymbol{R}l\rightarrow\boldsymbol{R}lk} \cdot \boldsymbol{DT}_{\boldsymbol{R}lk} \cdot x_k \qquad \text{Eq. 23}$$

On reaching this point the tolerance stack can be solved using either a worst case or statistical assessment can be performed and compared to the functional requirements of the assembly.

Although a well-established approach of tolerance analysis, the variation method has a number of shortcomings. The most formidable being the complexity in defining the differential assembly matrix ($\boldsymbol{DA}$). Solving this requires an implicit knowledge of the assembly system and forward knowledge of balancing the geometric variation and the assembly conditions. In response, a number of researchers have looked at addressing this problem. Sodhi and Turner [79] proposed a constrained-optimisation technique for the determination of an assembled part's position within an

assembly of non-ideal parts. They proposed the application of linearized rotational elements using the likely small scale of typical manufacturing error to their advantage. Wang and Ozsoy [80] proposed a method of mapping the fundamental assembly with a hierarchical data structure. The structure representing an assembly's connectivity information via a description of mating links, conditions, paths and features. The use of geometric reasoning has also been proposed as a method of solving the [81].

In an attempt to Solve the variation approach's assembly problem Whitney *et al* [82], proposed an adjustment of the variation approach, which focuses on assembly though the kinematic restraint of a component's movement. This approach is rooted in the author's earlier work, where the concept of Datum Flow Chains (DFC) was proposed. A DFC is a graphical concept that represents the component interactions of mating features within an assembly system[16]. By looking at the kinematic impact of the jointing/contact interfaces between assembled components the allowable motions between them can be identified. This is performed through the application of screw theory (section 2.3.4.3) to define the allowable motion in an inter-component joint, via a "twist" matrix [83]. In total seventeen kinematic joint type have been identifed and defined for use in the twist matrix [84].

Beyond the complexity of solving the assembly state the variation approach suffers a number of further short comings: an inability to resolve profile

based geometric inaccuracy's (although this can approximated via the faceting of freeform surfaces) [75, 76]; an inability to properly resolve functionally-coupled mating gaps (i.e. close running limits and fits) within assembly[78]; no support for the "envelope" or "independence" rules as defined by the ISO and ASME standards[77].

2.3.4.2.3 Matrix approaches

The matrix approach attempts to generate a description of the tolerance zones. These 4x4 matrix descriptions express the tolerance zones as geometric displacements, altering the nominal component geometry to the extremes of the tolerance zones [85]. The displacements are modelled as transformation matrices relative to the local (feature) reference frame, ignoring the invariant degrees-of-freedom of the tolerance zone. By way of example (Figure 2-10), for a cylindrical tolerance zone t applied along a vector $\boldsymbol{AB}$, the invariant degrees of freedom are the rotation around the cylindrical axis (X) and the translation along the same axis (X) – these are not captured in the matrix, as they have no displacement effect on the geometry. The remaining non-invariant translations (y and Z) and rotations (v and w) that constitute the geometries degrees-of-free are captured in the displacement matrix.

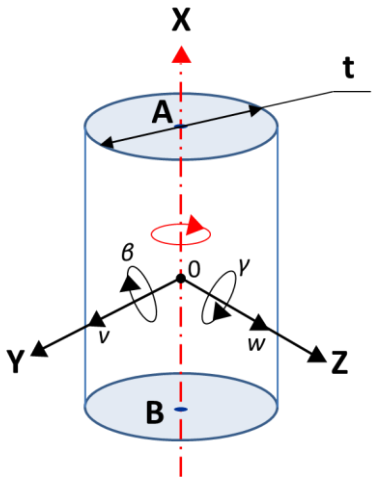


Figure 2-10 : Cylindrical tolerance zone

Based on the example in Figure 2-10 the homogeneous transformation matrix would be as shown in Eq. 24.

$$\boldsymbol{D}(v,w,\beta,\gamma) = \begin{bmatrix} \cos\gamma\cos\beta & -\sin\gamma & \cos\gamma\sin\beta & 0 \\ \sin\gamma\cos\beta & \cos\gamma & \sin\gamma\sin\beta & v \\ -\sin\beta & 0 & \cos\beta & w \\ 0 & 0 & 0 & 1 \end{bmatrix} \qquad \text{Eq. 24}$$

To ensure the vector segment ***AB*** then remains within the cylindrical tolerance zone (Eq. 25) is applied.

$$\sqrt{(Y_{dA}^2 + Z_{dA}^2)} \leq \frac{1}{2}t \quad with \quad \begin{bmatrix} X_{dA} \\ Y_{dA} \\ Z_{dA} \end{bmatrix} = D \cdot A$$

$$\sqrt{(Y_{dB}^2 + Z_{dB}^2)} \leq \frac{1}{2}t \quad with \quad \begin{bmatrix} X_{dB} \\ Y_{dB} \\ Z_{dB} \end{bmatrix} = D \cdot B \qquad Eq.\ 25$$

$$0 \leq \beta \leq \pi \quad and \quad 0 \leq \gamma \leq \pi$$

Using the two sets of formulae, the allowable influence of tolerance zone on the part is mathematically defined; with, Eq. 24 expressing the altered part

geometry along axis ***AB*** and Eq. 25 expressing the parameters of the tolerance zone.

The above example is based on a cylindrical tolerance zone, however nine (four surface and five volumetric) tolerances zones have been identified (from the ISO/ASME standards), and modelled [85].

The displacement matrices for multiple tolerance zones can be summed to assume the total displaced of a feature. For measurement between two features, the displacement must be performed on each of the features under review. Combining their maximum and minimum tolerance zone conditions in the global reference frame the worst-case relationship between them can be determined. This can be performed at either the part for TTRS or assembly level[72]. It should be noted that this method can identify only the worst case stack-up, and no SiQ output is possible with this approach.

2.3.4.2.4 Jacobian method

Proposed by Laperriere and Lafond [86] the Jacobian tolerance analysis method aims to mathematically quantify the kinematic dispersions between pairs of Functional Elements (FEs). These FEs can be: on the same component but distant for one another, "*internal pairs*"; or between the features of separate components that are in contact, "kinematic pairs" or "external pair" [87]. An analysis of the ultimate functional impact of the allowable manufacturing tolerance on a product can then be calculated by chaining together a number of FEs.

To perform the analysis the translation between the FEs of the ideal nominal geometry is modelled (Figure 2-11a). The modelling of the translation is preformed through the creation of six chained "*joints*", each representing a degree-of-freedom in the transform between the FEs. The joints ordered with the first three coordinate frames representing the global three orthogonal translations (XYZ) and the next three the global orthogonal rotations (around the XYZ axes). However, each joint is orientated so that it is always operating along or around its Z axis. The nominal joint model is then perturbed with small displacements to represent the possible manufacturing error (Figure 2-11b)

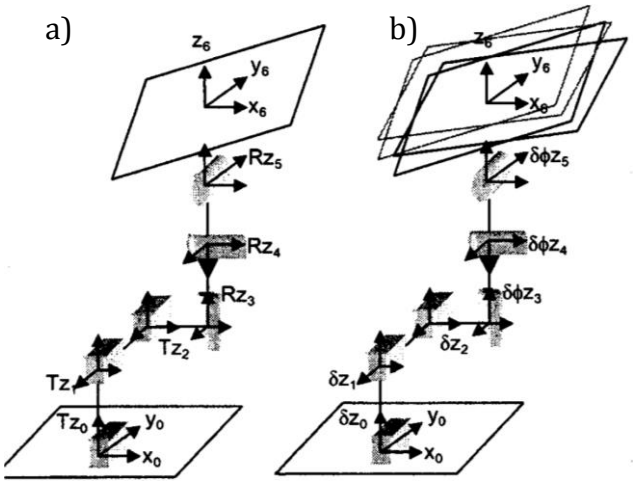


Figure 2-11 : The virtual joints of the Jacobian method, a) the nominal model, b) with small displacements to represent possible variance [87].

Once defined the six joints can be aggregated into a single transformation matrix, and then several of these transformation matrices (each representing a pair of FEs) can then be chained to create a tolerance stack-up. The Jacobian matrix can then be calculated; translating the

transformations into the global coordinate frame, and a worst case or statistical analysis of the tolerance chain performed.

As with each of the tolerance analysis methods discussed in this chapter, the Jacobian method has a number of shortcomings, namely: the Jacobian method is unable to account for assembly functional clearance (i.e. running fits); the system cannot accommodate nested tolerance systems (i.e. a geometric tolerance applied to a sub-assembly of a larger system, while the sub-assembly contains variance within itself); and the Jacobian method can't accommodate form based geometric tolerances [88].

2.3.4.3 *Small displacement torsors*

Based on screw parameters of commonly used in kinematic modelling [89]; torsors describe the viable kinematic motion allowed by a given geometric tolerance zone [90]. The identification of allowable motion between two surfaces is performed through the substitution of the component interface surfaces with an array of perpendicular screw parameters [91]. These parameters are expressed in the form of a torsor and can define any of seven tolerance types depending on the permitted kinematics at each given point in the array. Eq. 26 shows a typical torsor for a hypothetical point on a given surface, where the translations of point A are defined by u_A, v_A and w_A; and the rotations relative to perpendicular are expressed in α, β and γ [63].

$$\boldsymbol{T}_A = \begin{Bmatrix} \alpha & u_A \\ \beta & v_A \\ \gamma & w_A \end{Bmatrix}_{\boldsymbol{R}} \quad \text{Eq. 26}$$

The combined effect of the SDTs can be calculated by a union of the torsors to generate a global kinematic behaviour. This generates only a worst-case evaluation between the features, as the SDTs are based on an array of points so it is not possible to assign any meaningful statistical distribution for the given surface. The biggest benefit of the SDT approaches is its ability to capture small scale/micro manufacturing inaccuracies. Sergent *et al.* highlighted this ability by using the approach to describe surface flatness of a small stepped component [92]. However, the SDT methodology cannot currently capture tolerance networks or chains of dimensions. Also, in-line with the other tolerance analysis methodologies SDT cannot full resolve / capture form based tolerance zones.

2.3.4.3.1 Summary of tolerance analysis approaches

In summary, every current tolerance analysis has its limitations and cannot be applied for the prediction of circularity of an assembled ring. The numeric systems such as AWc or SiQ are relatively simple to implement but they never truly capture the geometric nature of the assembled parts. Moreover, to derive the tolerancing equations needed for their use can be overly complex for most assemblages. While, the vector loop, matrix, variational, Jacobian and Torsor geometric methods are more capable for complex assembly systems they too have problems in this application. None of the systems support (except vector loop) form based tolerances; the

ISO/ASME geometric category into which circularity falls (a key-characteristic of the target structure). Furthermore, some of the systems (Jacobean and torsor) do not support nested assembly structures. But, within the context of the present work there are two problems that affect all the reviewed systems: first, all the systems look at the local tolerancing conditions only – none of them support a global goal (i.e. the circularity of the **entire** assembly system); second, all of these systems output a likely range not an absolute value, in contrast given the fix location approach of traditional fixturing, outputting a statistical range implies that the assembly never truly fits the fixture (see chapter 5).

2.3.4.4 *Computer Aided Tolerancing (CAT)*

The use of Computer Aided Tolerancing (CAT) for assessing the Geometric Dimensioning and Tolerancing (GD&T) of assemblies has been investigated by a number of researchers [93-95]. These system are generally an embodiment of the variation or matrix analysis approaches, usually with some form of integrated statistical engine for Monte Carlo simulation of the assemblies [68]. Typically, these software packages integrate or interface with commercially available Computer Aided Design (CAD) packages [96-98]. Working in a 3D environment the CAT software allows the user to define geometric variation directly onto the parametric model or the assembly constraints. After being defined the manufacturing variation is then visualised as statistical feedback, or as an envelope that surrounds each of the assembly's components. Using this envelope as the component's

outer boundary, the component's assembled positions are then altered to reflect variance within the assembly. Many of these packages also support animation, showing the function of a mechanism under the given allowable geometric deviation conditions. Currently most commercial CAT systems only support rigid components; however using a CAT system and FEA simulation, Byungwoo et al [99] demonstrated a system that predicted assembly distortions for flexible components. This flexible component functionality is slowly being introduced into some commercial CAT packages.

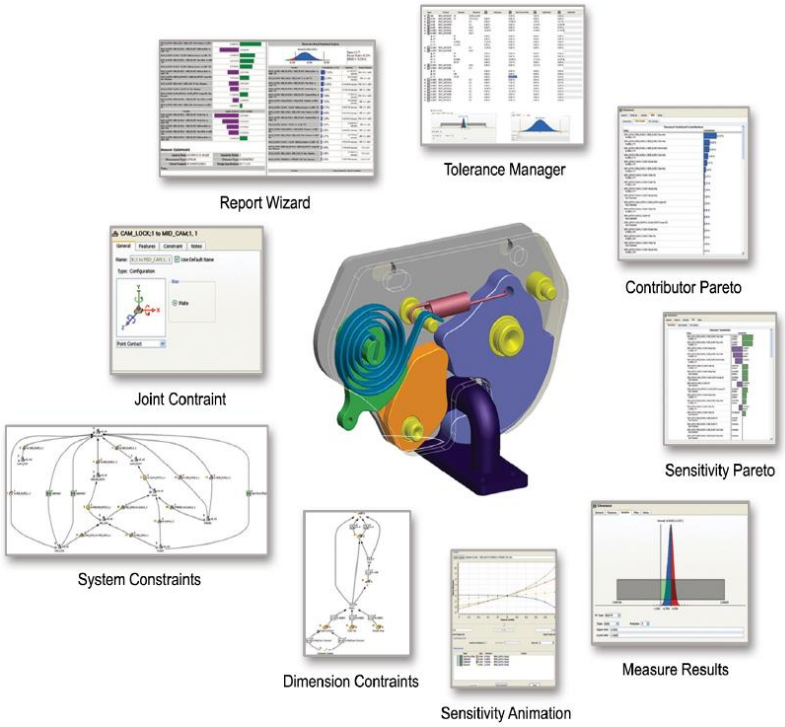


Figure 2-12 : Example of statistical output of typical CAT system [98]

A commercial CAT system could be used to model deviation with the annular assembly's components and predict the resultant circularity of the assembled structure. However, this is a reactive approach to the problem

at hand; a fundamental understanding of the causes of geometric deviation in the assembly would be more beneficial. This fundamental approach will act as the genesis of smarter "variation conscious" assembly techniques, so that an annular assembly's fixture is intrinsically enabled to build the best quality circular arrangement from any given set of components. Since CAT systems are based upon the reviewed tolerance analysis methods described in this chapter, CAT solutions inherently suffer from the problem of outputting a range rather that an absolute value.

2.3.5 Tolerance synthesis approaches

As discussed, tolerance analysis "stacks" the allowable variance in each component/feature to derive a final manufacturing variance for the function or feature under scrutiny. In contrast, tolerance synthesis approaches this tolerancing/variance problem from the opposite direction; starting at the tolerance requirements defined by the product's function and working back-down through the product/component hierarchy to impose the needed tolerances [100]. Frequently tolerance synthesis methods use statistical optimisation methods based on prior knowledge of the repeatability of a manufacturing process to derive its output. A benefit of this approach being that, tolerance synthesis can solve a tolerance problem in a single calculation, rather the requiring the iterative approach generally need for tolerance analysis [100]. However this prerequisite for an in-depth understanding a manufacturing process' capability, during the design process makes synthesis poorly suited to new product

introductions, so it's most frequent use is in cost optimisation of existing manufacturing processes. [22]. A further shortcoming of synthesis techniques is that the complexity of the modelling make them only suited to linear (no geometric) tolerance systems [22], Current synthesis methods fall into one of three main approaches namely:

- Statistical optimisation
- Quality engineering approaches
- Machine learning solutions

The Initial study of synthesis dates back to the 1970's, where Lagrange multipliers where used to solve non-linear computer models of a tolerance system [101-103]. Also during the 1970's Smathers and Ostwald [104] used the Bellmann's principle (dynamic programming) to solve a stochastic tolerance/cost optimisation model. Further to this, Ostwald and Huang [105] used Bala zero-one linear optimisation program to solve larger more complex tolerancing problems. The zero-one approach was then simplified for systems of greater complexity though the application integer programming [106, 107]. However, the approach was still very computationally intensive; a problem addressed by formulating the problem as a discrete linear optimisation problem by adding a reliability index into the calculations [108]. Although promising the linear discrete optimisation method struggled to converge to a satisfactory correlation between cost and quality for some nested assembly systems. Michael and Siddall [109, 110] solved this problem with a non-linear approach to the

discrete optimisation problem, however this was again computationally intense. Zhang and Wang [111] sort to address this issue with a mixed linear / non-linear method.

Quality engineering, as defined by Taguchi [9] are process control approaches base around “robust engineering” and look to create a robust fit for purpose product from the variational elements present within its production process. This method of quality control is grounded in a three phase methodology of; system design, parameter design and tolerance design. However, it is the parameter design that is pivotal in determining quality increases that minimise the impact on production costs [112]. Most of the quality engineering approaches to tolerance synthesis use a combination of ANalasis of VAriance (ANoVA), Taguchi loss function techniques and/or Design of Experiments (DoE) generally linked to a quality loss function [52, 100, 112-116].

The final tolerance synthesis category utilises the field of artificial intelligence to suggest the optimum tolerances. Early research relating to the use of machine intelligence for tolerance synthesis began in 1990’s with research into genetic algorithms [117-119]; later studies have examined the use of machine learning [120, 121], fuzzy logic [122], and neural networks [123, 124] to determine tolerances.

Within the context of the research problem presented in this thesis; synthesis could indeed be used to propose an optimised tolerancing scheme for segment ring shaped assemblies. This is especially true in terms of cost

optimisation, as similar industrial components have been in production for a number of years (as is common within the industries that utilise these types of structure). However, as with the tolerance analysis the output from these synthesis approaches would only suggest a likely range of diametric variance within the assemble ring. Again, therefore, whatever fixed nominal size you set the assembly fixture to (based on the synthesis output), it would never truly match the diameter of the assembly being built upon it – ultimately having a negative impact on the circularity of the built ring structure. A further problem with these approaches is that the complexity of the modelling quickly grows to unworkable levels with increases in system complexity [22]. Moreover, given that the sorts of structures discussed within this thesis are generally made of 50+ components all for which are require concurrent assembly; synthesis would be impractical in a commercial environment for these structures. A final issue with application of this synthesis to the problem hand is that tolerance synthesis is only suited to liner/parametric tolerancing schemes. Consequently, synthesis methods are not currently suitable for use with nonlinear geometric tolerances (such as circularity), which is at the heart of the work presented within this thesis.

2.4 Manufacturing process variability and Quality

Early eras in the post-industrialised world saw manufactures focusing on cost or volume of thought-put as the key markers for the effectiveness of production systems and processes. As corporations perceived competing

on the price as more important the quality of the product. However more recently, the guiding ethos of manufacturing has become that of “quality” [125]. Indeed, over 93% of fortune 500 companies now have in place some form of Total Quality Management (TQM) method [126]; who’s objective is to cut costs as an organisation through the improvement of quality, and in-turn reducing waste. This TQM trend traversed beyond just large multi-national companies with corporate entities of all sizes seeing benefits of this ethos [127, 128]. These quality management improvements can be embodied at every point of a business from management systems, to purchasing process, to manufacturing processes and the design of products. TQM is guided by six basic concepts [129]:

- A managerial commitment to quality, leading to an ethos of quality that filters down through every level of an organisation.
- Focus towards on the needs of the customer (be they internal or external).
- Full utilisation of the whole workforce through empowerment (using systems such as quality circles).
- Committing to continual improvement of production and commercial processes.
- Engaging supplies as partners.
- Establishing meaningful performance measurement methods.

2.4.1 Six Sigma

TQM itself contains a number of tools whose full description is beyond the scope of this thesis. However, one tool in particular – Six Sigma – is frequently used within manufacturing to improve the quality of a production process or the manufactured quality of the component; and thus it has relevance to the work presented. Six Sigma is a complex system for improving the robustness of any kind of process (although due to the context the focus here will be on manufacturing processes). Indeed as a methodology Six Sigma's successes are well documented, with corporations such as Motorola (who first developed the approach around 1985), General Electric, Allied Signal and Black and Decker all being early success stories [130].

Fundamentally, Six Sigma in manufacturing is concerned with controlling defects due to manufacturing variance. Moreover Six Sigma accepts that manufacturing variance is intrinsic any production process and understanding that each variance is an "opportunity" for creating a defect (i.e. producing a feature out of tolerance). Moreover, it is the goal of the Six Sigma methodology that the variance across a population of manufacture products, the non-defective products statically account ±6σ (standard deviations) of the population distributed about intended design nominal (i.e. mean) [131]. If achieved ±6σ, will result in 3.4 defects per million opportunities, or 99.9999998% of the product being within specification [132]. The core Six Sigma thinking is based of seven core ideologies [133]:

1. Focus on customer and key business processes as strategic objectives.
2. The use of project champions / sponsors.
3. Use of quantifiable measurements (such as defects per million).
4. Identify performance metrics for tracking progression that that give an indication of impact.
5. Staff training and project team placement to facilitate improved profitability, a removal of valueless tasks, improve quality and implementation speed.
6. Create a highly skilled hierarchy of experts (i.e. “green belt”, “black belt” and “master black belt”) who can foster staff training in six sigma thinking and lead project teams.
7. Set stretch objective, to encourage improvements beyond initial goals.

A further key concept of Six Sigma is that: the customers judge a product based on variance of a process, not its mean output [134]. Therefore, Six Sigma programs spend a great deal of their effort focused on the identification and reduction of output variance.

Although it is not a formal component of Six Sigma, DMAIC is commonly used problem solving structured approach used within Six Sigma activities. DMAIC is an acronym of the five steps defined within the methodology’s application, namely [131]:

Define: Recognize the improvement to be made; define customers need for the improvement; and construct a project team

Measure*:* Identify key parameters for measurement; collect required data; validate measurement approaches used; and determine process performance.

Analyse: Hypothesize root causes driving variance; determine underlying process capability; and investigate proposed root causes of variance

Improve: Identify potential solutions; quantify solution's impact and evaluate; and verify and approve solution.

Control: Cultivate a future on-going process management plan; monitor and control the process; develop a plan for future corrective actions, should the process drift into an unstable condition.

Although, many companies have shown to be successful in their application of Six Sigma, the approach is not without its critics; who suggest the approach is just an overly complex rebranding of existing quality methods [135, 136]. Besides, the approached evolved industrially and has seem little fundamental research performed by academia [137].

2.4.2 Six Sigma measurement/analysis methods

Six Sigma relies on a robust toolbox of data collection and statistical analysis methods to work effectively via the DMAIC framework [138]. Below common Six Sigma are brief described:

Statistical Process Control (SPC) - Although pre-dating TQM and Six Sigma by a significant margin (1930's), Statistical Process Control (SPC) has become firmly embedded within the Six Sigma approach. The basis of SPC is the control chart. To generate the chart the same process is performed several times (30+ repeats) to obtain a baseline mean and so a process ±3σ distribution can be calculated. Comparing future part batches to this bassline chart, shifts and changes in the underlying process can be seen.

Measurement System Analysis (MSA) – The quality of a product is relative its fulfilment of the customers functional requirements. Meteorology equipment is used by a manufacturer to challenge the component's geometry and ensure the end-user requirements are met, before it is delivered to the customer. MSA verifies the measurement methods and equipment used to ensure they truly reflect the output quality of the process properly. These studies are performed with idealised gauge components, using repeat measurements to validate the conformance process and equipment used.

Design of Experiments (DoE) – The variance within a manufacturing process is influenced by many parameters (e.g. temperature, tool-wear, control uncertainty, vibration…and so on). However, in all but the simplest of manufacturing systems each of these input parameters can have many effects on the output component. The Design of Experiments (DoE) methodology is a systematic approach for determining the complex operative space of the cause-effect relationships between a process' inputs

and its outputs. Indeed, if performed correctly DoE should result in a mathematic model the can predict any combination of outputs based on a set of defined inputs. In a seminal work on the subject Fisher [139] identified a number of key approaches used in the design of experiments these being:

- Randomized experimentation
- Optimal regression – using polynomial regression to graph each factor
- Sequential – Results of one experiment determines the inputs for the next
- Comparison – compare each experiment to a common control or baseline
- Statistical replication – Repeating experiments to understand errors and improve reliability of results.
- Blocking – Doing experiments in related batches
- Orthogonality – Run comparative contrasting experiments
- Factorial – smartly adjust multiple experimental inputs rather the "one-at-a-time".

Failure Modes and Effect Analysis (FMEA) – Developed by reliability engineers in the 1950s, FMEA is frequently used by Six Sigma Project teams. The process begins by assembling an expert team of stake holders, such as: the customer, manufacturing personnel, designers and quality engineers. The production process is then systematically charted, with the impact,

likelihood, and detection chance predictions for possible errors or variances at each step of manufacture. The identified error or variance sources are then graded with a Relative Priority Number (RPN) and tasks actioned with an eye of reducing each possible problem source. This is an iterative process which if performed effectively can resolve manufacturing issues before they manifest in production.

Quality control and capability analysis – On completion of a Six Sigma project it is important that the final quality of the improved process/product be expressed in a meaningful way. This is especially important against the key characteristics of the component or product. The required quantification can be done using the process capability index (Cpk), which shows a measurable relationship between process variability and the dimensional requirements of the product/feature. As Table 2-2 shows, the greater the Cpk index less likely defective parts will be produced by the process, therefore the target for a Six Sigma is two or greater.

Process	**Cpk**	**Spec range**	**Ppm defects**
Not capable	<1	±3σ	2700
Capable	1.33	±4σ	63.5
Very Capable	1.67	±5σ	0.6
Six Sigma	2	±6σ	0.002

Table 2-2 : Process capability (Cpk) implications [138]

In summary, TQM and Six Sigma could undoubtedly be used to improve the circular quality of a manufactured welded annular assembly. However there are two fundamental issues with this approach. Firstly, this method is somewhat reactionary requiring the assembly to be in production before

any meaningful data can levelled at the problem. Therefore, substantial resource (cost and/or time) will be required for what could be a poor initial solution, before correction begins and production moves towards a more suitable product solution. Admittedly, pre-production prototyping and pervious similar-too assemblies will offer some insight. However, existing assembly methods will normally already be optimised using these techniques (i.e. TQM, Six Sigma) and as chapter 4 will testify, current assembly method for annular structure are reaching the limits of their capabilities. Therefore, it is likely that relying on pre-existing historic knowledge of annular assembly build approaches will not address the problem at hand in a satisfactory way.

In-line with the other literature out-lined during this study, these TQM methods aim to reduce process variation. However, variation is still implicitly present within the assembly and its components. Therefore, the issue of fitting a ring structure of variable diameter onto the of a fixtures fixed location diameter is still present.

2.5 Assembly and variation management in the context of fixturing

The prime interest of research within the field of fixturing has been levelled at deterministically holding a single component. The established method for controlling Degree of Freedom (DoF) of a single prismatic part is the well-established 3-2-1 location methodology [140]. This approach offers a

reliable method of positioning a workpiece; however the part is still subject to some positional variability and location error. Camelio, Hu, and Zhong [141] expressed these location errors as the deviation between the World Coordinate System (WCS) or workpiece's nominal position and the Local Coordinate System (LCS) or workpiece's measured position. A homogeneous transformation matrix within Euclidean space using Cartesian coordinates is used to express this deviation. Song and Rong [142] built on this homogeneous matrix method, to propose a technique for establishing if a component is over or under constrained by its fixture.

Predicting the quality of workpiece-fixture location compliance is also an important consideration in the understanding fixturing error. This topic has seen a number of reports published [143-145] which makes use of a Finite Element Analysis (FEA) approach. These studies examined the consequence of clamping of components misshapen by manufacturing variance. The idea allowed for the adjustment of successive machining operations to compensate for the clamping deformations and location errors. Abellan-Nebot, Liu and Subiron [146] took a similar approach, embodying the idea in an "*active fixture*" with embedded sensors to physically measure workpiece error. In addition to this study a number of active fixture design approaches have also been proposed [140, 147-149], where location and clamping conditions are adjusted to balance errors transmitted from previous manufacturing stages.

For the fixture designer an assembly fixture constitutes a considerable design challenge. Each assembled component must be fully located and clamped in a position relative to the other components within the assembled structure. Moreover, to enable a jointing operation it is usual that at least one degree of freedom from each component is controlled by an interface with another component in the assembly, rather than the fixture (Figure 2-13). These component-component interactions will play a substantial role in deformation and conformity when considering the clamping forces in a fixture.

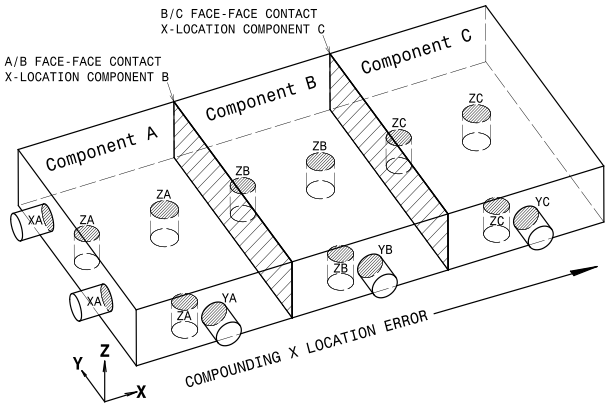


Figure 2-13 : The 3-2-1 approach when fixturing assemblies

Considering assembled components being dependent upon their neighbours for a least one DoF; two related studies [150, 151] attempting to minimise axial error build-up within a linear stack of cylindrical gas turbine components have been conducted. The authors used various build protocols in an attempt to evaluate and improve the co-axiality between segments and thus improve final assembly quality. Both studies showed the optimum build algorithm to be one of minimising the distance between the

component axis and the axis of the reference "table", rather than minimising the component-component axial distance. Although the face-face stacking contact is analogous to the inter-component contact seen within a segmented-ring assembly, these studies are based very specifically on linear assemblies where the use of axis-symmetric cylindrical segments allows for the rotation of a component to improve its fit. This advantageous situation cannot be extended to the assembly of segmented rings, where the segment components are axially asymmetric.

2.5.1 Weld fixturing

A fixture aligns the coordinate-frame of a component with that of a machine-tool or process. Once aligned the fixture's role is to hold the component in position resisting any process forces by the application for clamping forces. Therefore, as part of a fixture's design the orientation, magnitude and scale of any process forces must be considered, while allowing the process unrestricted physical access to the component. This implies that for each process type (e.g. grinding, drilling, water jetting, assembly and so on) the design of a fixture will change, as special consideration must be made for the requirements of each process. Exempli gratiā, a fixture used during a fusion welding process must contend with the thermal-mechanical forces that are generated along or perpendicular to the welded joint. However, despite the dependence of a fixture's design upon the process it serves, the focus in current scientific literature is on fixtures

used for conventional machining processes (e.g. milling and grinding) with relatively little interest being placed in other processes.

Schenk et al [152], look at the influence of fixture clamping upon weld distortion. The study examined in simulation and experimentally the seam weldings of lap and T-joints in thin plate material. Furthermore, the study looked at the several differing clamping approaches in a bid to understand their influence on the final weldments geometry, namely: cold release, open clamp once weld has cooled; hot release, open clamps directly after welding; transient clamping, applying the clamps progressively along the joint length as welding is performed; and preheated clamps, where the clamps are pre-heated to reduce thermal gradients. The results showed that the cold release clamping produced the least amount of distortion (although, it is likely at the cost of greater residual stress). While the transient clamping showed promise in reducing bowing in the welded plates. Ma et al. [8], undertook a similar study with a two-plate jig clamped (with a varying number of clamps) in an un-constrained two-plate weldment. Here the base findings showed that as the number of the clamps increased, so the degree of distortion present in the final weldment was reduced.

2.5.2 Stream of Variation Analysis (SOVA)

Stream of Variance Analysis (SoVA or SoV) is a state-space model representation of variation propagation through a Multi-stage Manufacturing Process (MMP) [153]. The approach was initially developed

in the 1990's in an attempt to analyse, optimise and predict the performance of complex automotive manufacturing systems during their design [154]. The state-space model captures and integrates: key product and process characteristics; information about tooling and fixturing (the process layout); assembly/manufacturing sequence; and metrology information (such as the location of measurement points and measurement uncertainty) [155]. For a MMP containing a total of N manufacturing stations (as shown in Figure 2-14), the SoVA state-space model is defined as [156]:

$$\boldsymbol{X}_k = \boldsymbol{A}_{k-1}\boldsymbol{X}_{k-1} + \boldsymbol{B}_k\boldsymbol{U}_k + \boldsymbol{W}_k \qquad \text{Eq. 27}$$

$$\boldsymbol{Y}_k = \boldsymbol{C}_k\boldsymbol{X}_k + \boldsymbol{V}_k, \qquad k = 1,2,\dots N \qquad \text{Eq. 28}$$

Where: $\boldsymbol{X}_k$is the state vector of deviation of the geometry created after the operation in station k; $\boldsymbol{U}_k$ is the process deviation of station k; $\boldsymbol{Y}_k$ is the product measurement of the KC within station k; $\boldsymbol{W}_k$ is the un-modelled variations in the manufacturing system for station k; $\boldsymbol{V}_k$ the measurement noise of the readings taken in station k; $\boldsymbol{A}_{k-1}$ is the "*dynamic matrix*" caused by the transfer between the preceding fixture $(k-1)$ and current (k) fixture; $\boldsymbol{B}_k$ is the "*input matrix*" or fixture layout of station k; and finally $\boldsymbol{C}_k$ the "*observation matrix*" or sensor layout of station k.

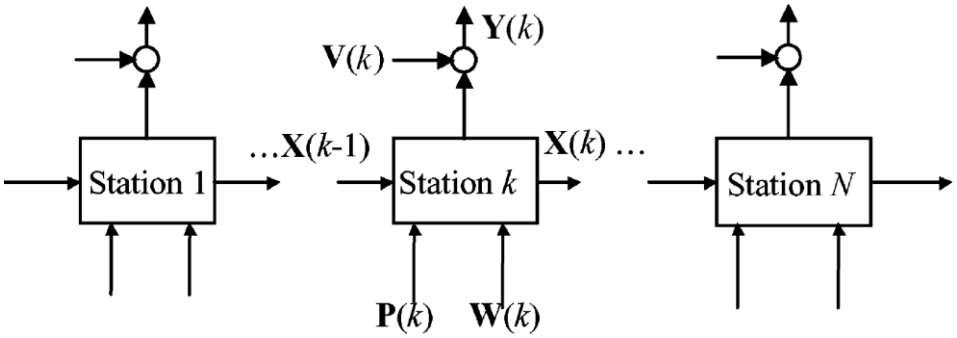


Figure 2-14 : Typical MMP showing space state model inputs [153]

For an MMP where only a single measurement is available at the end of the process (industrially the most common approach); Ding et al. [157] proposed Eq. 29 to determine likely quality of the observed assembly (assuming thin non-propagating lap-jointed components).

$$\boldsymbol{Y}_N = \sum_{k=1}^{N} \boldsymbol{C}_N \boldsymbol{\Phi}_{N,k} \boldsymbol{B}_k \boldsymbol{U}_k + \boldsymbol{C}_N \boldsymbol{\Phi}_{N,0} \boldsymbol{X}_0 + \varepsilon \qquad \text{Eq. 29}$$

Where, $\boldsymbol{\Phi}_{N,k}$ is the combined change of fixture layout through multiple manufacturing stations; $\boldsymbol{X}_0$ are the condition initial of the panels which contain imperfection due to manufacturing variance; and ε is the combine modelling and measurement uncertainty of the initial panels.

The bulk of SoVA research to date has focused on thin automotive or aerospace panel components conjoined via the spot welding or riveting of flanged faces. The fixturing scheme used in these automotive systems is the n-2-1 layout, rather than the traditional 3-2-1 approach use for rigid parts. This n-2-1 approach is required as the thin panels are compliant in one direction, and so require extra support (the flexibility being used to prevent

over-location). Moreover, these assemblies are generally fixtured via two location pins (one in a hole and one in a slot) and multiple Z-height support blocks [158]. As Figure 2-15 shows, this allows each panel to be individually located and misalignment taken-up by the width of the flange faces and/or deformation of the thin panel through clamping [159, 160].

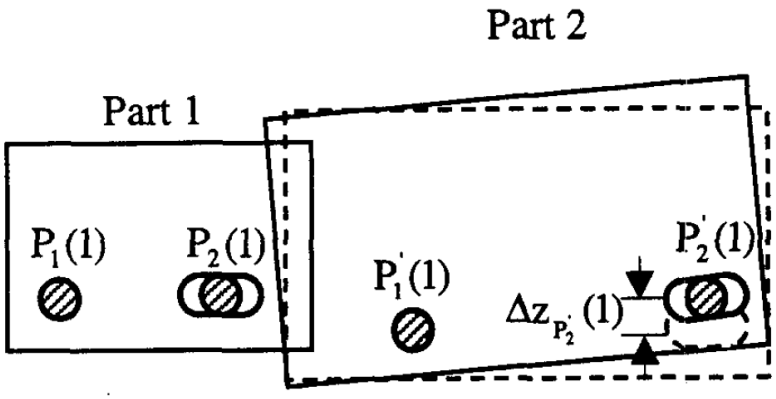


Figure 2-15 : Assembly/part/fixture variance being accommodated by flange width [158]

Due to the nature of thin automotive panels and their use of flanged interfaces and flexibility in the positioning of the spot weld/rivet; SoVA methods rarely account for the rigid-body interaction between assembled components. Indeed, many SoVA studies simplify the panel systems to a two dimensional representation of lap-jointed panels [161-163]. More complex three dimensional panel systems have been modelled using vector loop methods [164]. These more complex 3D models still simplify the interfacing joints of the panels (by virtue of compliance through their limit stiffness). However, they do permit the modelling of both butt joint and lap joint panel interfacing.

A few studies have examined the use of SoVA with fully-rigid solid-body parts. Rigid-body SoVA studies have been performed in both single station [165] and MMP [166, 167] systems. These rigid body studies pay a great deal of attention to the interface between the individual assembled components, as well as component-fixture interface; modelling these interfaces using the Whitney variation matrix model of kinematic joints (as discussed earlier in this chapter).

A key benefit of the SoVA over the pure tolerance analysis approaches is that the model incudes the entire manufacturing process, rather than just defining the geometry of the product. The inclusion of the complete production process allows diagnosis of the causes of production issues, be they: measurement uncertainties, fixturing error, transfer or assembly inaccuracies [168]. Given that it has been shown that, 70% of production errors can be attributed to fixturing related issues [169], so including fixturing within variance modelling is vital to increasing the accuracy such models. Indeed, the combined SoVA allows for "Root Cause Analysis" to be performed on a process' fixturing, so that likely sources of variation due to fixturing can be tracked and minimised [170].

As the variance modelling within SoVA is based on the same basic tolerance analysis approaches mentioned earlier in this literature study, it suffers from the same shortcomings; again making it poorly suited to the problem at hand. Moreover, the SoVA methodology outputs a range of likely variance in final assembled geometry. Again, this leads back to the position where a

traditional fixture has a fixed diameter for building an annular structure. As this fixed diameter can only be of one fixed size, so if the assembly varies even slightly from this intended diameter the structure being built will not interface correctly with the fixture's datum faces; reducing the influence of the fixture on the build process and impacting the geometric and parametric accuracy and repeatability of the annular assembly being constructed.

A further issue with SoVA is that it is not "goal seeking". The SoVA methodology can only predict the deviation of defined measurement points from their absolute target positions. SoVA has no mechanism for fitting those points to theoretical target geometries (i.e. a circle). Therefore considering an annular structure, the output deviations predicted by SoVA of the measurement points would bear no relevance to the global circularity goal of the annular structure being built. Therefore, currently SoVA cannot be used to suggest what the best build of an annual structure would be, so offering no insight into how to improve the geometrical quality of the assembly.

2.5.3 Metrology Assisted Assembly (MAA)

Metrology (or Measurement) Assisted Assembly (MAA), is a system of closed loop automated assembly with active highly-flexible fixturing and an integrated active measurement facility [171]. This system (shown Figure 2-16) enables the accurate assembly of large aerospace components using a reconfigurable assembly ideology to reduced tooling and rework costs

[172]. The ethos of MAA is a movement away from fixed geometry fixturing and towards flexible *"jigless"* assembly, via the application of flexible robotised assembly methods[173]. The key to utilising the flexible assembly methodology is attaining a best-fit of posture for the components being assembled within the reference frame of the current geometry of the assembly [174]; which requires the application of high resolution in-process 3D measurement systems to capture the component and assembly geometry and posture. The best fit posture computation is a two phase approach: firstly, determining (via measurement) the current position and orientation (i.e. DoF) of the component being assembled; and second, calculate the best-fit position of the component to the assembly geometry, with consideration of the GD&T / KC requirements of the final assembly [14].

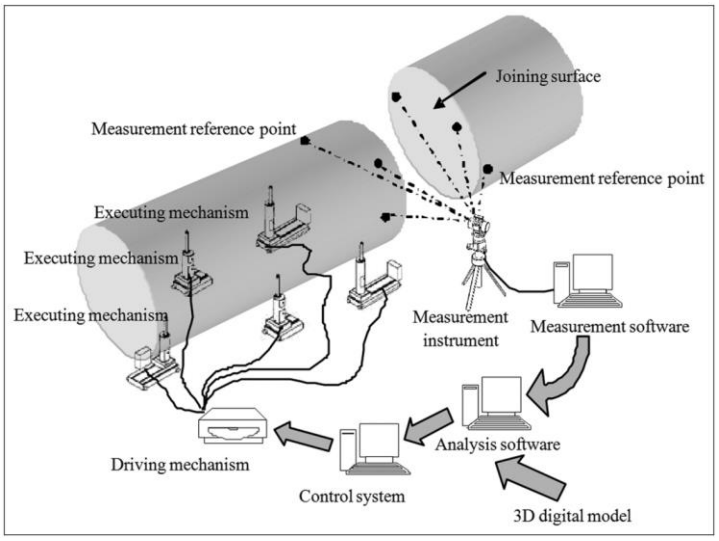


Figure 2-16 : MAA system diagrammatic overview [175]

A number of large-scale 3D metrology technologies have been investigated for utilisation in MAA systems[176], namely: iGPS, a commercially available

infrared laser beacon system from Nikon; HiBall, an infrared LED beacon system from 3rd Tech; digital theodolites; MScMS-1, a developmental ultrasound based system; MScMS-2, a developmental infrared photogrammetric system; and laser tracking with commercially available trackers. Of these approaches, laser tracking is the most common due to it high accuracy levels and existing utilisation of the technology within airframe construction industry [175]. However, laser trackers have a high per-unit cost, and a number of scanners are required for triangulation of a 3D point in Cartesian space. Trackers also require line-of-sight to the retroreflector markers; therefore on very large structures there is a further need for additional trackers.

Another large volume metrology technology Coherent Laser Radar (CLR) or LiDar (a concatenation of "*light"* and "*radar"*) [177]. Although this technology is less accurate than laser tracking, it is better performing than some of the other technologies utilised [178]. The use of LiDAR could also overcome another problem of MAA, in that current measurement technologies do not directly capture the component geometry fully, but instead a finite number of defined points (as markers), quantizing the geometry to just those points. In recognition of this Jamshidi *et al.* used LiDar in their study to capture actual component geometry and check of the assembled component [174]. However, LiDAR produces a vast quantity of metrological data in the form of a dense point cloud which requires substantial amounts of processing and storage (epically in large structures).

The majority of MAA research has focused on larger (generally airframe structures) components; however, a related study looked at a smaller aero-engine assembly [179]. The study investigated the assembly of a weldment consisting of four components: one U-shaped sheet metal part, two flat sheet metal parts and a cast hub. Two sensors where used to assist in the positioning of the component; a seam finding sensor and cross-shaped profile sensor. These sensors where added to a robot end-effector that contained a vacuum gripper to hold the parts being assembled. The end-effector was pre-measured establishing the Tooling Centre Point (TCP) relative to the robot and assembly reference frame. The loaded components where then guided to their assembled positions via a best fit algorithm and the live sensor data. Although some success was achieve, the authors found too much uncertainly in the system for a repeatable assembly; especially in the geometric form variance of the u-shaped sheet metal part and the datuming of the TCP.

At face value MAA is potentially applicable to the sorts of assembly problems that are at the heart of this thesis, but there are a number of none trivial problems that would need to be overcome. Firstly, at smaller scales the resolution of the system becomes of increasing importance, but as the assembly system scales down, components needed for the measurement (i.e. retroreflectors/ markers) must also be scaled. However, as these measurement markers influence the measurement (having the own manufacturing tolerance) so this will become increasingly important to control, as it become a larger proportion of the measurement being made.

Second, the ring assembly is a closed loop form, so each component has an influence on the size and quality of the final complete ring structure and all the sections of the ring must touch two other sections. Therefore, all the components of the assembly would need to be processed simultaneously and bought together, as a whole system. Bearing in mind that the industrial case study assembly contains 52 components this would be a mechanically challenging and very expensive. Furthermore, if the system was to embody the true spirit of MAA it would be jigless, requiring 52 robots and end-effectors to operate in unison (each with their own control and mechanical inaccuracies and uncertainties). The third issue is the difficulty of capturing geometric inaccuracy with the retroreflectors/markers. That is to say that, to capture a single geometric feature such as a mating face, three markers would be required per face, this would quickly pepper the parts in multiple marker in close proximity – potentially confusing any tracking system as especially as the multi-part assembly came together. This is especially problematic for solid non-compliant components, which would need aligning precisely. The final issue is with the control uncertainties of the automated assembly and positioning system. Moreover, as a fully automated assembly system would need to make small precise movements to create align the assembly mating faces, so mechanical inaccuracies and uncertainties become a serious concern (this was problem was observe in Jayaweera *et al.'s* aero-engine assembly study [179]).

2.6 Metrology and verification

This section of the literature review will look at the metrological aspects of the project, offering insight into the influence of measurement accuracy and uncertainty upon the project's methodology, experiential results and the conclusions.

2.6.1 Measurement Uncertainty

Uncertainty is defined as: "*parameter (of metrology), associated with the result of measurement, that characterizes the dispersion of values that could reasonably be attributed to the measurand*" [180]. Frequently confused with error and tolerance, measurement uncertainty expresses the confidence of the result of a single measurement within the context of a number of repeat measurements for the same feature and using the same equipment. By way of example, repeatedly measuring the length of a simple steel block with a CMM will generate a slightly different result with each measurement. Despite, the equipment and block being unchanged, the result will vary due to small unpredictable system variances; such as: the block may be subjected to heating by the operator handling it, or a cool draft may cool the block as a door is opened, encoder noise on the equipment may be present during the reading, a slight difference in the surface finish could affect the measurement slightly as a different measurement point is chosen for each measurement, the operator's skill level...and so on [181]. It should be noted that these factors are not avoidable measurement errors but unknown facets of the measurement process itself. These random independent

uncertainties are combined, so repeating any given measurement will generally produce a Gaussian spread of values about a nominal mean value; as predicted by Central Limit Theorem (CLT) [182]. Figure 2-17 shows a typical expectation for the generic block and CMM example. Looking at this figure it can be seen that the distribution of the measurement variation can be plotted as a density function or distribution. What is more, as the distribution is mathematically describable, so the probability of any single measurement falling within a given measurement range can be predicted. Therefore, using standard deviation and knowledge of the density function, the confidence of a single measurement can be expressed as "*XX±YY at a confidence of ZZ%*"; where *XX* is the measurement reading from the equipment, *YY* the likely deviation from the read due to the uncertainties, and *ZZ* the confidence of measurement falling within the stated deviation.

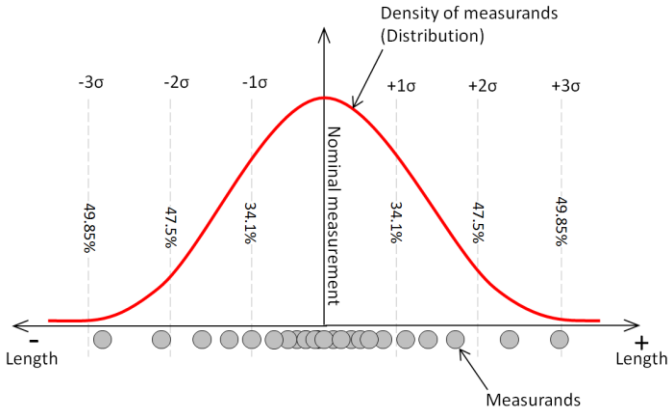


Figure 2-17 : A typical distribution of a measurement due to uncertainty

The confidence level is based a fundamental statistical knowledge of standard deviation (expressed as a σ or k value). Using the CMM and block example with its Gaussian distribution as an it can be shown the 68.1% of

all the measurement points will fall within a range of ±1σ (standard deviation) from the mean central value. Furthermore, 95% of the measurements will fall within ±2σ and 99.7% within ±3σ. Other distribution types such as rectangular, Cauchy, F, T, Chi squared, exponential and so on these confidence level as still predictable using standard deviation but will represent different confidence values. However, the most commons types for measurement uncertainty are Gaussian and rectangular (or uniform).

Some measurements require that several independent uncertainties be combined to obtain a final uncertainty value. Pharmaceuticals for example may contain several constituent chemicals that need to be weighed and combined accurately. Here the uncertainty in the weight of the resultant drug would contain the combined uncertainties of the individual components during weighing. A number of international regulatory bodies have established guidelines for the expression of, and combining of, uncertainties [180, 183, 184]; however none of these are de-facto legal standards but guidelines [185]. The ISO guidelines are split into three main documents: "*ISO/IEC Guide 99:2007 - International vocabulary of metrology -- Basic and general concepts and associated terms (VIM)*" [186]; "*ISO/IEC Guide 98-1:2009 - Uncertainty of measurement -- Part 1: Introduction to the expression of uncertainty in measurement*"[187]; and "*ISO/EC 98:2008 Uncertainty of measurement – Part 3: Guide to the expression of Uncertainty in Measurement (GUM)*" [184].

The ISO GUM guidelines identify two main classes of uncertainty, these being:

Type A: Uncertainties obtained directly through making repeat measurements and statistically determining the distribution and spread of the measurands. These are usually found to be a Gaussian probability density distribution.

Type B: Uncertainties obtained indirectly from source such as equipment datasheets or calibration certification. These are usually treated as a square probability distribution.

It is common for systems that amalgamate uncertainties to require a combination of both the A and B uncertainty types. When combining uncertainties (as in Eq.30) a number of measured values x_i, are combined by some function (f) to output some secondary measured value (Y).

$$Y = f(x_1, x_2, \dots x_n) \qquad \textit{Eq. 30}$$

Before combining uncertainties they must first be converted into a "*standard uncertainty*" using a Bayesian inference. For a Gaussian distribution Eq. 31 should be used to perform the conversion, where: u is the value of standard uncertainty, $\bar{x}$ is the standard deviations calculated from the measurement set, and n the number of measurements taken in the set. While, for a uniform/rectangular distribution Eq. 32 should be used. Where, a is

$$u = \frac{\bar{\mathrm{x}}}{\sqrt{n}} \qquad \textit{Eq. 31}$$

$$u = \frac{\mathrm{a}}{\sqrt{3}} \qquad \textit{Eq. 32}$$

It should be noted that these are based on the premise that the measurements probability density is ideally distributed without skew or kurtosis. As Eq. 33 shows, once converted into standard uncertainties (u), a number of uncertainties can be consolidated with a summation in quadrature to create "standard combined uncertainty" (u_c). To apply a confidence level u_c needs further multiplication with a coverage factor k (in standard deviations) to represent the full the "expanded uncertainty", U of the combined system (Eq. 34).

$$u_c = \sqrt{\sum_{i=1}^{n} {u_i}^2} \qquad \textit{Eq. 33}$$

$$U = u_c . k \qquad \textit{Eq. 34}$$

As Eq. 33, is only applicable to a linear systems, but partial derivatives can be utilised to calculate the consistent sensitivity coefficients in situations of weak non-linearity. Eq. 35, shows the non-linear form, again the result is an expanded uncertainty and is expressed at a single interval of standard deviation, so further processing is required via *Eq. 34*,

$$u_c \approx \sqrt{\sum_{i=1}^{n} \left(\frac{\partial f}{\partial x_i}\right)^2 \cdot u^2(x_i)} \qquad \textit{Eq. 35}$$

For situations of true non-linear most of the international uncertainty standards recommend the use of Eq. 36, which is based on a Taylor series first order expansion. Expanding the on the Taylor series principle the higher order expansions can also be used to estimate skew and kurtosis [188].

$$u_c \approx \sqrt{\sum_{i=1}^{n} \left(\frac{\partial f}{\partial x_i}\right)^2 \cdot u(x_i)^2 + 2\sum_{i=1}^{n}\sum_{j=i+1}^{n} \frac{\partial f}{\partial x_i}\frac{\partial f}{\partial x_i} u(x_i, x_j)} \qquad \text{Eq. 36}$$

2.6.2 Uncertainty and the implication for tolerances

A designer will place a tolerance on a given feature for the purpose of ensuring it's functional robustness in the final product despite the presence of implicit manufacturing variance. Moreover, with a tolerance the designer assigns is explicitly expressing the maximum allowable deviation of the manufactured component's geometry from nominal design ensuring the part performs its function as intended. Measurement uncertainty (should) play a role in the selection the manufacturing tolerance applied to the components as it adds an additional unknown boundary to the tolerance zone. By way of example, imagine a 10mm wide block with a tolerance of ±0.1mm; therefore, the block would be acceptable if manufactured at 10.08mm. Now, if the size of the block was then measured with a caliper

whose uncertainty is ±0.05 at 95% confidence; the block could be somewhere between 10.03 and 10.13, but still read 10.1mm on the measurement device for 95% of the time. Clearly, the upper limit would mean the block is potentially out-of-tolerance while the lower limit would be acceptable. This ambiguity would also be present at the lower limit of the tolerance zone also. This leads to four possible outcomes (Figure 2-18) when validating a manufactured component with a measurement:

Outcome 1: **Out-of-tolerance**, the measured valve is greater than the tolerance size of the part by a value greater than the uncertainty of the measurement system.

Outcome 2: **Indeterminate**, the measured valve is greater than the tolerance size of the part by a value less than the uncertainty of the measurement system.

Outcome 3: **Indeterminate**, the measured valve is less than the tolerance size of the part by a value less than the uncertainty of the measurement system.

Outcome 4: **Within tolerance**, the measured valve is less than the tolerance size of the part by a value greater than the uncertainty of the measurement system.

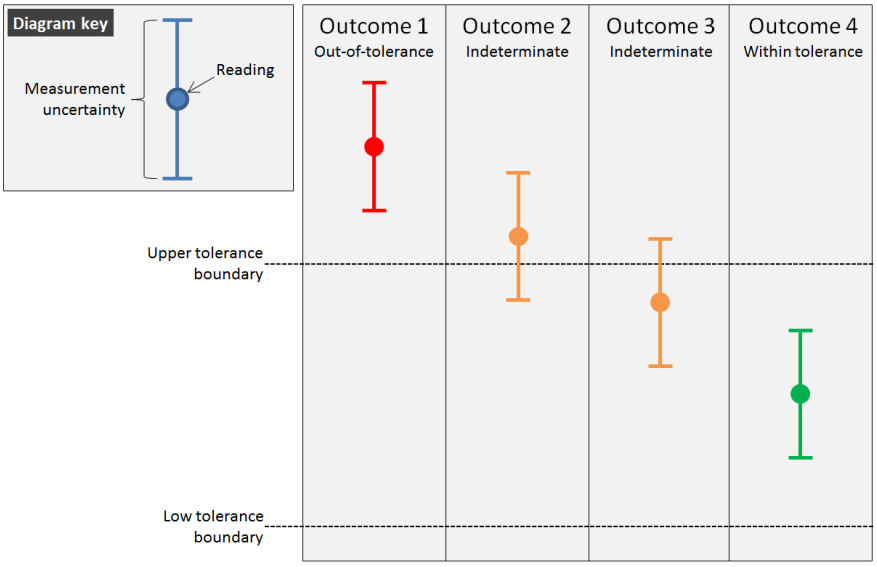


Figure 2-18 : Implications of uncertainty in the validation of tolerances

2.6.3 Coordinate Measurement Machine (CMM)

Figure 2-1 shows a typical Coordinate Measurement Machine (CMM); a measurement system typically capable measurements of ±0.001mm in resolution. A CMM is defined by ISO is as a: "measuring system with the means to move a probing system and capability to determine spatial coordinates on a workpiece surface" [189]. These systems can performer their measurement via either the physical contact of a probe touching the component, or some form of optical measurement system. CMM's output an XYZ point measure point cloud relative to a defined 0,0,0 origin (this origin usually being set using datum features on the geometry being measured). Component features such as planar faces can then be extracting by probing several points on the feature and mathematically processing those points to derive the underlying geometry. Typically, a Cartesian CMM comprises of three high precision encoded linear stages (one for each measurement

axis) that allow the probe to be moved freely within the measurement volume. Further to this, the CMM probe is also normally capable of the rotation in two axes; allow access to angled features for measurement.



Figure 2-19 : Typical gantry type CMM with contact probe

The metrological verification of CMM equipment is covered internationally by the ISO 10360 family of standards. ISO 10360 comprises ten related standards, being:

- ISO 10360-1:2000 - Geometrical Product Specifications (GPS) -- Acceptance and reverification tests for coordinate measuring machines (CMM) -- Part 1: Vocabulary.
- ISO 10360-2:2009 - Geometrical product specifications (GPS) -- Acceptance and reverification tests for coordinate measuring machines (CMM) -- Part 2: CMMs used for measuring linear dimensions.
- ISO 10360-3:2000 - Geometrical Product Specifications (GPS) -- Acceptance and reverification tests for coordinate measuring

machines (CMM) -- Part 3: CMMs with the axis of a rotary table as the fourth axis.

- ISO 10360-4:2000 - Geometrical Product Specifications (GPS) -- Acceptance and reverification tests for coordinate measuring machines (CMM) -- Part 4: CMMs used in scanning measuring mode.
- ISO 10360-5:2010 - Geometrical product specifications (GPS) -- Acceptance and reverification tests for coordinate measuring machines (CMM) -- Part 5: CMMs using single and multiple stylus contacting probing systems.
- ISO 10360-6:2001 - Geometrical Product Specifications (GPS) -- Acceptance and reverification tests for coordinate measuring machines (CMM) -- Part 6: Estimation of errors in computing Gaussian associated features.
- ISO 10360-7:2011 - Geometrical product specifications (GPS) -- Acceptance and reverification tests for coordinate measuring machines (CMM) -- Part 7: CMMs equipped with imaging probing systems.
- ISO 10360-8:2013 - Geometrical product specifications (GPS) -- Acceptance and reverification tests for coordinate measuring systems (CMS) -- Part 8: CMMs with optical distance sensors.
- ISO 10360-9:2016 - Geometrical product specifications (GPS) -- Acceptance and reverification tests for coordinate measuring systems (CMS) -- Part 9: CMMs with multiple probing systems.

- ISO 10360-10:2013 - Geometrical product specifications (GPS) -- Acceptance and reverification tests for coordinate measuring systems (CMS) -- Part 10: Laser trackers for measuring point-to-point distances.

While, the ISO standard for assessing CMM measurement uncertainties during these verification tests is covered by ISO/TS 23165:2006 [190].

Uncertainty for CMM measurements is complex and has been a long standing area of research area [191-195]. The complexity of CMM uncertainty primarily derives from each measurand being an amalgam of three independent measurement axes. Indeed, the United Kingdom's National Physical Laboratory (NPL) identified 21 sources of variation just in the mechanical systems of the three measurement axes used in a typical Cartesian CMM [196]. Additionally, factors such as: environmental factors (i.e. temperature, humidity, etc.); component factors (i.e. local surface roughness, part stiffness, etc.); Operator factors (i.e. skill); and systemic factors (i.e. software rounding, encoder noise, wear, etc.) can affect the whole system and/or induvial measurement axes. Geometric measurements further compound the issue of CMM uncertainty as they derive the measurement geometries by combining multiple measurands, best fitting them to reference geometry. Dhanish and Mathew [197] looked this uncertainty issue in greater depth in their study of circularity uncertainty when utilising a CMM. Unsurprisingly, they showed a link between the induvial measurand uncertainties and the overall uncertainty

of the measured circularity. The authors noted that the uncertainty was not only due to the equipment itself, but also the quantization of the measurement surface into a finite number of discrete points.

2.6.4 Photogrammetry

Photogrammetry has long standing use within the field of industrial meteorology, as it offers quick non-contact 2D/3D measurement of complex freeform geometries. Generally photogrammetry compares two or more photographs of the same scene, mathematically combining them to generate a measurement. To generate 3D measurements the combined photographs must be taken via different viewpoints, either through the use of multiple cameras or by moving single cameras. Once the images have been captured they are combined via triangulation for the geometry across the multiple images of the scene. Academic interest in photogrammetry began in the early 1980's where the foundations of the speckle pattern [198], laser speckle [199], and Moiré [200] approaches were set; while industrial application of 3D photogrammetry stretches back to the mid-1980's [201]. However, it wasn't until the shift towards the adoption of digital photography in the 1990's that technology mustered any industrial traction.

Being non-contact, fast in the acquisition of data and capable of capturing complex surfaces, photogrammetry is capable of measuring both static and dynamic (i.e. deformation due to vibration) systems [202]. While, photogrammetry systems are also available for measuring very small

objects (i.e. stereo-microscopy) [203] and very large systems (i.e. 3D satellite imagery) [204, 205]. However, despite these benefits, currently photogrammetry methods have a number of shortcomings, such as: a requirement for lines of sight during measurement; the processing of the images and resultant point cloud can be computationally intense; the edges of geometries are difficult to acquire cleanly; there is a need for consistent/even lighting of the subject during data-capture; and very reflective or matt surfaces can be difficult to capture without surface preparation (i.e. Ti-oxide spray)[206].

Photogrammetry measurement is a developing filed and as such the international standards bodies are somewhat lagging behind the technology [207]. The current ISO standard covering photogrammetry in the measurement is "*ISO 10360-7:2011 - Geometrical product specifications (GPS) -- Acceptance and reverification tests for coordinate measuring machines (CMM) -- Part 7: CMMs equipped with imaging probing systems*". However, this only expresses accuracy of these system in very board terms, and only from the standpoint of Length Measurement Error (LME); due in the main to the difficulties in validating a freeform surface[207]. The other international standard of note is the German VDI 2634 part 1, 2 and 3. These long standing VDI standards (pre-dating the ISO equivalent) also use LME to define measurement accuracy. As a consequence of shortcomings of these standards (i.e. only partially covering the capabilities of photogrammetry), so current photogrammetry systems do not offer full metrological traceability [208].

As part of this is research project two forms of photogrammetry were used, namely: speckled Dual Image Coloration (DIC), and structured light photogrammetry.

2.6.4.1 *Speckled Dual Image Coloration (DIC)*

Monoscopic speckled image photogrammetry begins by painting the object to be measured with a random speckled pattern [209]. This speckled pattern offers a constant reference pattern for the object. After photographing the object to record the initial state of the pattern; force can then be applied to the object distorting the measurement specimen (and thus the pattern). A second image can then be taken for comparison to the image of the initial state; associating the distance that induvial speckles have moved relative to the resolution of the camera sensor (in pixels/mm) and distance of the camera the object, the strain induced by the applied for can be measured. However, as only single camera is used movement can only be captured in a 2D plane, with any movement in the third dimension being misinterpreted by the measurement algorithm [210].

Using the same speckling methodology, but with the bioscopic or dual image capture (see Figure 2-20), the position of each speckle can be correlated the two images to create a 3D recording of the speckle pattern. Furthermore, just like the monoscopic system, taking an image set before and after the application of a distorting force, the strain and movement in the measured component can be observed; this time in three dimensions [211, 212]. The downside to the "*Dual Image Correlation*" (DIC) method is

that there are errors and uncertainties associated with the image correlation process due in the main to differences between the two cameras. The difference such as: lens dirt, distortion and aberration; lighting differences caused by viewing the object from differing positions; specular highlights moving between views on reflective surfaces; and CCD sensor noise and resolution [213]. However, despite this DIC sub-micron (0.16μm plane and 0.22μm spherical reported) measurement resolutions are possible with these systems [214].



Figure 2-20 : A typical dual image correlation system [215].

2.6.4.2 *Structured light photogrammetry*

Using speckle DIC, the component must be painted to create a reference pattern, however this is not always welcome, especially for production components. Structured light photogrammetry systems (Figure 2-21) sidestep this issue but using a digital projector (or less commonly fringe grating) to project a checkerboard pattern on to the component as it is measured. Again, viewing the pattern bioscopically, the captured imaged can be correlated via triangulation to build a 3D point-cloud of the surface

being measured [216, 217]. But, unlike speckle DIC, the reference pattern is not physically connected to the surface, so it won't show any strain information if a force is applied; it will only capture the form of the surface (i.e. deformations)

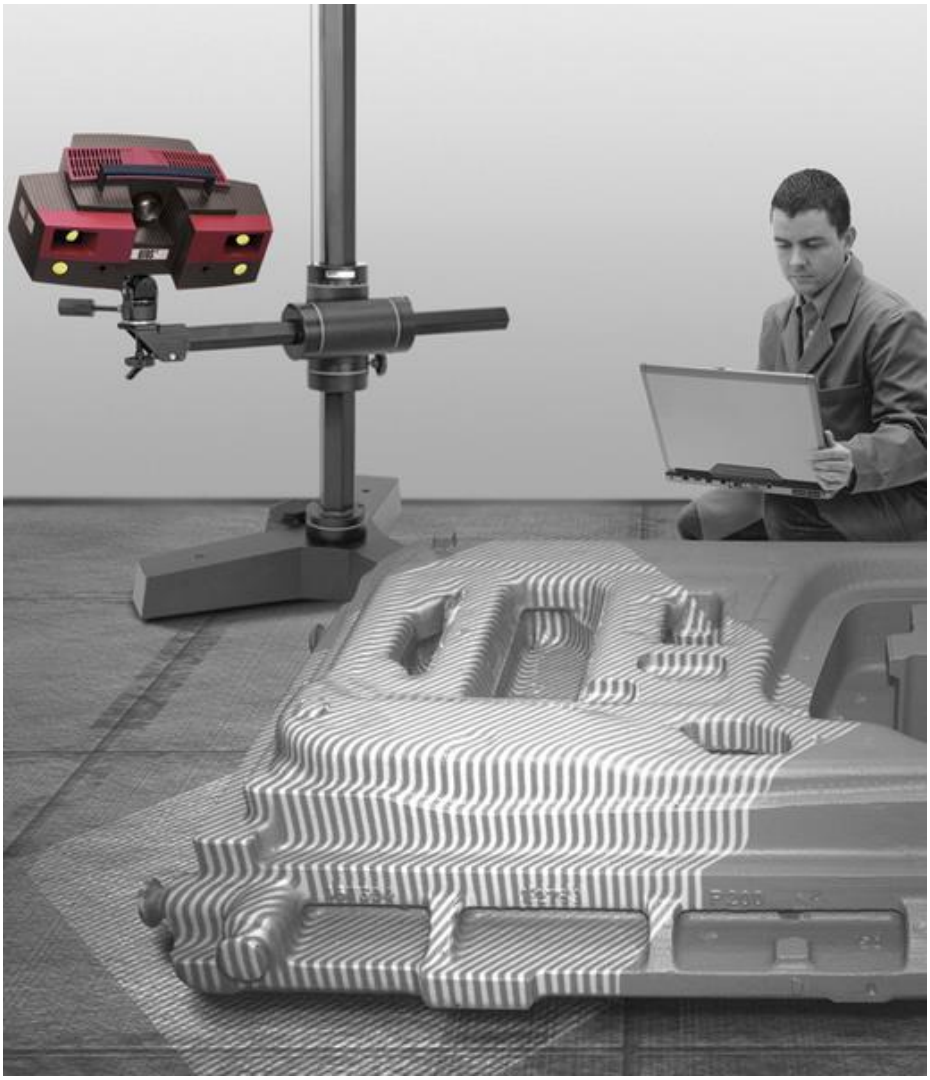


Figure 2-21 : A typical structured light photogrammetry scanner [218].

These systems are typically capable of measuring with a resolution of 20-100μm somewhat lower than that of a speckle DIC [219, 220]. As structured light photogrammetry also used bioscopic vision it suffers from

the same correlation uncertainties as the speckled DIC method. However, the projection of the reference pattern generates a number of additional uncertainties for the system, such as: line-of-sight issues; secondary reflections of the projected pattern; and the colour/reflectivity of the object being projected onto impacting the contrast/colour of the reference pattern [214]. Though, the application of a temporary Ti-oxide matting powder can reduce the impact of some reflectivity issues.

2.7 The influence of welding in assembly variation

The large metal ring structures which are the focus of this thesis are significant to a number of heavy industries, such as: aerospace gas turbines, power generation and heavy plant. However, as size and/or the complexity of such rings grows it becomes technically and financially less effective to produce these geometries in a single piece [221]. It is therefore common practice that large ring structures are assembled from smaller segmented components and then joined using fusion welding. However, creating a ring in this manner adds new sources of potential variations into the production process via manufacturing variance in component geometry, positional assembly errors and weld distortions. Arguably weld distortion is the least predictable of these, and in itself is driven by two main contributing factors; gap errors between the components to be conjoined and the shrinkage caused by the thermal cycle of the welding process [222].

2.7.1 The gas tungsten arc welding process

Gas Tungsten Arc Welding (GTAW) – also known as HeliArc or Tungsten Inert Gas (TIG), is an arc welding method that uses a non-consumable tungsten electrode, and a constant current to form an electrical plasma arc within a localised inert gas environment [7]. The arc's energy is principally conducted through the base material of the joint. This energy generates heat, melting the base material to form a molten weldpool. However, should this weldpool straddle the joint between two or more components then the molten material from both sides of the joint will mix [223, 224]. This mixing process is primarily driven by Marangoni (thermo-capillary) convection currents within the weld pool [225, 226]. A permanent bond between the components is then created once the pool is allowed to cool. The use of a shielded anaerobic welding environment enables traditionally difficult materials to be welded with GTAW, to a quality that matches Electron Beam Welding (EBW) or Laser Beam Welding (LBW), but at the fraction of the capital cost [221]. Furthermore, GTAW also offers a welding method that is virtually spatter-free, with low vaporisation of the base material and a separate filler material. These characteristics allow the GTAW process to forgo the use of a filler material altogether in certain beneficial circumstances, creating an autogenous welding process.

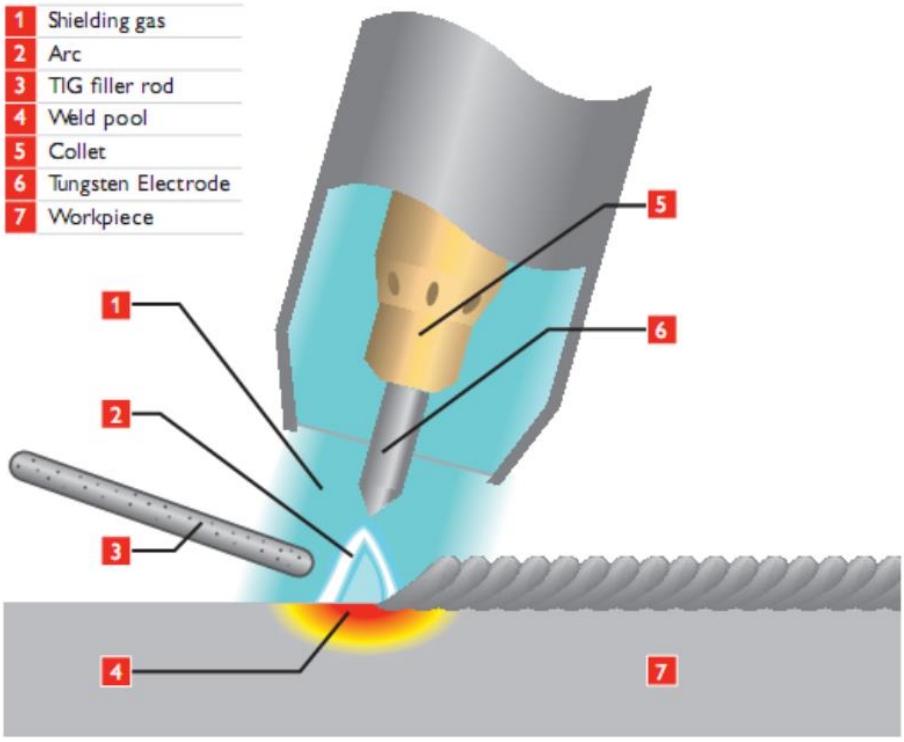


Figure 2-22 : The GTAW welding process [50]

2.7.2 The impact of assembly gaps on welding

The gaps between the constitutive elements of the assembly, caused by manufacturing, handling and location variations, add an extra degree of uncertainty into the welding process [227]. This is especially true when using an autogenous welding approach, as more energy must be put into the process to generate a sufficiently large weldpool in the base material, so that the gap may be bridged. The importance of considering assembly gap in the prediction of welding distortion has been highlighted by Denga et al. [228]. Their study used a thermal elastic finite element model to predict the distortion in a number of large assemblies. These assemblies constituted a flat steel plate with a lattice of reinforcements welded onto it. The study found that adding gaps to the model gave a good approximation

of the real world component. The authors also noted that distortion level often exceeded the size of the initial gaps in the final welded structure.

2.7.3 Tack welding

Tack welding is a prevalent technique that uses small locally fused joints. Its primary use is that of a temporary intermediate joint that stabilises the positions of an assembly's components prior to the application of a full seam weld. Industrially, this is useful for stabilising an assembly of components allowing it to be moved (between fixtures). Furthermore, it is also beneficial in situations where clamping an assembly may be overly complex or impinge the final production seam welding process/jointing method. Despite tack welding being industrially ubiquitous the majority of prior scientific interest in weld distortion has been with the final seam weld [229-233] or stitch weld runs [234]. Previous studies [223] have reported a complex relationship within a seam weld between the thermal expansion at the molten weldpool, and the contraction of the solidifying weld. This leads to residual stress along the length of a welded joint that can cause component deformations. However, the reduced size of a tack welds implies a reduction in these forces, and thus reduced component deformations when compared to the full seam weld. Indeed, new smaller mirco-tack welds are now employed on some welding equipment to reduce the distortion generated when compared to traditional tack-welds [235].

There are a small number of tack welding studies available, however they all examine tack welding as facet of a seam welding process, using it as a

Preliminary Weld Process (PWP). Jonsson et al. [236] examined the release of tack welded residual stresses (due to their melting), during the a seam welding operation. Moreover, the study found that the initial "locked-in" of residual stresses were dependent on the order in which the welds are performed; which in-turn influenced the severity of the distortions post seam weldment. Drawing an overarching conclusion from their study, the authors recommend performing all the tack welds as quickly as possible. This helps ensure previous welds are still warm and compliant when exposed to the thermo-mechanical forces of the proceeding tack welds. A similar study [237], looked at adding a tack welding process into an FEA seam welding simulation. This was to capture the release of residual stress on the melting of the tack welds. The authors found that their simulation better matched their experimental trials when the tack welding model was included.

In another study, considering weld root gaps on tack welded pipe flanges (115mm OD pipes), Abid and Siddique [238] found there to be little effect in axial displacement while varying the gap between 0.8 and 2.0mm. The study found that the angular position of the tack around the pipe circumference to be the most influential variable. However, for this study a Metal Arc Welding (GMAW) process was used, a process which utilises a consumable electrode filler material. Moreover, the addition of this filler material is likely to reduce the tack weld's shrinkage, replacing material lost through vaporisation or spatter.

2.8 Conclusions and identified research gaps

An overview summary of the reviewed tolerance / variation management approaches is shown in *Table 2-3*. The table also includes the proposed "variation conscious" methodology as presented in this thesis for comparison. The explanation of the table headings are:

- *Family* – What type of approach is it? (Synthesis or Analysis)
- *Description* – The approach's name
- *Worst-case* - Can the approach output (or input for synthesis) a worst-case answer for the tolerance system?
- *Statistical* - Can the approach output a statistical (SiQ/RSS) answer for the tolerance system?
- *Supported tolerance zones* – What ISO geometric tolerance zones are supported by the modelling?
- *Functional clearance* – Can the approach support functional clearances (i.e. limits and fits)?
- *Allows nested network* – Are sub-assembly networks supported?
- *Geometric goal seeking* – Can the approach fit an assembly to a goal geometry (i.e. improve an assembly for circularity)?
- *Output* - Is the output absolute or a range?

Family	Description	Worst-case	Statistical	Supported tolerance zones	Functional clearance	Allows nested network	Geometric goal seeking	Output	Notes
Proposed	**Variation Conscious**	**N/A**	**N/A**	**Contact only**	**No**	**No**	**Yes**	**Absolute**	
Analysis	Traditional Stacking	Yes	Yes	Contact only	No	No	No	± Range	Linear stack only
	Vector loop	Yes	Yes	Yes *	No	No	No	± Range	* Non-ISO compliant tolerance zones
	Variational	Yes	Yes	Non-form	Unclear	No	No	± Range	
	Variational kinematic joint	Yes	Yes	Non-form	Unclear	No	No	± Range	
	Matrix	Yes	No	Non-form	Yes	No	No	± Range	
	Jacobian	Yes	Yes	Non-form	Unclear	No	No	± Range	
	Torsor	Yes	No	Non-form	Yes	No	No	± Range	
	Steam-of-Variance	Yes	Yes	Non-form	Unclear	Yes	No	± Range	Allows for multi-station systems
Synthesis	Statistical optimisation	Yes	Yes	Non-form	Yes	Yes	No	± Range	
	Quality engineering	Yes	Yes	Non-form	Yes	Yes	No	± Range	
	Machine learning	Yes	Yes	Non-form	Yes	Yes	No	± Range	

Table 2-3 : Comparative overview table of variational management approaches

To summarise *Table 2-3*, none of the existing variation management approaches solve the problem at hand fully. As mentioned throughout this chapter all of these approaches produced a likely variance range as their output. A ranged output is of little use for a closed loop structure as current fixturing approaches utilise a fixed build diameter only; meaning that variability in the diameter of the assembly will prevent the assembly from truly matching the datum/location diameter of the fixture. Consequently, the fixture will not fully locate the components; ipso facto the fixture will have poor influence on the build quality of the constructed annular structure.

A further issue is that, all of the existing variation management methodologies are none goal seeking. The aim of the build process is to construct the most circular assembly possible. However, none of the approaches suggest how to do this and they only state the likely parametric output variance in the structure's diameter. Moreover, it is easy to turn a component (such as a flange or hub) to size so that it can be added to the resultant assembly during later manufacturing operations; however it is difficult to assemble (and weld) these extra hubs and flanges if there is a poor circular fit between the structure and the added parts. This issue is seen in the industrial case study structure (chapter 4) where a key characteristic of the assembly its circularity. A further issue with all of the examined variation management approaches is that they are incapable of capturing ISO standard form tolerances (the family of tolerances containing circularity and run-out). The vector loop method is capable of capturing

such form deviations, but it maps the tolerance zones using a non-ISO compliant approach, making it difficult to inspect for compliance in the manufactured part.

Computer Aided Tolerancing (CAT) is a capable software based solution, which uses the variation management techniques discussed within this literature review. Although, CAT could be leveled the problem at hand, there are a number of shortcomings. Firstly, the approach offers the designer no real insight into how to best design fixtures for assembled looped structures. Therefore, the designer is still "working blind" relying on his/her own instinct and experience, which is unlikely to reap any substantial quality improvements over previous fixturing. Second, as CAT is based on the existing underlying variation management and tolerance stacking methods, so it has a poor appreciation of the ISO form tolerances (such as run-out or circularity). The final issue it that being based upon existing tolerance stacking methods, CAT will output range value as its answer; which as previously discussed, is not suitable for the fixturing of ring structures.

Measurement Assisted Assembly (MAA) as an approach is poorly suited to the type of structure examined in this thesis. Currently, MAA has only been demonstrated on very large component assemblies. Moreover, the demonstrated MAA assemblies have generally been thin flanged faced panels (Whitney Type 2 structures), which allows for flexibility in the joint positions and mating geometry. To apply MAA to the solid-body geometry of a welded annular assembly a substantial number of issues would have to

overcome (which was testified by the attempts of other researchers). First, is the capture of the complex geometry; as MAA requires the use of retro-reflectors to track the position and orientation of the geometry. Moreover, each retro-reflector captures a single point, so defining a single planar face on a component requires three reflectors per face (the components under investigation have five planar faces per part that require tracking to allow assembly). Beyond, the number of reflectors is their size, which is not an issues for large aircraft airframe type assemblies, but is problematic at smaller scales. A further retro-reflector issue is visibility and extraction. The reflector's positions are record by laser tracker making line-of-sight a necessity; which is difficult to maintain as the components mounting face come together. Indeed, once the components are mated the reflector must be extracted so that they do not interfere with the welding, again this will be difficult. A further issue is tracking, as the reflector come into close proximity, it may be difficult to the laser trackers to distinguish which retro-reflector is which – leading to control system confusion. It should be noted at the point that, LiDar and photogrammetric systems may addresses some of these issues, but these methods generate huge amounts of data so require slow and complex data processing algorithms.

In its true essence MAA is aimed at removing dedicated fixturing, relying on advance robotics to position the components to be joined relative to one another in Euclidean space. However, current industrial robots are of relatively low positional accuracy, when compared to a dedicated fixture. This is relative inaccuracy is acceptable for very large thin-sheet structures

with flange mounting faces; they intrinsically contain some geometric and joint position flexibility to easy assembly. However, for welded solid bodies the flexibility is not present. Finally, these annular assemblies are complex, the exemplar Rolls-Royce Trent 900 front bearing housing ring of vanes contains 52 parts that would require simultaneously assembly. Moreover, having 52 robots and end-effectors working in such close proximity would be expensive, excessively complex mechanically and intolerably complex in terms of automation control software.

Total Quality Management (TQM) methods (inc. Six Sigma) could be used to improve the build quality of these type of structures, but they are a somewhat reactionary approach. TQM requires production to be underway so that data can gathered and used as the basis of corrective action. Although an exemplar assembly is shown within this thesis, and this could be used for the bases of a TQM study. This sort of study would offer no real solution for next generation of components, which are required (by market pressure) to be both larger and more circular. Importantly, by developing a fundamentally robust assembly methodology for ring shaped annular assemblies there will be a reduced need for these expensive and time consuming TQM methods. Also, these TQM methods aim to reduce the variance output of a production system, but they are still outputting a range values, which as previously discussed is poorly suited the assembly of ring shaped structures.

A final conclusion from this literature review is that the Preliminary Weld Process (PWP) - or tack welding - is an underserved area of scientific study.

While seam welding of all types is very well understood by science, tack welding is very poorly covered by existing literature. This is lack of scientific interest is surprising, as tack welding is somewhat of an industrially ubiquitous process. Moreover, tack welding is normally used to set the positions of components prior to final seam welding. Therefore, the PWP has an embedded and observable impact upon the ultimate geometric quality of a welded assembly. A tack weld is fundamentally different from a seam weld; it has a point focused instantaneous thermal profile as opposed to the seam weld which occurs over a much larger area and time period. A further difference is that seam welds normally use a filler material and tacks are autogenous so do not. Seam weld need this extra material due to their increased shrinkage as a result of martial loss (through spatter and vaporisation) and thermal contraction and volumetric solidification shrinkage. A final important point is that, given their highly localised nature of tack welds and their non-use of filler material, the PWP is especially vulnerable small gaps between assembled components.

2.9 Identified research gaps

On review of the current literature and in the context of the problem outlined at the beginning of this thesis, a number of research gaps have emerged. The identified gaps being:

- The need for a robust methodology for the prediction of the absolute size diametric of an annular assembly; this is needed to ensure that assembled components will fully contact the assembly fixture's

datum surfaces during assembly – fundamentally enabling the fixture greater influence on the build process and improving build circularity.

- A method for goal seeking circularity within a given set geometric set of components, while being mindfully of their likely geometric variance. Currently, no method of variation management is capable for fitting an assemblage of parts (with variance) onto a geometric target (i.e. reference circle). Filling the research gap will lead to an improvement within the assembled structures circularity.
- The development of a fixturing design ethos for the assembly fixtures of closed loop geometries. Current ring assembly methods are based on a fixed build diameter, where the fixture locators are set to match the nominal build diameter of the required structure; which is poorly suited to build closed loop assemblies. Therefore, what is needed is an innovate fixturing design guiding strategy that can utilise the proposed diametric size prediction approaches, so a fxturing approach is required
- Despite its industrial ubiquity, tack welding is poorly understood in the context of geometric distortion, especially considering its enhanced negative interaction with assembly gaps. Therefore, an understanding of the influence of assembly gaps on tack welding is and the resultant thermal-mechanical distortion is imperative, if a complete picture of the assembly of annular structures is to be understood.

3 Methodology

3.1 Introduction

This chapter will outline the methodology used to address the aim and objectives of this research project. Furthermore, it will describe broadly the overarching approach to the research, before breaking-down each of the project's phases and describing them in greater detail.

3.2 The Overarching Approach

This project is a multifaceted academic challenge, and seeks to examine: *(i)* modelling of component manufacturing variation; *(ii)* assembly error propagation; *(iii)* fixture enhancements for improved circularity; and *(iv)* thermo-mechanical PWP distortion. Consequently, the research requires an approach that breaks the project down into a number research phases.

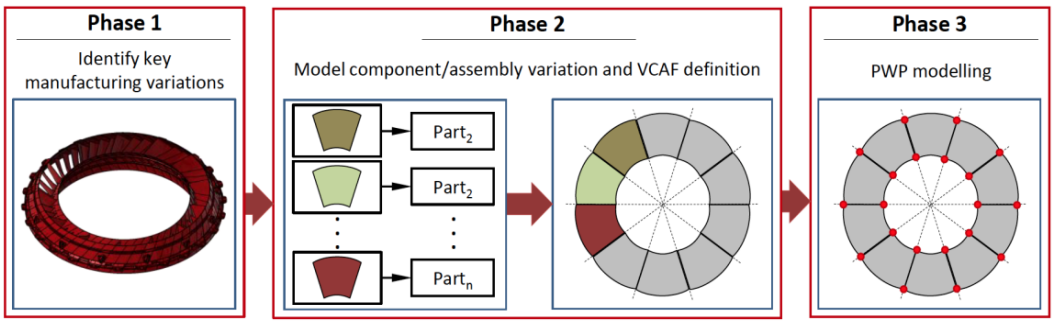


Figure 3-1: The overarching reseach methodology

Figure 3-1 shows the project's main phases and their relationship as an overview, the diagram identifies the phases as being:

Phase 1 (Chapter 4) - This project phase identified the geometric variation parameters (component, fixture and/or assembly) which have the greatest influence on the ring's final circularity (a key characteristic for the assembly). This was done with an in-depth geometric analysis of an illustrative industrial test-piece assembly (i.e T900 FBH RoV). The data from these studies was then used as the basis for mathematical modelling the variations of the components and assembly.

Phase 2 (Chapters 5 and 6) - The modelling of manufacturing variation within the components and assembly was a key goal of this project phase. Exploiting this knowledge the novel VCAF methods were defined, as component variance and its propagation through the assembly were better understood. During this phase of the project the VCAF approaches were also experimentally validated and compared to more traditional build techniques.

Phase 3 (Chapter 8) - Once the geometric conditions produced by assembling the components together were known, the effects of this variation upon the PWP were modelled and tested experimentally. This was done through first understanding the local weld conditions, and then extrapolating these results into the global assembly system. This step therefore defines the like output geometry from the process (i.e. as it leaves the assembly fixture)

These project phases will be described in greater depth in the proceeding sections of this chapter.

3.3 Phase 1 - Identify Key Manufacturing Variations

The first phase of the project was primarily focused upon defining and identifying the typical drivers of variation within the components of large annular assemblies. This definition will be acquired through a series of observational and metrological investigations, utilising an illustrative industrial test-piece assembly (T900 FBH RoV) as a typical example of such structures. Furthermore, this data will later be used as the basis of a mathematical model for typical component variation within annular assemblies.

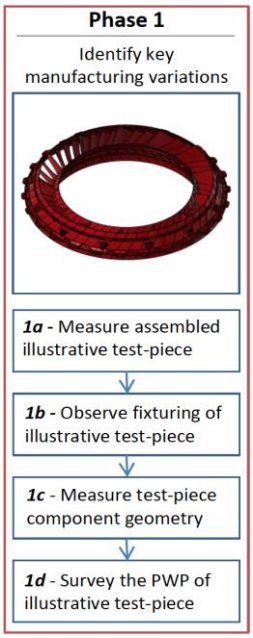


Figure 3-2: The project phase 1 methodology

As Figure 3-2 shows, phase 1 will be broken in to a number of further tasks, these tasks being;

1a - Measure assembled illustrative test-piece: An industrial test-piece weldment will be measured (primarily for circularity) as a reflection of a typical large annular welded assembly. This will highlight the current

challenges, geometric profile and tolerance expectations of "real-world" assemblies. Furthermore, as a repeating industrial component is to be used, so a number of assemblies can be measured, offering an aggregated overview of the quality and geometric conditions of the illustrative structure.

1b *- Observe fixturing for illustrative test-piece:* The current fixturing or assembly approach will have a substantial influence on the geometric quality of the illustrative industrial test-piece. Therefore, to give full meaning to assembly measurements taken from the test-piece, the current assembly fixturing must be observed and understood.

1c *- Measure test-piece component geometry:* To achieve a complete understanding of the illustrative assembly, the input components and the variation will also be measured. This will quantify the assembly input variation, allowing the relationship between the input component variation and output assembly geometry to be observed and documented.

1d *- Survey the PWP of illustrative test-piece:* The PWP of the test-piece will be observed and used as the basis for the weld modelling of the project. The information gathered will be of use both experimentally and for FEA models of the welding process.

3.4 Phase 2 - Model Variation and VCAF definition

Phase 2 utilises the information gained during the previous project phase to generate a mathematical model of manufacturing variation within an annular assembly's wedge shaped components. Moreover, this phase

looked to quantify the drivers of geometric deviation within the assembly system as a whole, paying close attention to those parameters which have the greatest influence on assembly circularity. Furthermore, it is from this modelling that the VCAF assembly methods are derived and defined. The defined assembly methodologies are then experimentally validated against traditional methods (as observed in phase 1) proving-out the legitimacy of the defined VCAF approaches.

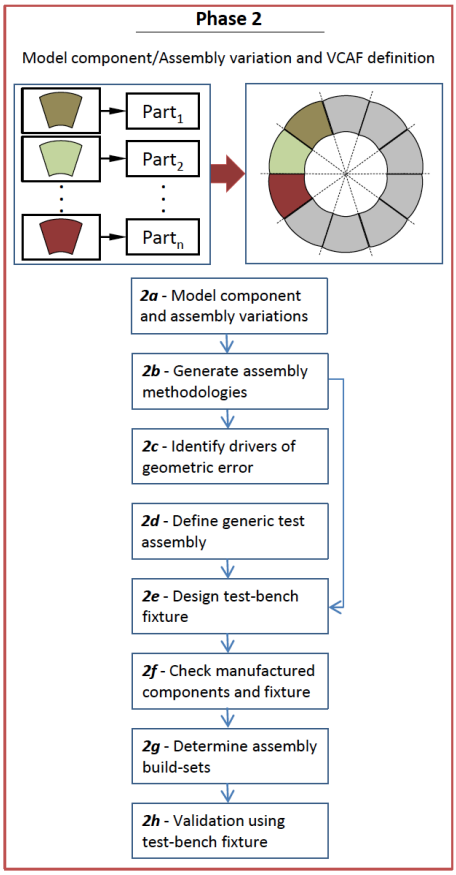


Figure 3-3: The project phase 2 methodology

Phase two (Figure 3-3) will have number of distinct tasks these are:

2a *- Model component and assembly variations:* Using the observations and numerical data accumulated during the geometric survey of the illustrative test-piece, a mathematical model of the component variation can be

defined. This model will address the key geometric parameters of the component (i.e. distance, radius, flatness, angular accuracy) and define their relationship to the fundamental key geometric (i.e. circularity, diameter, flatness) metrics of the pre-weld assembly.

2b *- Generate assembly methodologies*: Using the mathematical model of component and assembly variations (***2a***) the novel "variation conscious" assembly methods can be created. These VCAF methods will respond to the assembly components exact geometry, rather than the design nominal of the components. They intelligently adjust the fixture's locators, enhancing the in-fixture build conditions for circularity. Once identified, the VCAF and traditional fixturing approaches will be defined mathematically.

2c *- Identify sources of geometric error*: Even with the VCAF approaches there will likely remain a number of sources of non-circularity and geometric error within the constructed annular assemblies. This is because the manufactured components will geometrically deviate from the ideal design nominal, and this deviation will manifest itself in the assembly geometry. These sources of possible error were modelled (for both VCAF and traditional build approaches), so that they could be factored into the results of the experimental validation. The information was also required during the welding trials (phase 3) portion of this project, and was used to define the Local Weld Conditions (LWC).

2d *- Define generic test assembly:* To prove-out the VCAF approaches, a generic annular assembly was created for the purpose of physical validation. The generic assembly was designed with fully interchangeable

wedge components. This interchangeability enabled the use of components that contained intentional explicit errors alongside nominal components (containing only implicit manufacturing variations) during the assembly process. The inclusion of components with explicit errors allowed the response of the VCAF and traditional methods to be observed at more extreme (but controlled) levels of input variation.

2e *- Design test-bench fixture:* A flexible test-bench fixture was designed to perform the physical validation of the proposed VCAF methods. It was designed to construct the generic assembly (***2d***) using either a VCAF or a traditional fixturing approach. The development of a common test-bench platform negated the influence of differing fixture manufacturing variations on the results of the experimental validation. This is because the tested assembly/fixturing methods will be subject to common manufacturing errors within the test-bench fixture.

2f *- Check manufactured components and fixture:* The proposed VCAF build methods improve the fixture's set-up in response to the input variation of the assembly's components. Therefore, the geometric accuracy of the generic test assembly's components must be quantified before any experimental validation can take place. Furthermore, knowing the input variations also enabled the experimental testing of the traditional fixturing methods and their response to component variance. The accuracy of the manufactured fixture was also noted as this too will influence the quality of the assembly.

2g *- Determine assembly build-sets:* Each manufactured generic assembly component was assigned a unique identifier, against which their implicit and explicit manufacturing variations were logged. The identifiers were then used to pre-define a number of assembly build-sets that covered various build conditions, including; nominal, intentionally oversized and intentionally undersized assemblies. By building the same build-sets with each of the proposed VCAF and traditional fixturing methods, a like-for-like quality comparison between the differing assembly/fixturing methods could then be made.

2h *- Validation using test-bench fixture platform:* The proposed VCAF build methods were physically validated against the traditional fixturing approaches using the flexible test-bench fixture. Using each of the identified VCAF and traditional assembly approaches, the pre-defined build-sets were constructed within the test-bench fixture. These experimental build trials took place on the bed of a Coordinate Measurement Machine (CMM), so that each assembled ring could be measured in-situ. Furthermore, no welding process was performed in the fixture, so once an assembly had been measured the components could be unloaded. The fixture was then re-set so that the other assembly methodologies could be tested using the same components and build-set.

3.5 Phase 3 - PWP Modelling

The third phase of the project focuses on the PWP, which conjoins the assembled components into a stable structure ready for the final seam

welding process. This phase will be based on the observations of project phases 1 and 2, and examine the effects of the identified manufacturing variations and the influence of the build method upon the thermal-mechanical weld distortions. The observed geometry of the component/assembly variation will be tested experimentally in "per-joint" isolation, before being modelled using FEA. Once the per-joint Local Weld Conditions (LWC) are understood, a full ring welding trial will be performed. This will be followed by a FEA model of the whole assembly system during PWP welding. This final phase will ultimately predict the final process output, or the assembled geometry as it leaves the fixture.

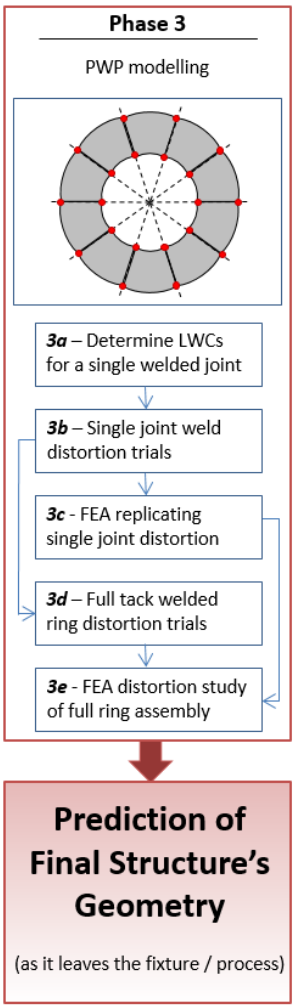


Figure 3-4: The project phase 3 methodology

Project phase 3 (Figure 3-4) will systemically build an understanding of the welding conditions via the following tasks:

3a *Determine LWCs for a single welded joint:* As a consequence of the knowledge gained during the process of identifying non-circularities and other geometric (assembly and components) errors during (***2c***) the LWC geometries can be defined. This will include any gaps and/or steps created by fitting non-ideal components into the assembled structure. Furthermore, this utilise the observations made during the PWP survey of the illustrative industrial test-piece assembly (***1d***).

3b *- Single joint weld distortion trials:* After identifying the LWC, the influence of assembly errors (such as gaps and misalignments) on the PWP was tested via a series of experimental trials. These trials replicated the LWC in isolation, so that the effects of the thermo-mechanical weld distortions could be observed on a single welded joint. Consequently, this enabled a more fundamental understanding of the mechanisms of the localised weld distortion, as the influence of the other parts of the assembly are negated.

3c *- FEA replicating single joint distortion:* FEA studies of the Isolated single-joint LWC were performed. These studies underpinned an understanding of the influence of the LWC within the entire assembly system.

3d *- Full tack welded ring distortion trials:* Weld trials were performed on a series of full ring assemblies, these trials expanded on the single-joint LCW knowledge to encompass the macro weld distortions present in a complete

assembly. Moreover, these trials also examined the influence of weld sequence upon the final distorted shape of the assembly.

3e *- FEA distortion study of full ring assembly:* This FEA studies aims to replicate the experimental full-ring weld trials, using the single joint model as the basis. This will prove-out the implications and relevance of the of the LCW and weld order in the context of the global weld distortion of a complete ring structure. Furthermore, the output of 3e will complete the predictive framework for the assembled structure's geometry based on the component, assembly and weld variances.

3.6 Conclusion

This chapter has outlined the three project phases and the overarching approach used in addressing the project's research objectives. The first of the three project phases identifies the key variation drivers within large annular assemblies via the geometric study of an illustrative test-piece assembly. Next, Phase two models the component and assembly variation drivers, so that variation conscious fixturing methods can be proposed. Finally, phase three models the LWC and global thermal-mechanical weld distortion of the PWP. Working in this manner has generated a tiered workflow for the project, with each phase building on the knowledge of the previous project phases. From this approach has grown a deep understanding of the geometric variance of annular assemblies constructed from wedge shaped components. This understanding begins with the micro-level of component manufacturing variation, and eventually extends

up to encompass the assembly wide thermal-distortion of the PWP. Moreover the ultimate output of the three phase is a framework for a complete understanding of the assemble and weld processes so that better quality geometrically and predictable annular structures can be built in the future

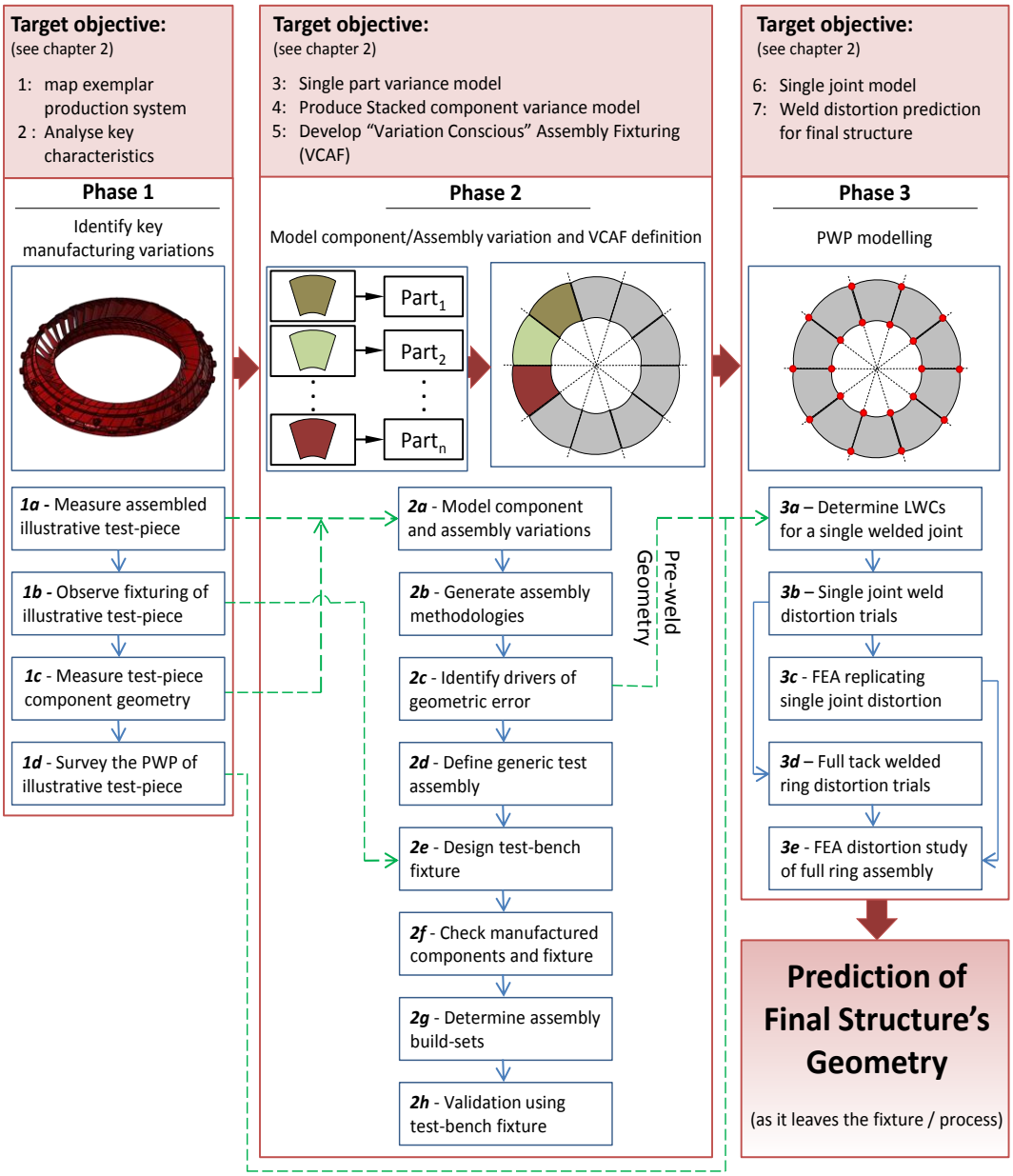


Figure 3-5: Complete project methodology flowchart

Figure 3-5 shows an expanded flowchart of the main tasks required to realise each of the project's phases. This diagram also shows the interrelationships between the differing tasks of the project, and how they interact outside of the specific project phases. The methodology laid-out in this chapter demonstrates the approach taken in broad terms, the in-depth specific procedures (i.e. the experimental/trial procedures) will be discussed in the relevant chapters of this thesis.

4 Identifying Key Manufacturing Variations: Critical Analysis of an Existing Annular Weldment Assembly System

4.1 Introduction

Presented within this chapter is the critical analysis of an exemplar existing industrial assembly system (Figure 4-1). In terms of research project the need for this analysis was twofold; firstly, it allows the typical sources of manufacturing variation within a modern annular assembly process to be identified and characterised (leading to modelling in later chapters). Secondly, it defines the current functional (i.e. accuracy, circularity) and technical (i.e. required manufacturing processes) expectations for the creation of these types of structure within the high precision aero-engine industry.

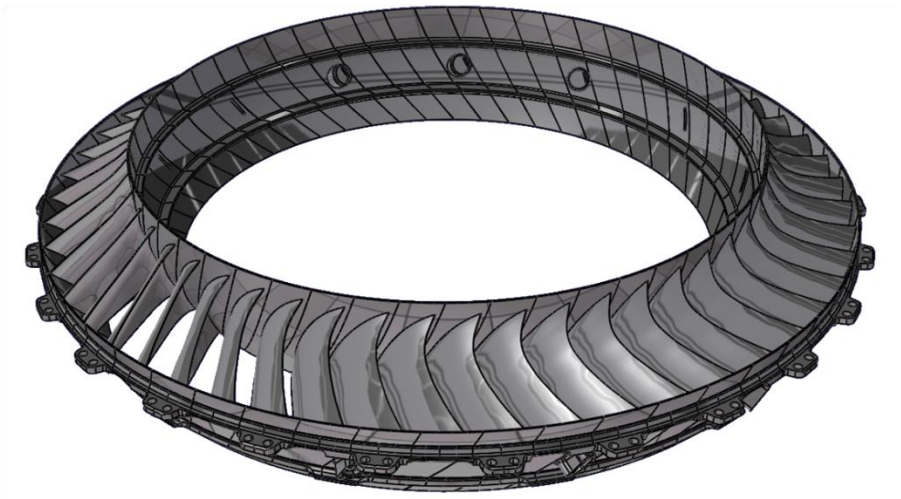


Figure 4-1: The illustrative annular assembly.

For the purpose of this study Rolls-Royce offered the Trent 900 (T900) Front Bearing Housing (FBH) Ring of Vanes (RoV), as an illustrative annular assembly. The analysis of the assembly process for the illustrative annular assembly consisted of the following tasks;

Analysis of illustrative annular assembly production data*:* A fully assembled illustrative annular assembly was studied, exemplifying the typical geometric output of a typical modern assembly system when faced with a ring shaped assembly. This enabled a qualification of the current expectations for output quality of the existing assembly system, and highlighted potential issues with the current methodology.

Evaluation of variability of component geometry: The component parts of the illustrative annular assembly were measured, so that the input variation into the annular assembly system could be understood. This data was then scrutinised for a causal link between the observed component geometry and the final assembled structure.

Evaluation of fixturing for the illustrative annular assembly: As the fixture has a fundamental effect upon the quality of the assembled structure, so the fixture used for illustrative annular assembly was surveyed. Special attention during this survey was paid to the fixture's location strategy.

Survey of illustrative annular assembly PWP: The preliminary welding process of the illustrative annular assembly was surveyed, so that a typical approach to tack welding within a manufacturing environment could be

appreciated. Observations made during this survey would then function as the process basis for the FEA welding simulations.

4.2 The illustrative annular test-piece assembly

The T900 FBH RoV (Figure 4-3) illustrative industrial test-piece is a large ring assembly with an internal diameter of 1037mm, an external diameter of 1560mm, and a vertical height of 300mm. This weldment is assembled from fifty-two wedge-shaped titanium alloy (Ti-6Al-4V) vanes, which are face-face abutted to form the annular structure. These vanes consist of an I-shape wedge geometry, which has an aerofoil acting as the vertical portion of the "I"; while, the upper and lower horizontal bars of the "I" are contact faces that mate to the neighbouring components. These upper and lower contact faces are in reality wedge faced arches, and are referred to as either the upper/lower platform, or as the outer/inner annulus. Each wedge has a basic wedge angle of 6.92° (360°/52), however the face-face contact surfaces are at double compounded angles.

Beyond the basic assembly geometry, Figure 4-2 shows that there are also two basic vane types used within the assembly; standard and service. Although both vane types have the same geometry in the upper and lower platforms, they do differ in the aerofoil; where the service vanes are thicker (≈2.0mm) in cross-section with a wider aerofoil chord length. These vanes are then mixed at a 3:1 ratio within the assembled structure, with the bias being toward the standard vane type. Adding further to the complexity, there are also a number of service and standard vane variants, each with

specialised features related to their function. Because of this vane specialisation, the component load sequence must be carefully controlled, ensuring each vane type is loaded into the assembly at the correct location.

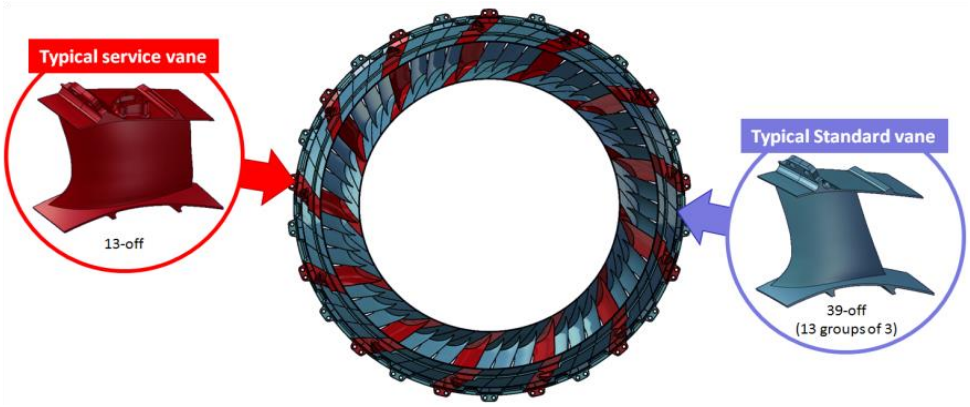


Figure 4-2: The distirbuton of standard and service vanes within RoV.

4.2.1 Assembly Key Characteristics

The most important features of the assembly are considered to be the gas-wash faces (Figure 4-3). The quality of these surfaces is especially important for engine efficiency, as steps between the vanes on these surfaces would interrupt the smooth airflow through the engine creating unwanted eddies. The EBW does perform a smoothing wash-weld of the gas-wash faces as its final process. However, the wash-weld can only blend a maximum step size of 0.5mm, and there are no post-process machining operations to correct for larger steps. For this reason the gas-wash face a key characteristic of the assembly and controlled with a surface profile tolerance throughout the assembly process; even at the cost of other features if needed (as these generally have a machining allowance in their geometry).

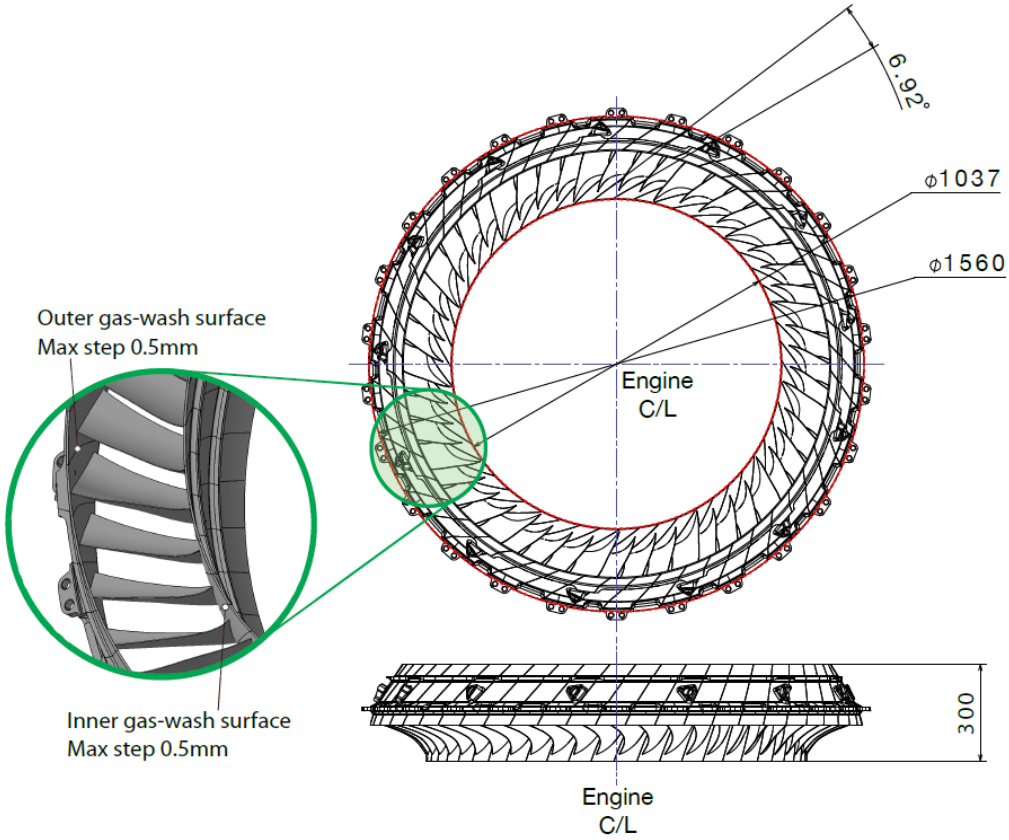


Figure 4-3: Overall dimension of the illustrative annular assembly.

The second key characteristic for the assembly is its circularity. The assembly engineering drawings controls the circularity of the assembly to ±0.15mm. Circularity is important for subsequent assembly process; more so than the diameter dimension. This is because welding a turned item of high circularity to a non-circular assembly would give differing widths to the weld gap – leading to asymmetry in weld shrinkage and thus residual stresses. Moreover, asymmetric residual stresses would cause assembly warpage and disfigurement, which would compound assembly difficulties further through the production process.

4.2.2 Vane datums

The vanes are wedge-shaped I-beam components, which stack together to create the closed ring assembly. Moreover, as Figure 4-4(a) shows each vane contains a number of manufacturing datum points. These datums follow a scientifically well understood 3-2-1 location scheme [140, 239], and are used to deterministically position the vanes during manufacture. These datums are consistent across all vane types, enabling common production tooling to be used in the vane's manufacture. The FK Point is of particular importance within this datuming scheme, as it acts as the origin for the Local Coordinate System (LCS) and as the machining datum for the inter-component contact surfaces.

The assembly stages of production use a different datuming methodology to that of manufacture, and does not conform to the traditional 3-2-1 approach. This difference in locator scheme is driven by the requirement for a face-face contact between the components. Moreover, it is the face-face contact condition between a vane and its neighbour, which controls each vane's assembled angular position. For this reason, the datums used within the assembly are restricted to the "A" face and the FK point (Figure 4-4(b)). The "A" face is used as the main support surface and controls the relative height of each vane, while the FK point carries over from the manufacturing datum scheme and controls each vane's radial position.

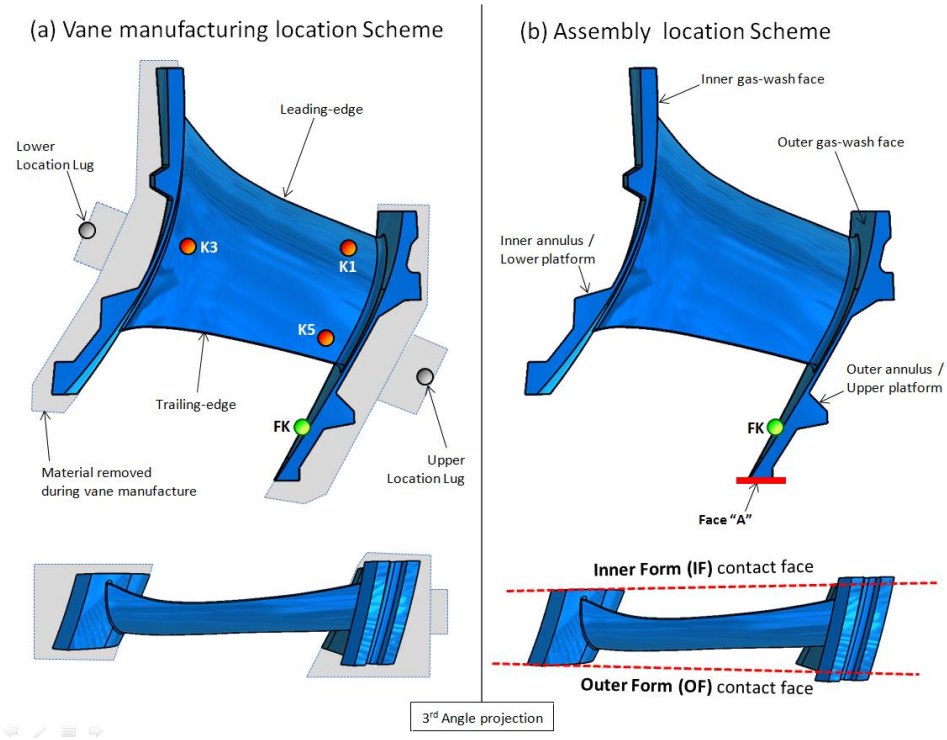


Figure 4-4: Vane datum schemes: (a) manufacture, (b) assembly.

4.2.3 Overview of the annular assembly manufacturing process

The scope of this project is in the RoV assembly only, however the wider context of the assembly is required to fully understand the structure. Currently the illustrative annular assembly is manufactured in a six stage process consisting of the following steps:

Vane manufacture: The vanes are manufactured from a forged near net-shape blank, which is machined to achieve the final geometry and surface finish. Once complete each vane is then CMM checked to ensure it conforms to the Condition of Supply (CoS) drawing, before being assembled.

RoV assembly and initial PWP: The vanes are manually loaded into the assembly fixture eight or nine at a time, to create a "build segment". Once formed the current build segment is then PWP welded together to stabilise

its geometry. The next segment then uses the end of the previous build segment as its starting point, this process continues until a complete ring is constructed.

Secondary PWP: Because the assembly fixture obscures some of the required PWP weld positions, so it is not possible to perform all the necessary welding within the assembly fixture. However, enough welds have been performed up to this point that the assembly may be unclamped, flipped-over, and placed onto a support table, where the welding can be completed.

Electron beam welding: The assembled ring is loaded into an Electron Beam Welder (EBW), where it is PWP welded (again) and seam welded, before the final wash weld is performed.

Metrology: The fully welded ring assembly is CMM measured. As part of these measurements the centre axis of the assembly is determined. This information is then used in the ensuing turning and machining operations.

Machining Operations: The ring assembly is machined, to achieve the required geometric and functional tolerances and the necessary surface finishes. These are in effect clean-up operations, which prepare the weldment for the additional assembly operations later in the manufacturing process (these extra steps are outside the scope of study for this project).

4.3 Analysis of illustrative assembly production data

To understand the geometric output limitations of the current assembly system, existing manufacturing data was scrutinised. The benefit of analysing this data was that it offered an aggregated view of a number of assemblies. This enabled a more balanced view of the assembly system's output, reducing the influence of anomalies within the dataset. The CMM data used for this study was extracted from the illustrative annular assembly after the EBW process (manufacturing stage iv). This data is used identify which three equidistant vanes within the assembly are positioned closest to the radial nominal. The identified vanes are then used as clamping points during the post-weld turning and milling operations.

The production data for nineteen structures was used for this analysis, with each dataset containing two measurement groups. One of which broadly measured the assembly's circular run-out and another its flatness. The first of these measurement groups contained the radial distance of each vane's FK datum point (see Figure 4-4) to the assembly's axis, indicating the weldments approximate circular run-out. While, the second measurement group contained the deviation of "A" face (see Figure 4-4) from nominal, which is akin to flatness. The measurements were only available in hardcopy, so they were manually input into a spreadsheet to enable a greater depth of interrogation for the data.

4.3.1 Approximate circular run-out findings

The smallest value for the FK point to axis measurement, was subtracted from the largest (Figure 4-5) for each dataset and plotted. Although technically this data is that of circular run-out [37], it must really be considered an approximation, as it contains only fifty-two data-points over the rings circumference. The plot shows an average approximated circular run-out of 1.56mm (±0.034 at 95% confidence), which equates to a 0.23% error on the nominal 678.5mm radius of the assembly. The plot also shows a total spread of between 1.05mm and 2.43mm (both ±0.034 at 95% confidence) within the nineteen RoV datasets.

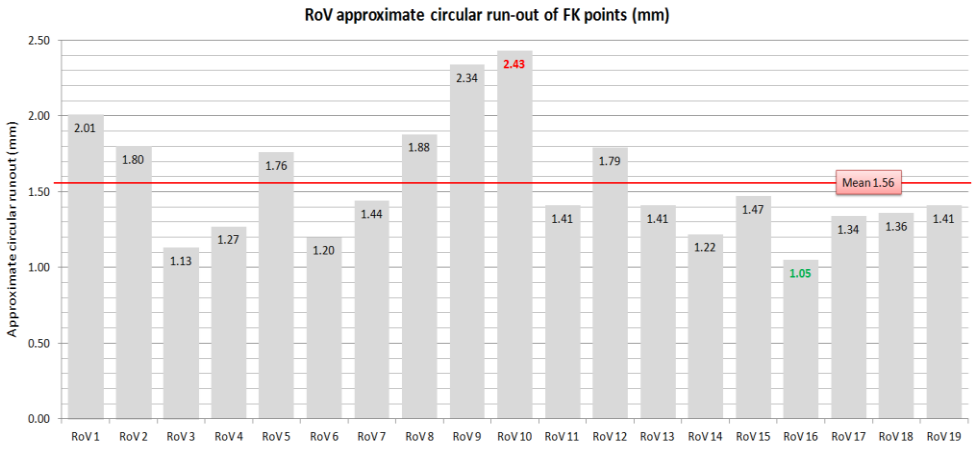


Figure 4-5: Approximated run-out for the illustrative annular assembly.

The radial position of each vane's FK point was also plotted against the vane's position within the assembly across the nineteen datasets (Figure 4-6). What is interesting looking at this graph is the large amount of variance in the position of the FK point for any given vane. The mean variance in the radial position of the FK points being 1.22mm (±0.034 at 95% confidence), while the largest deviation being 2.40mm and the

smallest being 0.68mm (both ±0.034 at 95% confidence). The trend within this "noise" only really becomes apparent upon consolidating the data and plotting it to show the mean radial position of each vane.

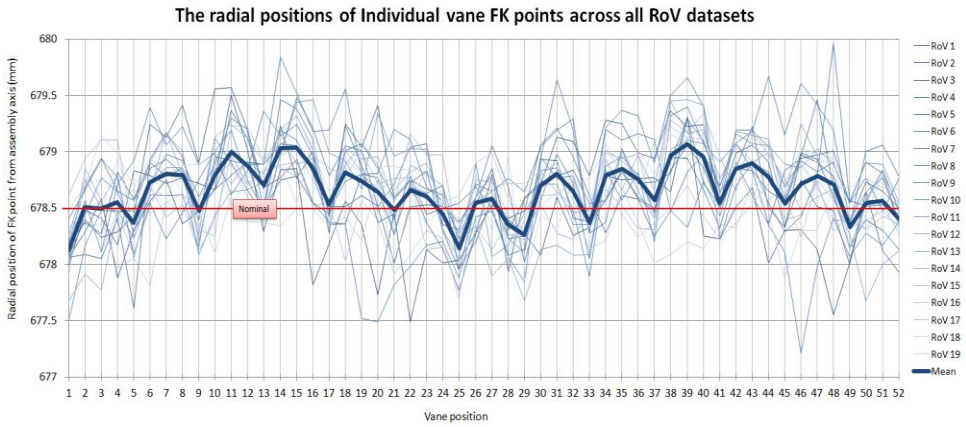


Figure 4-6: Radial FK point values for all datasets.

Plotting the mean radial position of each FK point in a "radar" style plot (Figure 4-7) gives a good overview for the output geometry of the illustrative annular assembly and its production process. As Figure 4-7 shows, the typical output geometry is an elliptical form, punctuated with lobed protuberances. The geometric source of these "petalled" lobes becomes apparent only once the distribution of the standard and service vanes is added into the graph. Adding this information data to the plot shows that; the standard vanes appear to create the peaks within the plot, while the service vanes pull the geometry inwards. This information suggests a geometric difference between the two vane types, despite their design intent of being geometrically identical in terms of assembly features. Furthermore, this geometric differential is fundamentally influencing the assembly process and circularity of the final structure.

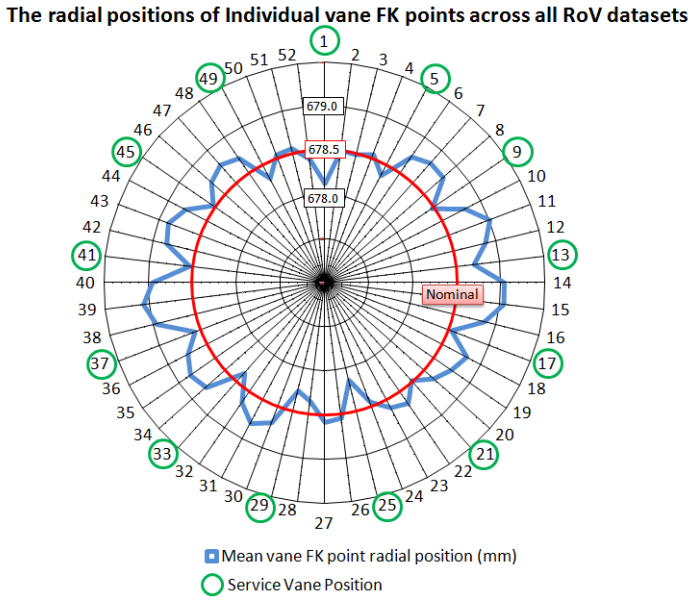


Figure 4-7: Radar plot of FK point mean radial position.

4.3.2 Flatness measurement findings

The manufacturing data for the deviation in height of face "A" also underwent numerical scrutiny. This data was transposed into an approximation of ISO 1101 [37] geometric out-of-plane flatness measurement, by converting these plus/minus data points into an absolute range. Once converted, this data then offered the out-of-plane flatness of the entire assembly, but as it is based on a single measurement point per vane, so it gives no indication of the flatness for individual "A" faces. As Figure 4-8 shows, the measured flatness across the nineteen RoV's sampled had a mean flatness of 0.91mm (±0.013 at 95% confidence), and within a range of 1.41mm to 0.62mm (both ±0.013 at 95% confidence).

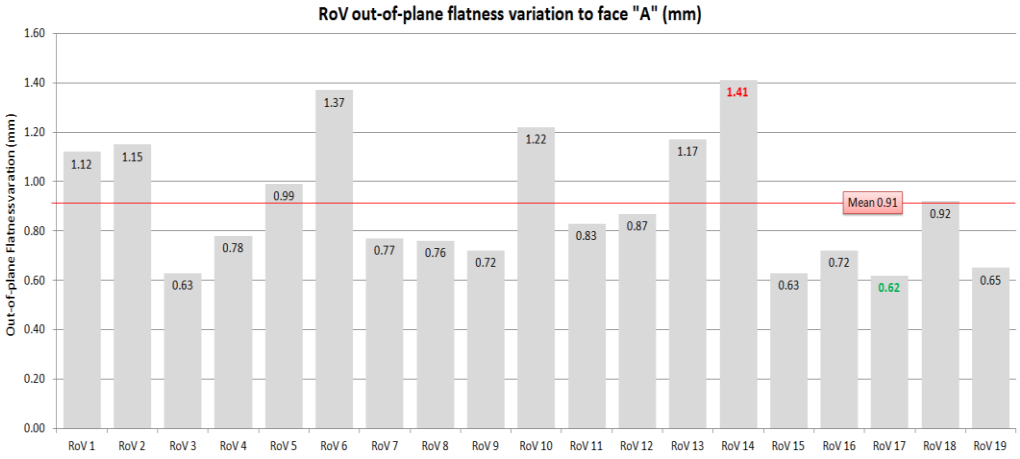


Figure 4-8: Out-of-plane values for illustrative annular assemblies.

Shown in Figure 4-9, the flatness data was also plotted per vane across all nineteen datasets. The plot shows an average variance in out-of-plane error per vane of 0.74mm, with the best performing vane being 0.42mm, and the worst performing 1.21mm (all ±0.013 at 95% confidence).

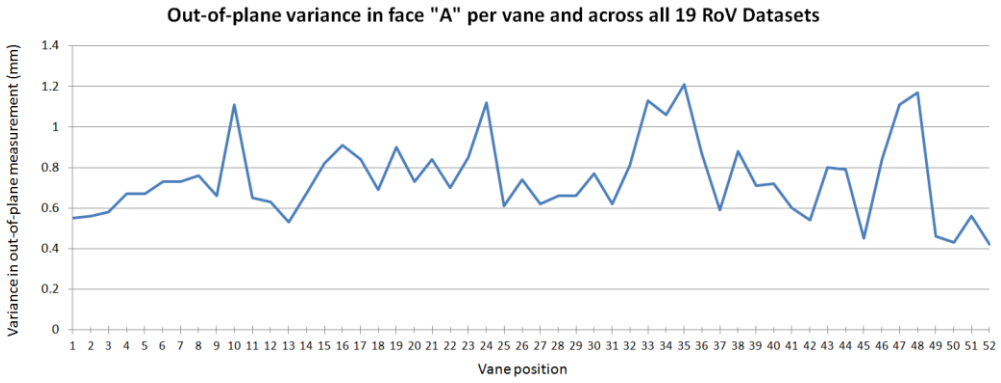


Figure 4-9: Variance in out-of-plane measurement per vane.

However, rather than flatness, a more interesting result can be seen in a plot of the height of each vane's "A" face relative to the design nominal (Figure 4-10). What is immediately striking about this plot is its similarity to the earlier approximate circular run-out plot (Figure 4-6).

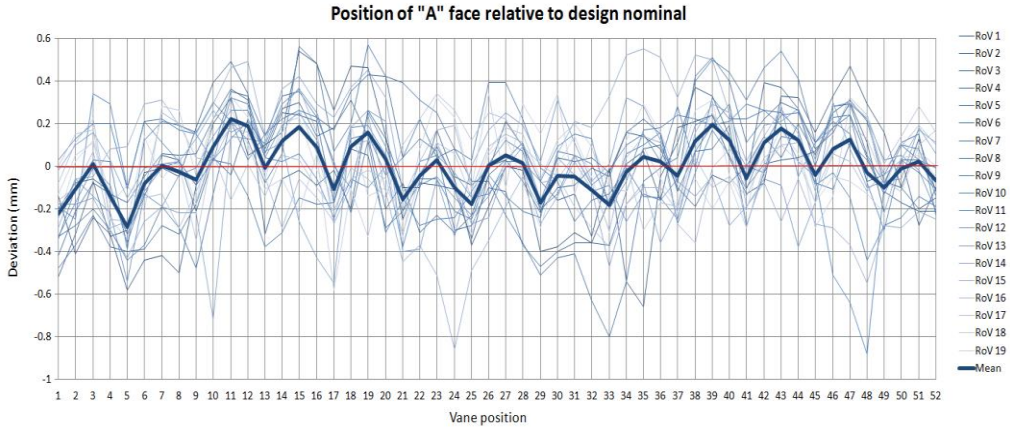


Figure 4-10: Positional deviation of "A" face from designed nominal.

To highlight this similarity, Figure 4-11 shows a comparative plot of the radial position of each vane's FK point and "A" face deviation. Looking at this plot, it would appear that the geometric variations in both flatness and circular run-out are being driven by the same variation source. That said, from the examination of the assembly's approximate circular run-out, a correlation between variation within the assembly geometry and the two vane types was found; this trend too, is also apparent within this plot of mean flatness.

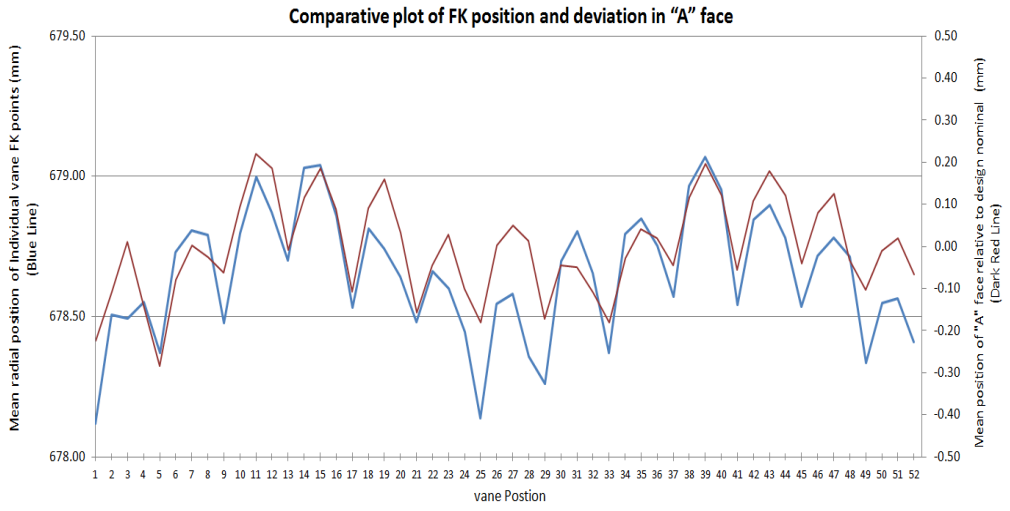


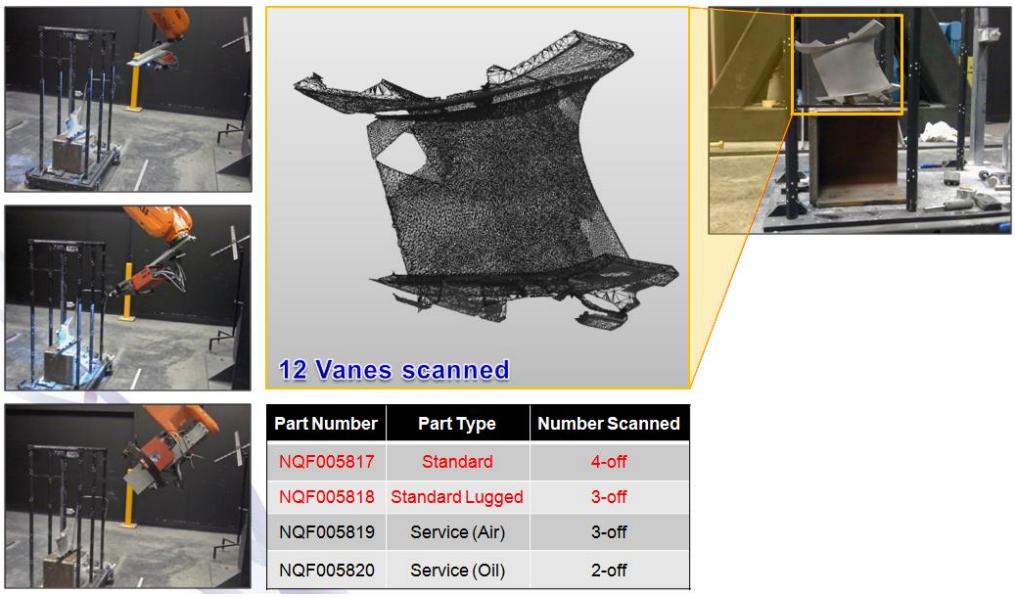
Figure 4-11: Comparative plot of FK position and deviation in "A" face.

4.4 Analysis of the illustrative annular assembly's components

As the two vane types were influencing the illustrative annular assembly final shape in differing ways, a geometric analysis was undertaken to quantify the root cause of this observation. This study aimed to compare the two vane types to their nominal design intent, so that the differences between the two geometries could be better understood.

Every manufactured vane component undergoes a CMM quality control check, the data from which could certainly be used for this study. However, these CMM measurements are performed while the vanes are clamped into an inspection fixture, and this clamping may be influencing the measurement results. For this reason, it was decided that the study should forgo the use of the production inspection fixturing and the CMM, and measure the parts in a free-state condition. To achieve this free-state condition a non-contact 3D scanner was used to perform the required measurements.

A set of twelve production (seven standard and five service) ready vanes were acquired for scanning. After coating with a specialised temporary matting spray, each component was scanned using an ATOS II white light optical scanner attached to an industrial ABB robot (Figure 4-12). The PolyWorks software was then used to capture the scan data, before exporting it as a stereolithography (.STL) file, so that the measurement point-cloud could be loaded in to a CAD package for further processing.



Part Number	Part Type	Number Scanned
NQF005817	Standard	4-off
NQF005818	Standard Lugged	3-off
NQF005819	Service (Air)	3-off
NQF005820	Service (Oil)	2-off

Figure 4-12: Scanning the vanes of the RoV

To compare between the scanned vanes and the nominal CAD model (or design intent) the point-cloud was loaded into the CAD package Catia V5. However, the CAD software could not directly measure between the point-cloud and the solid model of the vane geometry. Also, as the vanes were scanned in an unfixtured free-state, so the point-clouds lacked a common Cartesian coordinate system; preventing them from being reliably aligned with either each other or the nominal CAD model. So, due to these reasons the measured point-clouds were manually converted (Figure 4-13) into a surface model with a common origin, which then enabled the comparison to be performed.

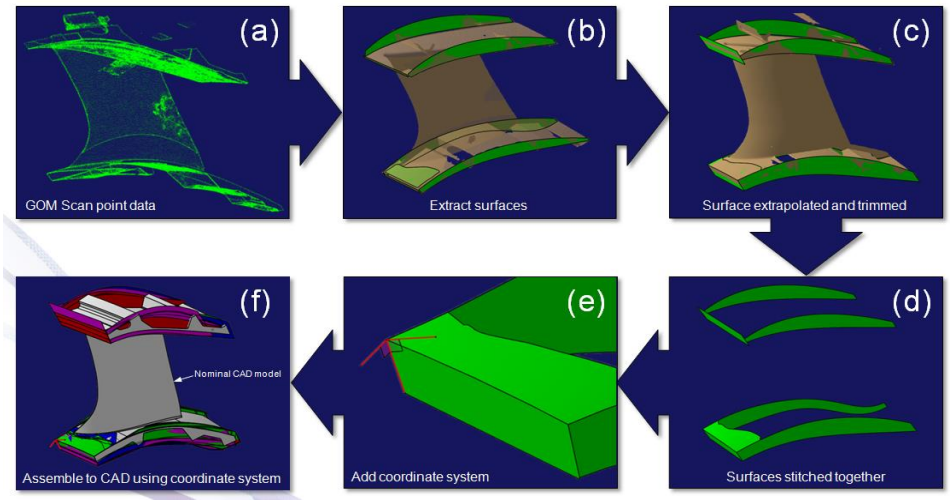


Figure 4-13: Converting point-cloud measurement to surface model

The conversion steps required for each component were:

a) Import measurement point-cloud into Catia V5.

b) For each face of interest, extract the bounding points and use these points to construct a surface. The extracted bounding points should be a small distance (≈1-2mm) from the edge of the surface being extracted, as measurement noise makes defining an edge unreliable when using optical scanning methods [ref].

c) Extrapolate the constructed surfaces so that they intersect.

d) Trim and stitch together each of the constructed surfaces, this is to reconstruct the edge and corner geometry.

e) Choosing a corner common to all the scanned vanes, create a coordinate system by aligning the axes to the intersecting planes. A corresponding coordinate system is also required within the nominal CAD model.

f) Assemble the geometry to be interrogated by aligning the constructed coordinate systems.

4.4.1 Interrogation of vane scan data

Examining the converted point-clouds within Catia, the vane geometry aligned well to the nominal CAD model, and all the vanes also conformed to the tolerances stated on the engineering drawing. However, it became apparent that the vane's geometry also contained a small (previously unknown) mono-directional twist, between the upper and lower platforms, with its axes running through the aerofoil (Figure 4-14).

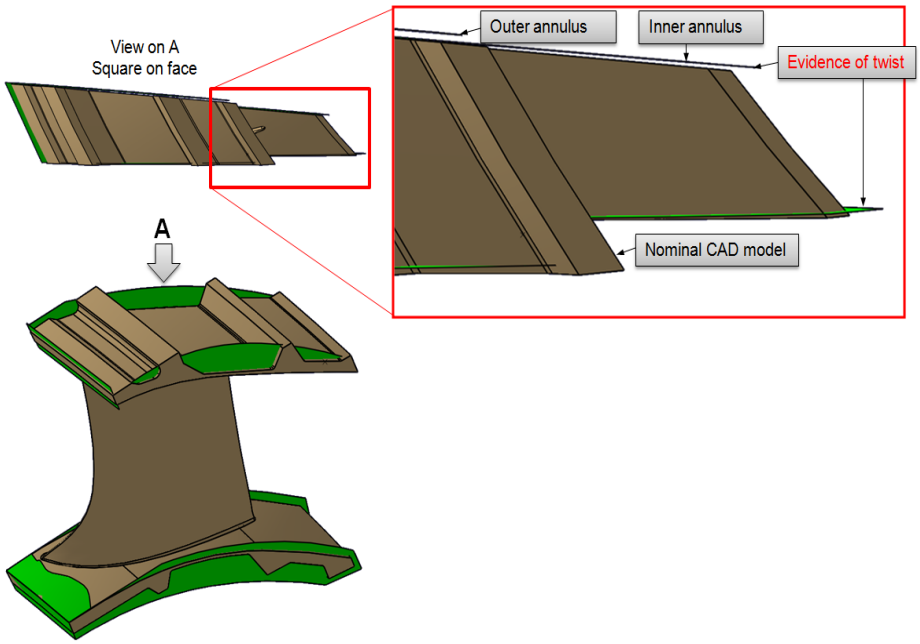


Figure 4-14: Typical scan result with mono-directional twist

As Figure 4-15 and Figure 4-16 show, the degree of mono-directional twist differed between the service (0.36°CCW average ±4.2x10-4° at 95% confidence) and standard (0.59° CCW average ±4.2x10-4° at 95% confidence) vanes, with the standard vanes exhibiting a 63% larger twist.

Part Type	Lower IF	Lower OF	Lower Leading Edge	Outer IF	Outer OF	Outer Leading Edge
Standard Vane	0.227°	0.213°	0.002°	0.587°	0.492°	0.160°
Standard Vane	0.227°	0.168°	0.005°	0.607°	0.494°	0.208°
Standard Vane	0.281°	0.248°	0.008°	0.592°	0.593°	0.189°
Standard Vane	0.241°	0.191°	0.020°	0.641°	0.442°	0.200°
Standard Vane	0.246°	0.252°	0.000°	0.550°	0.451°	0.155°
Standard Vane	0.265°	0.241°	0.080°	0.557°	0.515°	0.204°
Standard Vane	0.258°	0.222°	0.003°	0.595°	0.561°	0.215°
Service Vane	0.272°	0.258°	0.012°	0.446°	0.398°	0.096°
Service Vane	0.255°	0.266°	0.010°	0.411°	0.421°	0.060°
Service Vane	0.248°	0.221°	0.040°	0.360°	0.330°	0.051°
Service Vane	0.287°	0.229°	0.002°	0.291°	0.248°	0.007°
Service Vane	0.276°	0.265°	0.006°	0.453°	0.403°	0.101°

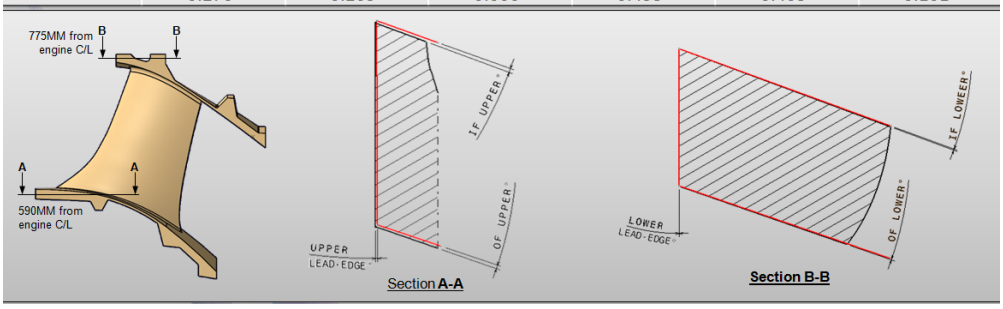
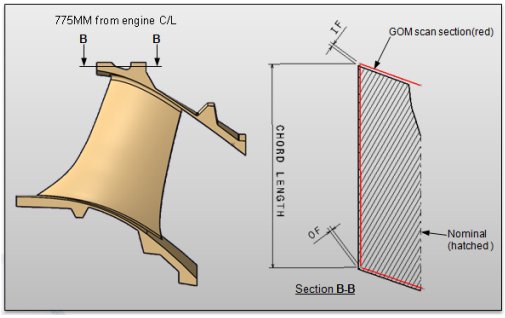


Figure 4-15: Angular of vane scan data (all ±4.2x10-4° at 95% confidence)



Part Number	IF offset (mm)	OF offset (mm)	Chord (mm)
CAD Nominal	N/a	N/a	97.46
Standard	1.49	1.52	97.68
Standard	1.34	1.44	97.55
Standard	1.38	1.53	97.63
Standard	1.41	1.51	97.57
Standard	1.34	1.41	97.63
Standard	1.01	1.23	97.50
Standard	1.29	1.43	97.66
Service	0.98	0.94	97.55
Service	1.07	0.98	97.57
Service	0.60	0.66	97.43
Service	0.57	0.64	97.35
Service	0.84	0.85	97.52

Figure 4-16: Vane upper platform displacement *(±0.0111 at 95% confidence)*

This mono-directional twist has the effect of increasing the out-of-plane (flatness) error across the inter-component contact surfaces. However, given that the twist had not been previously identified by the end users, it must be that the twist was flattened-out by the clamping forces of the CMM fixture. It stands to reason therefore, that it must be possible to squeeze the twist flat within the assembly fixture also. Squeezing the vane flat in this way, would elastically deform it, resulting in a reactive spring force from

the vane. The wedge shape of the vane then makes it likely that this reactive spring force will be resolved outwards. This may explain the lobes within the assembly's output geometry, as these too, appear to be pushing only outwards. Even if this predicted flattening is not occurring, or the flattening is only partial the twist is in effect making each wedge slightly wider than the anticipated design nominal. This will inevitably affect the fit of each wedge into the assembly system, and as Figure 4-17 shows, an oversized component is most likely to be pushed outwards. From this standpoint, it is easy to see why the standard vanes with their greater degree of distortion, are more likely to be outboard of their intended nominal radial assembly position.

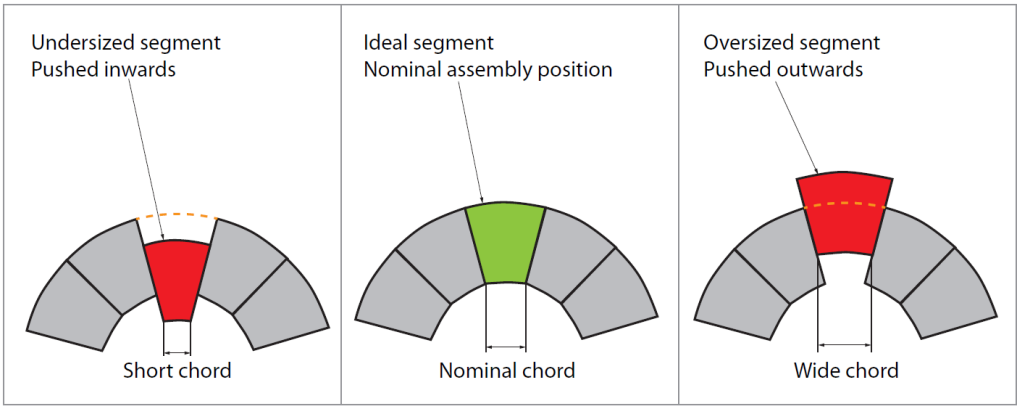


Figure 4-17: The likely position of vane based on chord width

Further evidence for a twist as the source of the lobed assembly geometry can also be seen in the extracted flatness data. Figure 4-11 showed previously that, a plot of averaged deviation in the height of the "A" face exhibited a similar profile to that of the averaged approximate circular run-out. However, the surfaces inspected to extract these measurements are perpendicular to each other; this implies that the driving source of the lobes

must affect both of these surfaces simultaneously. A twist in the geometry would most certainly distort the relative positions of all the surfaces of the upper and lower platforms, making it a good candidate to explain the observed geometry.

4.4.2 Further investigation of component mono-directional twist

With further investigation, the mono-directional twist was tracked back to an encapsulation technique used in the production of the vane. This technique uses a low-melt eutectic bismuth alloy (58% Bi and 42% Sn) to support the aerofoil during the machining of the inter-component contact surfaces. The "True Alloy" used for this encapsulation has a liquidus of 138°C, and it was found (though an FEA study and experimentation) that this heat caused thermal expansion of the aerofoil, inducing the twist. Furthermore, as the aerofoils differ in thickness and chord length between the standard and service vanes, so too did the amount of twist.

4.5 Appraisal of illustrative annular assembly fixturing

The assembly fixture and its ability to accommodate system wide manufacturing variance will have a substantial effect on the final structures geometric quality. Therefore, to give full meaning to the measurements taken from the illustrative annular assembly, the current assembly fixturing must also be observed and understood.

The fixture used for the assembly of the illustrative annular assembly is a large manual load and clamping fixture that utilises fixed radial locators situated at the assembly's outer annulus. It also contains two support faces,

with a height drop between them to accommodate the vanes offset geometry. A non-contact visual reference pin is also included at the leading edge of the upper platform to assist the operator with component alignment during the build process. Finally, each component is secured via two bolt-down strap clamps, which pull the vane down onto the support faces mentioned earlier.

The current build fixture uses a segmented build strategy (Figure 4-18) to construct the final assembly. This is done through the use of two datum stocks, one being “fixed” and the other “floating”. The fixed stock creates a datum face in the position of the 52nd vane, while the floating stock is positioned at the end of the current build segment. The vanes are then stacked in pre-defined sets of either eight or nine to fill the gap between the stocks. Once complete each build segment is then PWP welded to stabilise the assembly, before the floating stock is moved to the end position of the next build segment. The process then continues this way until the last build segment is reached, whereupon both stocks are removed from the fixture, allowing completion of the ring.

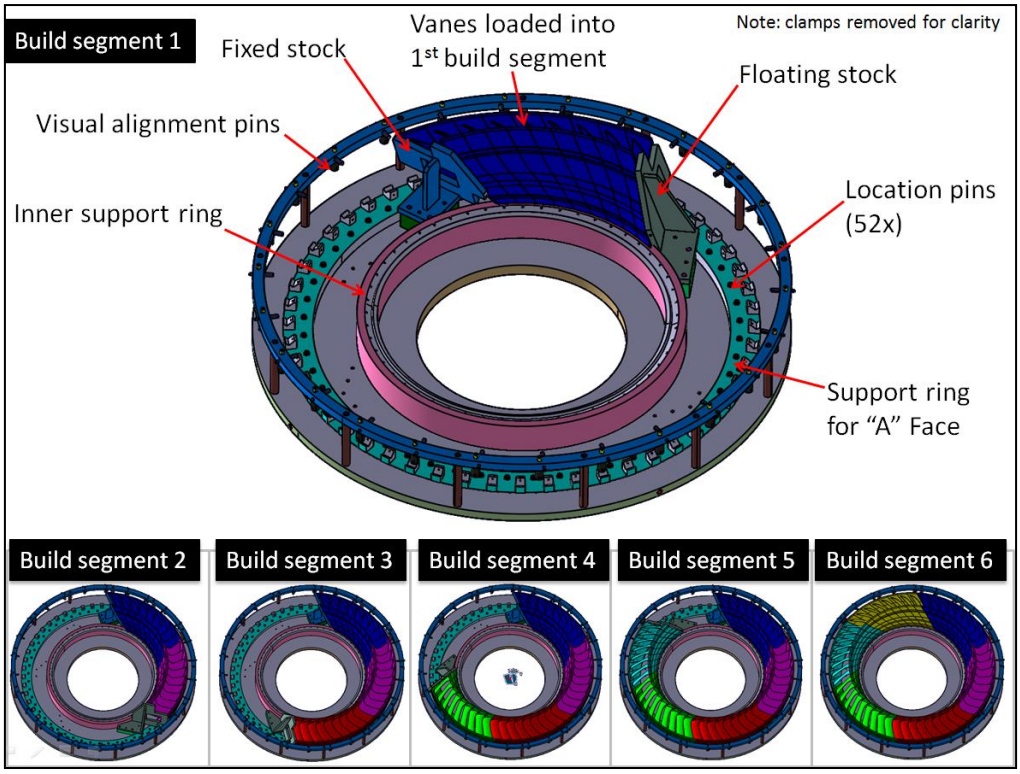


Figure 4-18: Segmented build approach of illustrative annular assembly

Plotting the position of the segment breaks against the approximate circular run-out (Figure 4-19), the geometric influence of the stocks can be seen within the output geometry of the welded assembly. Looking at this plot shows that, the vanes positioned directly after the end of a segment generally have a positional deviation approaching zero. This is probably because the stock being very solid causes an extra flattening of the vane's twist, allowing it to sit in a position that is much closer to the build nominal. Consequently, this implies that positions not in contact with the fixed or floating stocks are not fully located. This is because the components that surround them are also subject to spring-like elastic deformation, and therefore, are less rigid allowing the components to flex.

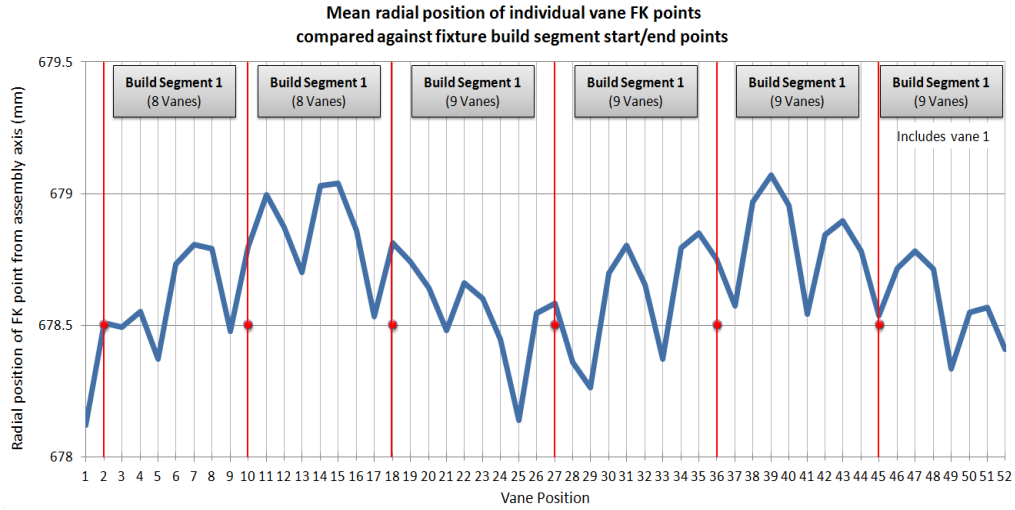


Figure 4-19: Build segment breaks against approximate run-out

4.6 Survey of illustrative annular assembly PWP

The current fixture build process uses an in-fixture PWP or tack welding process to stabilise each build segment once it has been constructed. These temporary 2mm deep, Ø6-8mm PWP welds are performed using a Gas Tungsten Arc Welding (GTAW) process. These welds are only temporary, as they are replaced by the EB welder prior to the final seam and wash welding processes. This replacement is essential as the GTAW preliminary welds are too weak to withstand the thermal stresses induced during EB welding. While EB tack welds, are considerably deeper in penetration and free from atmospheric contamination (which creates brittleness in welded titanium), making them stronger and more ductile. As the GTAW welds are entirely temporary, so with experience Rolls-Royce has found no need for the use of a consumable filler rod, making the GTAW PWP an autogenous process. However, this autogenous process may be at the cost of generating

larger weld distortions, as the base material lost through vaporisation and spatter is not replaced by filler.

In-fixture welding allows each vane to be deterministically positioned during the welding process, improving geometric accuracy in the finished structure. However, the downside of this approach is that, the fixture impinges the welding process, masking three of the eight welds required to stabilise each vane. To achieve the masked welds, the assembled RoV is removed from the fixture, turned-over, and placed on a support bench, so that the final welds can be performed, before being loaded into the EBW. Another well documented issue with in-fixture welding [152, 240] is that by constraining the components during the welding process, the residual stresses within the final weldment are increased. Therefore, given the large volume of welding that takes place within the EBW; this would generate substantially greater residual stresses than the PWP process, if the RoV was fully restrained on a vane-by-vane basis. However, conjoining the RoV assembly with a PWP process prior to the seam welding, substantially reduces the clamping within the EB welder (to just four clamps for the entire RoV structure).

An interesting point noted while observing the PWP of the illustrative annular assembly is that: it seems current practice for the operator to use the welding process to manage small assembly gaps. It was observed that the operator insightfully addressed small misalignments within the assembly by adjusting the weld order. Working in this way he was able to either reduce or entirely close small inter-component gaps during the

assembly's construction. To achieve this closure the operator would weld the gap positions first, using the welds shrinkage on solidification to pull the gaps shut. Once all the gaps were closed the remaining joint positions were welded to finish off the structure. This effect may only be possible because of the autogenous PWP used, as removing the filler material from the process increases welds shrinkage. However, the use of an autogenous PWP requires that larger gaps be G-clamped (flattening the twist), as the lack of filler material makes it difficult to generate a large enough weldpool to bridge the gap between the components [241].

4.7 Conclusions

During this chapter an in-depth critical analysis of an existing assembly/fixturing system has been presented. An exemplar the build process for an illustrative annular assembly (T900 FBH RoV), constructed from wedge shape components has been studied. This assembly has been systematically tracked through its production process using: specific measurement, first-hand observation and manufacturing data. The data has shown that the current assembly system is producing a high quality output structure with just 0.23% radial error, there is as always however, room for further improvement.

This study has isolated a number of sources of manufacturing variation typical to the production of large welded ring assemblies. Carrying forward the identified sources of variation, a system wide assembly model can be created, which in-turn can be used as the backbone for the development of

variation conscious fixturing methodologies. Therefore, a number of useful conclusions can be pulled from this study, these being;

1. Many of the components within the assembly have specialist features, which must appear at a specific point within the rings circumference. This prevents the use of swapping components to match the assembly build conditions. Moreover, the components are supplied as a specific build-set, severely reducing the available pool of exchangeable components.
2. All the components are CMM checked prior to assembly, so the geometric quality of each component is known with a high degree of certainty before it enters the assembly fixture. This allows the "pre-tuning" of the assembly fixture to address the quality of the incoming components.
3. The production of a closed loop requires each component to contact its neighbouring components. This implies that the assembly's integrity is dependent on the quality of the face-face contact between components. This means that the fixture cannot locate the components in all Degrees of Freedom (DoF), as the face-face contact acts as the angular location for each component. Consequently, these fixtures cannot utilise the well-established 3-2-1 fixturing scheme.
4. The closed loop structure and face-face contact between components leads to a stacking of component variation, as each component is abutted to the preceding components. This stacking suggests that the assembly's circumference is proportional to the

sum of the stacked component chord lengths, so the assembly's circumference (and thus diameter) is variable. However, current fixturing methods generally do not offer variability in their location scheme.

5. The use of a segmented build process can be seen in the geometry of the assembled structure. Additionally, by welding a completed segment before building the next, each segment is likely to be influenced by weld distortion in the preceding segments. For these reasons replacing the segmented build, with a "single-hit" build methodology will probably create more consistent output geometry.
6. A consistent component is a key parameter in assembly quality. By way of example, if all the vanes had the same degree of twist (driven by stiffness) they would probably nest together, however it is the difference in twist that caused lobe geometry seen in the assembly.

Beyond conclusions concerning the assembly and fixturing, a number of important verdicts can also be drawn from observations of the illustrative annular assemblies PWP. These findings will be pulled into the welding study and used as the basis to the welding portion of this project. The findings are:

7. The PWP weld sequence can be used to influence the quality of the assembly, offering the apparent ability to control some assembly imperfections.

8. There appears to be a gap closing weld mechanism at work, which is probably exaggerated by the autogenous weld process, which increases weld shrinkage. However, it might be that weld shrinkage is just locally flattening the observed twist in the component.

5 A model of component and assembly variation

5.1 Introduction

In this chapter the effects of component and assembly variation upon annular structures will be modelled and defined mathematically. This modelling will be based upon the observations made during the critical analysis of the illustrative industrial test-piece assembly (chapter 4), and will take into account the identified sources of manufacturing variation made during that study. The model will initially define mathematically the variation within Key Characteristic (KCs) of the wedge-shaped components. Once this variation is defined the knowledge will then be used as the basis of the VCAF methodologies, before being utilised in the design of a fixture (chapter 6). Finally, the geometric drivers of non-circularity (the assembly KC) within the VCAF methodologies will be identified and modelled mathematically, allowing an understanding of the ultimate limits of these methodologies.

5.1.1 Assumptions

In order to enable the modelling of the assembly system a number of assumptions have been made about the components and assembly. These assumptions are based on the observations made during the study of the illustrative industrial test-piece and its production process. The assumptions are:

- The holistic circularity of the assembly is the quality metric of highest functional importance (i.e. the key characteristic) to the resultant annular structure, and so will be the focus of the mathematical model. Furthermore, assembly circularity is considered of greater importance than other assembly parameters such as: diametric accuracy, flatness or the absolute position of individual component features.
- Each component is unique and cannot be exchanged for other components within the assembly.
- The assembly is constructed from abutted I-shaped wedge components (shown Figure 5-1), with each having the same nominal wedge angle.
- The components used within the assembly are considered perfectly rigid non-deformable bodies.
- To create a closed segmented ring assembly each wedge must contact the components either side.
- The components are located on the internal radial face.

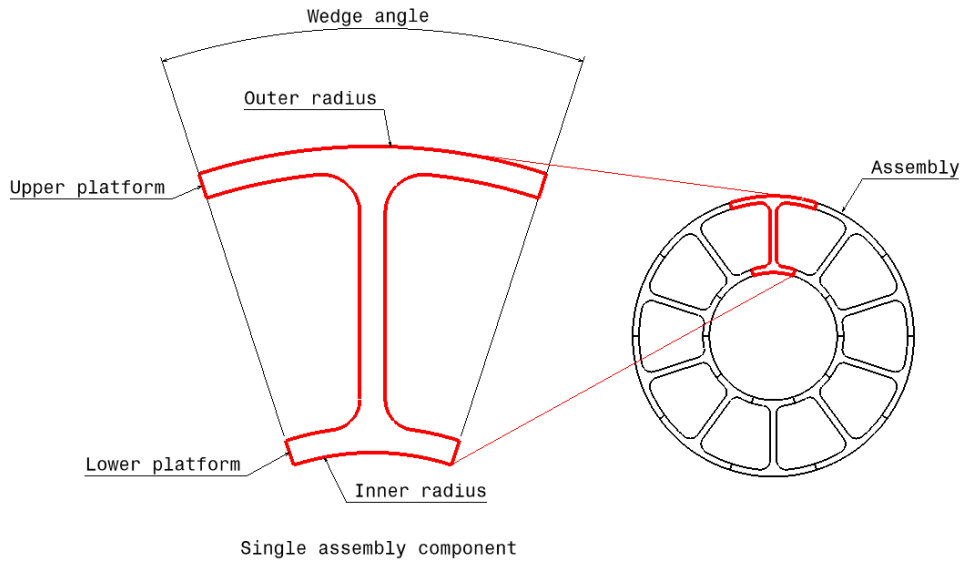


Figure 5-1 : Assumed typical style of component geometry

5.2 A model of manufacturing variation within wedge shaped assembly components.

During the geometric analysis of the illustrative industrial test-piece assembly, it was noted that the assembly contained the stacked variation of the component widths / chord lengths. The stacking of this variation was due to the requirement for a face-face contact between the assembly's components. Furthermore, the study also highlighted the influence of the component's chord length on its radial position within the assembly; with component exhibiting an oversized chord being pushed outwards. Consequently, it becomes apparent that the chordal length is the component's KC, given its fundamental importance to the quality of the assembled structure. With this in mind, the effects of component manufacturing variation upon the chord length was modelled

mathematically; so that, this could be later extrapolated into a model of the assembly system.

Eq. 1 shows a mathematical definition of an arc's chordal length, where; C is the chord length, R is the arc radius and θ the swept angle (shown diagrammatically in Figure 5-2).

$$C = 2R\,sin\left(\frac{1}{2}\theta\right) \qquad \text{Eq. 1}$$

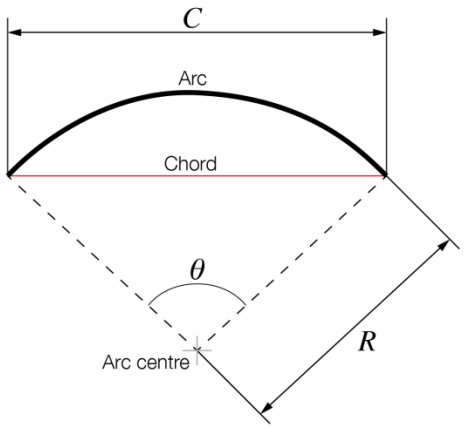


Figure 5-2 : Definition of chordal length

Although Eq. 1 defines the length of an arc's chord, it is too simplified a representation for the assembly's components. This is because the equation makes no account for the upper and lower platform geometry of the component (Figure 5-3a). The issue with this is the two platforms will be subject to implicit manufacturing variation, making it unlikely that their arc endpoints will be perfectly collinear (Figure 5-3b & Figure 5-3c). However, as there is a prerequisite for each vane to contact its neighbour, so either of these platforms can influence the effective width of the component in the context of the assembly.

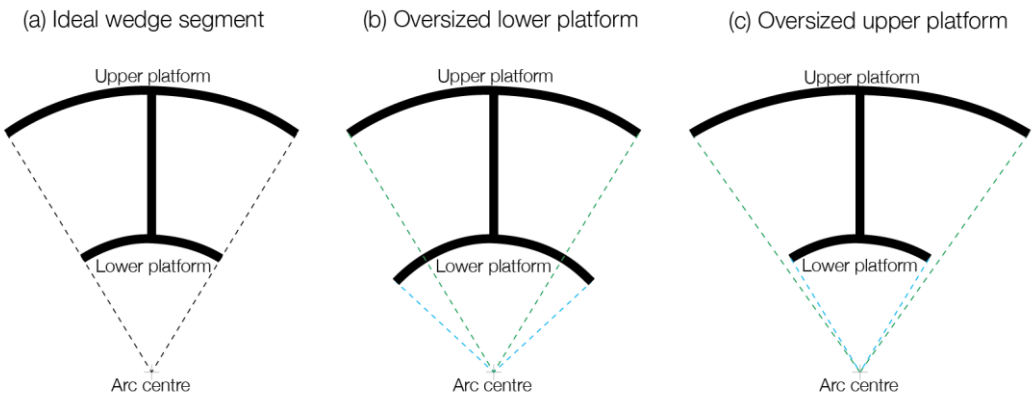


Figure 5-3 : The effect of manufacturing variation within the upper and lower platforms upon component width

5.2.1 True wedge angle

As Figure 5-4 shows, to calculate an accurate representation of the component's chord length the "true" wedge angle (γ_i) of the component must be calculated to accounting for the upper and lower platform geometries, and their implicit manufacturing variations. The initial step in determining the value of γ_i is to calculate the inner and outer chord lengths (IC_i and OC_i) using Eq. 2 and Eq. 3. Where, $I\theta_i$ is $\angle I_a I_b$, $I\theta_i$ is $\angle O_a O_b$, while IR_i and OR_i are the inner and outer radii respectively.

$$IC_i = 2 \cdot IR_i \, sin\left(\frac{1}{2} I\theta_i\right) \quad \text{Eq. 2}$$

$$OC_i = 2 \cdot OR_i \, sin\left(\frac{1}{2} O\theta_i\right) \quad \text{Eq. 3}$$

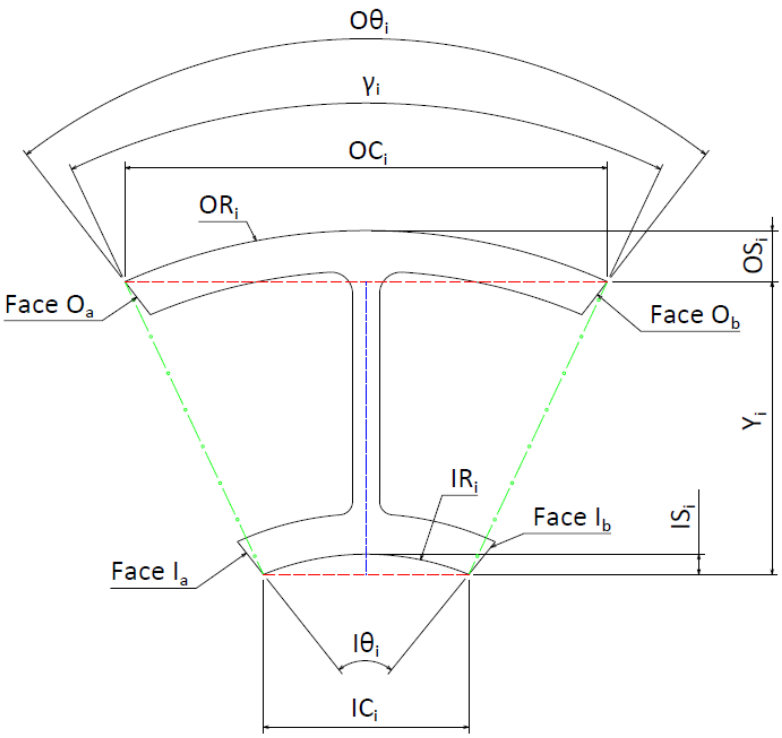


Figure 5-4 : The wedge components true angle

Classical geometric equations (Pythagoras theory) Eq. 4 and Eq. 5 are then used to calculate the upper and lower platform sagitta (IS_i and OS_i).

$$IS_i = IR_i - \sqrt{{IR_i}^2 - \left(\frac{1}{2}IC_i\right)^2} \qquad \text{Eq. 4}$$

$$OS_i = OR_i - \sqrt{{OR_i}^2 - \left(\frac{1}{2}OC_i\right)^2} \qquad \text{Eq. 5}$$

Eq. 6 is then used to generate the vertical height (Y_i) between IC_i and OC_i using sagitta of the arcs and the radii.

$$Y_i = (OR_i - OS_i) - (IR_i - IS_i) \qquad \text{Eq. 6}$$

Using Y_i and the half difference between IC_i and OC_i the true angle γ_i the component can then be calculated using trigonometry, as shown in Eq. 7.

$$\gamma_i = 2 \cdot \tan^{-1}\left(\frac{\frac{1}{2}OC_i - \frac{1}{2}IC_i}{Y_i}\right) \quad \text{Eq. 7}$$

Once γ_i has been calculated, the value can then be to used generate an adjusted inner chord length (IC_i') using *Eq. 8*.

$$IC_i' = 2 \cdot IR_i \, sin\left(\frac{1}{2}I\theta_i\right) \quad \text{Eq. 8}$$

The IC_i' describes a truer representation of the components chord length, and accommodates the implicit manufacturing variations found within the upper and lower platform geometries.

5.2.2 Out-of-plane error

The calculation of γ_i defines the angle between the theoretical face-face contact planes of the components based upon the positions of their upper and lower platforms. However as Figure 5-5 shows, the upper and lower platform faces are in themselves planes, and these planes will never be truly parallel. For this reason, the out-of-plane variation (parallelism) between the faces (O_aI_a and O_bI_b) must also be accounted for within the chord length calculation. This parallelism error will increase the chord length of the component to create an effective final inner chord length (EIC_i).

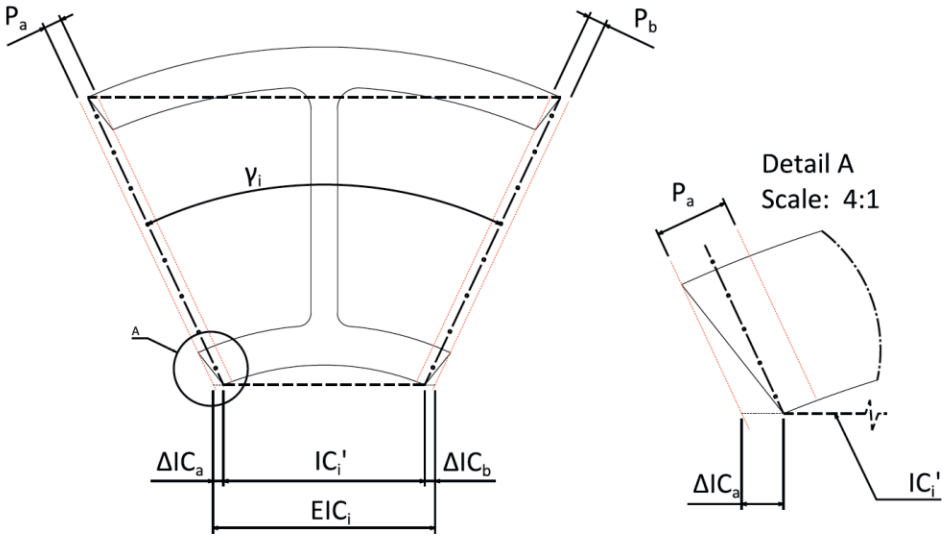


Figure 5-5 : The influence of out-of-plane error on the effective chord

Looking at Eq. 9, the method used in accounting for this parallelism error is outlined. In this equation ΔIC_a and ΔIC_b are the ISO 1101 parallelism errors (P_a and P_b) resolved along the direction of the IC_i' chord line.

$$EIC_i = IC_i' + \Delta IC_a + \Delta IC_b \qquad \text{Eq. 9}$$

Eq. 10 expresses the expanded form of *Eq. 9*, to show how the parallelism errors were resolved along the direction of the chord.

$$EIC_i = IC_i' + \left(\frac{\frac{1}{2}P_a}{\cos\left(\frac{1}{2}\gamma_i\right)}\right) + \left(\frac{\frac{1}{2}P_b}{\cos\left(\frac{1}{2}\gamma_i\right)}\right) \qquad \text{Eq. 10}$$

In summary, the presented model generates values for the effective chord length (EIC_i) and true wedge angle (γ_i) of the component's geometry. Moreover, these two values capture the typical manufacturing variations observed during the critical analysis of the illustrative industrial test-piece.

Therefore, as the chord length is implicit to assembly quality, so effective chord length (EIC_i) and true wedge angle (γ_i) are the true KCs of the wedge components. This knowledge is useful as the manufacturing variability is implicit to each of the I-shaped wedge components, and it will ultimately influence the resulting circularity of the annular assembly. This knowledge further enables the tuning of the assembly method, allowing adaption of the assembly approach to respond to the manufacturing variability within the system.

5.3 Definition of VCAF assembly methodologies

The traditional fixturing stratagem for the production of annular assemblies is to place fixed datum locators at a nominal radial position. Each assembly component is then positioned so that it touches a datum locator; deterministically defining its position relative to the assembly's centre. In a practical setting the benefit of this Fixed Datum (FD) approach is primarily one of simplicity (and thus cost). However, the method assumes a nominal build condition, and takes no account for the variation within the assembly's components. Moreover, as the components are stacked to create a ring, so deviation in the individual component chord lengths will alter the build diameter of the assembly. While, the nature of this closed loop system implies that a change in any single component will influence the geometry of the entire assembly system. Given that manufacturing variability is inevitable, it is therefore, all but impossible that the assemblies components will be geometrically nominal. This leads to two possible assembly outcomes; either the ring will be oversized, so it will not touch all the datum

locators; or the ring will be undersized, preventing it from being fully closed around the locators.

Using the foreknowledge of the effective chord length (EIC_i) and true wedge angle (γ_i) are component and thus assembly KCs, it has been possible to develop novel assembly methodologies that are variation "conscious". The proposed methods alter the fixture's datum locators specifically to suit the incoming variation of the components. This enhances the assembly's build quality by intelligently compensating for the manufacturing variation with the "smart" adjustment of location scheme within the fixture. Working in this way the best quality assembly will be produced for each given set of assembly components. The proposed VCAF methods are:

The geometric assembly method (Section 5.4): An approach that simplifies the system to a cyclic n-side polygon which is then constrained to a theoretical build circle.

The translation method (Section 5.5): This scheme calculates the ideal radial position of each wedge component by correcting the theoretical angle of the chord length relative to the assembly centre.

5.4 The geometric assembly methods

The fundamental premise of the geometric assembly methods is to simplify the assembly system to a cyclic n-side irregular polygon, with the polygon's sides being constructed from the chord lengths of the assembly's components. Once the polygon's sides are defined, they are constrained to

a fitted theoretical build circle, which ensures the circularity (the ultimate assembly KC) of the assembly. This polygonal approach replicates what was observed during the analysis of the illustrative industrial test-piece; that is the stacking of the component chord widths, causes the theoretical build circle's diameter to shrink or grow based on the amount of variation within the system. The use of a polygon has the added benefit that it ensures that each component is able to achieve at least a point contact with its neighbours.

During this project to two polygonal assembly methodologies have been identified. These two methods are differentiated by the position of the theoretical base circle relative to the position of the datum locators. The identified geometric methods are:

Circumscribed Geometric (CG): As Figure 5-6a shows, the circumscribed approach places the inter-component joints onto the theoretical build circle, to which the smallest possible circle is fit externally around the polygon.

Inscribed Geometric (IG): Shown in Figure 5-6b, this approach uses an inscribed theoretical build circle, to place the fixture's locators at the tangency point of the theoretical build circle and polygon sides. The inscribed circle is the largest possible circle that fits within the polygon.

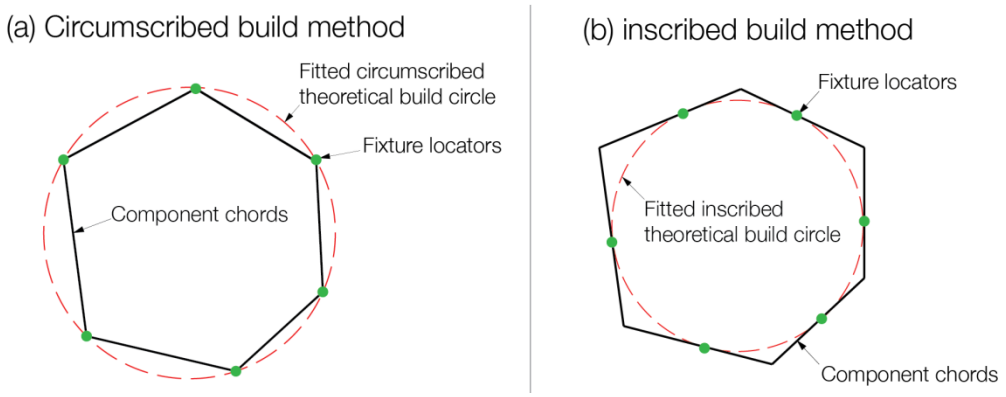


Figure 5-6 : Geometric build methods; (a) Circumscribe, (b) Inscribed

Potentially both the CG and IG approaches control the circularity errors within the final assembly. However, the two methods require differing mathematical models to describe their layout and how they respond to the input variation of the system.

5.4.1 The circumscribed geometric methodology

Figure 5-7 shows the basic lay-out of the CG VCAF method. As described previously, this approach utilises an n-sided irregular polygon that is constrained to a theoretical circumscribed build circle. While, the locators' angular positions are determined by the inter-component joint positions of the parts to be assembled.

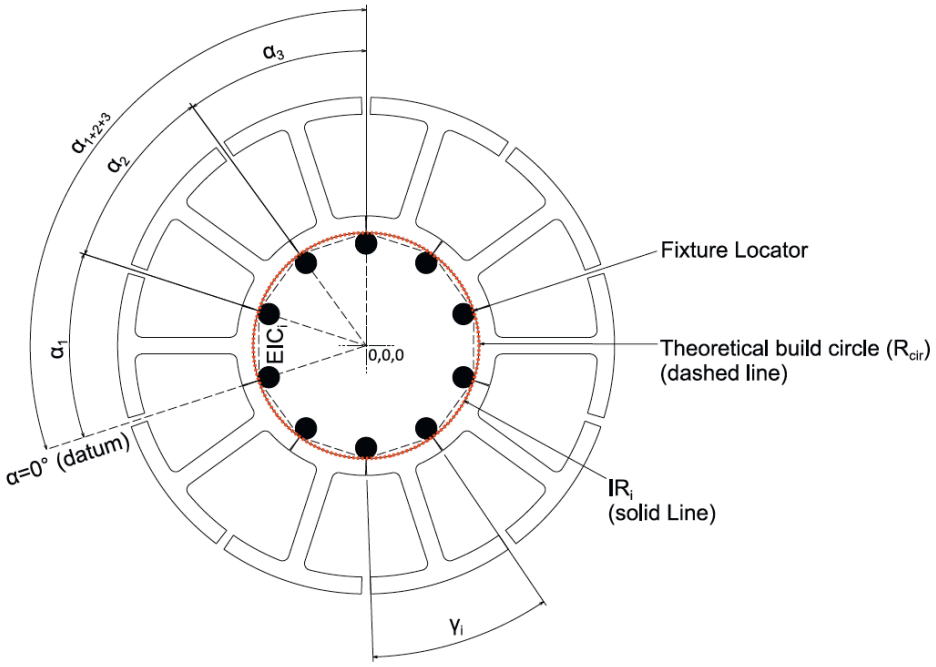


Figure 5-7 : The CG build methodology

5.1.1.1 *Precise Calculation of the theoretical build diameter*

To use this build method it is imperative that the size of the theoretical build circle be calculated prior to assembly. However, the method for calculating the theoretical build circle is not exactly straightforward, as the formulation differs depending on the number of components within the assembly. *Eq. 11* shows the principal formulation for calculating the radius of the theoretical circumscribed build circle (R_{cir}) irrespective of the number of components within the assembly.

$$2\pi = \sum_{i=1}^{n} 2 \cdot \sin^{-1}\left(\frac{\frac{1}{2}EIC_i}{R_{cir}}\right) \qquad \text{Eq. 11}$$

This equation utilises the fundamental geometric law that; within a closed polygon the sum of the internal angles equals 2π radians. *Eq. 11* calculates

the sum of the angles created by each chord length relative to the assembly's centre. So, to find the size of the theoretical build circle, this equation can then be rearranged to make R_{cir} subject. Working in this way the exact theoretical build circle can be determined; however the rearrangement of this formula is computationally complex especially in larger assemblies.

This approach for calculating the circumscribed build circle has been verified with a CAD study. The study was performed using several parametric sketches (Figure 5-8 shows two examples) each containing a closed polygon with a circle constrained to it. The constrained circle was then measured and compared to the results of the calculation. In each case the calculation robustly predicted the size of the circumscribed circle with a high degree of accuracy.

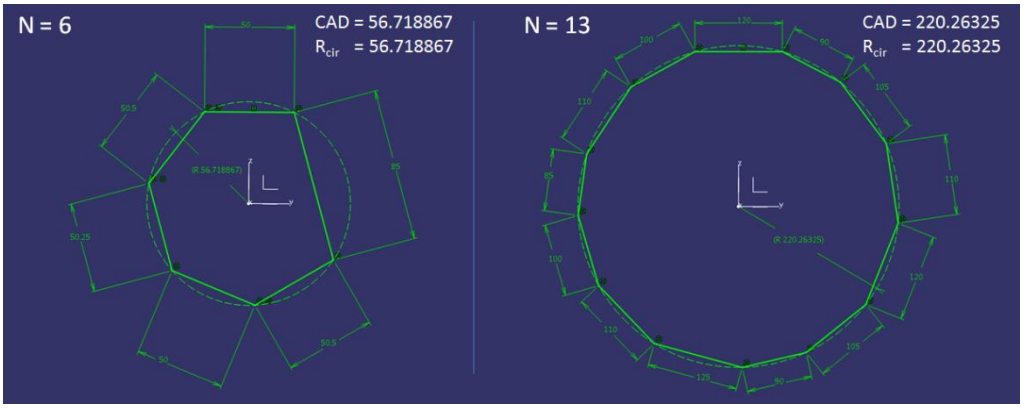


Figure 5-8 : Typical CAD sketches used in verified of CG set-up model

A final step in using the CG build methodology is to generate the true radial positions for the fixture's datum locators. In order to do this, the diameter of the location pins should also be accounted for using Eq. 12. Where, *LD* is

the nominal diameter of the fixture's location pins, and Rb is the build radius of the fixture.

$$Rb = R_{cir} - \left(\frac{LD}{2}\right) \quad \text{Eq. 12}$$

5.1.1.2 *Estimated calculation of the theoretical build diameter*

Beyond the exact calculation for the theoretical build diameter of the CG method, an estimated approach was also developed. This estimated approach offers a computationally less intense method of deriving R_{cir}, but at the cost of overall accuracy. The estimated approach is based upon the geometric equation (*Eq. 13*) for the calculation of a circumscribed circle of a regular polygon with n sides, where L is the length of the regular polygon's sides.

$$R_{cir} = \frac{\frac{1}{2}L}{\sin\left(\frac{\pi}{n}\right)} \quad \text{Eq. 13}$$

As *Eq. 13* is intended for an idealised regular polygon, it assumes there is no variability within the lengths of the polygon's sides. However, as a manufactured system will intrinsically contain some variation, so the chord lengths (EIC_i) within the assembly need to be aggregated to summarise the system's variability, as shown in *Eq. 14*.

$$R_{cir} = \frac{\frac{1}{2}\overline{EIC_i}}{\sin\left(\frac{\pi}{n}\right)} \quad \text{Eq. 14}$$

As *Eq. 14* uses an averaging method, a small scale Monte Carlo study was undertaken in order to verify the quality of the estimate. The Monte Carlo study saw the generation of 500 random, normally distributed chord lengths. These randomised chord lengths where based on a 10 segment assembly, with a 200mm nominal internal diameter; giving a nominal length of 61.803mm at a 36° wedge angle. A standard deviation of 5mm was applied to the chord lengths during the randomisation. This distribution interval is somewhat inflated when compared to what would be expected from an accurate manufacturing process. However, the expectation is that the averaging estimate would become less accurate as variation within the dataset increased, so an exaggerated distribution interval would highlight the estimates robustness.

The 500 chord lengths were assembled to create 50 sample polygons. Arithmetic (*Eq. 15*) and geometric (*Eq. 16*) averaging methods were then used to estimate the radial size of the theoretical build circle.

$$R_{cir} = \frac{\frac{1}{n}\sum_{i=1}^{n}\frac{1}{2}EIC_i}{\sin\left(\frac{\pi}{n}\right)} \qquad \text{Eq. 15}$$

$$R_{cir} = \frac{\sqrt[n]{\prod_{i=1}^{n}\frac{1}{2}EIC_i}}{\sin\left(\frac{\pi}{n}\right)} \qquad \text{Eq. 16}$$

Using the same randomised data as the averaging predictions, a parameterised CAD sketch was used to geometrically construct each of the

polygons (via a design table). The circumscribed circle for each of the 50 polygons was then measured. Using the CAD results as the base values, the averaged estimates (arithmetic and geometric) where then subtracted from these CAD measurements and plotted (Figure 5-9).

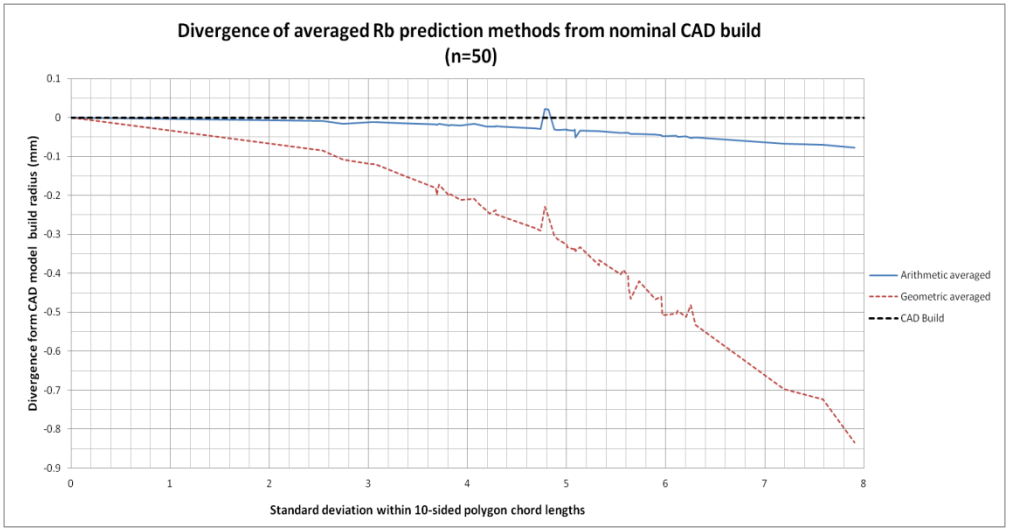


Figure 5-9 : Comparison of averaging methods verified against CAD nominal

The results showed that the arithmetic averaging method, gave a good approximation of the theoretical build diameter even with exaggerated amounts of variability in the chord length data. The plot also shows that the geometric averaging method fared less well, especially at higher levels of deviation. A further point of note is that both methods show a tendency to underestimate the circumscribed circle's resultant diameter.

5.1.1.3 *The locators angular position*

The CG methodology requires that the fixture's locators are placed radially at the theoretical build diameter (R_{cir}). While the angular position of each locator is dictated by the interface/joints between the components. However, the angular position of each locator relative to the centre of the

assembly will alter depending upon the size of the theoretical build circle. This is shown in Figure 5-10, because the chord moves from the radial position R_{cir} to $R_{cir}{}'$, the angle relative to the assembly centre also changes from β_i to β_i'. This implies that the angular position of each locator cannot be determined using just the true angle (γ_i) of each component. Therefore, the angular position of each fixture locator must be calculated based upon the value of R_{cir}.

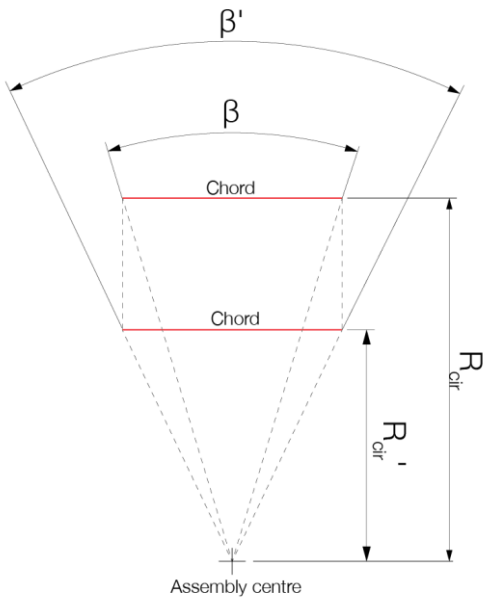


Figure 5-10 : Assembly angle in respect to chord's radial position.

Using an inverse trigonometric function *Eq. 17* derives the angle of "current" locator (β_i) relative to the assembly's centre before, summing it with the previous angle calculations to obtain the current angular position of the system.

$$\beta_i = 2 \cdot \sin^{-1}\left(\frac{\frac{1}{2}EIC_i}{R_{cir}}\right) + \sum_{i=1}^{n-1} \beta_{i-1} \qquad \text{Eq. 17}$$

In summary, the CG VCAF method uses a circumscribed theoretical build circle, which is calculated in response to the incoming variation of the components. The diametric size of this theoretical build circle can be calculated using one of two methods, either: *Eq. 11*, an exact but computationally complex approach; or *Eq. 15* a robust estimated approach. The positions of the fixtures locators can then be computed using *Eq. 12* (radial position) and *Eq. 17* (angular position).

5.4.2 The inscribed geometric methodology

Figure 5-11 shows the basic lay-out of the IG VCAF method. This build methodology uses an n-sided irregular polygon that is constrained to a theoretical inscribed build circle. Using this approach the angular position of the datums are determined by the tangency points of the polygon against the inscribed circle.

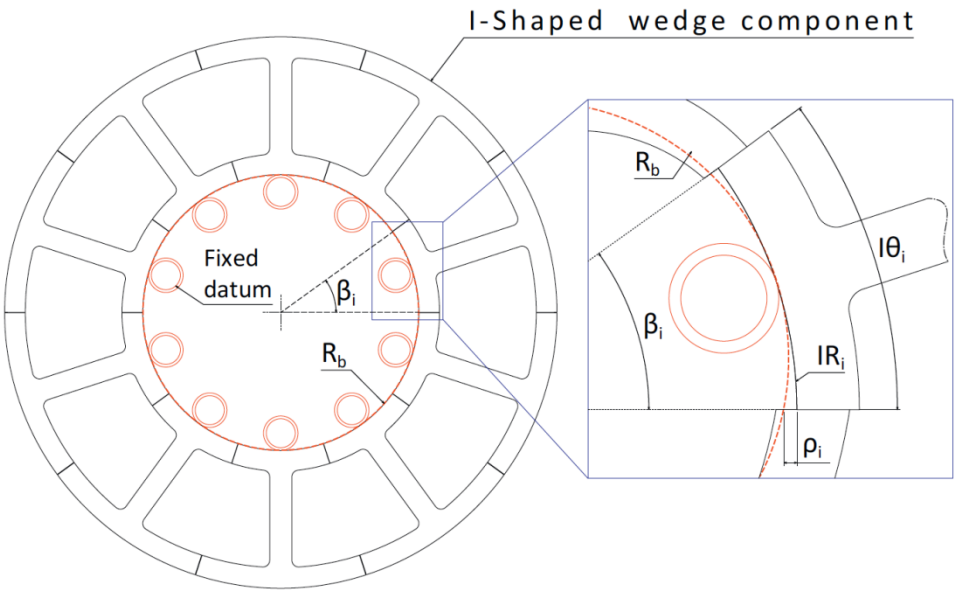


Figure 5-11 : The IG build methodology

5.1.1.4 *The calculation for the theoretical build diameter*

Unlike the CG method, the IG method appears to have no precise formulation for calculating the theoretical build circle (R_{ins}), so it relies instead upon an estimated calculation. The lack of a precise solution is due to the congruency between the chordal tangency points and the theoretical build circle (discussed in greater depth in section 5.1.1.5). Due to this, the geometry contains too many unknown quantities (i.e. build radius, locale of tangency points and/or wedge angles) to allow the creation of a discrete formulation. Consequently, the estimated calculation for R_{ins} must utilise the geometric equation of an inscribed circle of a regular polygon as its basis (*Eq. 18*).

$$R_{ins} = \frac{\frac{1}{2}L}{\tan\left(\frac{\pi}{n}\right)} \qquad \text{Eq. 18}$$

In-line with the approximation method used for the CG approach, this equation anticipates an ideal regular polygon, so must be transposed into *Eq. 19* to account for the manufacturing deviation within the assembly system.

$$R_{ins} = \frac{\frac{1}{2}\overline{EIC_i}}{\tan\left(\frac{\pi}{n}\right)} \qquad \text{Eq. 19}$$

As with the CG build previously, a comparative CAD study was performed to verify the best averaging method for use within *Eq. 19*. The same approach and chord length data was used for both CAD studies, but *Eq. 20* and *Eq. 21* were used in the R_{ins} CAD study, instead of *Eq. 15* and *Eq. 16*.

$$R_{ins} = \frac{\frac{1}{n}\sum_{i=1}^{n}\frac{1}{2}EIC_i}{\tan\left(\frac{\pi}{n}\right)} \qquad \text{Eq. 20}$$

$$R_{ins} = \frac{\sqrt[n]{\prod_{i=1}^{n}\frac{1}{2}EIC_i}}{\tan\left(\frac{\pi}{n}\right)} \qquad \text{Eq. 21}$$

The results (Figure 5-12) of the inscribed CAD verification study showed a more erratic response to manufacturing variation than the CG build approach. This erratic response appears to increase substantially as the chord length variations exceeded 3mm of standard deviation within a given assembly. However, of the two equations under scrutiny the geometric averaging method (*Eq. 21*) appear to offer a slightly more reliable

prediction. Also in contrast to the CG approach, the IG build approach appears to slightly overestimate the size of the theoretical build circle.

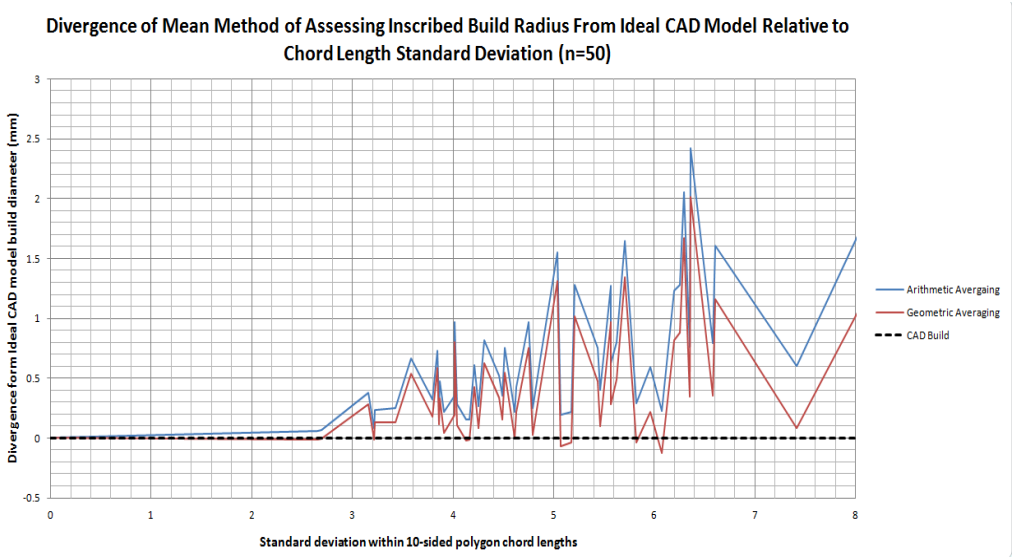


Figure 5-12 : Comparison of averaging methods against CAD nominal

The IG build methodology does not place the fixture's locators directly onto the theoretical build circle. Therefore, in order to calculate the radial position of each fixture locator (FL_i), the sagitta of the arc segment and the diameter of the datum locator (LD), must also be considered (Eq. 22)

$$FL_i = R_{ins} + \left(IR_i - \sqrt{IR_i^2 - \left(\frac{EIC_i}{2}\right)^2} \right) - \frac{LD}{2} \qquad \text{Eq. 22}$$

5.1.1.5 *The locators angular position*

As defined previously, the IG approach places the fixture's datum locators at the tangency point between the theoretical build circle and the component's chord. However, this tangency point will move along the chordal line, its position being dependent upon the ratio of its length relative to the chord lengths of the neighbouring components. The reason

for this movement in the tangency point is due to a fundamental geometric theorem [242], that; two tangential lines drawn externally to a circle and originating from the same point will be congruent. This can be seen in Figure 5-13, where both line segments labelled "T_1" are the same length, as are "T_2", "T_3" and so on. However, because the lines $EIC_1, EIC_2 \cdots EIC_5$ are of differing lengths, so the tangency point changes its position based on the length of each line relative to its neighbours. This situation implies that in order to find the position of any single locator the entire system must be solved. Consequently, the more components an assembly system has, the more complex the solution becomes. For brevity therefore, the system shown in Figure 5-13 will be used as an example of how to solve these systems.

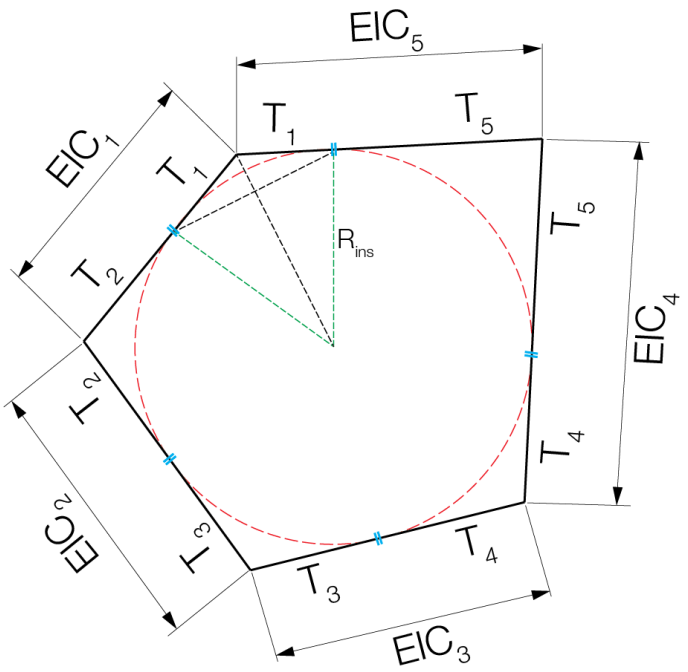


Figure 5-13 : The influence of line length upon tangency point

Looking at Figure 5-13, equations Eq. 23 to Eq. 27 are true.

$$EIC_1 = T_1 + T_2 \qquad \text{Eq. 23}$$

$$T_2 = EIC_2 - T_3 \qquad \textit{Eq. 24}$$

$$T_3 = EIC_3 - T_4 \qquad \text{Eq. 25}$$

$$T_4 = EIC_5 - T_5 \qquad \text{Eq. 26}$$

$$T_5 = EIC_5 - T_1 \qquad \text{Eq. 27}$$

Therefore, substituting Eq. 24 into Eq. 23, creates Eq. 28.

$$EIC_1 = T_1 + (EIC_2 - T_2) \qquad \textit{Eq. 28}$$

Building upon this, and substituting Eq. 25 into Eq. 28, derives Eq. 29.

$$EIC_1 = T_1 + \big(EIC_2 - (EIC_3 - T_4)\big) \qquad \textit{Eq. 29}$$

This substitution continues until all the terms are combined into one equation, so for the example polygon Eq. 30 would result.

$$EIC_1 = T_1 + \Big(EIC_2 - \big(EIC_3 - \big(EIC_4 - (EIC_5 - T_1)\big)\big)\Big) \qquad \textit{Eq. 30}$$

Expanding the bracket of Eq. 30 generates Eq. 31.

$$EIC_1 = T_1 + EIC_2 - EIC_3 + EIC_4 - EIC_5 + T_1 \qquad \textit{Eq. 31}$$

Eq. 31 can then be rearranging to make length T_1 the subject, (Eq. 32) to find the position of the tangency point.

$$T_1 = \frac{EIC_1 - EIC_2 + EIC_3 - EIC_4 + EIC_1}{2} \qquad \textit{Eq. 32}$$

Once the position of a single tangency point has been isolated, the others within the system can be defined easily, due to the congruency within the geometry; especially, as the lengths of the polygon's sides are known through chord measurements and EIC_i calculations. An inverse trigonometric function can then be used to calculate the angular position of the fixture's locators, Eq. 33.

$$\alpha_i = \left(\sum_{i=1}^{n} \alpha_{i-1}\right) + 2 \cdot \sin^{-1}\left(\frac{T_i}{R_{ins}}\right) \qquad \textit{Eq. 33}$$

These calculations have been checked against a number of CAD sketches (Figure 5-14). In the comparison between the sketches and calculations a strong correlation was demonstrated, however there is a substantial limitation to the IG approach. The limitation is that, the angular positions / tangency points of the fixtures locators can only be calculated for polygons with an odd number of sides. This issue arises while expanding brackets of the conjoined equation. During this expansion an odd sided polygon derives a form of the type shown in Eq. 34, while an even sided polygon will take on the form shown in Eq. 35.

$$EIC_1 = T_1 + EIC_2 - EIC_3 \cdots \cdots EIC_n + T_1 \qquad \text{Eq. 34}$$

$$EIC_1 = T_1 + EIC_2 - EIC_3 \cdots \cdots EIC_n - T_1 \qquad \text{Eq. 35}$$

As can be seen, Eq. 35's expanded form shows a $-T_1$ as the equation's final term. This $-T_1$ term cancels-out the $T_1 +$ at the start of the equation,

causing the formulation to breakdown (resulting in zero). This problem would appear therefore to be an issue of systemic symmetry, with an odd-sided polygon braking this symmetry. As an interesting side note, the parametric CAD sketches also did not resolve when drawing even-sided inscribed polygons. It was tried in several different CAD packages, and each one generated an over-constrained sketch condition when all the side lengths were added. Given the mathematical sketch description used within the CAD software differs from the method outlined here, it would suggest that this problem is inherent to the geometric form, rather than the model presented.

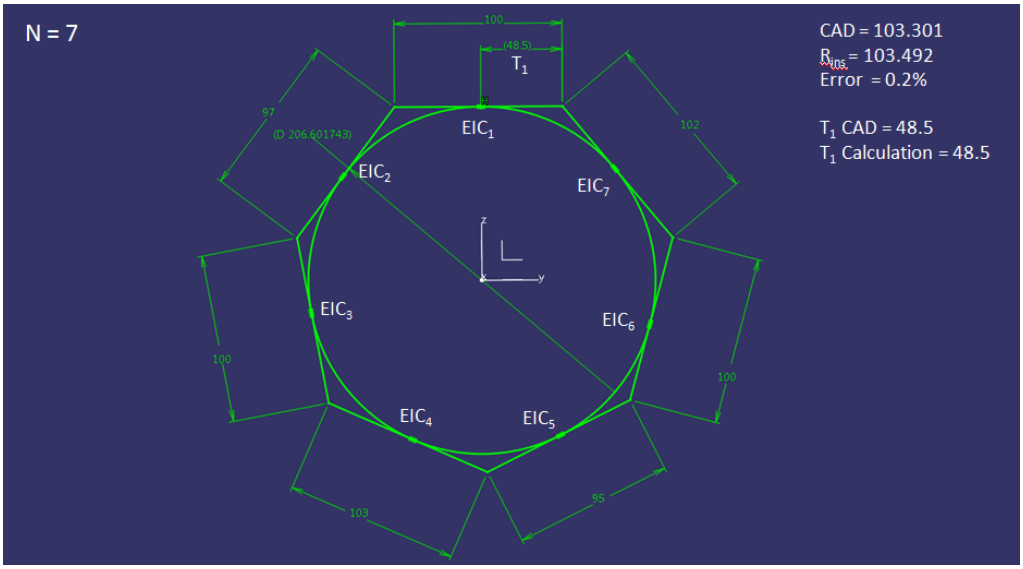


Figure 5-14 : A typical CAD sketch, used as verified of IG set-up model

To summarise the IG build method, the radial position of the fixture's datum locators can be identified using Eq. 22, after the pre-calculation of the theoretical build circle (Eq. 21). While, the angular position for each locator block can be found with Eq. 33. The formulation expressed in this study appears to show a reliable build prediction (especially at low levels of

component variation), however the IG approach appears fundamentally flawed; being constrained to assemblies with an odd number of parts/side.

5.4.3 Angular breaking errors

A fundamental prerequisite for creating a closed polygonal form is that the sum of the internal angles (shown α_n in Figure 5-15) must equal 2π radians. However, given the implicit manufacturing variation within the components, it is essentially impossible that the sum of the assembly's component wedge angles (γ_i) will equal precisely 2π radians.

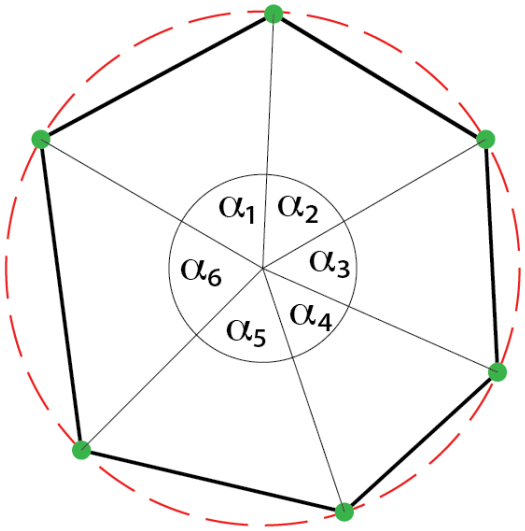


Figure 5-15 : The internal angles of a polygon

The most likely scenario therefore is that the annular summation within the assembly will either be <2π or >2π radians. The consequence of these two geometric conditions is shown in Figure 5-16a and Figure 5-16b, where small angular fractures can be seen at the inner or outer circumference of the assembled geometry. The position of these "angular breaking errors" is

dependent entirely upon the sum of γ_i within the assembly. In assemblies where the sum of the component angles is less than 2π radians, the angular breaking errors will occur at the outer edge of the assembly. Inversely, if the sum of the angles is greater than 2π radians they will occur at the inner edge of the assembly. Furthermore, these angular breaking errors are systemic geometric conditions, in that; if some wedges are oversized, but the sum of the assembly is actually undersized, then **all** the angular breaking errors will occur at the outer edge. To state another way, there will be no mixing of the internal and external angular breaking errors within a single assembly.

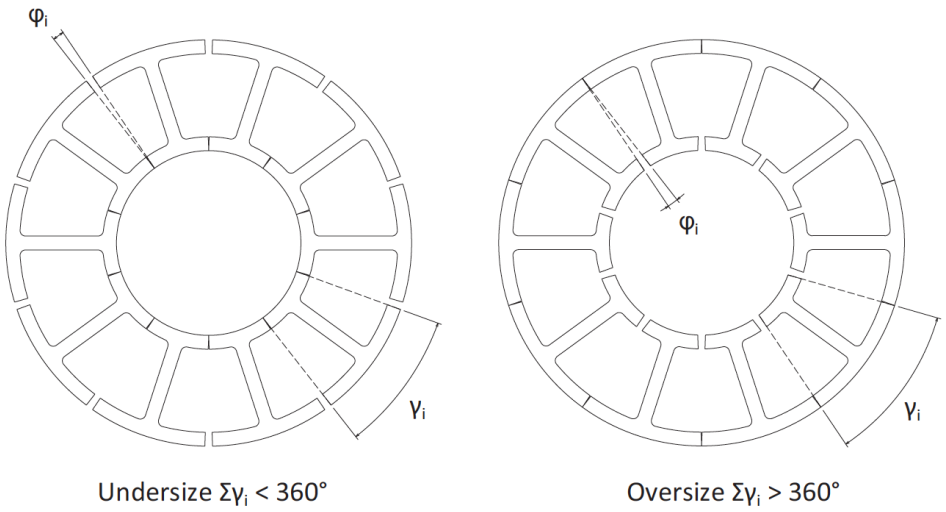


Figure 5-16 : Undersized (a) and oversized (b) assembled wedge angles

This known, the amount of angular breaking present in any given assembly can be quantified with Eq. 36, where $\sum \varphi_i$ is the total amount of angular breaking error present at either the outer (if negative) or inner (if positive) circumference of the ring. This knowledge reinforces the importance of the "true" wedge angle as key characteristic, as γ_i has two impacts upon

assembly quality. Moreover, γ_i determines the size and position of assembly gaps (which impact welding – see chapter 7), as well as the length of the component chord.

$$\sum_{i=1}^{n} \varphi_i = 2\pi - \sum_{i=1}^{n} \gamma_i \qquad \textit{Eq. 36}$$

As previously noted, any manufactured component contains intrinsic manufacturing variations, it is therefore all but impossible that the sum of the wedge angles within an assembly will equal precisely 2π radians. The inference of this situation is that none of the components within the assembly are likely to have a full-face contact with their neighbours. Instead, each assembly component will exhibit a point contact with its neighbours. Consequently, defining the fixture location scheme through the application of the typical 3-2-1 methodology; the inter-component contact face must be considered a single point contact. This implies that if a single locator is placed at the inner radius (i.e. IG approach), the component is likely to exhibit an ability to rotate (rock) about the location pin's axis. However, by placing the inner radius on to a theoretical location line (i.e. by placing two locators on the inner radius), this rotational DoF will then be blocked.

The position of the angular breaking errors within the assembly has a profound implication for the location strategy used in a given fixture. This is especially true when using a datuming approach which places locators at the inter-component joints, such as the CG method. In these situations the positions of the angular breaking errors must be controlled, so that they do

not fall on the location faces of the assembly; that is, for an oversized assembly (>2π radians) the location should be at the outer circumference of the assembly, while for an undersized assembly (<2π radians) the locators should be placed on the inner radius. This approach avoids the geometric ambiguity caused by the components contacting the locator at the angular breaks, increasing repeatability of the assembly process. In addition, the mathematics used in the pre-calculation of R_{cir} or R_{ins}, must be adapted to utilise either the inner or outer polygonal chord chain depending upon the net geometric conditions of the assembly. Performing the R_{cir} or R_{ins} calculation using the wrong (inner or outer) polygon chain is likely to inhibit the fixture's ability to locate the assembly fully.

For the reason of avoiding the angular breaking errors splits at fixture locator positions, it stands to reason that the assembly tolerances must be biased to support the intended fixturing location approach. To maintain manufacturing repeatability, it is essential that the underlying net geometric conditions be consistently either under or oversized. Moreover, if an internal location scheme is used in a fixture, every assembly must be undersized, so the assembly's components should be designed with a minus-minus tolerance. While, for an external location scheme a plus-plus tolerance approach must be taken. Consequently, it is essential that a plus-minus tolerance scheme is not used in an annular assembly, as it may be that tolerance stacking leads to assemblies being constructed that are not correct to the locator positions. The consequence therefore of a plus-minus

component tolerance scheme would potentially be a loss of production repeatability.

5.5 The translational build method

Figure 5-17 shows, the Translation Build (TB) VCAF approach which corrects per-part chord length manufacturing variation by individually adjusting each components radial position relative to the assembly's centre. Using this mechanism each component's chord is placed in its true position, rather than trying to fit all the assembly components to a common reference circle, as seen in the geometric (CG and IG) methods.

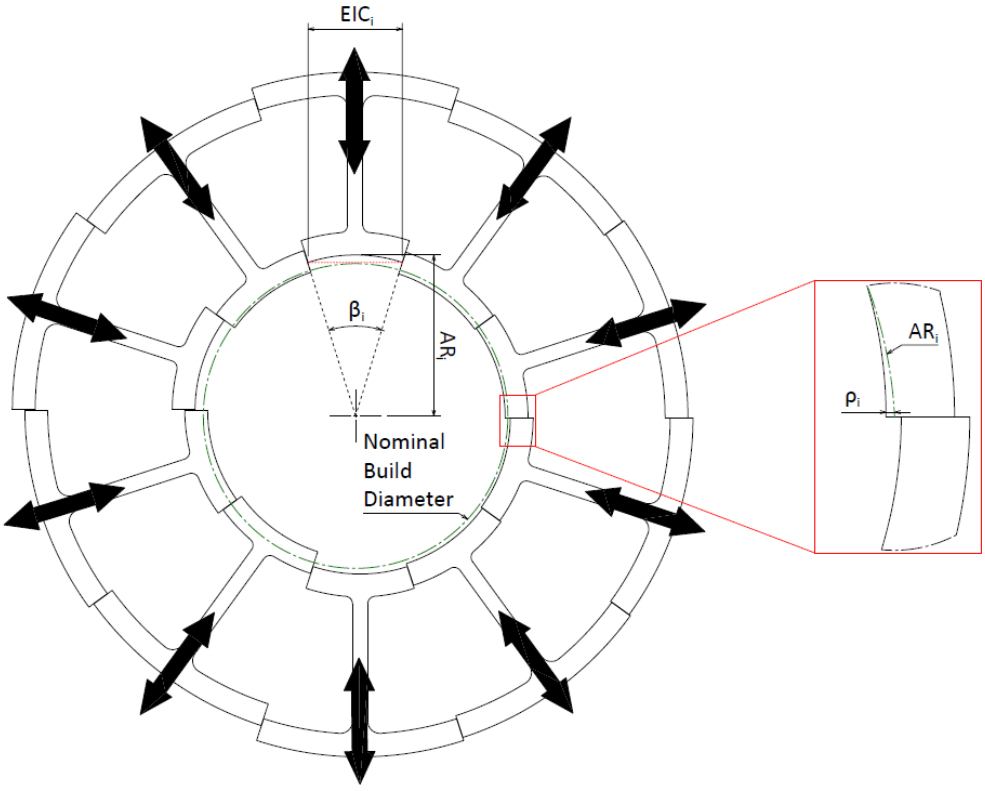


Figure 5-17 : The TB methodology

Looking again at Figure 5-18, striking a line from both ends of the EIC_i to the assembly centre a theoretical angle β_i is created. This angle is

dependent upon the chord's distance from the centre of the assembly, with it becoming more obtuse as the EIC_i chordal line moves towards the assemblies centre, and more acute as its position is pushed further outwards. However, the fundamental geometric theorems still apply to the system, so in order to create a fully closed system Eq. 37 must hold true.

$$2\pi = \sum_{i=0}^{n} \beta_i \qquad \textit{Eq. 37}$$

In an idealised closed ring assembly system with zero variation within the components, the nominal component angle (α) is 2π radians divided by the number of segments (n) in the assembly, as expressed in Eq. 38.

$$\alpha = \frac{2\pi}{n} \qquad \textit{Eq. 38}$$

As the TB methodology seeks to consolidate the requirements of Eq. 37 and Eq. 38, by independently translating each component radially so that its β_i angle matches the nominal α angle of the idealised assembly system. As a consequence of β_i being based upon the EIC_i, so the translation will be considerate of any manufacturing variation within the chordal length, ensuring each component is positioned in its true position.

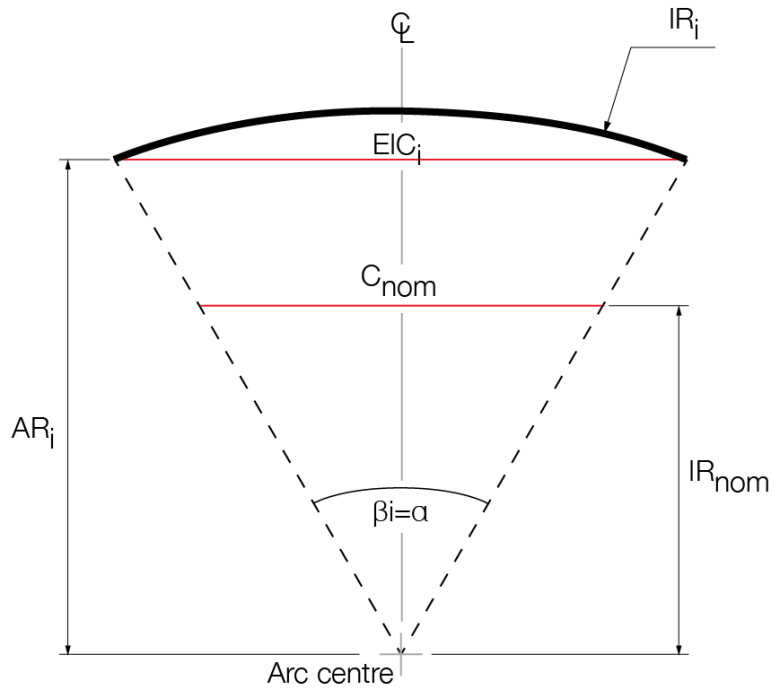


Figure 5-18 : Translation of the choral line' EIC_i to correct β_i

Eq. 39 shows the calculation required to define a component's assembly radial position (AR_i), which corrects the manufacturing variation within its chord length by matching the β_i and α angles.

$$AR_i = \frac{\frac{1}{2}EIC_i}{\sin\left(\frac{\pi}{n}\right)} \qquad \textit{Eq. 39}$$

As each of the assembly's components are moved independently of their neighbours, so it is likely that stepping will occur between each component. Furthermore, as each wedge has its own intrinsic manufacturing variation, which varies on a per-part basis, so each wedge will require a different corrective radial position. The consequence of this is that a single common datum-locator block cannot be used at the joint positions (as with the CG build method), as the datum locator will only touch one of the components,

not both. Instead a central (chord mid-point) locator should be used in a manner similar to the IG method. Moreover, as the locator is to be positioned at the centre of the EIC_i chordal length, so the chord Sagitta and the diameter of the fixture location pins must be considered during the calculation of the corrected radial position. Eq. 40 shows the calculation of the corrected build radius (Rb_i) to include the Sagitta height and pin diameter, where LD_i is the diameter of the location pin used for fixturing.

$$Rb_i = AR_i + \left(IR_i - \sqrt{IR_i^2 \left(\frac{EIC_i}{2}\right)^2} \right) - \frac{LD_i}{2} \qquad Eq.\ 40$$

A repercussion of the TB method matching the β_i and α values is that the angular positions of the fixture's locator blocks will remain constant at α radians for the whole assembly. As a consequential benefit the degree of angular breaking within a TB assembly is likely to be lower than that of an assembly constructed using a geometric technique. However, this is at the cost of stepping within the inner and outer circumference of the assembly. But, as the exemplar assembly of chapter 4

In summary, the TB build method translates each individual component radially to correct the manufacturing variations within the EIC_i chord length KC. The TB method manages this through matching the angle of the measured chord relative to the assembly centre (β_i) to the nominal assembly wedge angle (α). The assembled radial position of the EIC_i chord, AR_i can be calculated for each assembled component using Eq. 39. However, Eq. 40 should be used to calculate the radial placement of the

fixture datum locators. While, the angular position will match the nominal wedge angle (α) for the assemblies components, which can be calculated using Eq. 38.

5.6 Intrinsic non-circularities

In each of the VCAF build approaches outlined, the radial position of the assembled components are altered either en-masse or individually to correct for manufacturing variability in the component's chord length. This positional change alters the inner diameter of the physical embodiment of the assembly from that of the design nominal. However, the diameter of the assembled components will still be manufactured in accordance with the design nominal of the assembly. Add to this, the implicit manufacturing variation in the component's inner radius, and these factors combine to make the geometry of the assembly's inner/outer diameter quite uncertain. This disparity between the theoretical build diameter and the component's inner radial geometry is resolved in one of two geometric forms by the fixture, either; a lobed form (Figure 5-19a) or stepping (Figure 5-19b). The resolution of the inner radii geometric uncertainties within the fixture is dependent upon the position of the locators relative to the chord length. Moreover, given that circularity is a KC of the final annular structure, so consideration of these intrinsic non-circularities is needed for a full quality impact of assembly/part variation.

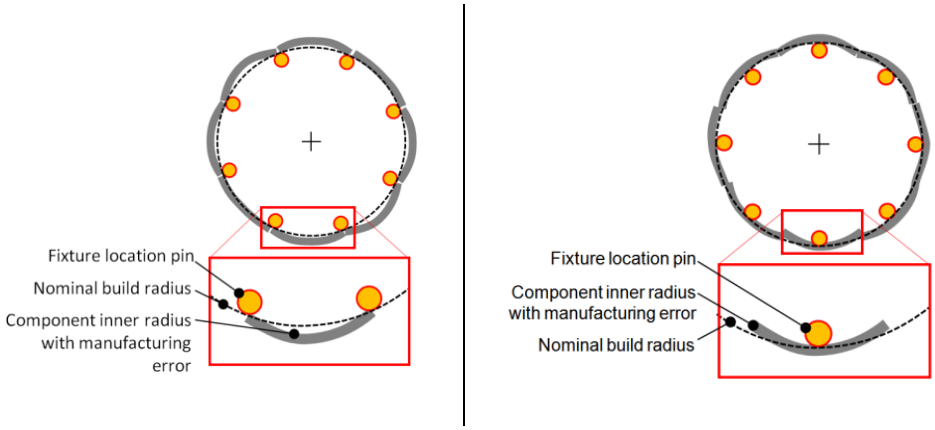


Figure 5-19 : a) Lobed geometry b) Stepped geometry

5.6.1 Lobed non-circularities

The lobed form of non-circularity is primarily evident in fixture location schemes where the fixture locators are placed at the joints between the components (i.e. the CG build method). As Figure 5-20 shows, the non-circularity in the lobed case originates from the difference between the theoretical build diameter and the radius of the component, and is driven by them both sharing a common chordal line (EIC_i).

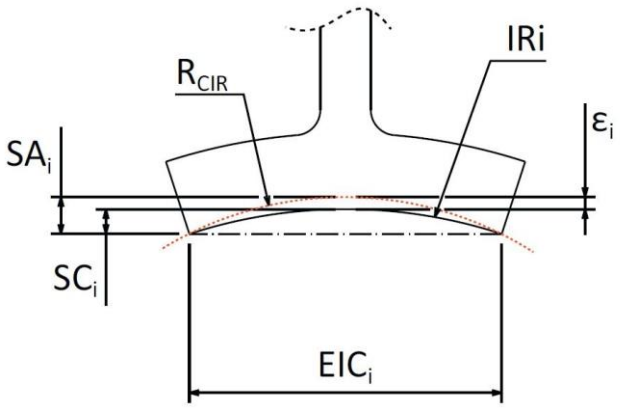


Figure 5-20 : Lobed non-circularity type

In these conditions the deviation from the assembly's nominal circular geometry (ε_i) can be found by subtracting the sagitta of the theoretical

build circle used in the assembly (SA_i), from the sagitta of the component geometry (SC_i). This is calculation is expressed in Eq. 41. As a point of interest, for an internally located assembly R_{cir} will always be smaller than IR_i. Indeed, should IR_i be smaller than R_{cir} then the assembly will fail to resolve to a fully closed geometric form.

$$\varepsilon_i = SC_i - SA_i \qquad \textit{Eq. 41}$$

Eq. 42 shows the expansion of Eq. 41 to show the influential geometric factors which drive the lobed non-circularities.

$$\varepsilon_i = \left(IR_i - \sqrt{IR_i^2 - \left(\frac{EIC_i}{2}\right)^2}\right) - \left(R_{cir} - \sqrt{R_{cir}^2 - \left(\frac{EIC_i}{2}\right)^2}\right) \qquad \textit{Eq. 42}$$

In order to determine the circularity of the resultant assembly, the Eq. 42 calculation must be performed for every component within the assembly. From this calculated dataset the largest value (ε_{max}) will reflect the MZC for the assembly, while R_{cir} will be the IMZCI (with the OMZCI therefore being R_{cir} + ε_{max}). It should be noted that this calculation assembly assumes a perfect idealised fixture, so the ε_{max} actually represents the highest possible circularity that could be attained using the build method and components. Moreover, in reality further sources of manufacturing and fixturing variation will be present in the system leading to higher "real world" MZC measurements.

5.6.2 Stepped non-circularities

The stepped non-circularities (Figure 5-21) are intrinsic to the locator schemes where the datum locators are placed at the mid-point of the

chordal line. These stepped non-circularities are of particular interest, as they not only impact the assembly's circularity KC but also the profile KC requirement (which ensure an uninterrupted airflow). The steps are created by an incongruity between the manufactured inner diameter of the components and the build diameter of the assembly. In addition, the inner radius (IR_i) of each component is also subject to independent manufacturing variations, so the stepping will also be driven by the relative differences in inner radius between neighbouring components.

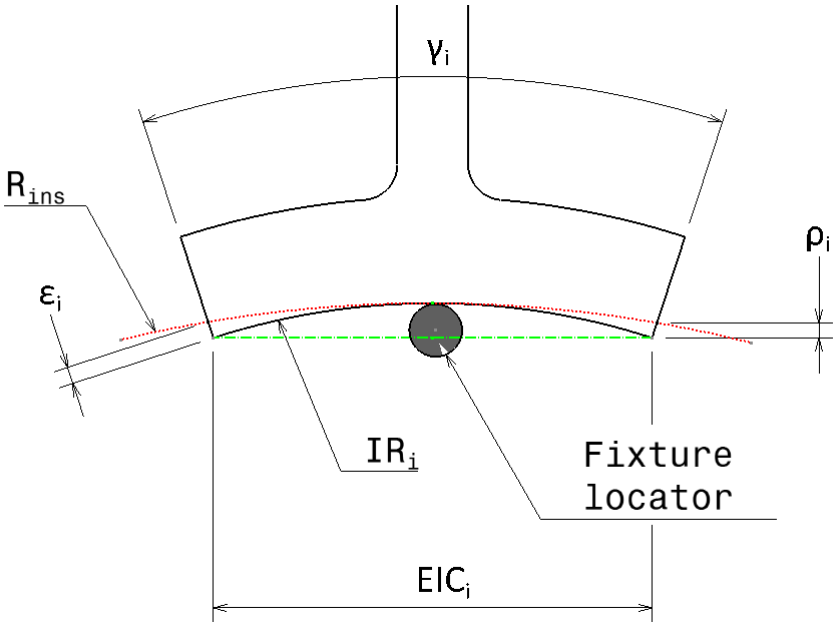


Figure 5-21 : Stepped non-circularities

To calculate the extent of the stepping, the height change between the sagitta of the assembly and the component must be calculated as per Eq. 41. However, the expanded version of this equation differs from the previous CG incarnation (Eq. 42), requiring instead that Eq. 43 is used for IG or Eq. 44 for a TB location scheme.

$$\varepsilon_i = \left(R_{ins} - \sqrt{R_{ins}^2 - \left(\frac{EIC_i}{2}\right)^2}\right) - \left(IR_i - \sqrt{IR_i^2 - \left(\frac{EIC_i}{2}\right)^2}\right) \qquad \textit{Eq. 43}$$

$$\varepsilon_i = \left(AR_i - \sqrt{AR_i^2 - \left(\frac{EIC_i}{2}\right)^2}\right) - \left(IR_i - \sqrt{IR_i^2 - \left(\frac{EIC_i}{2}\right)^2}\right) \qquad \text{Eq. 44}$$

These equations generate the vertical drop distance between the assembly and component sagitta, however the step offset occurs at the angle of the wedge face. Therefore, this value must be projected onto the angled face of the component, to give the size of the step (ρ_i) at edge of the component. This projection can be perform using Eq. 45.

$$\rho_i = \frac{\varepsilon_i}{\cos\left(\frac{\gamma_i}{2}\right)} \qquad \textit{Eq. 45}$$

The size of any step can then be calculated comparing the ρ_i value for any two adjacent components. While, in terms of the ISO circularity measurement for the IG build method the largest ρ_i absolute value within the assembled components (ρ_{max}) will be equivalent to the MZC.

Although Eq. 45 is the final calculation step of the IG build method, the TB VCAF approach require a further stage of calculation. This extra stage is required to account for the displacement used to correct manufacturing variation in the EIC_i chordal length. Eq. 46 shows the calculation required to determine the per-part translation step (ρ_i').

$$\rho_i' = \rho_i + AR_i \qquad \textit{Eq. 46}$$

It terms of the ISO measurement of the geometric circularity for the TB assembly methodology, the smallest value of ρ_i' (ρ_{min}') will equate to the

IMZCI, while the largest value of ρ_i' (ρ_{max}') will equate to the OMZCI. The MZC will be determined by the subtraction of the ρ_{min}' from the ρ_{max}'. Again, as with the lobed non-circularity predictions the results show the idealised maximum possible level of circularity for the component set under scrutiny. In reality however, lower levels of circularity will be exhibited by the assembly, due to: fixturing error, inter-component contact incoherence and measure uncertainties.

5.7 Conclusions

This chapter has laid out a mathematical description of the likely geometric variance present within the wedge components of large annular structures. This mathematical description was then combined with observations made during the study of the illustrative industrial test-piece (chapter 4), to generate the VCAF assembly methodologies. Two fundamental VCAF approaches were then proposed (both based on the effective chord length KC), these being:

The geometric build methods: These approaches constrain a polygonal representation of the assembly system onto a theoretical build circle. The theoretical build circle can be either circumscribed (CG) or inscribed (IG).

The translation build method: This correction method is performed by the application of a per-part radial translation. The TB approach corrects the theoretical angle between a component's chord length and the assembly centre, matching it to the design nominal.

Each of the proposed VCAF assembly approaches (CG, IG & TB) were expressed mathematically. Moreover, for the geometric build methods; the CG build scheme was defined using both a precise (but computational intensive) and estimated calculation approaches. While, for the IG build method only an estimated prediction of the theoretical build circle could be presented.

Beyond the definition of the VCAF methodologies themselves, the influence of the angular braking errors was discussed (and the influence of the γ_i KC upon them). These triangular gaps are generated when the sum of the component's wedge angles do not equate to 2π radians. Furthermore, the influence of these gaps on the ideal positions of the fixture's datum locators, and how the position of these errors can be controlled by effective component tolerancing has also been discussed. Finally, the fundamental intrinsic non-circularities which determine the maximum quality (i.e. minimum circularity) possible for any given set of components was discussed and defined.

From the information presented within this chapter a number of conclusions can be drawn, the most significant of these being:

- The generation of angular breaking errors has important implications for the datuming scheme of a given fixture. Moreover, where the sum of angles used within an assembly exceeds 2π radians external location should be used; while, if the sum of the angles is below 2π radians then internal location should be used.

This ideology is especially pertinent if the fixture's datum locators are to be placed at the components joint positions, as with the CG build method.

- When designing the components for an annular assembly, it is important to be mindful of the tolerances; if it is intended that the components be internally located then a -/- approach should be adopted for the wedge faces; while, the for externally located assemblies a +/+ approach should be adopted. Moreover, the worst possible approach is a +/- method, which would create location ambiguity within the assembly and a lessening of repeatability irrespective of the location scheme used.
- Inevitable angular breaking errors, prevent true face-face contact from occurring between the assembly components. Therefore, these faces must be considered a point contact. This influences the fixture's lay-out, so that in order to achieve a 3-2-1 datum layout for each component, the inner radial face of the component must be controlled by two locator blocks. The use of a single block is likely to permit the rotation of the part around the locators pin axis.
- The sum of the assembled component wedge angles will directly affect the fixtures location strategy. For example, in assemblies where the total sum of the angles is greater than 2π radians, the inter-component contact points will occur at the outer edge of the assembly. This will require the chord line calculations to be performed for the outer edge chords, as this is the position of the closed polygonal loop. Similarly, should the sum of the angles be less

than 2π radians then the calculations should be performed using the inner chordal polygonal chain.

- The IG method can only be used for assemblies with an odd number of components. This flaw makes it difficult to recommend as a generalised fixturing approach, especially given its inability to resolve a precise solution for the theoretical build circle. Moreover, this approach also, uses a mid-point datum locator, which as mentioned previously is likely to permit rocking. For these reasons this assembly technique will not be tested experimentally.
- There are two forms of intrinsic non-circularity, and any given assembly will contain at least one of the identified geometries (either lobed or stepped). The stepped non-circularity is the least desirable due to its impact on the assemblies profile KC requirement for uninterrupted airflow.

A final note: The VCAF models outline in this chapter have a generic reach beyond just the circular structures of the sort outlined in chapter 4. Moreover, as the CG and TB methods are based on polygonal systems, so any closed loop structures could be modelled in this way. This make the VCAF approaches are equally applicable to rectangular, trapezoid or other polygonal forms (be they regular or irregular). Using them in this more generic way would require the use of component lengths as the component KC, rather than a chord length. Additionally, with a more mathematically complex chord description it should also be possible to model elliptical assembly systems as well.

6 Validation of VCAF build approaches

6.1 Introduction

Presented in this chapter is the physical validation of the proposed VCAF assembly methodologies as defined in Chapter 5. During the validation process the VCAF approaches were tested against, and compared too, the traditional industrially prevalent Fixed Datum (FD) build approaches. This comparison was performed through the embodiment of a generic multi-segment test-bench assembly, which was designed to include exaggerated explicit manufacturing variance within its structure. While, to facilitate the testing, a novel flexible fixture which allowed the construction of the test-bench assembly using either FD or VCAF build methods was designed and built. The creation of this flexible fixture therefore enabled the same assemblies to be constructed using either a traditional or VCAF approach within a consistent fixturing system. Moreover, by building the same assemblies, using the same components within the same fixture, a quantified like-for-like comparison between the different fixturing stratagems and their response to systemic manufacturing variation can be made. Practically, using this modus operandi, 64 assemblies were constructed and inspected with a CMM for circularity and diametric accuracy. Also, along with the measurements the presence of assembly gaps was also noted as these will potentially impact the integrity of the preliminary welding process (PWP) - which will be discussed in chapter 7.

Finally, the presence of non-circularity drivers (chapter 5) was also tested and validated experimentally.

6.2 The generic test-bench assembly

For the purposes of validation experimentation a test-bench assembly was required to embody the manufacturing variance present within a typical large assembled annular structure. This test-bench assembly would then be used in conjunction with a flexible fixture to validate the proposed VCAF build methods, allowing their ultimate build quality to be compared with that of the traditional FD fixturing approaches. The test-bench assembly was designed to contain known explicit manufacturing errors, along with the inevitable implicit manufacturing variance. The explicit manufacturing errors were purposefully exaggerated from the typical implicit manufacturing variation; the reason for this was twofold: Firstly, it increased any observable differences between the proposed VCAF and traditional build methods, reducing the influence of measurement uncertainty and "noise" within the results; and secondly, increasing systemic errors within each build trial would "stress test" each build method so that robustness could be observed.

6.2.1 The design

The chosen test-bench assembly (shown in Figure 6-1)[1] was a ten segment mild-steel structure, constructed from abutted I-shaped wedges. The 25mm thick ring assembly was designed to have a nominal internal diameter of 200mm and a nominal external diameter of 440mm. While the thickness of the upper and lower platforms, and the vertical centre span between them was a consistent 10mm. In terms of the angle, the components had a nominal 36° angle between the inter-component contact faces. Although ten nominal components were created, an extra eight components with an explicit angular error were also manufactured. Of these eight components, four were manufactured 2° oversized (38°), and four where manufactured 2° undersized (34°). These extra components therefore, allowed controlled deviation from the assembly's from design nominal, so that exaggerated error can be inducted into the assembly system as needed.

[1] Full engineering drawings for the assembly and components are included in the appendices.

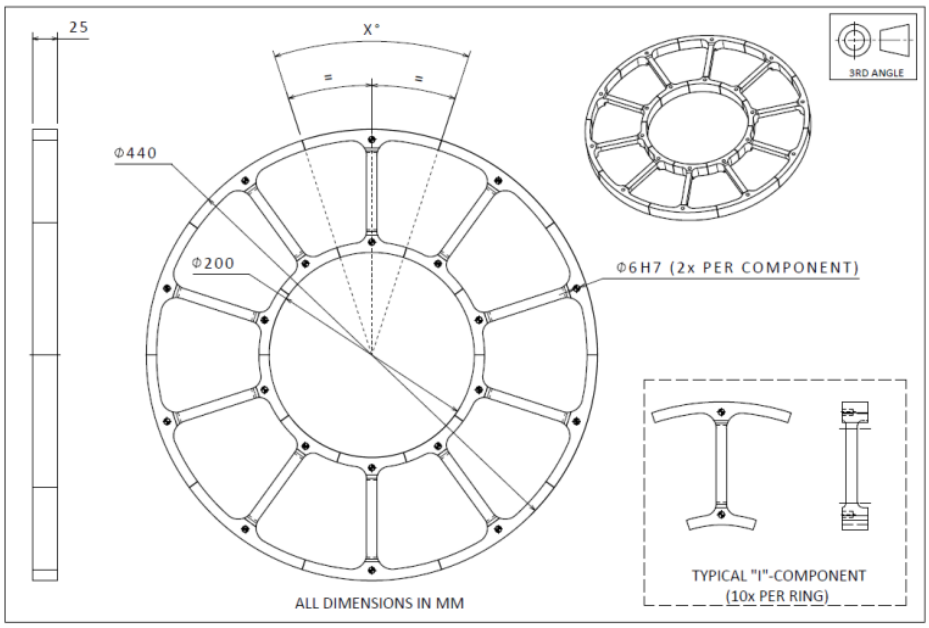
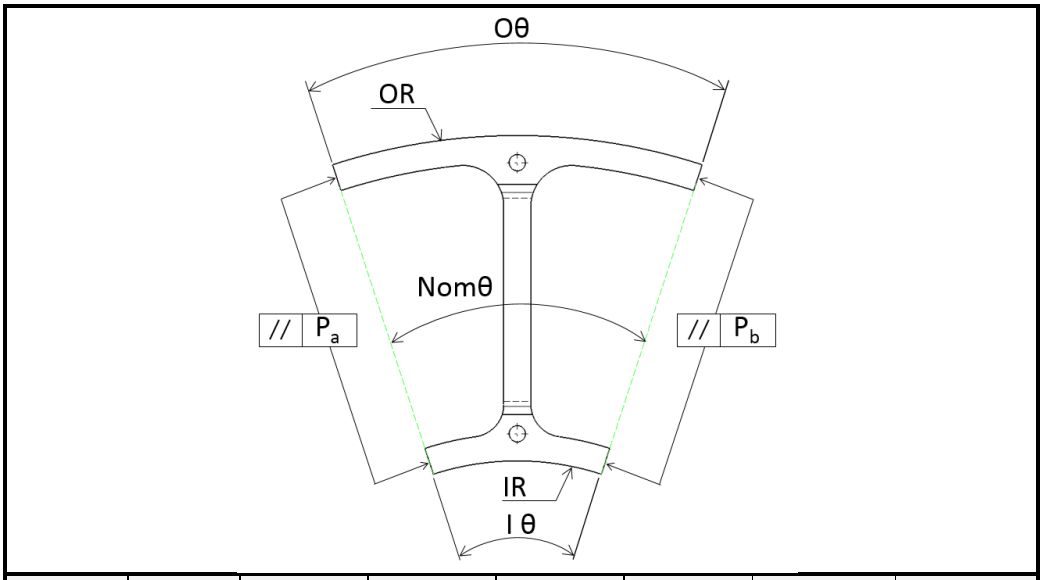


Figure 6-1 : Drawing of generic test-bench assembly

In addition to the profile geometries, two Ø6H7 datum dowel holes (located on the part centre-line) were also included within the design of the components. These holes where included as measurement datums to allow the automated CMM validation of each component. Each component was also marked with a unique identifier, to enable the tracking of which components where used during which assembly build process.

6.2.2 Validation of manufactured geometry

Once the components had been manufactured they were examined using a CMM to determine the degree of implicit variance present in each part (Table 6-1). The upper and lower platforms; inner and outer radii; and the parallelisms between the faces I_aO_a and the faces I_bO_b (Figure 6-1) where measured for each of the manufactured parts. This data was then logged against each components unique identifier to create a numeric picture of variation within the components.



Identifier	Nomθ Nominal angle (°)	Iθ Measured inner platform angle (°)	Oθ Measured outer platform angle (°)	IR Measured inner radius (mm)	OR Measured outer radius (mm)	Pa Parallelism (mm)	Pb Parallelism (mm)
34-1	34.00	33.928	33.922	199.487	441.504	0.196	0.170
34-2	34.00	33.951	34.060	205.595	441.087	0.050	0.200
34-3	34.00	33.934	34.013	199.952	435.293	0.202	0.143
34-4	34.00	33.926	33.919	199.689	438.572	0.133	0.117
36-1	36.00	35.972	36.069	198.642	441.647	0.097	0.101
36-2	36.00	35.904	36.070	199.201	441.812	0.241	0.064
36-3	36.00	35.914	36.109	197.936	441.53	0.316	0.052
36-4	36.00	35.939	36.264	199.37	441.518	0.181	0.065
36-5	36.00	35.961	36.136	199.258	438.778	0.05	0.259
36-6	36.00	35.976	36.085	197.836	434.911	0.215	0.494
36-7	36.00	35.983	36.000	199.588	441.428	0.136	0.130
36-8	36.00	35.994	36.026	198.997	438.569	0.157	0.228
36-9	36.00	36.015	36.052	199.189	441.402	0.126	0.157
36-10	36.00	35.838	36.027	196.996	441.934	0.339	0.049
38-1	38.00	37.856	37.870	200.061	438.128	0.130	0.036
38-2	38.00	37.957	37.897	199.963	440.554	0.178	0.070
38-3	38.00	37.811	37.593	200.265	440.181	0.124	0.091
38-4	38.00	38.087	37.755	199.898	439.698	0.369	0.195

Uncertainties (see appendix):

Angular measurements ±4.2x10^{-4} at 95% confidence
Radial measurements ±0.0099 at 95% confidence
Parallelism measurements ±0.0022 at 95% confidence

Table 6-1 : Component measurements

The measurement data was processed (Table 6-2) using the approaches outlined in chapter 5 to generate the "true" wedge angle (γ_i) and effective chord length (EIC_i) required for the set-up of the CG build method. The absolute radial position (AR_i) for each part was also pre-calculated, as required by the TB build method (which is also shown in this table).

Identifier	γ_i (°)	EIC_i (mm)	AR_i (mm)
34-1	33.9169	58.2907	94.3163
34-2	34.1552	60.4515	97.8120
34-3	34.0792	58.6536	94.9036
34-4	33.9135	58.2902	94.3155
36-1	36.1486	61.7559	99.9225
36-2	36.2064	62.0638	100.4214
36-3	36.2678	61.7007	99.8339
36-4	36.5316	62.5140	101.1498
36-5	36.2813	62.1522	100.5645
36-6	36.1760	61.4951	99.5011
36-7	36.0140	61.7818	99.9652
36-8	36.0528	61.6469	99.7468
36-9	36.0818	61.8664	100.1019
36-10	36.1790	61.18669	99.0021
38-1	37.8818	64.9753	105.1322
38-2	37.8470	64.8972	105.0058
38-3	37.4112	64.3291	104.0867
38-4	37.4780	64.2187	103.9081

Table 6-2 : Calculated component data

6.3 Design experiential test-bench fixturing

In order to experimentally validate the VCAF build methods a fixture for the test-bench assembly was required. The design intention for this fixture was to generate a fixturing system capable of building the test-bench assembly using the CG, TB and traditional FD all within the same tool. The benefit of this being that errors within system related to the quality of the fixture will be common between the build methods, so any observed geometric differences within the assembly will primarily be driven by the build approach itself. Moreover, as all assembly builds will reuse the same pool of 18 components, so by the same token the component variations will also be consistent, negating the influence of these factors when considering the output structure's geometry.

6.3.1 Requirements of the design

It was decided that four build approaches would be validated using the fixture, these being: a Fixed Datum Inscribed (FDI) build (Figure 6-2a), a traditional fixed build approach where the fixture's datums are positioned at the nominal midpoint of the component's chord; a Fixed Datum Circumscribed (FDC) build method (Figure 6-2b), a traditional fixed approach where the fixture datums are placed at the inter-component joints; the CG method (Figure 6-2c); and finally, the TB method (Figure 6-2d) . The IG build method would not be tested during the validation process due to the shortcomings highlighted in chapter 5.

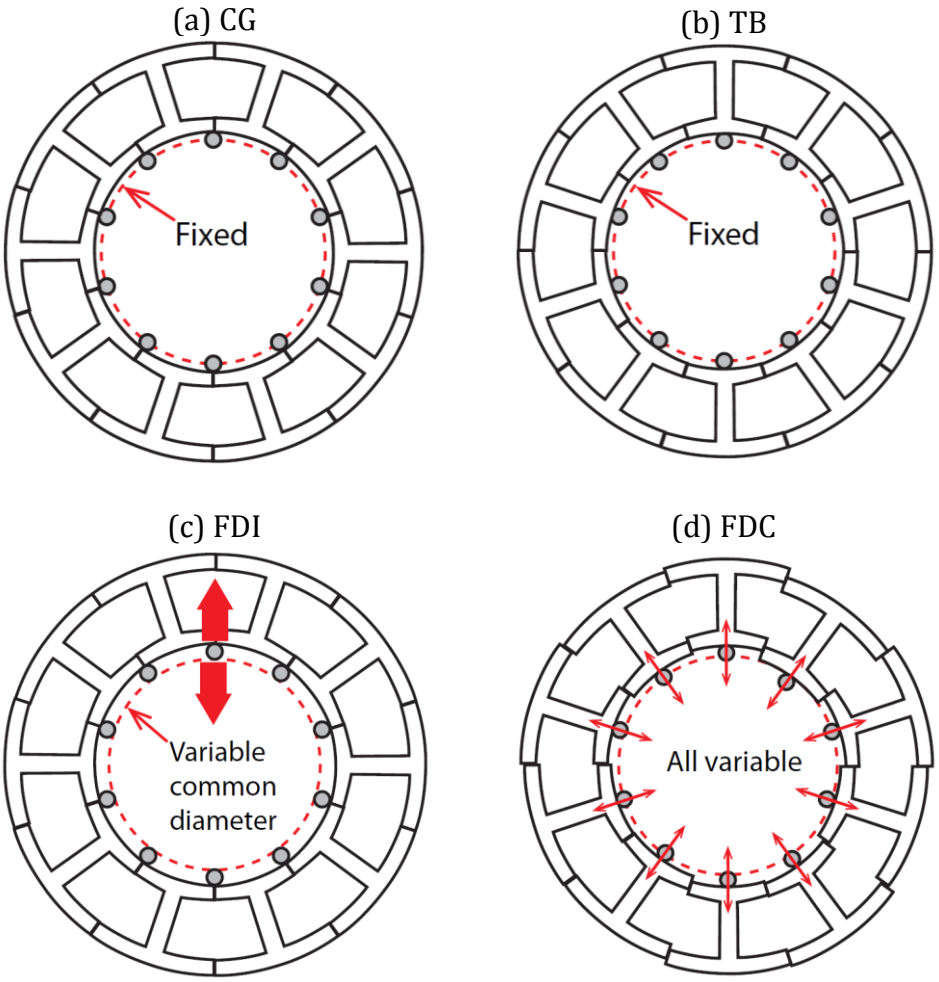


Figure 6-2: The build methods validated: a) CG, b) TB, c) FDI and d) FDC

To make the flexible test-bench fixture capable of supporting the dissonant requirements of the VCAF and traditional FD build approaches, a number of functional design requirements must be fulfilled. These design requirements being;

- The design should radially locate the components of the test-bench assembly on their internal diameter.
- The fixture's build diameter should be adjustable to support the testing of the CG approach. Each locator must also be capable of being repositioned independently along the radial line to allow testing of the TB fixturing

methodology. However, the fixture must also support the locking of the fixture's datum locators to the nominal build diameter, so that the FDI and FDC methodologies can be tested.

- The fixture's locator blocks should also be angularly repositionable, with the ability to lock the datums at the assembly's nominal (36°) angular locator spacing. Again, this is required to fulfil the requirements of both FD and VCAF fixturing approaches.

- As the position of the fixture's datum locators are to be moveable (to support the VCAF builds), so the fixture's design should contain high accuracy datum measurement features to enable the verification of the fixture's set-up.

6.3.2 The design concepts

During the design cycle of the flexible fixture a number of design concepts were generated. The designs were primarily driven by the requirement to allow a change in the fixture's datum diameter, so that the VCAF builds could be supported by the final fixture. Moreover, some of the concepts were noteworthy in their ingenuity and have been filed for patenting with UKPO (presented within the appendices), three of these will be discussed prior to describing the final design. The three most notable designs were the Eccentric Cam (EC) design, Fixed Ring Linkage (FRL) design and Scissor Linkage (SL) design.

6.3.2.1 *The EC design*

The EC design (Figure 6-3a) is based around a spiral profiled cam. As Figure 6-3b shows, each cam is attached (via a pivot pin) to a fixed inner ring and contains an integral spur gear which meshes with an internally toothed ring gear. On twisting the outer toothed ring relative to the fixed inner ring, the cams turn in unison increasing the effective diameter by virtue of the spiral location face of each cam (Figure 6-3c).). Furthermore, each spiral cam can also include a flexure face design, to "take-up" local surface defects and small amounts of geometric deviation. However, these flexures are only truly suited to clamping applications, rather than location.

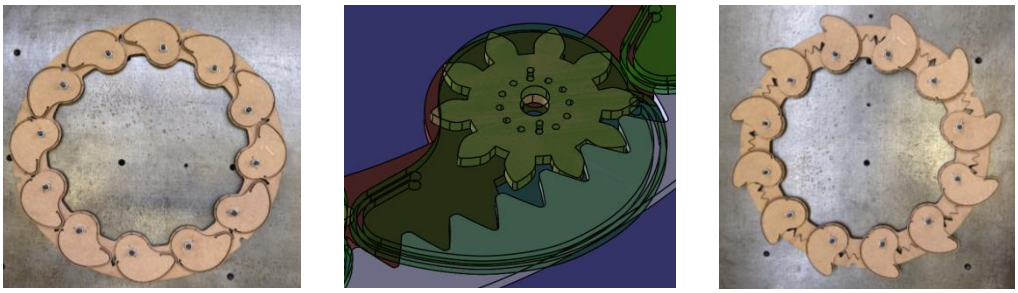


Figure 6-3 : a) EC prototype closed, b) Cam detail, c) EC prototype open

6.3.2.2 *The FRL design*

The FRL design (Figure 6-4a) uses a linkage based approach to alter the fixture's build diameter. As Figure 6-4b shows, this fixture operates by rotating a fixed inner ring relative to a concentric fixed outer ring. This relative motion drives a linkage, which in turn pivots a locator arm outwards, and it is this unfurling mechanism which offers the diametric change. For this particular design, the components to be assembled would then be positioned at the tips of the arm locator.

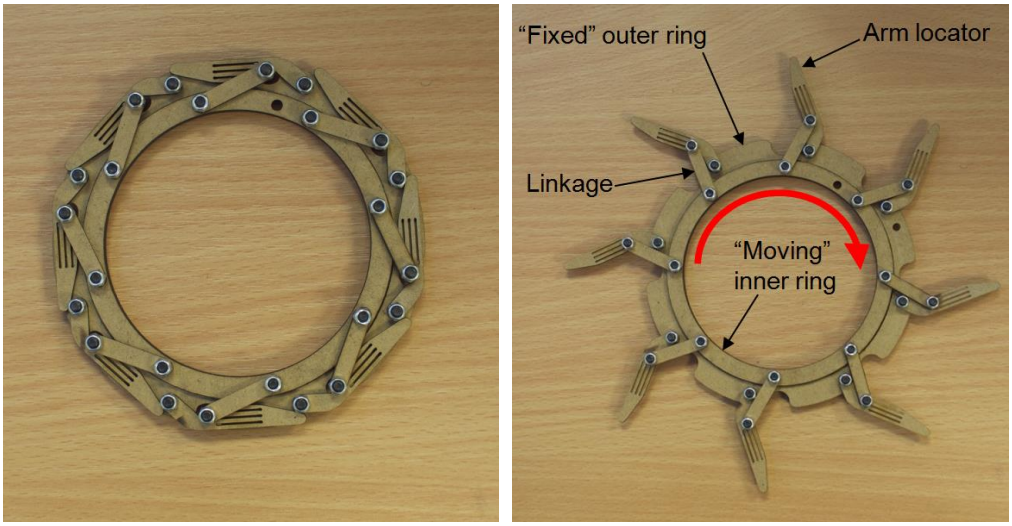


Figure 6-4 : a) FRL design in closed, and b) unfurled positions

6.3.2.3 *The SL design*

The SL design (shown Figure 6-5) uses a ring constructed from a chain of coupled scissor linkages. The ends of each linkage pair is attached to its neighbours, so by changing the angle of one linkage pair, all the scissors within the chain will adjust to match the angle of the initial driving linkage pair. As a Consequence, the size of the global chain system is defined by the angle between any given scissor linkage; so that, as the angle between the legs of the linkage becomes more obtuse the overall diameter of the fixture shrinks, while as the angle becomes more acute the fixture's diameter increases. In order to apply a component clamping force a sliding location foot was included at the interface between each scissor linkage and its neighbours. Each location foot had a fixed pivot at one end, and a slot along which the second pivot could slide. Each location foot also contained a conformable contact face which touched the fixtured component's inner surface.



Figure 6-5 : SL prototype (30mm range) inside Ø420mm component

As Figure 6-6 shows, this design was able to adapt to fixture components within a large diametric range; the range being defined by the length of the legs of the scissor linkages and the slot within each foot.

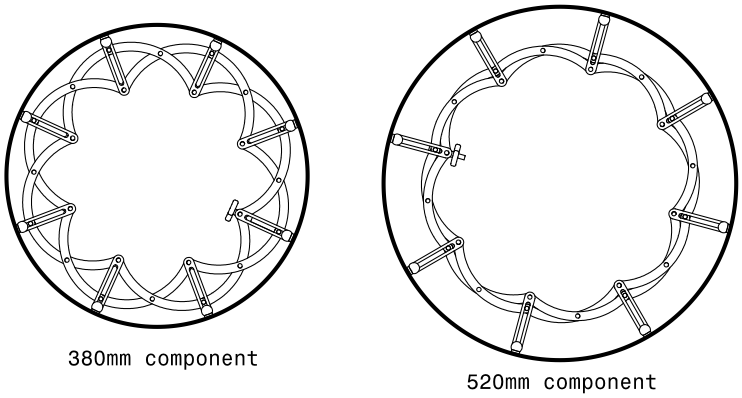


Figure 6-6 : A single SL fixture clamping Ø380mm and Ø520mm cylinders.

6.3.2.4 *Stacked designs*

It became apparent while designing the EC, FRL and SL fixturing system, that components of a more complex cross-section could be accommodated with relative ease by stacking several fixtures together (shown Figure 6-7a). As these designs are adaptable in diameter; they can be loaded into a component and expanded, conforming to the inner profile of the part to be fixtured. Furthermore, this is possible even if the part contains an overhang

or undercut within the geometry. Figure 6-7b shows some of the sorts of wall profiles that could possibly be fixtured this way.

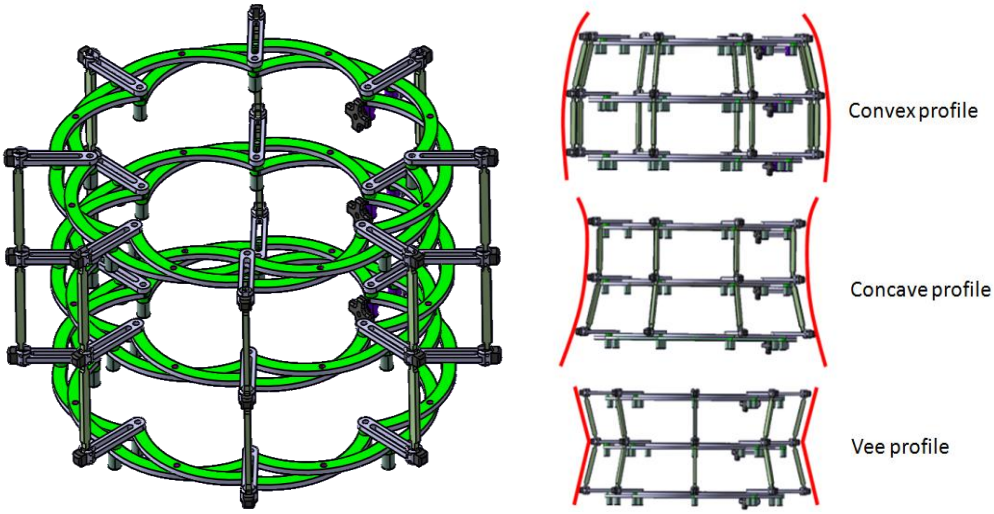


Figure 6-7 : a) Stacked SL fixtures, b) profiles capable of being clamped

6.3.3 The flexible fixture's final design

Although the EC, FRL and SL designs are very efficient in allowing for the global contraction and expansion of the fixture's build diameter, these designs suffer from an inflexibility within the independent and individual positioning of the fixture's locators. Consequently, these designs prevent the required variance of either the angular or radial positions of each fixture locator, which makes these designs unworkable for true variation conscious fixturing. As a consequence a more traditional design approach was required for the flexible fixture's design.

Figure 6-8 shows the final iteration of the flexible fixture's design[2] used to experimentally build the test-bench assembly. This fixture contains two

[2] Full engineering drawings for the fixture are included in the appendices.

main “units”, these being: a structural base unit and ten Locate and Clamp Carriage Units (LaCCU) – one per assembled component.

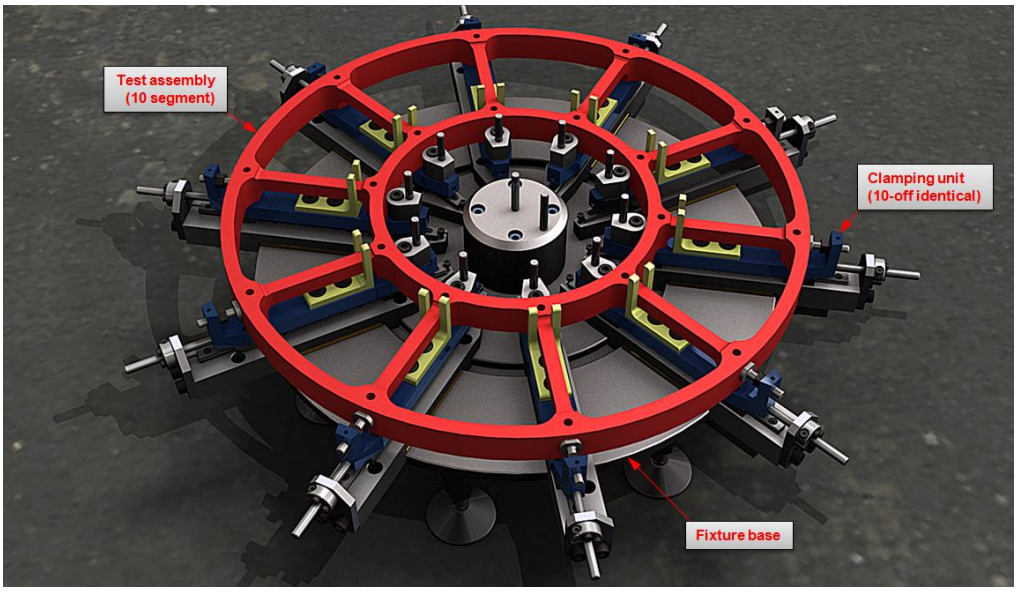


Figure 6-8 : The final flexible fixture design for the test-bench assembly.

The fixture’s core operating principle, which is the key enabler to its build configuration flexibility, is shown in Figure 6-9. This figure shows, how each of the LaCCU units is constrained between two concentric running edges (shown red) built into the base unit. These machined running edges allow each LaCCU to be independently adjusted angularly, while ensuring each carriage remains on the radial line. A further DoF is then added into the fixture’s design by the inclusion of a linear slide within each LaCCU, which allows each carriage (and thus the component held within it) to be positioned at a radial distance. This high degree of positional flexibility is the engine which enables the final fixture’s design to support FD and VCAF build methods all within the same test platform.

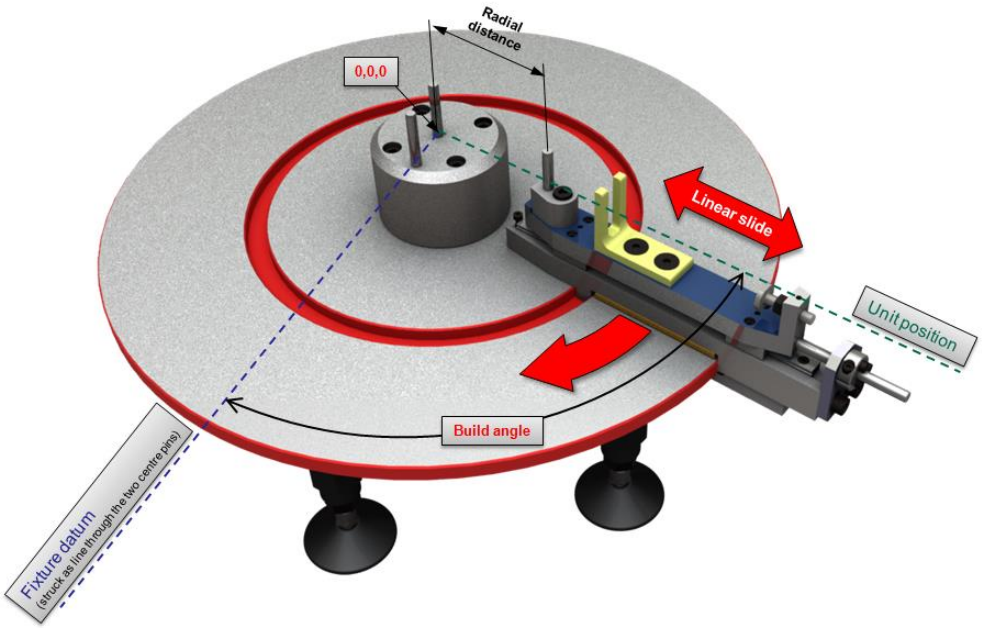
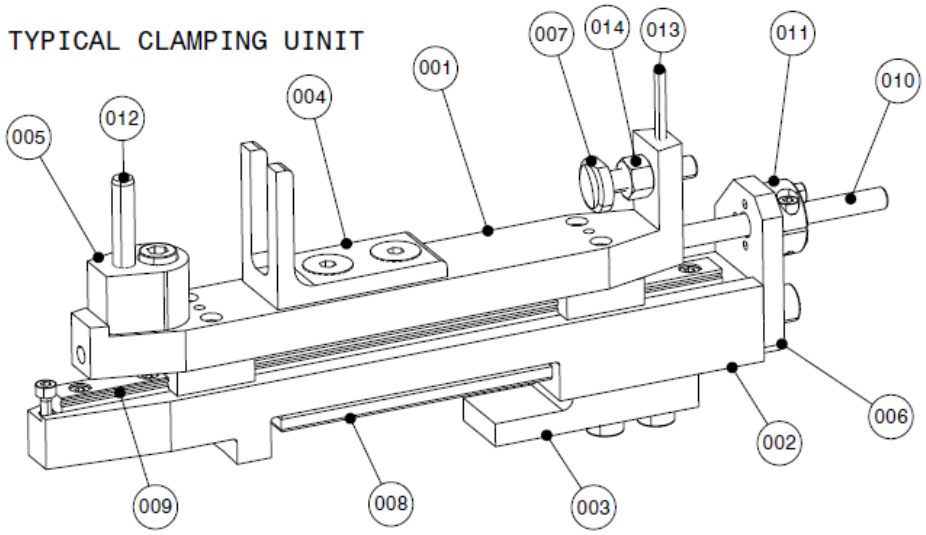


Figure 6-9 : The flexible fixture's operating principle

6.3.3.1 *The LaCCU's make-up*

Each LaCCU is sits upon a graphite impregnated phosphor-bronze bearing pad (Figure 6-10 item 008), which is attached to the underside of the lower radial carriage (Figure 6-10 item 002). This arrangement allows each LaCCU to easily slide on the greased upper face of the base unit, so that each LaCCU may be positioned angularly. A single test-bench assembly component is loaded into each LaCCU, and clamped between a threaded clamping block (Figure 6-10item 007) and the datum locator block (Figure 6-10 item 005). To assist with the loading and location of the wedge component a rough locator (Figure 6-10 item 005) is provided. This clamping assembly then sits atop a linear slide (Figure 6-10 item 009), allowing the component and clamping arrangement to be translated along the radial line. Once positioned, the unit is then locked in place with the angular "bolt-down" locking plate (Figure 6-10 item 003) and split collar rod clamp (Figure 6-10 item 011). The flexibility of this design

permits a total inner diametric build range of 180-225mm, and a ±10° angular envelope per LaCCU.



ITEM	QTY	DESCRIPTION
001	1x	UPPER LINEAR CARRIAGE
002	1x	LOWER RADIAL CARRIAGE
003	1x	LOCKING PLATE
004	1x	ROUGH LOCATOR
005	1x	LOCATOR BLOCK
006	1x	REAR PLATE
007	1x	THREADED CLAMP
008	1x	GRAPHITE IMPREGNATED BRONZE SLIDE PLATE
009	1x	CAGED BALL LINEAR SLIDE
010	1x	HARDENED GUIDE ROD
011	1x	SPLIT COLLAR ROD CLAMP
012	1x	DOWEL PIN (PRIMARY DATUM)
013	1x	DOWEL PIN (SECONARDY DATUM)
015	1x	THREADED CLAMP LOCKING NUT

Figure 6-10 : General assembly of fixture and clamping units

To allow a consistent and repeatable measurement of the fixture experimental set-up, each of the ten clamping units also contained two datum dowels (Ø6 mm inner most and Ø3mm outermost). These reference dowels are used to reference the angular and radial position of each LaCCU relative to the fixture's centre (this will be discussed in greater detail later). An assistive datuming plate (Figure 6-11) was also created to align each LaCCU's outer (Ø6 mm) reference dowel relative to the fixture's master datums. Using this jig-plate would set the

fixture for a nominal build, with each LaCCU being equi-spaced at 36° and their datum locator blocks all being positioned to a build diameter of 200mm.

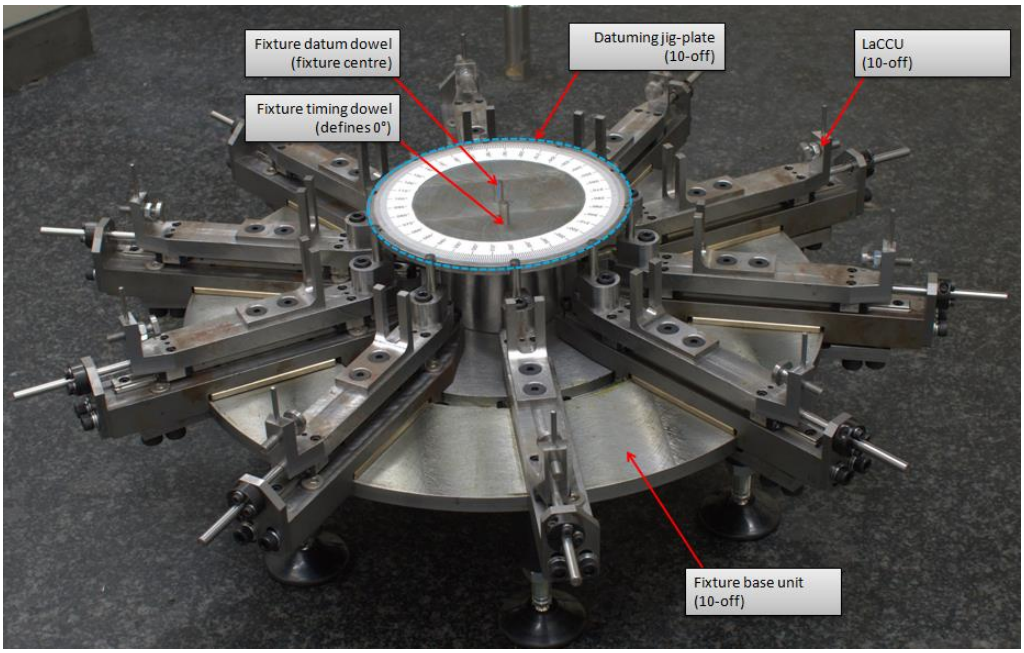


Figure 6-11 : Datum jig-plate for setting the nominl postion of LaCCU

6.3.4 Validation of manufactured accuracy of the flexible fixture

Before any assembly builds were performed the flexible fixture was tested to understand its accuracy and repeatability. The purpose of this testing was to profile the fixture's inherent manufacturing errors and offer a quantification of their possible effect upon output assembly quality. The test was performed by setting the radial and angular positions of all the fixture's LaCCU's using the datuming jig-plate. The positions of each LaCCU's inner (Ø6mm) datum dowels were then measured using a Mitutoyo Euro-C-A-121210 Coordinate Measurement Machine (CMM). The test was performed three times, with the LaCCU being re-datumed after each cycle of the trial. The aggregated results and comparison to the design nominal are presented in Uncertainties (*see appendix):*

Angular measurements ±4.2x10-4 at 95% confidence
Linear measurements ±0.0111 at 95% confidence

Table 6-3.

Angle between adjacent unit datum dowels (inner Ø6mm)				**Radial distance from fixture centre to LaCCU datum dowel (inner Ø6mm)**			
Design nominal (°)	**CMM mean** (°)	**Max/min** (°)	**Standard dev.** (°)	**Design Nominal** (mm)	**CMM mean** (mm)	**Max/min** (mm)	**Standard dev.** (mm)
36.00	36.024	+0.628 -0.353	0.280	82.00	82.130	+0.192 -0.140	0.120

Uncertainties (see appendix):

Angular measurements ±4.2x10^{-4} at 95% confidence
Linear measurements ±0.0111 at 95% confidence

Table 6-3 : CMM results of fixture accuracy and repeatability testing

Looking at the data presented, it becomes apparent that the level of positional accuracy achieved by the flexible test fixture's design is relatively low when compared to that of a traditional static fixture. Nonetheless, these inaccuracies are inherent to the use of the running fits required to make the flexible fixture reconfigurable. Moreover, the employment of these types of fits will always be subject to some degree of "play" where ever their used, meaning there will always be some trade-off in static accuracy if reconfigureability is required within the fixture.

6.4 Experimental validation; the evaluation of build error

To qualify the effect of each of the proposed VCAF build methodologies upon the geometric quality (circularity) of the test-bench assembly and compare them to the more traditional FD approaches, a series of experimental build trials were performed. The premise of these trials was to build the same assembly (with the same implicit and explicit

manufacturing variation) using each assembly method within the same assembly fixture; allowing a "like-for-like" comparison of circularity between structures built using the different fixturing approaches.

6.4.1 The build sets

Before testing could begin, a series of test ring assemblies (build-sets) were defined using the available pool of manufactured wedge components. Using these components, four fundamental distributions of assembly variation are possible, these being:

A. Nominal build - containing only components with implicit errors to give a net build condition of $\approx 2\pi$ radians.

B. Balanced build - containing the same number of explicitly oversized and undersized components, these are mixed with nominal components to give a net build condition of $\approx 2\pi$ radians.

C. Oversized build – containing a mix of explicitly oversized and nominal components to give a $>2\pi$ radians net build condition.

D. Undersized build - containing a mix of explicitly oversized and nominal components to give a $<2\pi$ radians net build condition.

To understand the full capabilities of the FD and VCAF fixturing approaches each of these fundamental variation distributions were built in the fixture experimentally. To ensure all possible variation distributions were tested a series of 16 assembly build-sets (four per distribution) were pre-defined. The components used in each build-set were picked pseudo-randomly,

from the nominal, oversized and undersized component pools as required by the overall distribution of each set. Each distribution category (with the exception of the nominal / implicit variation only build-sets) were further divided into either two or four degrees of error. A complete breakdown of the components used within each build-set is shown in Table 6-4.

		Component number at unit Position										
Build ID	Explicit error	Unit 1	Unit 2	Unit 3	Unit 4	Unit 5	Unit 6	Unit 7	Unit 8	Unit 9	Unit 10	
A1	0°	36-4	36-8	36-10	36-5	36-1	36-6	36-3	36-9	36-7	36-2	Nominal
A2	0°	36-5	36-4	36-2	36-8	36-9	36-3	36-10	36-7	36-6	36-1	
A3	0°	36-1	36-4	36-3	36-6	36-8	36-9	36-10	36-2	36-7	36-5	
A4	0°	36-2	36-7	36-5	36-8	36-4	36-1	36-9	36-10	36-6	36-3	
B1	±2°	36-3	36-1	34-2	36-8	36-4	36-7	38-3	36-9	36-2	36-5	Balanced
B2	±2°	36-1	34-3	36-6	36-2	36-8	36-10	36-5	36-7	36-4	38-4	
B3	±4°	36-10	36-5	34-1	36-2	38-4	34-4	36-3	36-1	38-2	36-4	
B4	±4°	34-2	36-2	36-8	38-3	36-7	38-1	36-1	36-6	34-3	36-9	
C1	+2°	36-8	38-4	36-5	36-4	36-2	36-10	36-6	36-9	36-1	36-3	Oversize
C2	+2°	36-10	36-9	36-3	36-1	36-5	36-4	38-2	36-8	36-6	36-7	
C3	+4°	38-3	36-10	36-2	36-8	36-3	36-4	36-7	38-1	36-5	36-9	
C4	+4°	36-1	36-6	38-2	36-3	38-3	36-9	36-5	36-7	36-10	36-4	
D1	-2°	36-7	36-6	34-2	36-9	36-4	36-2	36-8	36-3	36-5	36-10	Undersize
D2	-2°	36-6	36-9	36-10	36-5	36-1	34-4	36-7	36-4	36-2	36-3	
D3	-4°	36-1	36-4	36-7	34-3	36-6	36-2	36-9	36-8	36-3	34-1	
D4	-4°	36-2	34-3	36-3	36-8	36-6	36-10	36-5	34-4	36-4	36-7	

38-X = 38° Oversized segment 34-X = 34° Undersized segment 36-X = Nominal (no explicit error)

Table 6-4 : The build-set definitions arranged by distribution category

Table 6-4 defines not only which components are used within a given build-set, but also their position within the fixture. This is done by defining which LaCCU each component part is loaded into; with unit 1 being directly in-line with the fixture's datum timing dowel (**Error! Hyperlink reference not valid.**) and then numbering the LaCCU clockwise around the fixture.

Working in this way ensured that the same components were used in the same positions for each experimental build irrespective of the build methodology being investigated.

6.4.2 The testing procedure

The validation was performed by building each of the sixteen pre-defined build-sets in the flexible fixture, using the FDI, FDC, TB and CG datuming approaches. Once built, each assembled structure was then interrogated for circularity and diametric size using a CMM. A flowchart showing the experimental and set-up processes for each build type is shown in Figure 6-12.

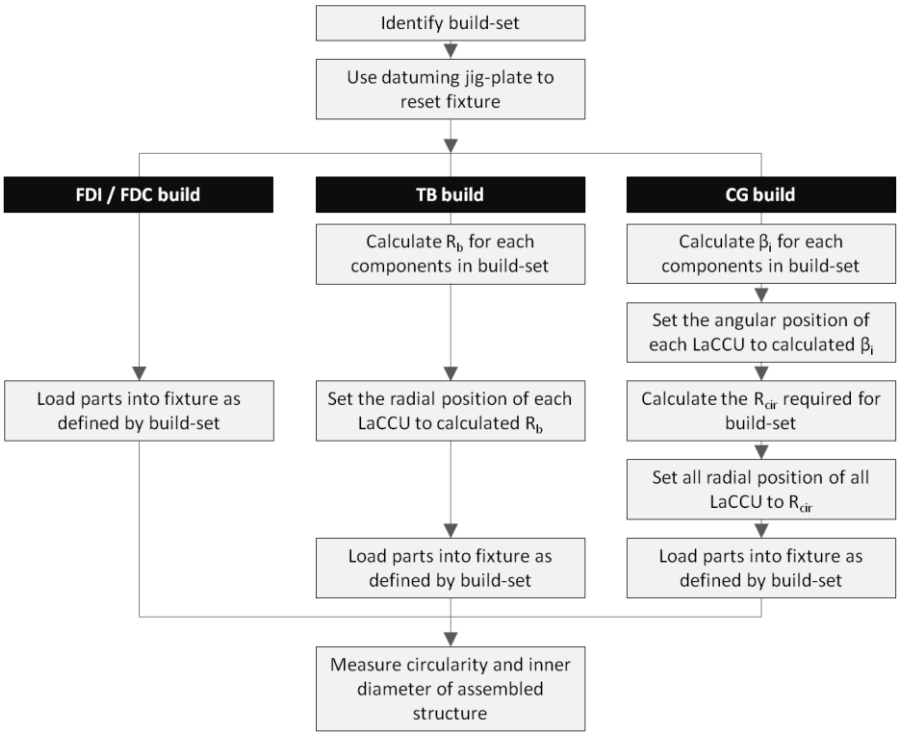


Figure 6-12 : Flow chart of experimental process

Each build trial began with identifying the build-set to be constructed. Once this had been determined, the datum jig-plate was used to prime the fixture LaCCUs, setting them to their nominal/home position with a 200mm internal build diameter and 36° between the locators. Once the LaCCUs

were set, the jig-plate was then removed, so as to not impinge on the assembly process. The next step of the build would depend upon the location methodology undergoing trial. The options being:

FDI build set-up – This build requires no further adjustment to the positions of the LaCCUs, as the jig-plate sets the fixture correctly for the build. Using the build-set table (**Error! Hyperlink reference not valid.**), each identified component is then loaded into the specified LaCCU. The rough locator built into each LaCCU is used, so that each part sits with the datum locator at the mid-point of its inner radius.

FDC build set-up - Again, this build requires no further adjustment of the fixture once set with the jig-plate. The components identified in the build-set table (**Error! Hyperlink reference not valid.**) are loaded into the LaCCU, as identified on the table. However, with the FDI build the components should be loaded so that the datum locators are positioned at the inter-components joints (i.e not using rough locators).

TB set-up – For the TB build the radial position of each LaCCU requires adjustment. The amount of adjustment required is determined with the model presented in chapter 5. However, for speed the adjustments were pre-calculated for the test-bench assembly components (presented in **Error! Hyperlink reference not valid.**). The radial distance of each LaCCU was set using a digital calliper, via a measurement between the fixture's centre datum dowel and the inner datum dowel of the LaCCU. A small guide (shown **Error! Hyperlink reference not valid.**) was used to ensure the measurement was parallel to the fixture's base plate. The TB method

requires no angular adjustment, so once the LaCCU radial positions are set, the components can be loaded into the fixture, as per the build-set. For the TB method the locators are positioned at the centre of the component's inner radius using the rough locators of the LaCCU as a guide.

CG build set-up – The CG build method requires adjustment of both the angular and radial positions of each LaCCU. The angular adjustment required for each LaCCU was calculated based on the component being loaded into it, as described in chapter 5. Again for speed, the required angular values for all the test-bench components were pre-calculated and tabulated (**Error! Hyperlink reference not valid.**). The angular position of each LaCCU was then set using the angular scale (±0.50°) which is built into datum jig-plate. The CG build method required the theoretical build circle (R_{cir}) to be calculated for the given build-set. Once R_{cir} was established (see chapter 5) all the LaCCU were positioned to this diameter, using a digital calliper and the calliper guide component. Finally, each build-set component was loaded into the LaCCU as specified in the table.

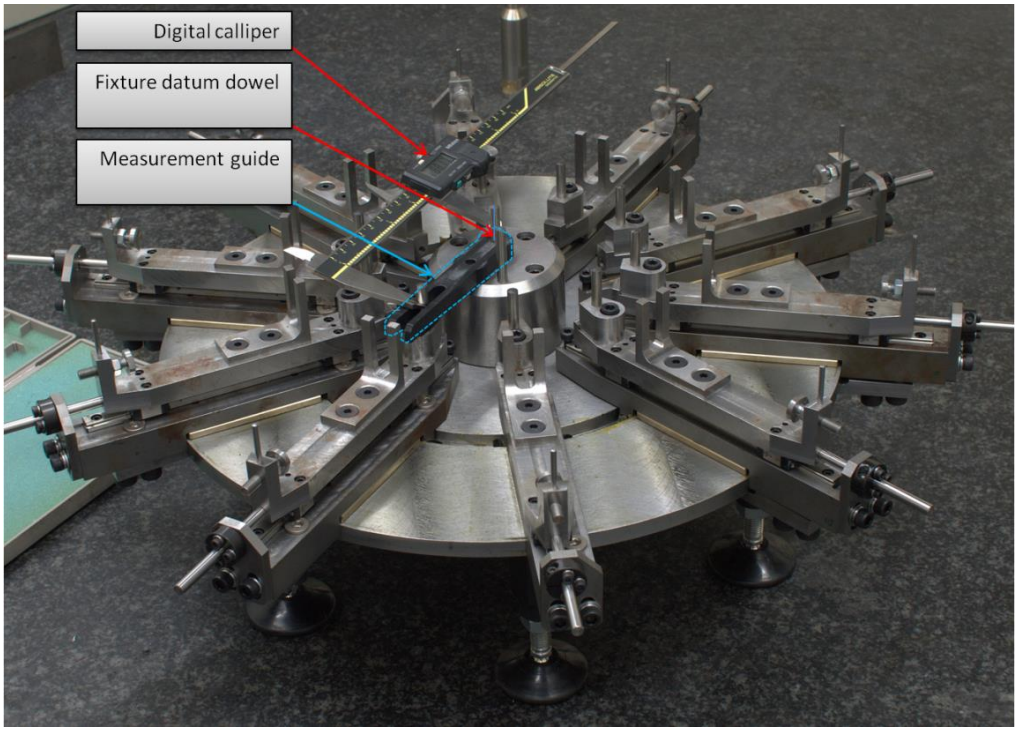


Figure 6-13 : Positioning a LaCCU using the calliper guide component

On completion, each assembled structure was interrogated using a Mitutoyo Euro-C-A-121210 CMM. Using the CMM, the internal diameter and circularity of each assembly was measured using a total of 20 points (two per component, at third intervals along the inner radius). Along with these measurements the presence and position of any angular breaking errors or assembly gaps was also noted.

6.4.3 The results and discussion

The collated results for the experimental builds are shown in Table 6-5. This table shows: the distribution category, the total error within each build, the measured mean diameter, the MZC, the diametric deviation of the Inner Minimum Zone reference CIrcle (IMZCI) and Outer Minimum Zone reference CIrcle (OMZCI) for all the build approaches. The table also shows the calculated

R_{cir} of each of the CG builds to allow comparison with the experimentally measured results.

Looking at the results table, the oversized (C1-C4) TB results are shown as "Build not possible". This result was recorded as the remaining gap after assembling nine components was too small to accept the final segment. The reason for this is the oversized distribution condition of these build-sets. Moreover, as stated in chapter 5, the components in an oversized assembly contact at the outer edge, leaving angular breaking errors at the inner edge. Consequently, the outer diameter controls the assembly's required location diameter for an oversized build. However, the mathematics used in calculating the LaCCU positions during this study are based upon the component's inner diameter (an assumption stated in chapter 5), so the wrong translated position is being calculated for the components within these oversized build-sets.

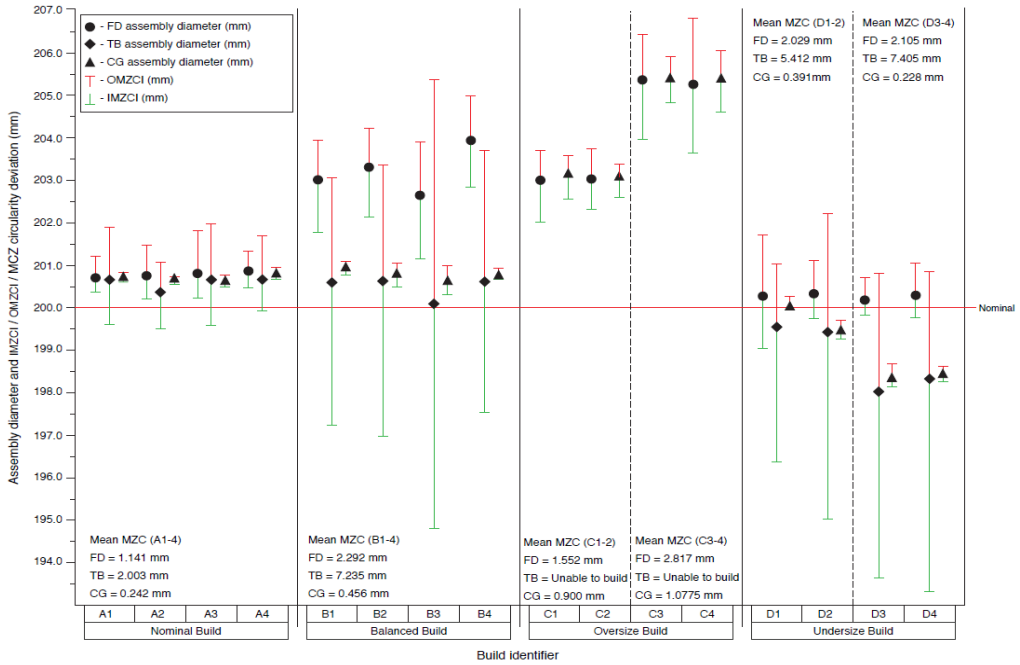
Build-set ID	$\sum_{i=1}^{n} \gamma_i$ (°)	Fixed Datums Inscribed (FDI)			Fixed Datums Circumscribed (FDC)			Translational Build (TB)			Circumscribed Geometric (CG)				
		Mean Diameter (n=20) (mm)	MZC (mm)	+OMZCI - IMZCI (mm)	Mean Diameter (n=20) (mm)	MZC (mm)	+OMZCI - IMZCI (mm)	Mean Diameter (n=20) (mm)	MZC (mm)	+OMZCI - IMZCI (mm)	Calculated Diameter $2R_{cir}$ (mm)	Mean Diameter (n=20) (mm)	MZC (mm)	+OMZCI - IMZCI (mm)	
A1	359.496	200.706	0.841	+0.511 -0.330	200.722	0.637	+0.348 -0.218	200.661	2.287	+1.239 -1.048	200.324	200.740	0.225	+0.124 -0.101	Nominal build
A2	359.496	200.755	1.258	+0.711 -0.547	200.670	0.464	+0.245 -0.218	200.667	1.573	+0.715 -0.858	200.324	200.702	0.188	+0.069 -0.119	
A3	359.496	200.709	1.595	+1.011 -0.585	200.668	0.472	+0.256 -0.216	200.661	2.389	+1.317 -1.072	200.324	200.747	0.280	+0.156 -0.124	
A4	359.496	200.766	0.888	+0.467 -0.401	200.689	0.524	+0.237 -0.287	200.668	1.763	+1.030 -0.763	200.324	200.822	0.274	+0.144 -0.130	
B1	359.427	203.013	2.186	+0.931 -1.235	200.714	0.542	+0.280 -0.262	200.587	5.830	+2.469 -3.361	201.049	200.967	0.321	+0.148 -0.173	Balanced error
B2	359.588	203.309	2.085	+0.923 -1.162	200.695	0.719	+0.262 -0.427	200.619	6.373	+2.728 -3.645	200.274	200.817	0.563	+0.267 -0.295	
B3	359.426	202.648	2.753	+1.249 -1.504	200.746	0.812	+0.330 -0.427	200.086	12.851	+5.276 -5.296	200.009	200.647	0.678	+0.366 -0.311	
B4	359.388	203.939	2.144	+1.041 -1.103	200.741	0.993	+0.567 -0.426	200.606	6.164	+3.079 -3.086	200.781	200.786	0.260	+0.172 -0.088	
C1	361.600	203.032	1.688	+0.703 -0.995	203.008	1.800	+1.062 -0.783	Build not possible			201.218	203.170	1.015	+0.427 -0.588	Oversize
C2	361.549	203.032	1.415	+0.704 -0.711	203.046	1.455	+0.686 -0.769	Build not possible			201.269	203.103	0.785	+0.299 -0.486	
C3	363.215	205.364	2.471	+1.067 -1.404	205.378	1.572	+0.713 -0.859	Build not possible			202.219	205.417	1.079	+0.515 -0.564	
C4	363.366	205.259	3.164	+1.560 -1.604	205.394	2.098	+0.878 -1.219	Build not possible			202.138	205.407	1.431	+0.662 -0.769	
D1	357.475	200.276	2.681	+1.448 -1.233	200.293	0.573	+0.217 -0.356	199.555	4.648	+1.480 -3.168	200.108	200.047	0.337	+0.252 -0.086	Undersize
D2	357.428	200.332	1.376	+0.786 -0.590	200.471	0.514	+0.233 -0.282	199.430	6.175	+2.004 -4.171	199.232	199.482	0.444	+0.251 -0.194	
D3	355.559	200.183	0.883	+0.525 -0.359	200.407	0.745	+0.436 -0.308	198.281	9.389	+2.786 -4.393	198.180	198.363	0.546	+0.346 -0.201	
D4	355.396	200.294	1.297	+0.771 -0.526	200.385	0.894	+0.395 -0.499	198.329	7.630	+2.520 -5.110	198.189	198.457	0.349	+0.182 -0.167	

Table 6-5 : Results of experimental build trials (Uncertainties for diametric measurements ±0.0099 at 95% confidence – see appendix)

The results in Table 6-5 is expressed graphically in Figure 6-14, where the inner diameter (a point), OMZCI (a red bar), IMZCI (a green bar) are expressed for each build-set. This plot also articulates the MZC for each build-set as the height difference across the red and green bars, with a smaller height being more circular.

Looking at this plot the first thing to become apparent is that (unsurprisingly) each fixturing method gave its best result for both diametric accuracy and circularity KC when assembling the build-sets with the least amounts of component variation (A1-A4). Inversely, at the other end of the scale, all the fixturing methods exhibited their worst diametric accuracy when faced with the oversized (>2π radians) build-sets. Moreover, both the diametric accuracy and circularity KC of each assembly worsened as these build-sets became increasingly oversized, so that the results for C1 and C2 exhibit better circularity and diametric accuracy than those for C3 and C4. The reason for this poor build quality is because the mathematics for each fixturing approach is based upon the inner diameter of the assembly. However, in reality the build diameter of an oversized assembly is controlled by the outer edge of the assembly (as a consequence of the components true angle γ_i KC), which is not considered in the current assembly modelling. As a consequence, the CG, FDI and FDC results are much aligned with one another in the oversized C1-C4 builds, as the low location integrity of the fixturing in these build-sets means the fixture is having little effect on assembly quality.

Also obvious from the plot of the trial results is that the TB fixturing method appears to exhibit by far the worst circularity of all the fixturing approaches (for reasons which will be explained later), however it is not necessarily the worst performing build approach in terms of diametric accuracy.



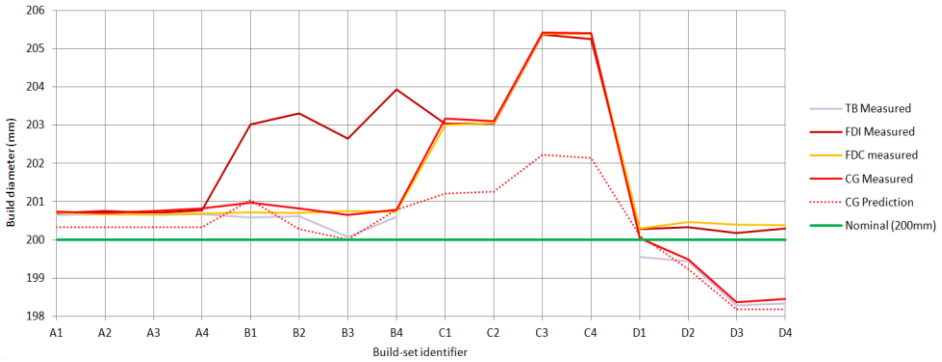
Uncertainties in diameter measurements ±0.0099 at 95% confidence – see appendix

Figure 6-14 : A graphic represeantation of the build results

6.4.3.1 *Results analysis; the inner diameter*

Figure 6-15 shows the inner diameter of each constructed assembly plotted against the build-set (from *Table 6-5*), as well as the R_{cir} prediction generated by the CG fixturing method (also from *Table 6-5*). This plot shows the underlying trends within the experimental data allowing for easy comparison between the differing fixturing approaches. However, it should be remembered that build diameter is not a KC for the assembly – as

circularity is functionally of greater importance making it a KC of the assembly.



Uncertainties in diameter measurements ±0.0099 at 95% confidence – see appendix

Figure 6-15 : Measured inner diameter against build-set

The results showed, that the fixed diameter (FDI and FDC) build methods always appear to produce an inner diameter greater than 200mm after the structure is assembled, even when faced with an undersized build-set distribution. This is likely due to the fixed nature of these methods, as the diameter of the locators is fixed at 200mm, so the only direction the components could possibly move is outwards, resulting in the observed oversized assemblies. Although, as a side-note, when looking at the true wedge angle (γ_i) KC of the components containing only implicit manufacturing variation (see Table 6-1), these components all have a true wedge angle slightly larger than the nominal 36° (averaged γ_i 36.114°). This is due in the main to the out-of-plane error between the inner and outer inter-component contact faces. This trend for slightly oversized implicit variation only components can be seen in Figure 6-15, where the CG prediction for the implicit only build-sets (A1-A4) shows a result a little above that of the nominal/error free line.

The diametric results demonstrated that all build approaches are generally in agreement in the size of the constructed inner diameter of the assembly. However, the FDI build deviated from the results shown by the other build methods when faced with the balanced distribution build-sets (B1-B4), where its diametric response to the input variation becomes somewhat erratic. The reason for this erratic behaviour may be that the FDI build approach uses a single locator block at the mid-point of the inner edge of the component. Moreover, this location rationale theoretically allows the component to rock about the locator until it contacts a neighbouring component, which will then block the rotational DoF. The mixture of over and undersized components within the balance build-set may make this situation less predictable at a local level, as the angular breaking errors are less consistent; which is reflected in the system wide results. The TB build method is also based upon the same location strategy, with a single mid-point datum locator. However, the TB approach did not exhibit the same diametric response to the balanced build-sets as the FDI method. This could be evidence of the per-part correction used in the TB approach addressing this issue and stabilising local variance to produce a more repeatable global build result.

An interesting result shown in Figure 6-15 is the synergy between the TB fixturing method and the CG methods R_{cir} prediction. The diametric accuracy of the TB approach appears to track R_{cir} across all the build-sets (where the builds were possible), and was a closer match than even the physical CG build results in a number of trials. Moreover, this observation

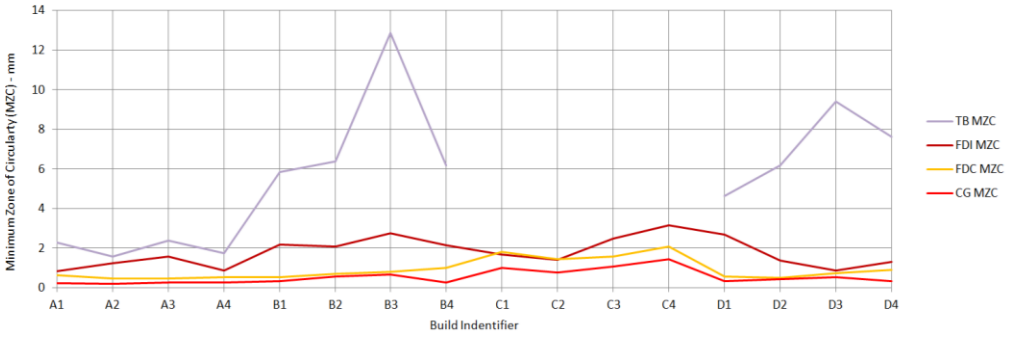
is interesting as both VCAF methods are based on different mathematic models, yet it appears that they generate similar results for the size of the assembly's inner diameter.

6.4.3.2 *Result analysis; circularity*

Figure 6-16 plots the circularity (from *Table 6-5*) of each build-set, when constructed using each of the four fixturing methodologies. This plot shows the resultant MZC (as deviation, expressed in mm) for each of the assembled structures. The plot shows a consistent trend between the differing fixturing approaches with the CG method exhibiting the most circular build outcomes (and thus best performing in terms of the assembly KC). While, this is tracked closely by the FDC build method, which consistently produced the next best assemblies in terms of circularity. The common factor between these approaches is that the locators are positioned at the inter-component joints, rather the mid-point of the inner radius. Placing the fixture's datum locators at the inter-component joint positions will ensure each component is located via a line, rather than a single point. A component located via a single central point can pivot about its locator until it contacts an adjacent component, while for a component located via a line this rotational DoF is not possible. Furthermore, this two datum approach uses the geometric stability of the fixture to control this rotational DoF, rather than relying on the unpredictable geometry of the adjacent components. Besides, given what has been shown about angular breaking errors and the inevitable gaps they produce, these error features

will give the components room to move, reducing the geometric quality of any assemblies which utilise a mid-radial point location scheme.

The TB approach exhibited by far the worst circularity of all the build methods. This is because this approach not only uses a single mid-radial locator, but also the approach fundamentally generates stepping within the assembly geometry through its translation of each component. Moreover, this make the TB approach poor in terms of both the circularity KC and profile KC (for airflow) required by the assembly. Looking back at the tabulated pre-calculation for the TB translations (*Table 6-2*), it can be seen that by combining the calculated translations (AR_i) for the most oversized and the most undersized components, a stepping of ≈11mm is predicted, and this prediction is borne out in the observations made within the experimental results.



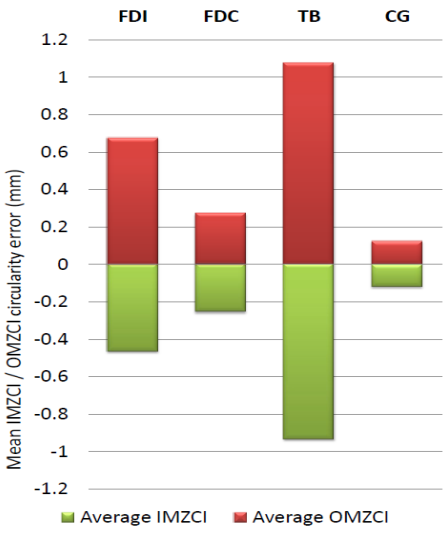
Uncertainties in diameter measurements ±0.0099 at 95% confidence – see appendix

Figure 6-16 : MZC measurements against build-set

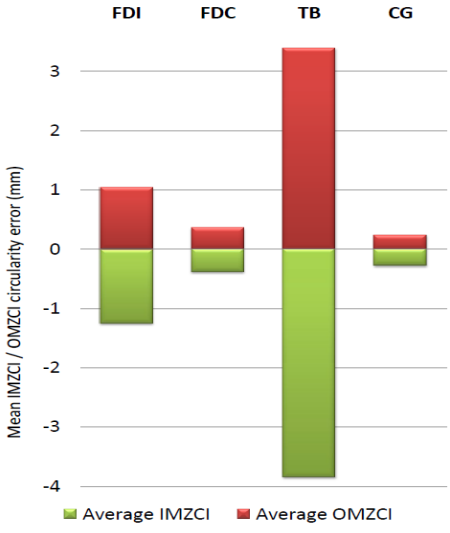
A more generalised view of the experimental circularity measurements can be seen in Figure 6-15 (a-f). These figures present graphically the underlying IMZCI, and OMZCI data averaged across each build-set distribution category. These figures also show the oversized and

undersized build-set distribution categories sub-divided into two and four degrees of error per assembly. These averaged results exhibit the same principal pattern as the other circularity results, with; the CG fixturing producing the most circular assemblies, closely followed by the FDC method, then the FDI approach and finally the TB method which consistently gave the least circular assemblies.

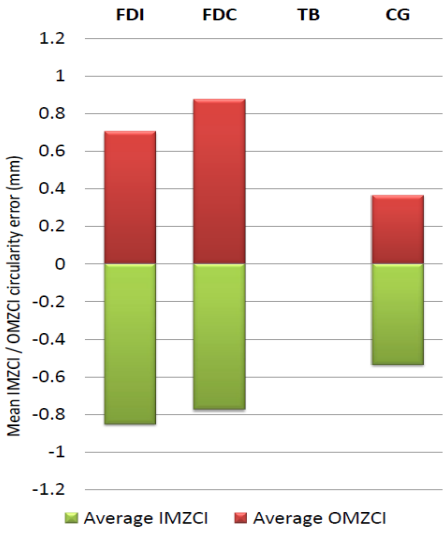
a) Averaged A1-A4 build-set results



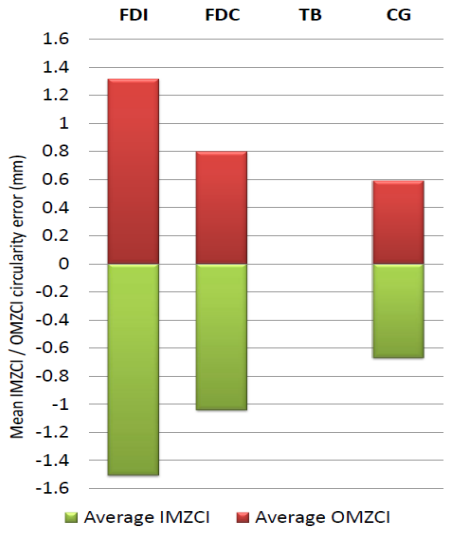
b) Averaged B1-B4 build-set results

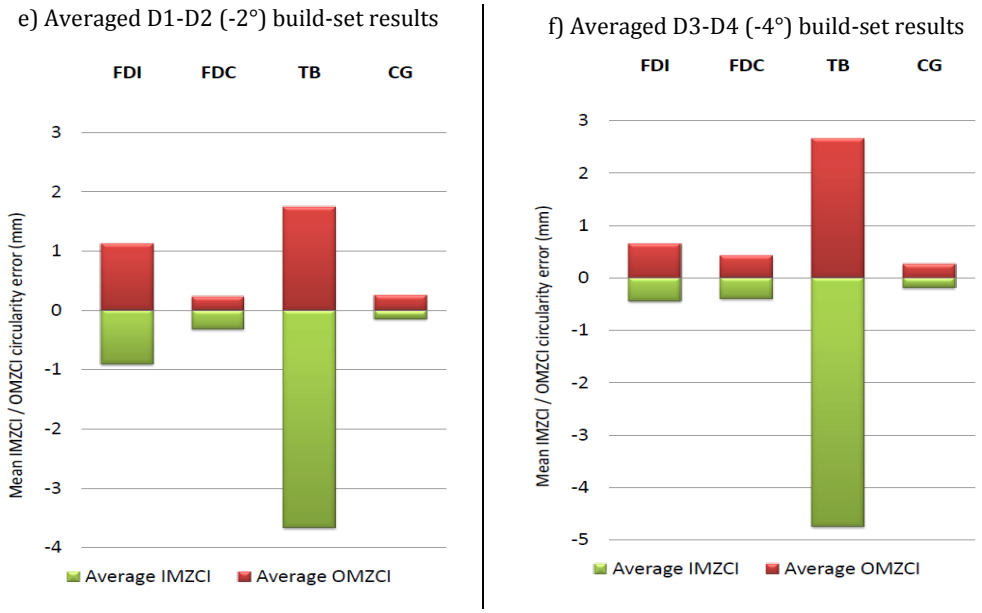


c) Averaged C1-C2 (+2°) build-set results



d) Averaged C3-C4 (+4°) build-set results





Uncertainties in diametric measurements ±0.0099 at 95% confidence – see appendix

Figure 6-17 : Graphs of the averaged build-set results

6.4.3.3 *Result analysis; angular breaking errors*

In addition to the numeric measurements taken during the assembly process, the presence and position of any assembly breaks and gaps was also recorded. Recording this information is important for two main reasons: firstly, gaps within the assembly will potentially impact the integrity of the preliminary welding process (PWP) - which will be discussed further in chapter 7; and secondly, the presence of gaps (especially at the inner radius) signals an incomplete build, as the assembled components have failed to generate a fully closed ring structure (as defined by the assumptions in chapter 5). Also, gaps could potentially impact the profile assembly KC as they can lead to shrinkage in the seam welds final seam weld (although these are beyond this project's scope)

Table 6-6 shows the summarised results of the observations made during the assembly process.

Build ID	Distribution	FDI	FDC	TB	CG
A1-A4	Implicit only	None	None	None	None
B1-B4	Balanced (±)	Both	Both	None	Outer radius
C1-C4	Oversized (+)	Inner radius	Inner radius	Build not possible	Inner radius
D1-D4	Undersized (-)	Inner radius	Inner radius	None at -2° / Outer radius at -4°	Outer radius

Table 6-6 : Observed assembly gaps within assembled structures

The first point of note when looking at Table 6-6 is that all the build methods failed to generate a fully closed assembly when faced with an assembly whose net angular distribution exceeded 2π radians (build-sets C1-C4). This situation exists because the angular breaking errors within an oversized assembly will always manifest at the inner radius (see chapter 5). Besides this, the models used to set-up of the VCAF fixturing methods are based on controlling of the inner diameter of the assembly (via the component's inner chord length). Therefore, the VCAF methods were always going to miscalculate the build diameter of an oversized assembly. The mathematic model presented within chapter 5 for the VCAF fixturing approaches should be adaptable to calculate for the outer edge of the assembly, and thus be usable for oversized assemblies. However, the assumptions for this project stated that this study was interested only in the inner diameter of the assembly, so adjusting the model to account for errors in the outer edge of the assembly was outside the scope of the project.

Looking at the more traditional fixturing methods; both FDI and FDC approaches exhibited angular breaking at the inner edge when constructing undersized assemblies (see Figure 6-18). At first glance this appears contradictory to what is known about angular breaking errors, as they would normally occur at the outer edge of an undersized assembly. However, because the FDI and FDC build methods use a fixed location diameter of 200mm, so to fit the assembly around the fixture's location pins the undersized geometry was stretched and distorted. Consequently, it was this stretching of the assembly which prevented inter-component contact at the inner edge of the assembly, and thus inducing the breaks at the inner edge rather than outer edge of the assembly. Therefore, the gaps observed in these two assembly types where not really angular breaking errors at all, but a geometric consequence of stretching the assembly's geometry.

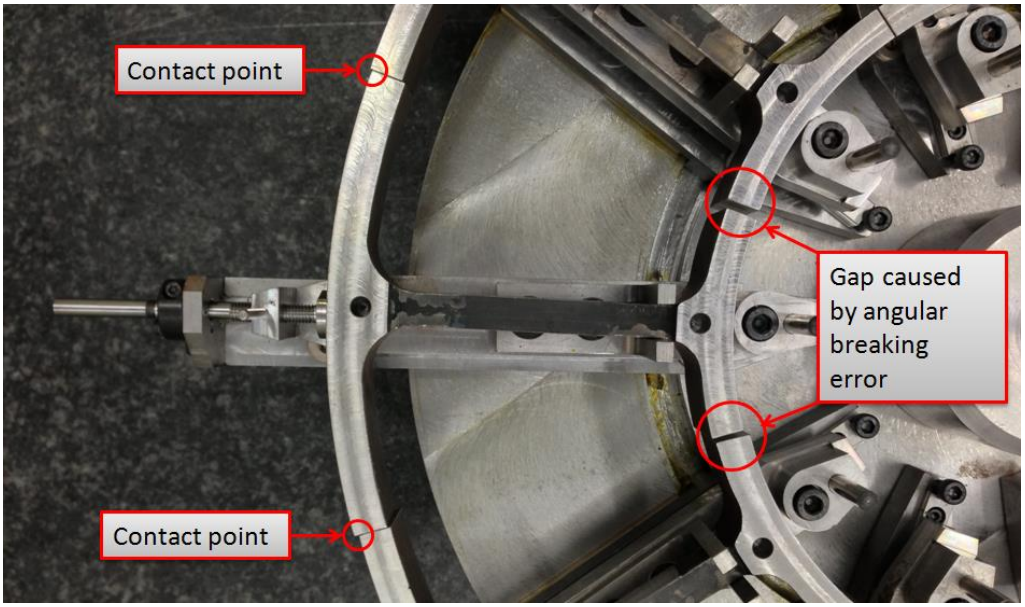


Figure 6-18 : Gaps observed in diametrically undersized builds when using FDI method.

The VCAF methods performed well for the presence of angular breaking and gap errors, with both the CG and TB methods creating closed assemblies in all build-sets except those which were oversized. The TB method in particular performed favourably when compare to the other fixturing methodologies, showing good control of gaps and angular breaking errors, even when faced with elevated levels of explicit component variation.

6.5 Experimental validation; non-circularity drivers

In chapter 5 the presence and nature of inherent loss of circularity within annular assemblies was discussed, along with its importance as an assembly key characteristic. During the discussion two main forms of non-circularity driver were identified and modelled mathematically, these being; the lobed and the stepped types. In addition, chapter 5 explained why the stepped non-circularity was undesirable in term of the assembly profile KC. In order to physically confirm the presence of these geometric conditions and verify the numeric modelling a series of experimental trials were performed using the test-bench assembly and flexible fixture.

6.5.1 The testing procedure

The procedure for experimentally validating the modelling of the inherent loss of circularity is expressed as a flow chart in Figure 6-19. Fundamentally, the procedure was similar to that of the experimental validation for the VCAF approaches. However, these trials used only the

build-sets containing implicit variation (A1-A4), which were constructed using the FDI and FDC fixturing methods only. In total therefore, the trial consisted of eight assembly builds, with the FDC method being used to test for the lobed non-circularities, and the FDI method being used to test for the stepped non-circularities.

Each trial began by setting the fixture to its nominal build position (internal datum diameter of 200mm and 36° between LaCCU) using the datum jig-plate. The components where then loaded into the LaCCU as defined by Table 6-4. While, depending on the fixturing method being used the datum was positioned at either the mid-point of the inner radius (FDI) or at the inter-component joint positions (FDC). Once the assembly had been constructed the inner diameter of the structure was measured twice using a CMM; once at the mid-point of each component (n=10) and again at each joint position for each component (n=20). In an ideal assembly there would be no difference between these two measurements as the ring structure would be perfectly circular, however in reality the two values will differ due to component and assembly variance (i.e. inherent loss of circularity). Therefore, by subtracting these two values from each other (and dividing by two to convert diameter to radius) gives a reflection of inherent non-circularity for each assembled build-set. This value can then be compared to the modelled inherent non-circularity as described in chapter 5.

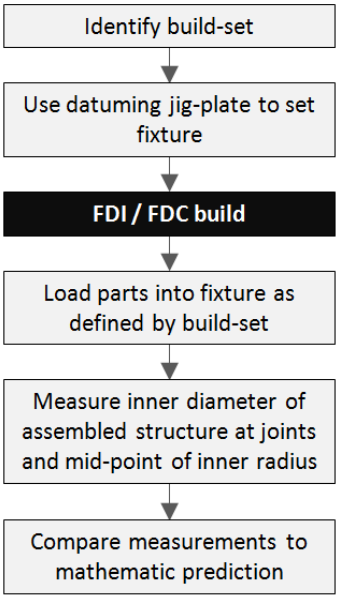


Figure 6-19 : procedure for validating non-circularity driver model

6.5.2 The results and discussion

6.5.2.1 *Result analysis; lobed non-circularities*

Uncertainties in *diameter measurements ±0.0099 at 95% confidence – see appendix*

Table 6-7 shows the result of the experimental investigation into the lobed non-circularities, on the A1-A4 build-sets, and FDC fixturing approach. The experimentally measured results of these build-sets generated an averaged value of 0.026mm (±0.0099 at 95% confidence*)* for the inherent non-circularity. For comparison, calculating the inherent non-circularity as defined in chapter 5 generates a result of 0.015mm, when based on a fixture location diameter of 200mm. This calculated figure is very close to the experimentally measured values, with the discrepancy probably being down to the fixture's actual location diameter not matching the idealised

value used in the calculation. However, a close agreement between these experimental results and the calculation is clearly evident in this instance.

Build ID	Measured mean diameter at joint (n=20)	Measured mean diameter mid-point (n=10)	Measured mean inherent non-circularity
A1	200.722	200.782	0.030
A2	200.670	200.720	0.025
A3	200.668	200.713	0.023
A4	200.689	200.738	0.025
Averaged	200.688	200.738	**0.026**

Uncertainties in diameter measurements ±0.0099 at 95% confidence – see appendix

Table 6-7 : Results for lobed non-circualirties build trials

6.5.2.2 *Result analysis; stepped non-circularities*

Uncertainties in *diameter measurements ±0.0099 at 95% confidence – see appendix*

Table 6-8 shows the experimental results for the measurement of stepped inherent non-circularities, within the A1-A4 build-sets constructed via the FDI fixturing approach. Typically, the stepped non-circularities were easier to observe in-fixture (see Figure *6-20*) than the lobed type non-circularities, due to the more defined visual point of reference (however, please note that some of the stepping will be likely due to the component pivoting on the single central locator). As Uncertainties in *diameter measurements ±0.0099 at 95% confidence – see appendix*

Table 6-8 shows, the testing generated an averaged stepping of 0.031mm (±0.0099 at 95% confidence*)*, but the mathematical model from chapter 5 generated a prediction (ρ_{max}) of 0.015mm. Although, looking at the table,

there may be an outlying data point skewing the average, as the A1 build-set result is twice that of the other build-sets. Also, the experimental measurement will of course be subject to many of the same measurement and fixturing uncertainties as the lobed non-circularity. Nonetheless, there is an extra disparity between the calculated and experimental values, which is probably due to the FDI build method, and its propensity to rock about the single mid-point locator. And yet, although this value is less coherent than the lobed non-circularities it is still within the right order of magnitude to be a meaningful result.

Build ID	Measured Mean Diameter At Joint (n=20)	Measured Mean Diameter Mid-point (n=10)	Measured Mean Inherent non- circularity
A1	200.600	200.707	0.054
A2	200.661	200.710	0.025
A3	200.649	200.696	0.024
A4	200.660	200.704	0.022
Averaged	200.642	200.704	**0.031**

Uncertainties in diameter measurements ±0.0099 at 95% confidence – see appendix

Table 6-8 : Results for stepped non-circualirties build trials

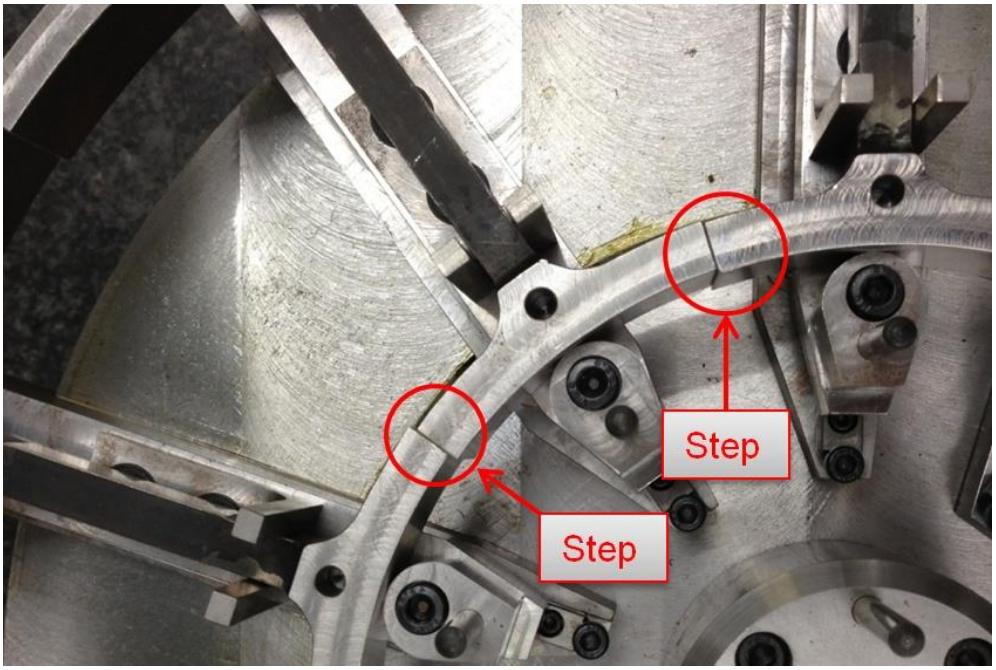


Figure 6-20 : A typical stepped type non-circualarties

6.6 Conclusions

In this chapter the VCAF ideas presented within chapter 5 were experimentally investigated. This exploration as performed through the conduit of a generic test-bench assembly and a pool of components with both implicit and explicit manufacturing variance. To construct the test-bench assembly a novel flexible fixture was designed and built. This fixture allowed the construction of the test-bench assembly using traditional (FDI and FDC) and VACF (CG and TB) fixturing methodologies within the same fixturing environment. As a consequence of the common fixture and pool of components a direct "like-for-like" comparison between the assembled results could be made, as any difference between the resultant structures will be a direct consequence of the fixturing approach rather than any other significant factor. Using the assembly and fixture, a series of 64

experimental assembly builds where performed utilising nominal, balanced, oversized and undersized component variance distributions (build-sets). During the experimental trials it was found that the proposed VCAF CG method performed the most consistently in terms of circularity (a KC for the assembly), outperforming the fixed datum traditional approaches. While, the TB VCAF method was shown to be the worst performing fixturing approach for circularity by some margin (falling short in terms of the circularity and the profile KC requirement of the exemplar assembly). The TB approach was however the most reliable for constructing closed gap-free assemblies. Also validated experimentally during these trials were the calculations for inherent non-circularities (from chapter 5), which determine the absolute minimum (best) circularity possible for any given set of components used in the construction of an annular assembly.

In summary, a number of conclusions can be drawn from the work discussed within this chapter, these being:

- In terms of the KC for assembly circularity a consistent pattern of results emerged during the physical build trials. The CG fixturing approach consistently produced the most circular assembled structures. While the FDC and then the FDI approaches produced the next best assemblies in terms of circularity. Finally, the TB method created the least circular structures by some margin, which was due to stepping caused as a consequence of the per-part translation used

in this build method. Consequently, the TB method was the worst performing method for overall geometric quality, failing to control either the profile or circularity KCs for the assembly adequately.

- In terms of the completeness of the builds (at the inner edge) the TB method was the best performing fixturing approach, producing fully closed assembly loops in all-but the oversized build-sets (C1-C4). However at the other end of the scale, the traditional fixed (FDI and FDC) approaches failed to create closed rings in all build conditions except the implicit only build-sets (A1-A4). The reason for their failure is a mixture of trying to stretch an undersized assembly to fit the fix location diameter, and a poor adaption to the angular breaking errors (caused by poor conformance to the component's true angle KC). In contrast the TB method's adaption to angular breaking appears to be very effective and reasonably robust.

- The ideas (in chapter 5) that: the components within an oversized assembly will resolve to make point contact at the outer edge of the assembly and generate angular breaking errors at the inner edge of the structure; while, the components of an undersized assembly will contact at the inner edge and generate angular breaking errors at the assembly's outer edge, is supported fully by the experimental observations. This is seen in the poor circularity response of each build method when applied to the oversized build-sets (C1-C4). Moreover, the VCAF methods failed in these oversized situations as their location modelling is based on the inner diameter of the assembly, and as the inter-component contact

occurs at the assembly's outer edge, so the fixture will not locate the assembly's components as intended. Therefore, it would be recommended looking at the experimental results that oversized assemblies should be located externally, while undersized assemblies should be internally located during fixturing.

- It was observed during the experimentation that the fixturing approaches which use two locators at the inter-component joint positions (i.e. CG and FDC) allowed the fixture to control an extra degree of freedom when compared to the other build methods. That is to say, the approaches with a single locator at the centre of their inner radius (i.e. TB and FDI) allowed the components within the assembly to pivot about this central location point. Moreover, any angular breaking errors within the assembly's make-up gives the components room to move within these fixturing methods making them particularly sensitive to angular breaking errors; again due the by poor control of the component's true angle KC. Conversely, within the fixturing methodologies which contained two datum locators, this rotation was blocked by the predictable geometry of the fixture making their builds more consistent and less sensitive to assembly gaps and angular breaking errors.

- The predicted inherent non-circularities were observed experimentally. Furthermore, the measured result showed a strong correlation with the mathematic prediction made within chapter 5. Although, the scale of these geometries is relatively small, but they do define the absolute limit of the circularity possible for a given set of components.

7 Investigations into the interaction between PWP and angular breaking error within weld ring assemblies.

7.1 Introduction

As discussed in chapter 5, if the sum of the wedge angles used within an annular assembly is not exactly equal to 2π radians, then angular breaking errors will be present within the final assembled structure. Given the imperfect nature of real-world manufacturing, the components of an annular assembly will contain at least some variation within their production, so in practical terms every manufactured annular assembly will contain angular breaking to some degree. However, as the positions of the angular breaking errors are dependent upon the net build conditions of the assembly, so the actual positions of the angular breaking errors can be controlled with careful tolerancing of the components. With this in mind, it has been shown in chapter 5 that, oversized assemblies will have angular breaking errors induced at their inner edge, while undersized assemblies will have angular breaking errors induced at their outer edge.

As the basic aim of this research project is to understand the key construction parameters for the creation of high quality welded ring assemblies, so a question to ask around the angular breaking errors and the gaps they create is: how do these angular breaking error gaps interact with

the Preliminary Welding Process (PWP)? This question is especially pertinent for several reasons: Firstly, to align with the illustrative industrial test-piece (chapter 4) the PWP process being explored during this project is autogenous, so there is no filler material to bridge any gaps (which is likely to make this welding type more sensitive to joint imperfections); Secondly, the PWP sets the relative positions of the components for the final seam welding process, so it is important in terms of the geometry of the ultimate weldment; Finally, the PWP is a highly localised point welding process making it more susceptible to localised geometric conditions (and air is a poor thermal and electrical conductor).

7.1.1 Chapter outline

During this chapter the thermal-mechanical interplay between an autogenous PWP and an assembly's angular breaking errors will be explored.

The chapter begins with an analysis of an unconstrained assembly of two plates separated by a small gap during an autogenous tack welding process. This study was performed to better understand the fundamental thermo-mechanical conditions at a local level, and was a first step in understanding more complex multi-part assemblies.

Next, a fixtured two component welded assembly was examined. This weld trial used a fixture to represent the rigid-body inter-component contact of an annular assembly's components during a PWP. Once the free-state and

fixtured assembly's welding conditions have been investigated the focus of this chapter will switch to investigate full ring assemblies. The full ring studies documented in this chapter are: a rigid-body geometric study, an experimental weld study and a finite element process simulation. These full ring investigations create a picture of the global interplay between the angular breaking errors and the PWP. Furthermore, they offer an understanding of the global thermal-mechanical distortions likely when manufacturing a typical welded annular structure.

7.2 Welded plates experimentation

To understand the assembly wide influence of the angular breaking errors upon the weld distortion of the PWP, it is important to first appreciate the thermal-mechanical distortions as a per-joint mechanism. To achieve this appreciation, a series of welding trials were performed using pairs of plates (in both a free-state and fixtured), which were conjoined using a GTAW PWP. Supporting these physical weld trials was a number of FEA simulations were also generated.

7.2.1 Free-state welding

The initial welding trials were performed using a pair of plates that where welded in an unconstrained state. The premise being that by fusion welding two plates, which are separated by a small gap, in a state free from the influence of any fixturing or adjacent components, a clear indication of any underlying distortion mechanisms can be obtained. Moreover, once this

local weld condition is defined it can then be extrapolated for a system wide prediction of thermal-mechanical weld distortion.

7.2.1.1 *Experimental testing*

During the welding trials, pairs of 52mm x 100mm x 12mm Ti-6Al-4V plates were joined manually via an autogenous GTAW Direct Current Electrode Negative (DCEN) fusion welding process. To generate a repeatable edge for welding each plate had one of its 100mm edges machined to a 3.2 Ra finish[3]. A simplified representation of the angular breaking errors was then created by separating each pair of plates with a parallel gap of 0.0, 0.5 or 1.0mm between the plate's machined faces. In total the testing was performed with three plate pairs at each gap width.

To measure any distortions generated by the welding process a Dantec Dynamics Q400 Dual Image Correlation (DIC) was used during the welding trials. The DIC was chosen as it would allow accurate in-situ measurements of the assembly to be taken in three-dimensions without impinging on the welding process. However, only pre and post weld measurements could be made during the experiments, as the intense light generated by the welding process's plasma arc has the potential to damage the DIC's optical sensors. The DIC system needs a unique visual reference to track the movements within the objects being measured; therefore each block to be welded was

[3] Full engineering drawings are included in the appendices

painted white and speckled with black spray prior to the experimental procedure. This generated a random, but locally unique surface pattern that the DIC's software could track across measurement frames.

The actual experimental set-up (Figure 7-1) saw a pair of plates separated by a shim (not used in the 0.0mm gap assembly), the plate pair was then constrained between two ground steel setting blocks. Once the gap was set, the shim was slid from between the plates, and the setting blocks removed. A DIC image was then taken logging the assembly's pre-weld state. A 8-12mm long PWP GTAW weld with a 100A constant current (at 24 volts) was then manually performed. Post-weld, shielding gas was applied for a further 15 seconds to minimise atmospheric pollution of the molten weldpool. Once the weld was fully complete and cooled (to room temperature) a second DIC image was taken to record the post-weld geometry of the assembly.

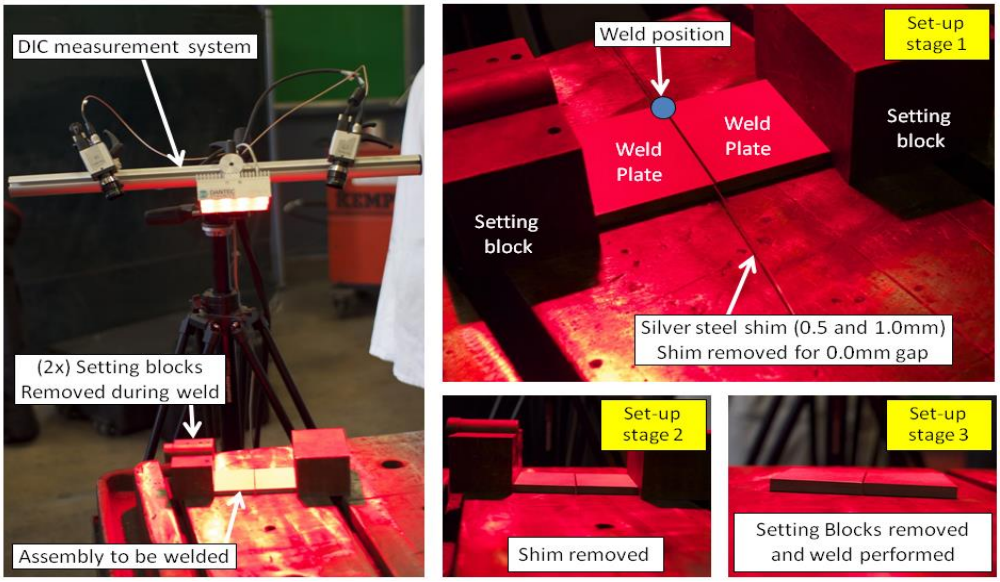


Figure 7-1 : Experimental pre-weld set-up procedure

7.2.1.2 *Experimental testing results*

The results of the three weld trials are shown in Table 7-1; where the measured gap closure, an image of sample and the DIC measurements results are tabulated per weld gap.

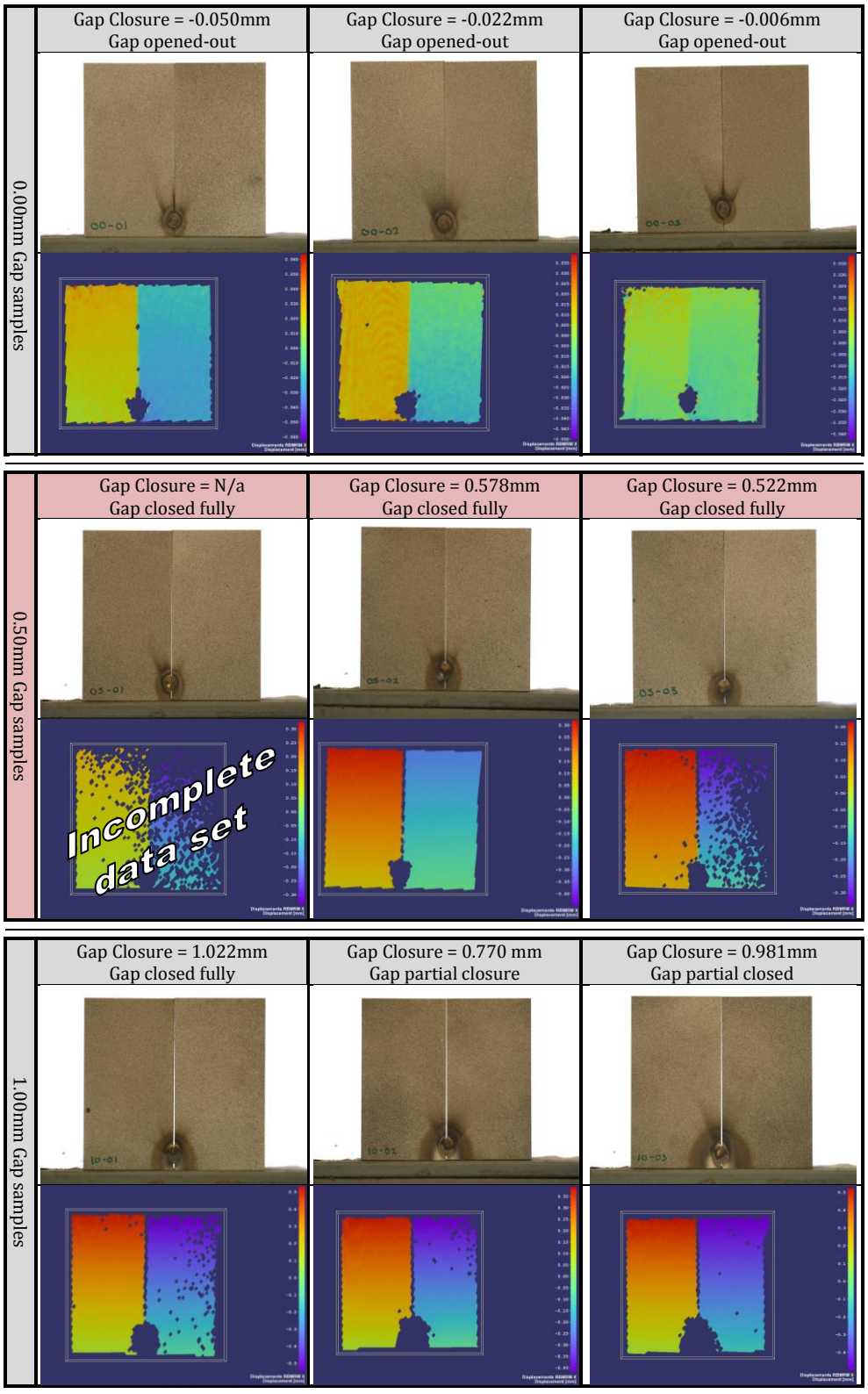


Table 7-1 Result of free-state welding trials

The results showed that the assemblies which contained a gap (the 0.5 and 1.0mm samples) experienced at least some degree of gap closure due to the welding process. The gap closure witnessed in the 0.5 and 1.0mm samples (Figure 7-2) occurred predominantly at the point furthest from the weld site. However, the DIC results showed that despite the partial closure, the gap's width remained virtually unchanged near the weld site. The lack of gap closure near the weld suggests that the traditional seam welding shrinkage mechanisms (i.e. volumetric weld shrinkage and the loss of material through spatter or vaporisation) are not the main mechanisms of gap closure in this system. The amount of gap closure was variable, and appears to be around 1.0mm as a maximum, as only one-out-of-three of the 1.0mm samples demonstrated a full gap closure. This is in contrast to the 0.5mm samples, which all saw the gap close at the point furthest from the weld. However, despite the observed values, the weight or length of the welded components may impact the degree of gap closure exhibited.

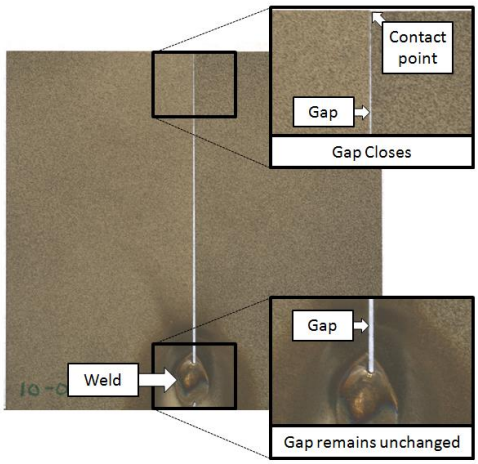


Figure 7-2 : A gap closure result of the free-state welding trials

The trial results also showed that when the samples with no gap, the weldment exhibited a small opening-out of the joint to 0.02-0.05mm. This is most likely due to localised thermal expansion exceeding the post-weld volumetric weld shrinkage. That is to say that, the weld shrinkage is not causing enough shrinkage in the experimental assembly system to close the gap after is has been opened-out by the thermal expansion of the weld cycle. However, it should also be noted that given the size of the gap, the result could possibly be due to DIC measurement noise.

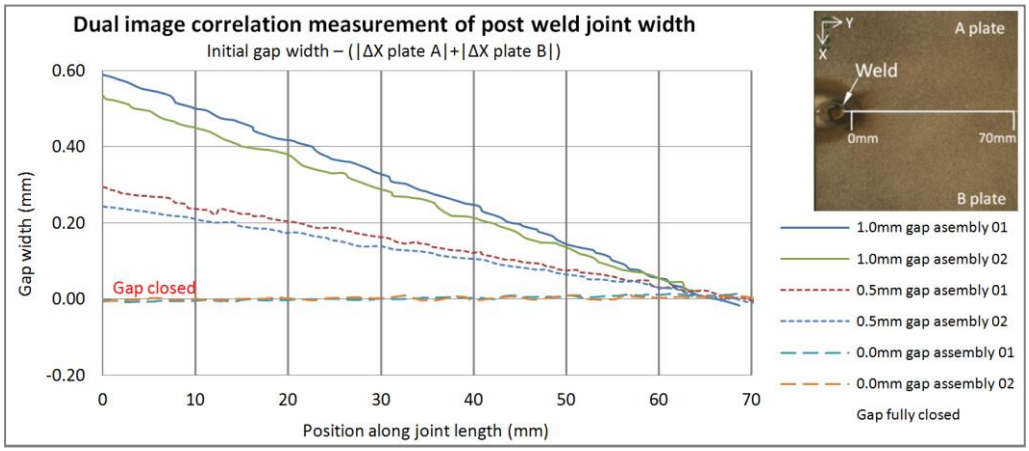


Figure 7-3: Plot of DIC camera gap size results

7.2.1.3 *FE modelling of 0.5mm assembly*

To better understand the processes at work in the free-state weld experiments a FE model was produced of the weld process. This FE model was a non-linear transient thermo-mechanical simulation performed using Visual-weld software by ESI. Using the software the two plates of the assembly were modelled separated by a 0.5mm gap. They were modelled using linear hexahedron continuum elements and assigned a Ti-6Al-4V material. The plates were modelled so that the elements were distributed

with a linear bias towards the welded zone refining the mesh in the areas of most interest. The model also contained a node-to-surface contact boundary condition between the opposing surfaces inside the joint, which was to ensure the interaction between the two plate bodies could be captured.

A filler material was modelled at the weld site bridging the gap between the plate bodies so that heat could transfer across the joint void. Defining this filler material were specialised "chewing gum" elements; which begin the simulation with a modulus of elasticity of $1x10^{-5}$ times that of the base material (Ti-6Al-4V in this model). This low-stiffness state persists until the filler is heated above its melting temperature (1660°C), whereupon its phase changes to adopt the modulus of elasticity of the base material [243].

The bench used in the "real-world" experiment was captured in the FE model through the use of directional boundary conditions. These directional boundary conditions blocked movement of the plate models in the –Z (i.e. through the bench) direction only, and allowed the components to move freely in the XY & +Z directions. To prevent uncontrolled Rigid Body Motion (RBM) in the +Z direction the weight of each part was simulated via a point force applied at the approximate centre of gravity of each plate. This simulated weight was then applied in the –Z direction, pushing the part onto the virtual bench. Finally, as there is no friction within the simulation between the plates and "bench", a node on one of the plates was fully constrained in the X and Y directions. This boundary condition

was required to prevent the uncontrolled RBM of the assembly during welding, but it was only required on one plate as the chewing gum filler material would prevent RBM in the second plate.

To model the heat-source in the FE software the physical size of the weldpool was measured from the experimental weldments. This offered the height and width dimensions of the heat-source for use in the FE model of the process. To obtain the penetration one of the zero gap weldments was split-open to expose the weld in cross-section (Figure 7-4), allowing a depth measurement to be made. The weld was found to typically be 7-9mm wide, 9-13mm long, with a penetration depth of ≈3mm.

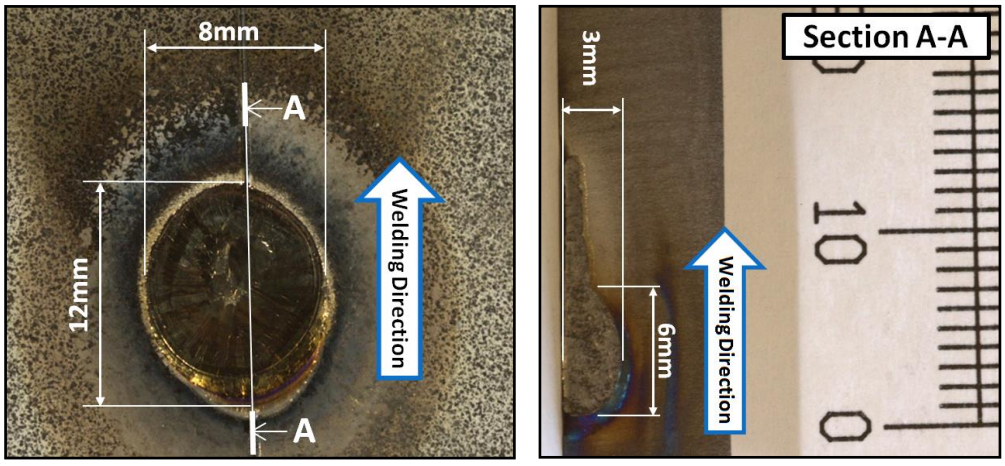


Figure 7-4 : Typical PWP weld and crosss-section

Along with the heat-source's geometric data, the weld power per unit length – or flux - was also required for the modelling process. To extract this data from the experimental set-up the thermal flux estimated from the measured physical weld using a method proposed by Pichot et al.[244]. Their approach shown in Eq.1 uses Q to represent the homogeneous

thermal flux (W/mm) for a given weld power P, and R as radius of the disc through which the power is transferred.

$$Q = \frac{P}{\pi \cdot R^2} \qquad (1)$$

To calculate the power in the used in welding process (assuming 100% efficiency) the fundamental power equation (Eq.2) can be used. In this equation P is the weld power in Watts, V is the potential difference in volts and I is the current in Amperes.

$$P = VI \qquad (2)$$

For the given experimental set-up the potential difference used during welding was 24V and the current 100A, deriving a flux (Q) of 381 W/mm if Eq.1 and Eq.2 are used.

7.2.1.4 *Modelling results*

The results of the simulation showed a similar resultant geometry to that observe during the experimental testing (Figure 7-5). That is, with a point contact occurring at the edge furthest from the weld site, while a negligible degree of closure occurring locally to the weld itself.

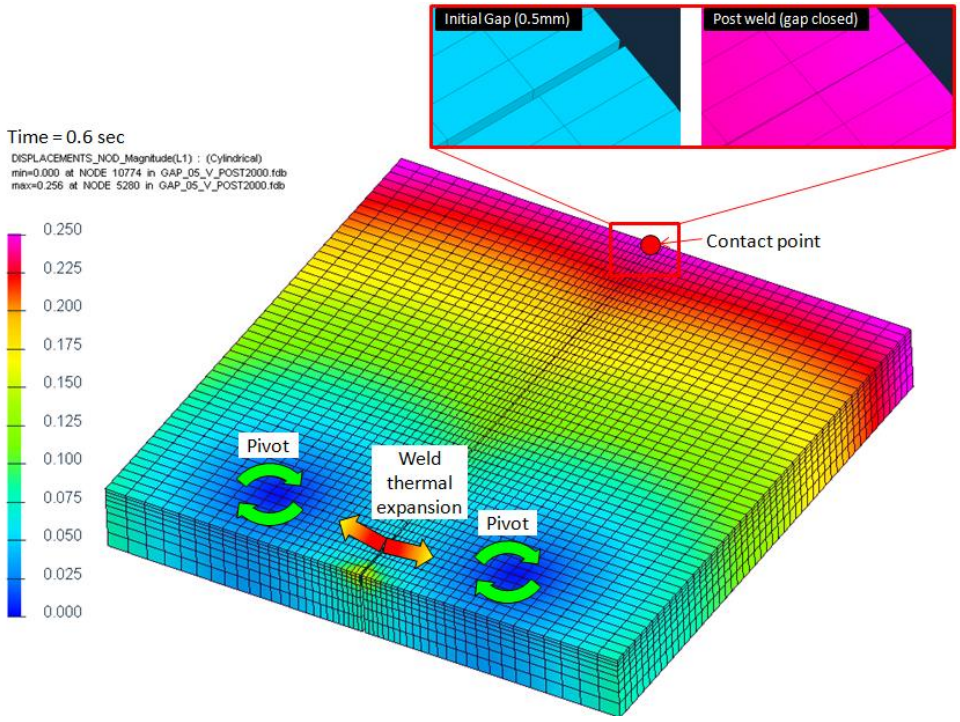


Figure 7-5 : Displacement results of free-state weld simualtion

Interestingly, this point tracks the welds movement along the joint, so as the weld moves forward so too will the pivot point. This suggests that the length of the PWP weld is critical to the described closure effect. In that, if the length of the weld increases the contact point will re-open, as the pivot moves down the assembly. This is possibly why the point contact mechanism has not been previously noted in studies looking at full seam welds, but as the PWP is a point welding approach so this pivot mechanism has become apparent in the results. This mechanism is potentially important, as many industrial processes use the PWP to set the positions of an assembly's components prior to the final seam welding operation, so this effect will influence the final geometry of a weldment. That said, in most industrial applications the components will be located/datumed and

clamped, which may block the effect, so it is only truly apparent in a free-state welding condition.

7.2.2 Constrained state welding

Although the free-state welding trials tell us a great deal about the underlying distortion mechanism of the PWP, it is not a good facsimile of the true in-fixture geometric conditions found in the creation of a welded ring assembly. That is to say, the free-state welding trials ignore several key-features of the assembly's local weld conditions, these being: the influence of the neighbouring components; and the gap will be V-shaped with a pre-existing point contact, rather than parallel. To address these shortcomings, a new set of weld trials were performed using a new two plate assembly. This time, the plates were designed to include a small V-shaped gap, while the presence of neighbouring components was replicated via a small weld fixture.

7.2.2.1 *The weld fixture and components*

The constrained plates welding trial was performed using eight pairs of 120mm x 55mm x 3mm thick mild-steel plates. Each plate contained a 0.125°±0.05° angle along one of its long edges, so that when two plates were placed together as a mirrored pair they would generate a 0.25°±0.1° V-shaped gap between them (Figure 7-6). Each plate also contained a dowel hole which was used to set the position of the plates in the fixture (via a stab-pin). These set-up datum holes were only used to position the assembly's components prior to welding, and were carefully removed

before any welds were performed. The plate's design also contains a concave datum surface for timing the plates rotationally, against a pin in the fixture. This concave face and pin arrangement was put in place to simulate the components rigid-body interaction with its neighbouring components, making this test more reflective of the local weld conditions of a full ring structure. As these pins are a facsimile of the adjacent components in the full assembly they remain in place throughout the welding process. Finally, a Ø11 clearance hole (for an M10 bolt) was also included in the plate so that a bolt can be used to clamp the plates to the fixture[4].

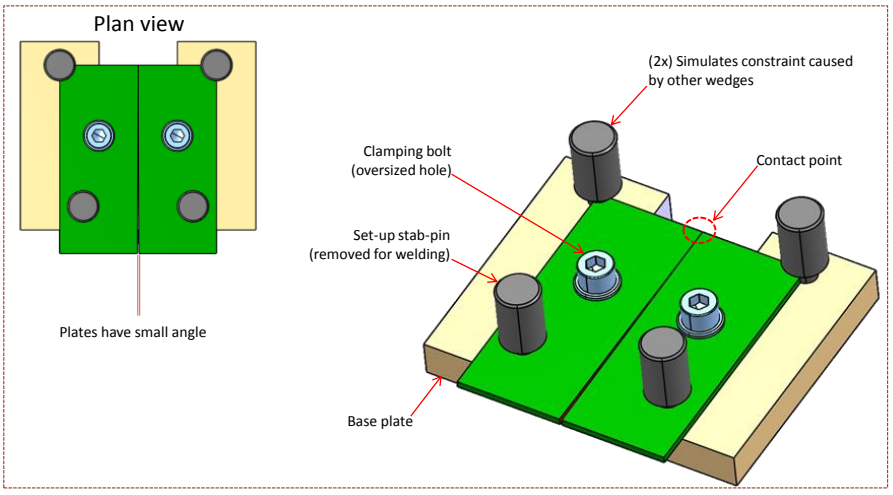


Figure 7-6 : The plates and fixture for the constained plate weld trial

Figure 7-7 shows a flow diagram of the fixture and the basic process for setting-up the assembly ready for welding. Step 1, shows the fixture base plate onto which a pair of plates are placed. Step 2, a pair of weld plates are positioned symmetrically on the fixture base plate, so that the angled faces

[4] Full engineering drawings for the plates and fixture are included in the appendix.

of the weld plates generate a V-gap along the centre-line of the fixture. Step 3, the four datum stab pins are then inserted into the fixture, which pass through the weld plates into the fixture base; locating the assembly using the main datum hole and the concave datum feature. Step 4, the clamp down bolts are inserted and tightened, before the full location stab-pins are removed (to leaving just the locators at the concave datum surfaces) – step 5. The assembly is then set for the welding operation (step 6).

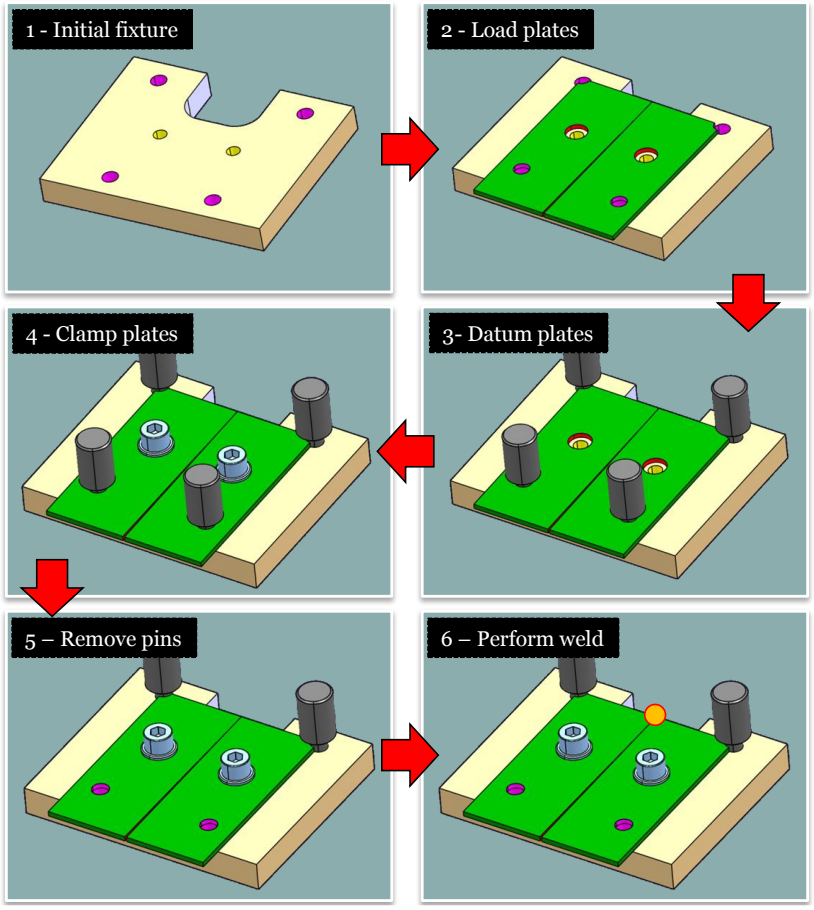


Figure 7-7 : The constained plate fixture operation sequence.

7.2.2.2 *The testing*

As with the previous weld experimentation, each assembly was painted matt white and speckled with black spray-paint, so that the Dantec

Dynamics Q400 DIC system could be used to measure the weld deformation. An assembly was then loaded into the fixture, and had its initial geometric state recorded via the DIC before any welding was performed (as shown in Figure 7-8). The PWP was then carried out manually using a GTAW DCEN autogenous welding process. Four welding configurations were experimentally trialled, these being: (a) welding only the outer edge gap-end of the assembly's joint; (b) welding only the contact-point of the joint; (c) welding the contact-point and then the gap-end of the joint; and finally, (d) welding the gap-end and then the contact-end of the joint. Each of these configurations where welded twice (giving eight samples in total), with the DIC camera being used to record the assembly's geometric state after each weld. The final geometry of the assembly was recorded with the DIC system once all the welding had been performed and the assembly had cooled to approximately room temperature (judged by touch).

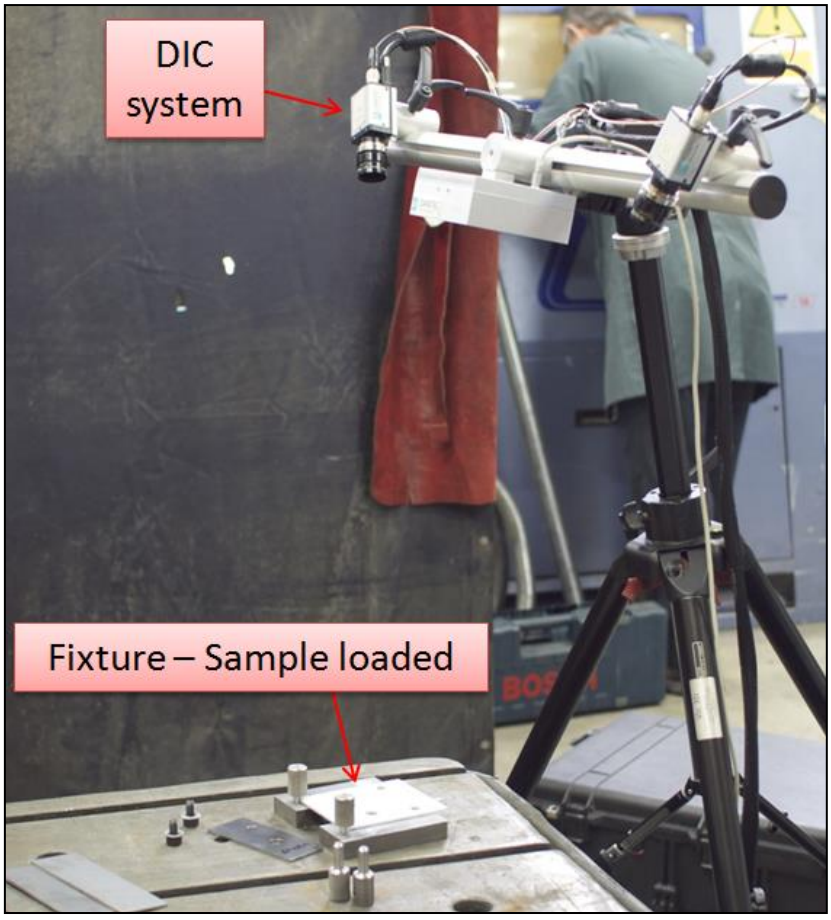


Figure 7-8 : The constrained welding trial set-up

7.2.2.3 *The results*

An overview of the results for the constrained plate trials are shown in Table 7-2. Looking at this data, the first point of note is that all the V-gaps welded during the trial opened outwards; widening the V. This contrasts the earlier free-state welding trials, which saw all the samples containing a gap exhibit at least some degree of gap closure due to the PWP. It was also observed that the degree of gap widening varied with the location of the initial weld. That is to say, when a weld sequence was begun at the contact end of the V-joint, the resultant weldment consistently exhibited a higher degree of joint widening than sequences which welded the gap-end of the

joint first. Indeed, because of this widening, it was not possible to complete all of the weld trial weld combinations. This was especially problematic in assemblies where the contact edge of the joint was welded first; with the initial weld opening-out the gap and making it too wide for the weldpool to bridge. This situation might be rectifiable with the inclusion of a filler material in the welding process, but the scope of this project is to examine only autogenous welds.

In the multi-weld trial assemblies which were possible (i.e. weld gap-end and then contact-end of the joint), the second weld appears to have little effect on the width of the v-gap. This is probably because the first weld fixes the geometry of the assembly and its stiffness is then great enough to resist the thermal effects of the second weld, reducing its influence on the final geometry of the fused assembly.

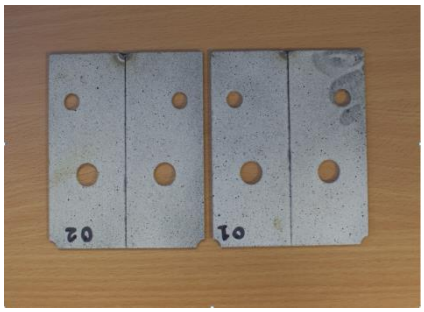
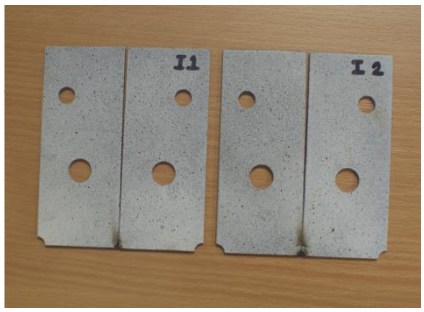
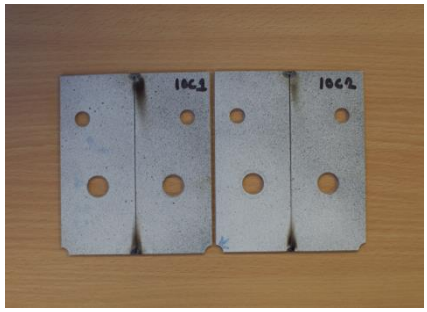
Weld position	Image of weldment	Result overview
Gap edge only		Sample 1 Opened-out 0.158 mm
		Sample 2 Opened-out 0.211 mm
Contact edge only		Sample 1 Opened-out 0.954 mm
		Sample 2 Opened-out 1.530 mm
Gap edge then contact edge		Sample 1 Opened-out 0.189 mm
		Sample 2 Opened-out 0.188 mm
Contact edge then gap edge		Sample 1 Opened-out 1.084 mm
		Sample 2 Opened-out 1.380 mm

Table 7-2 : Result of constrained welding trial

More in-depth analysis of the joint geometry can be seen in Figure 7-9 and Figure 7-10. These plots (from the DIC data) show the movement of each plate relative to its pre-weld position, so that the width change of the V-gap is the difference between the two lines. Furthermore, these plots show the change in gap width against the length along the joint, with zero being the contact-end of the joint. Finally, the graphs have been separated (for clarity) into single stage (Figure 7-9) and multi-stage welding configuration (Figure 7-10).

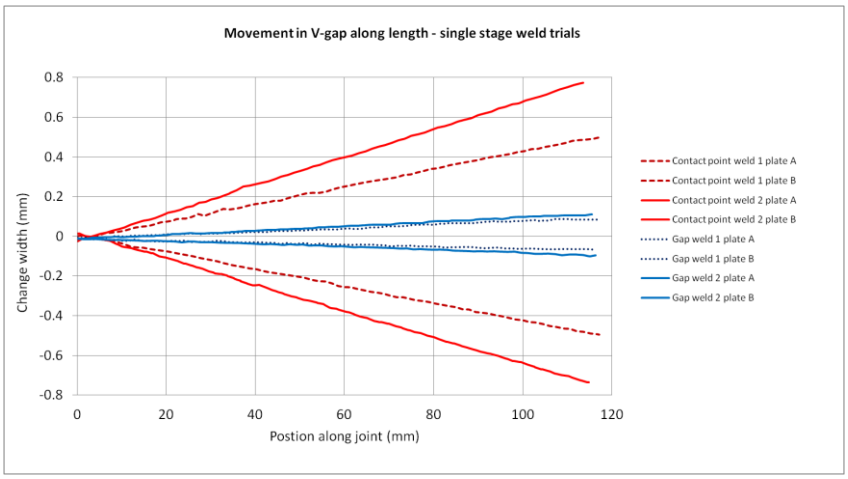


Figure 7-9 : Plate movment along joint – single stage weld processes

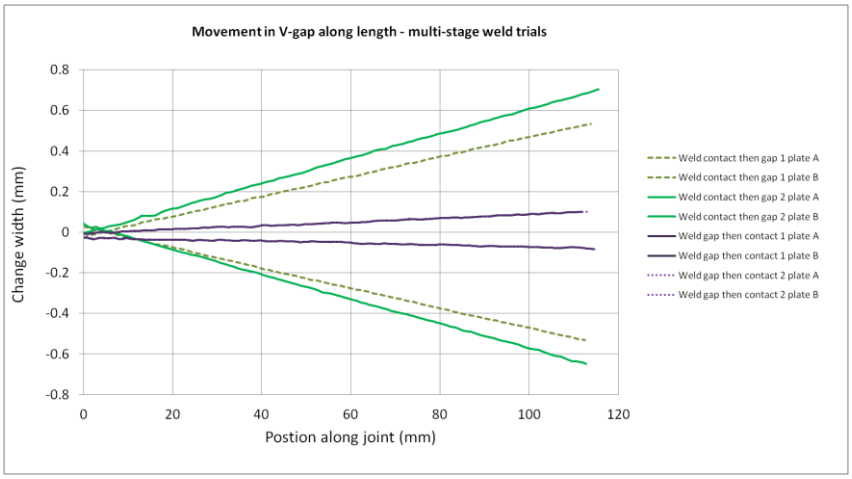


Figure 7-10: Plate movment along joint – single stage weld processes

These plots reinforce the observation that it is the placement of the first weld which determines the final gap geometry. This idea can be seen in the similarity between the single and multi-weld plots, which suggests that the second weld added little to the overall assembly distortion.

These plots also help explain how the assembly is geometrically capable of widening the gap. That is to say, given that the assembly's plates are constrained via fixed datum pins and a solid point contact between each plate they should not be capable of rigid body motion. However, looking closely at the plots it can be seen that in the trial where the contact edges are welded first (shown at 0 along the X-scale) the plates exhibit a negative movement in the plate positions. This suggests that the welding process is melting the point contact, and weld shrinkage is then pulling the plates into the gap generated by this melting. Moreover, given that the contraction is highly localised it is likely the weld shrinkage is then pivoting the gap open (in a manner similar to the pivoting seen in the earlier free-state trials).

A similar mechanism may be present within the results of the "weld gap-end and then contact point" samples (Figure 7-10), however in these instances as the weld is placed at the gap end of the joint it will have created shrinkage and residual stresses which are trapped by the fixed datums and the contact point geometry. Welding the contact point then melts the interface between the two plates allowing the stresses to be released. This then results in an opening-out at the contact point (shown at 0 along the X-scale).

To summarise the free-state and constrained plate weld trials; when two plates are welded in a free unconstrained state, the highly localise thermal expansion of the PWP pivots the gaps closed at the point furthest from the weld-site. However, constraining the plates to replicate the typical in-fixture geometric conditions of a full ring assembly, the v-gap opens outwards upon welding. Furthermore, it is likely that the melting of the point contacts between the components during the PWP, generates space for the parts to move enabling the observed expansion in the gap. Consequently, welding the gap end of the join first, locks the position of the geometry prior to melting this contact point. This reduces the influence of the "room to move" created by melting of the inter-component contact point.

7.3 Weld rings experimentation

Although the plate welding trials offer an insight into the fundamental conditions and distortion mechanisms at a local level, it is also important to understand the influence of these local phenomena at a global level. To that end, a series of physical and virtual (via FE simulation) segmented welded ring assemblies have been produced. The subsequent weldments (be they physical or virtual) have then been examined to identify the distortion geometries which define their final geometry.

7.3.1 Fundamental distortion shapes

Given what has been previously established concerning the angular breaking errors within a typical segmented ring structure (chapter 5) and their interaction with the welding process (this chapter), an interesting question to answer would be; what geometric form would an assembly resolve to produce should it be possible to fully close the angular breaking error gaps with the welding process? Answering this question may offer a prediction of the final geometric form of a ring weldment.

To answer the posed question a physical test was performed using six ten-segment ring assemblies, constructed from laser-cut 3mm sheet material and assembled with adhesive. Within each of these test assemblies the wedge angle of the components was adjusted (see Table 7-3) to impose a known amount angular breaking into each assembly. During the construction of each ring, the V-shaped gaps generated by the angular breaking errors where forced closed during gluing.

Ring ID	Nominal wedge angle (θ°)	Error per segment (°)	Total error in assembly (°)
1	33	-3°	-30°
2	34	-2°	-20°
3	35	-1°	-10°
4	37	+1°	+10°
5	38	+2°	+20°
6	39	+3°	+30°

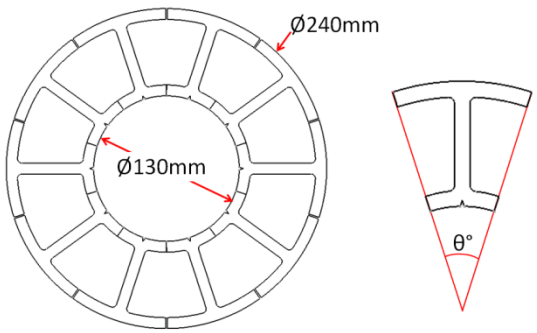


Table 7-3 : Gap clousre assemblies induced errors

The resultant structures once assembled showed two fundamental geometries emerging. The first, was a quantised conical geometry (Figure 7-11a), which was observed in assemblies were the sum of the wedge angles was <2π radians. The second geometric form was a quantised saddle (Figure 7-11b), which was observed only in assemblies where the sum of the wedge angles was >2π radians. Both of the geometries are described as "quantised" as their final form is an approximation constructed from the fixed geometry of the component parts. That is to say, the conical shape is not truly round, but instead an approximation constructed via a ten-sided polyhedral form. However, in both cases the distortion being generated is due to the change in the relative circumference length of the inner and outer diameters as the angular breaking gaps are forced closed.

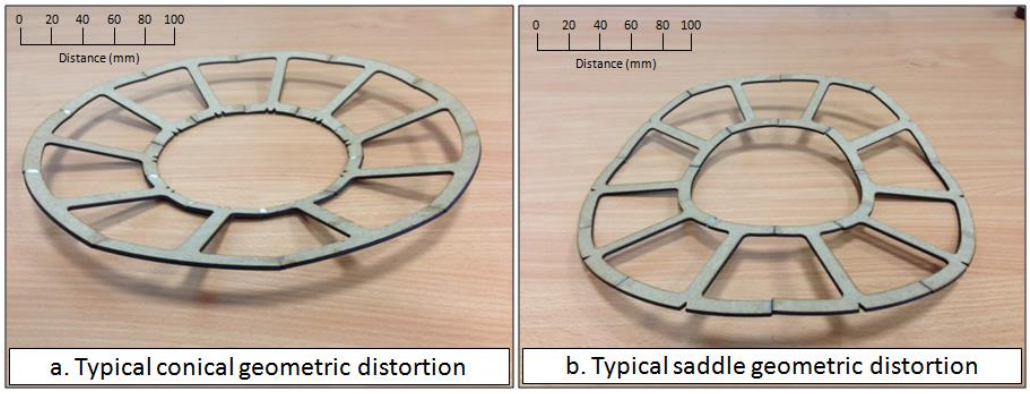


Figure 7-11 : Typical structures quantised a) conic, and b) saddle

Examining the assembled structures further it becomes apparent that the greater the angular error within the assembly, the more severe the resultant geometric distortion (Table 7-4). This increased distortion manifested itself as an out-of-plane error within the assembly, so that the Z-height (vertical height perpendicular to the plane of assembly) increases

in-line with angular error. A further observation about the two geometries is that the quantised conic form is far more stable and predictable geometrically than the quantised saddle. Moreover, the saddle's geometry comprised of two high and two low lobes, which were positioned perpendicular to each other about the centre axis/hole. However, these lobes could easily be manipulated by hand and repositioned as the structure was flimsy. This contrasted to the conic form which was structurally very robust. It should also be noted that the conical structures were also easier to assemble than their saddle counterparts; which is most likely due to the geometric stability of the final form factor of the assembly.

Ring	Total assembly error (°)	Resultant geometry	Out-of-plane Error (mm)
1	-30°	Conic	82
2	-20°	Conic	75
3	-10°	Conic	38
4	10°	Saddle	12
5	20°	Saddle	15
6	30°	Saddle	25

Table 7-4 : Out-of-plane error in assembled ring geometry

In summary, the knowledge generated during this study suggests that when defining a welded ring structure, the designer should specify a minus-minus tolerance in the component's wedge angle. This will force the sum of the component's wedge angles to be $<2\pi$ radians, which in turn will push the angular breaking gaps to the outer edge of the assembly and contact points to the inner edge of the assembly. Working with this ethos, will generate a quantised conic distortion in the completed weldment. Moreover, given the

improved geometric stability of the conic form; this will make for a more favourable build outcome in a manufacturing environment than the unpredictable (thus less repeatable) and geometrically less stable quantised saddle form.

7.3.2 Physical weld trials

To understand the influence of the PWP interaction with the inevitable assembly gaps in the context of a full ring structure a welding trial using full segmented ring assemblies was undertaken. These full-ring trials would expand on the knowledge generated during the free-state and constrained plate welding trials, to explore the interplay between the PWP and V-shaped angular breaking gaps in a full-ring assembly rather than an isolated context. To do this three weld configuration would be tested: the first, (A), weld the outer joints of the ring with an autogenous PWP; the second, (B), weld only the inner joints of the ring with an autogenous PWP; and finally, (C), weld both the outer and inner joints of the ring with an autogenous PWP.

To perform the full ring welding trials a six segment ring assembly and simplified weld fixture were designed (Figure 7-12)[5]. The base geometry of the segmented ring had an internal diameter of 200mm and an external diameter of 440mm, and was manufactured from 3mm mild steel plate.

[5] Full engineering drawings are included in the appendices.

Each wedge component was specified with a nominal wedge 60° angle. Unlike the previous trials no explicit manufacturing error was induced in the angular face of the components, as this test was intended to be a closer approximation of "real-world" assembly conditions than previous trials. To assist in the pre-weld assembly of the segments, each wedge part contained a single oversized (Ø14 clearance hole for an M10 bolt) hole at the centre of each component. This hole was not intended to locate the components via the bolts, but instead it acted as a rough guide to assembly when loading the parts into the fixture. Furthermore, as the premise of this trial was to better understand the interactions between components during the PWP, and not the influence of the fixture. As a consequence, the bolts used in the fixture were left loose during welding, so that there were no clamping forces influencing the weldment's geometry.

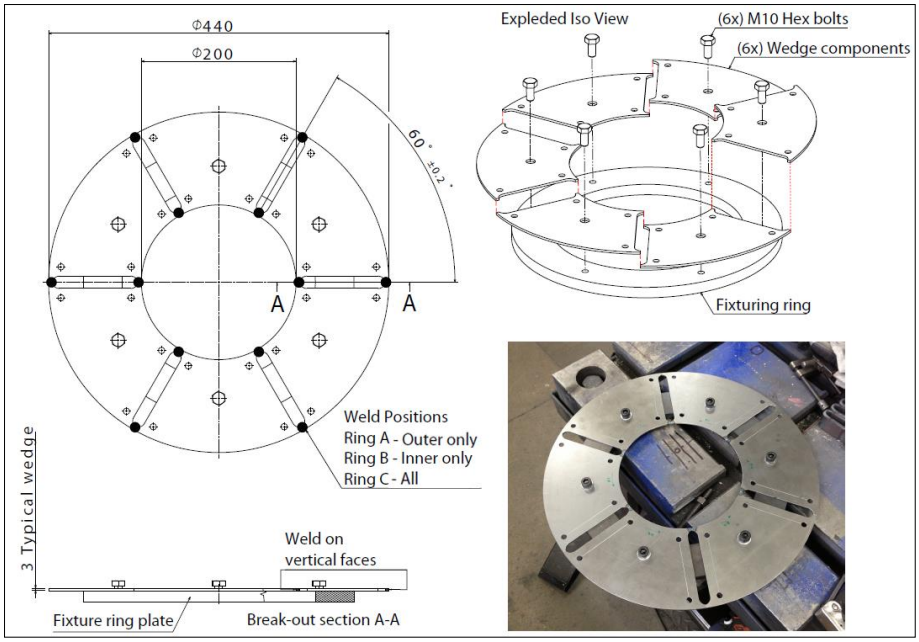


Figure 7-12 : Experimental test ring assembly and fixture

For testing three assemblies were produced from a batch of eighteen manufactured wedge components. To quantify the quality and position of the angular breaking errors within these assemblies, the wedge angle of each component was measured using a Mitutoyo Euro-C-A-121210 Coordinate Measurement Machine (CMM). From these measurements, the nominal wedge angle was found to be 60.05°, with a total range of ±0.03° across the pool of components. The implication of this is that all the constructed assemblies would be slightly oversized (i.e. >2π radians), so the contact points for all the assemblies would be at the outer edge of the assembly and the gaps at the inner edge. Beyond identifying the angular breaking errors, each assembly was also measured pre-weld to give a snapshot of the assembly's geometry before welding. To do this each assembly was CMM measured (two points per segment) for inner diameter, inner diameter circularity and assembly flatness. The results of these pre-weld assembly measurements are shown in Table 7-5

Ring Designation	**Positions to be welded**	**Inner Diameter (n=12)** (mm)	**Inner Circularity (n=12)** (mm)	**Assembly Flatness (n=12)** (mm)
A	Outer only	200.306	0.325	0.348
B	Inner only	200.284	0.395	0.424
C	Both (Outer then inner)	200.585	0.863	0.3519

Flatness measurements ±0.00266 at 95% confidence
Diametric measurements ±0.0099 at 95% confidence

Table 7-5 : Pre-weld assembly measurements

Once the pre-weld geometric state of each assembly had been recorded, each assembly was then welded sequentially counter-clockwise using constant current (25A) autogenous GTAW process. Each joint was tacked on the vertical (3mm) edge face of the component, rather than the top face. This approach was to prevent a biasing of the heat distribution by heating one side of the plate, reducing the likelihood of inducing a traditional "butterfly" type weld distortion. Moreover, this approach should offer a clearer picture of the weld distortions due to the assembly gaps rather than those created via skewed heating or offset weld shrinkage. Once complete, the welded ring assemblies were then measured for inner diameter, inner diameter circularity and assembly flatness using the same CMM and approach as the pre-weld measurements (Table 7-6)

Ring Designation	**Positions to be welded**	**Inner Diameter (n=12)** (mm)	**Inner Circularity (n=12)** (mm)	**Flatness (n=12)** (mm)
A	Outer only	200.049	0.593	0.613
B	Inner only	200.034	0.292	5.51
C	Both (Outer then inner)	200.223	0.309	0.158

Flatness measurements ±0.00266 at 95% confidence
Diametric measurements ±0.0099 at 95% confidence

Table 7-6 : Post-weld assembly measurements

Comparing the pre and post weld measurements a number of interesting observations can be made. Firstly, the welding has improved the circularity of most of the rings, with the exception of the A (weld inner only) ring.

Secondly, most of the weld scenarios exhibited a loss of flatness between the pre and post weld geometry. Finally, all the welded rings exhibited a reduction in their inner diameter of ≈0.3mm, irrespective of the number or position of the welds.

As stated, the out-of-flatness data shown in the Flatness measurements *±0.00266 at 95% confidence*

Diametric measurements ±0.0099 at 95% confidence

Table 7-6 was generated using a CMM to measure data two-points per segment. However, looking at the finished weldments this did not appear to fully represent the true distortion within the structures. Therefore, to get a more complete representation of the weld distorted geometry, the weldments were also measured on the CMM using a contact scanning probe. The probe was set to scan the assembly in 2mm wide passes (Figure 7-13), and the data was then loaded in Catia V5R20 CAD software for comparison to the nominal CAD model. Figure 7-14 shows the results, as a vertical height disparity between the nominal CAD file and the measured samples (in MM).

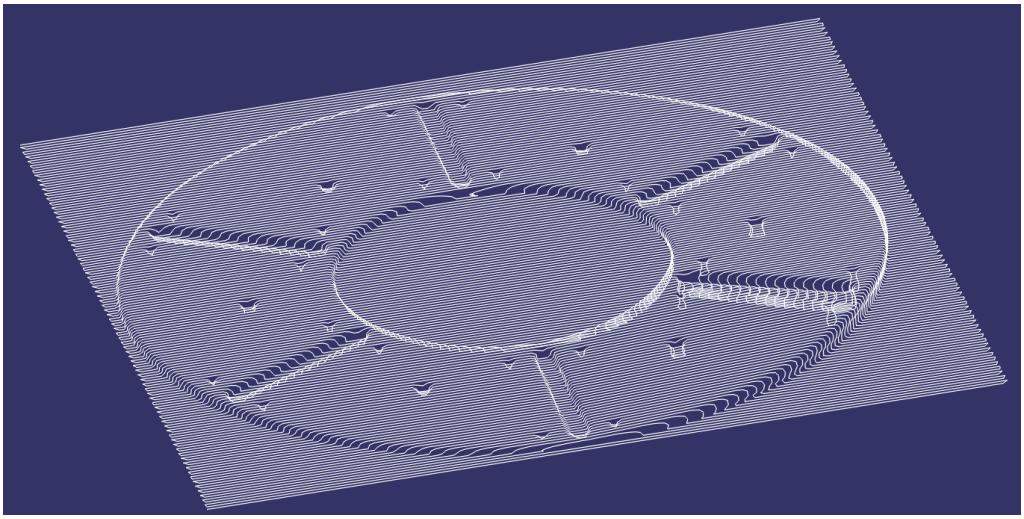
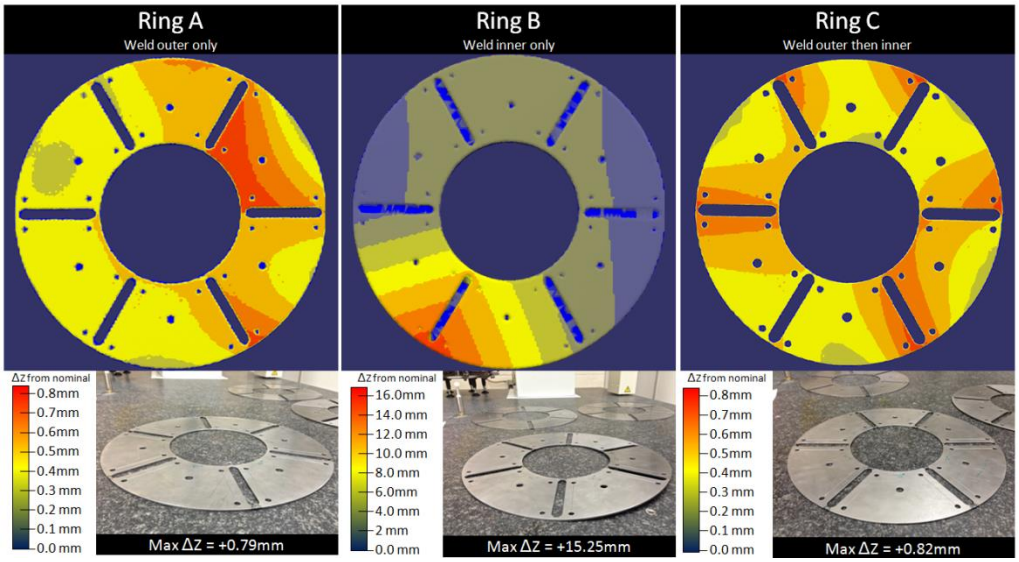


Figure 7-13 : Typical scan of welded ring, with 2mm slice resolultion.



Flatness measurements ±0.00266 at 95% confidence

Figure 7-14 : Results of CMM contact scanning

The scans showed in greater detail the out-of-plane distortion within the assemblies. They showed that the A and C rings distorted a little less than 1mm, while the B ring distorted 15mm. Although, the scans clearly showed the geometric form of each ring, it is difficult to identify the resolved geometry. Having said that however, the three welded rings look more like the quantised saddle than the quantised conic geometry.

Given that each weld was carefully placed on the vertical (3mm) face of the welded components to deliberately avoid off-set thermal loading, where could this out-of-plane distortion have come from? Considering the previous geometric and weld studies presented, what appears likely is that the out-of-plane distortion within the ring weldments is due to the closure of the angular breaking gaps driven by volumetric shrinkage of the welds. This hypothesis is reinforced when considering the previous study; which showed exactly this type of distortion when the angular breaking gaps were forced closed. Furthermore, add to this the well documented volumetric shrinkage of welds [223, 224, 237, 245], and a strong case is presented. This mechanism may also help explain why the assemblies welded at the contact points first (the A & C rings) performed better in terms of flatness than the assembly whose initial welds were placed at the gap end of the joint (the B ring). To explain, welding the contact point first forces the weld shrinkage to pull against the solid geometry of the components, rather than trying to pull an assembly gap closed. Furthermore, once this initial weld has solidified, it stabilises the assembly joint, and the stiffness of this solid weld then resists the shrinkage of any subsequent welds. Having said that, to perform an autogenous weld the contact point must be melted (at least partially) to generate a weldpool. This melting of the base material then allows for a small amount of weld shrinkage in the assembly; which is seen as a small reduction in the weldment's diameter and the out-of-plane error observed of the A and C rings. Interestingly, this shrinkage in diameter is beneficial in reducing the severity of the distortion caused by subsequent

welds. This is because the loss of base material at the point contact will reduce the widths of the assembly gaps slightly within the ring structure. This may explain the similarity of the results between the A ring (weld outer only) and the C rings (outer then inner), when looking at flatness. Moreover, as the B ring (weld inner only) placed the initial welds straight onto the angular breaking gaps, so it has not benefited from the reduction in gap width or the extra structural rigidity. Consequently, the B ring produced the most pronounced out-of-plane error as due to the weld shrinkage pulled the error gaps closed.

To test the link between gap closure and out-of-plane weld distortion all the weldments where examined under a Keyance optical microscope at 50x magnification. The results of the microscopy (Figure 7-15) clearly support the hypothesis described above, with the most distorted weldment (B ring – weld inner only) clearly showing full gap closure at both the inner and outer edges of the assembly's joints. While, the A (weld outer only) and C (weld outer then inner) rings show closure only at the contact-point (outer edge) of the weldment. The observation, that the gap at the inner edge of the C ring is not fully closed, suggests that the stiffness of the initial weld (at the contact-point/outer edge) resists the volumetric shrinkage of the second weld at the gap-end of the joint (inner edge).

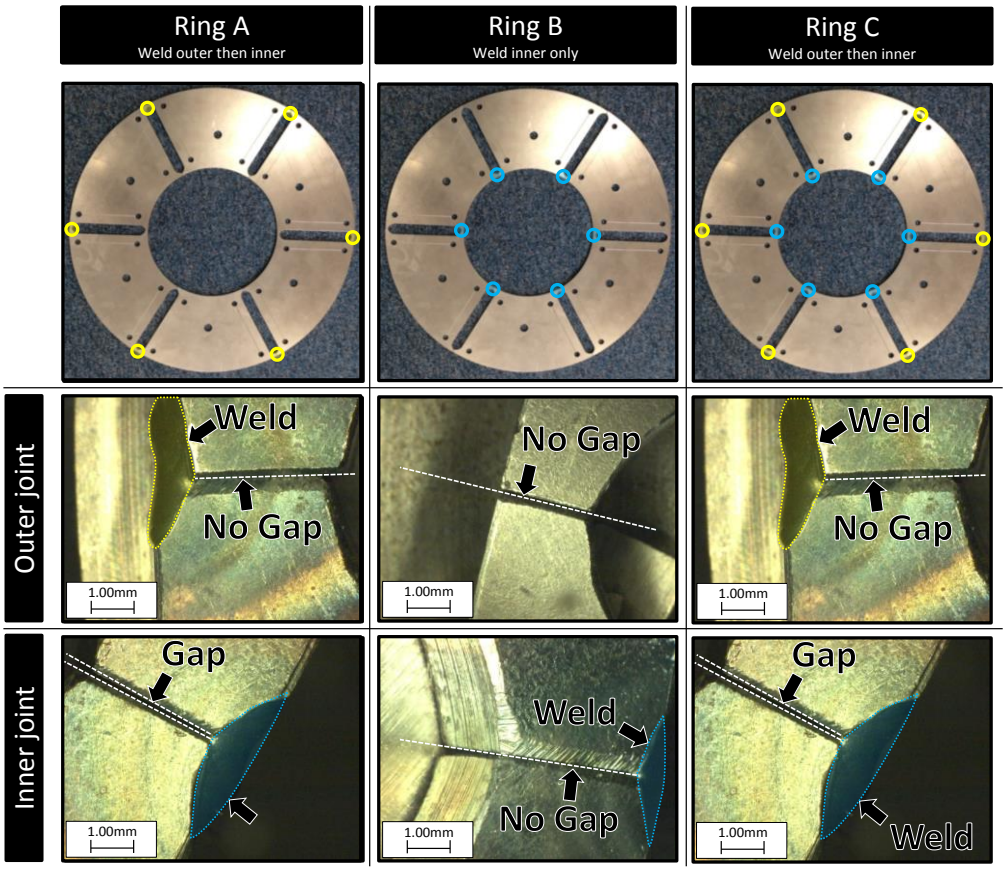


Figure 7-15 : Welded ring joints observed with 50x optical mircoscope

7.3.3 FE Modelling

To further understand the mechanisms at play during the PWP of a full ring structure a series of finite element analysis (FEA) simulations were undertaken using ESI Visual-weld. The base ring assembly was modelled using linear prismatic continuum elements. To match the manufactured condition of the physical trials, the wedge shaped assembly parts were modelled using a steel material with an angle of 60.05° between the mating faces (Figure 7-16). 0.6mm elements were used in the model of the components; this ensured there were enough elements to accommodate the Goldak double ellipsoid heat source model within the 3mm thickness of

the plate. A 3mm long by 6mm wide weld with a 2mm penetration depth (all measured from the experimental samples) was used for the simulations. While, a welding speed of 1.5mm/s (measured during the trials) with two-seconds being left idle between each weld in the sequence was used, along with a weld power of 265 W/mm (from Eq.1 and Eq.2). As the mesh used in this simulation was quite fine the centre geometry of each component was removed in an effort to lower the number of elements being processed in the simulation. Again, a "chewing gum" filler material was used to ensure heat transfer across the assembly gaps without influencing the movement of the components. Also, Node-to-face contact boundary conditions were added between adjacent assembly components, facilitating realistic rigid body interactions. In addition to the contact boundary conditions, each assembly component also had a stop condition applied to its underside. It was applied to four nodes towards the extremities of the part, and prevented movement in the –Z direction, this acted acting as a representation of each component's contact with the fixture. An external force of 1.8N was also added to the simulation as a representation of the components weight (measured from the manufactured parts). However, because there were no nodes at the component's centre of gravity, the force was evenly distributed between four nodes towards the edges of the components. Finally, to prevent rigid body motion in the assembly, two nodes in the first welded component where fixed in the XY directions.

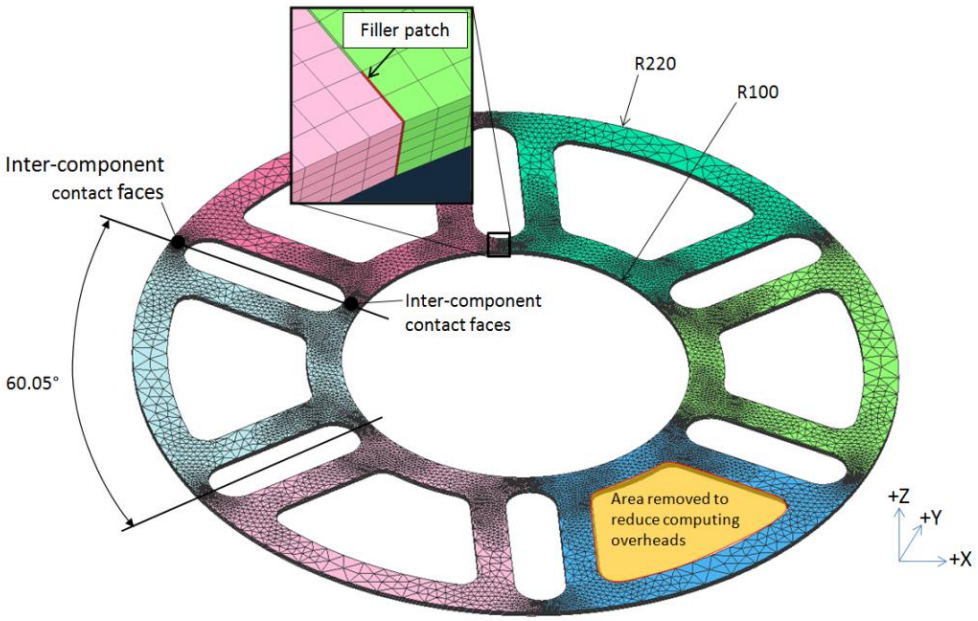


Figure 7-16 : Set-up for weld simulation

Using this simulation set-up, four variants of the welding simulation were run: A – Outer welds only; B – inner welds only; C – outer welds and then inner welds; and D – inner welds and then outer welds. The resultant simulations aligned well with the physical weld trials, with the exception of simulation D which was only performed as a simulation. The results of the simulation are expressed within Table 7-7, where the maximum out-of-plane error, description of resolved geometric form, and an image of the simulations results are shown. The results shown are all taken 300 seconds into the simulation.

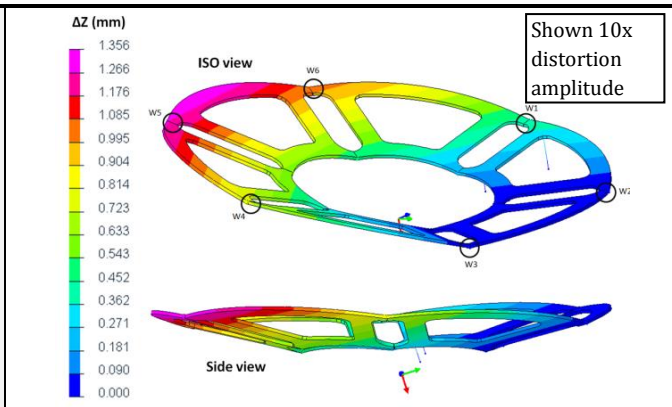
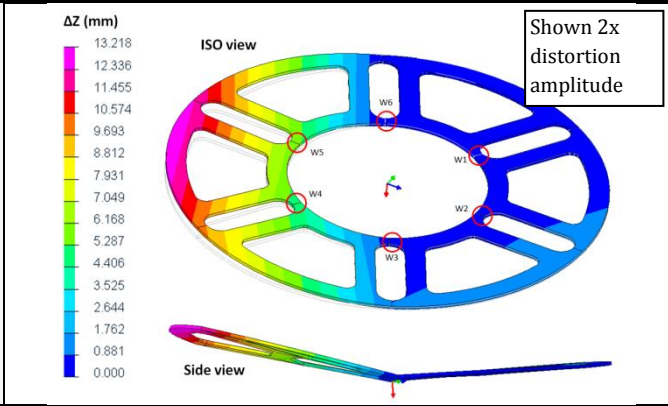
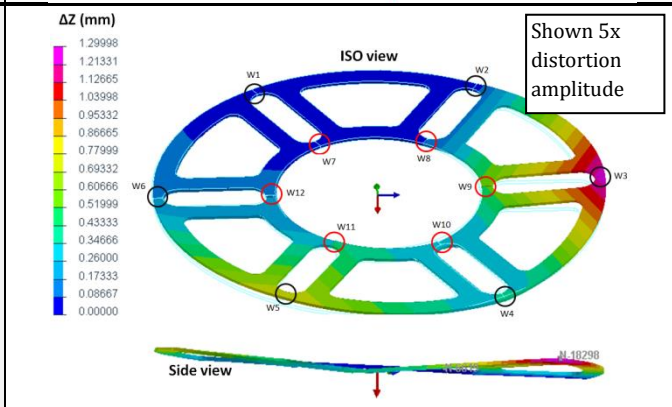
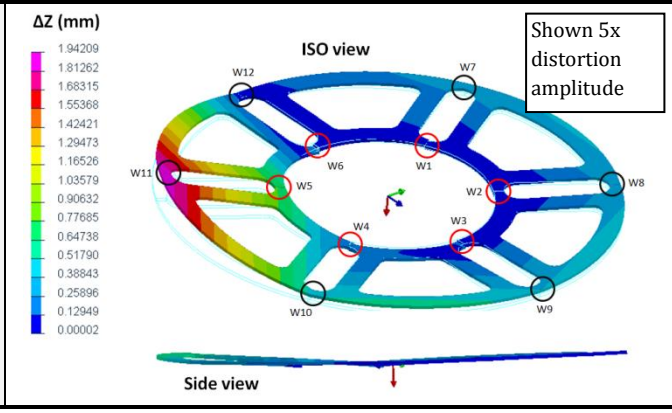
Simulation A (Weld outer only)		**Out-of -plane error:** 1.356mm **Shape resolved:** Quantized conic
Simulation B (Weld inner only)		**Out-of -plane error:** 13.218mm **Shape resolved:** V-bend
Simulation C (Weld outer then inner)		**Out-of -plane error:** 1.300mm **Shape resolved:** Quantized conic
Simulation D (Weld inner then outer)		**Out-of -plane error:** 1.942mm **Shape resolved:** V-bend

Table 7-7 : FEA weld Simulation results

Looking at the simulation results there is a small disparity between the simulated and physical results, with the simulated results generally showing a slightly higher level of distortion. This disparity is probably due to the idealised nature of the simulation against the variable nature of the manual “real world” weld operation. However, there is a clear correlation between the observed results of the physical trials and FEA simulations. By way of example, the B simulation results were only the gap end of the joint was welded exhibited by far the largest out-of-plane distortion of the four simulations. While, the A and C simulations where the contact point was welded first showed a significantly smaller amount of distortion. The D simulation result is perhaps the most surprising, as this exhibited a much lower level of distortion than expected. However, given the good correlation between the other physical and simulated results, it is reasonable to assume that the D simulation results also bare a good resemblance to reality. The reason for the lower overall geometric distortion levels in the D simulation is likely due to residual stresses generated during the first welding operation being released by the second welding operation. That is to say, welding the inner/gap edge first, the weld shrinkage will pull the assembly gap shut, but the geometry of the ring will resist this contraction, leading to the generation of residual stresses within the system. However, the second welding operation then melts the point contacts at the outer edge of the assembly, giving the geometry space to move. Consequently, this extra room releases the trapped residual stresses, allowing the geometric distortions to relax. Traditionally, a similar

mechanism is observed when unclamping an assembly which has been constrained with clamps during a welding operation [152, 227].

Looking at the final geometric forms of the FE study assemblies, many of them appear to contain a folded or V-shaped distortion, rather than one of the two identified fundamental forms. This V-distortion is likely a consequence of the sequential welding process; as each small PWP weld is likely to have solidified before the next weld in the sequence is performed. Consequently, as the welding process moves around the ring's components, each welded position is not independent of the welds which precede it. This is likely to make the last welded position very distorted if a fully closed ring is to be generated (which is observed in both the B simulation Table 7-7, and the B weld ring - Figure 7-14). This is a very different situation to the glued trial with the laser-cut components, where the entire structure was in effect joined at the same time in one operation.

Finally, looking at the FE results, the A ring simulation appears to be somewhat at odds with the findings of the fundamental distortion shapes trial. Moreover, because the A ring is welded at the outer edge only it would be expected that this would generate a quantised saddle geometry, while the simulation actually resolved to a quantised conic. However, this approach is welding the contact points at the outer edge of the ring, so it is not closing any existing gaps. As a consequence, this welding scheme differs from the quantised saddle results of the geometric study. However, having said that, the welding at the outer edge will melt the inter-component

contact points, giving each component room to move under the effect of the weld shrinkage. While, the extra room interacting with the weld shrinkage then pulls the components together, closing the gap at the inner edge, not the outer edge (Figure 7-17). Hence, as the closure is then occurring at the inner edge the assembly will resolve to a conic shape.

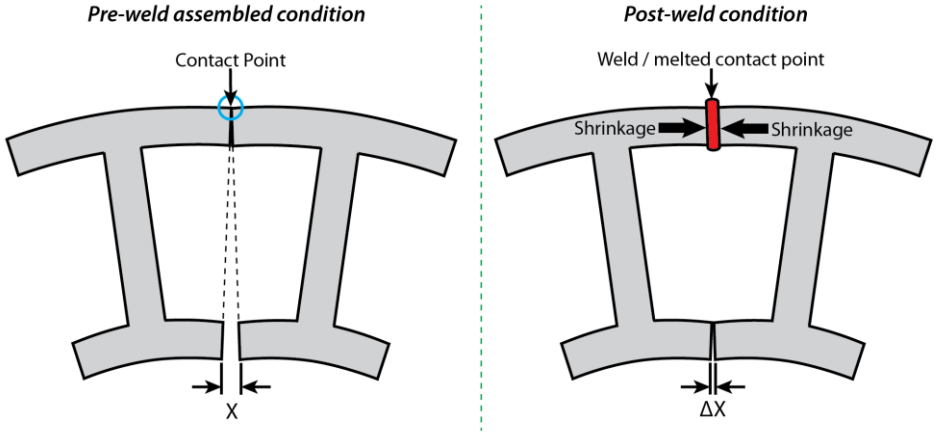


Figure 7-17 : The effect of melting contact on gap-end of the joint.

7.4 Conclusions

Previous chapters have identified angular breaking errors as being V-shaped assembly gaps caused by manufacturing variance within an annular assembly's components. It has also been shown that although the position of these gaps can be controlled through tolerancing, they are inevitable to some degree when assembling a ring shaped structure from wedge shaped components. With this in mind, it has been the focus of this chapter to examine the influence of these angular breaking errors upon the weld distortion generated by the highly localised Preliminary Weld Process (PWP) - or tack welding as it is colloquially known.

Initially this chapter presented an examination of the fundamental interaction between the small assembly gaps and the thermal-mechanical weld distortions. This was done both experimentally and via a non-linear finite element model. This first stage of the investigation was performed using iterations of a simple two plate assembly, which contained a small parallel gap between the plates. These simple assemblies were then manually GTAW welded in a free-state (i.e. without the influence of any fixturing), to show the fundamental inter-play between the gap and the welding process.

Building on the free-state welding trials, a series of fixtured welding trials were performed. The aim of this fixtured trial was to replicate the influence of the neighbouring components on the system during welding. For these welding trials, the gap between the two plates was deliberately designed to be V-shaped to replicate a typical angular breaking error.

After the fixtured welding trials, a non-welded assembly experiment was undertaken to understand the geometric effect of forcing the angular breaking errors within an annual assembly closed. This experiment saw the creation of six ten-segment laser-cut assemblies, each with differing amounts of explicit angular error within their geometry. Assembling these ring structures in such a way as to force the assembly gaps closed then offered an insight into the types of weld distortions likely in a full ring assembly.

Finally, tying together the knowledge gained in this chapter, a series of welded rings were created. These welded 6-segment 3mm thick mild steel rings had an internal diameter of 200mm and outer diameter of 440mm, The geometry and welding process used to construct these physical ring was then replicated using finite element software.

Based on the experimentation and finite element modelling outlined in this chapter, a number of conclusions can be drawn from the work presented, these can be summarised as:

- When performing a PWP on an unconstrained "free-state" assembly made-up of two plates separated by a small parallel gap; the plates are pushed apart by the highly localised thermal expansion of the welding process. This thermally driven movement is then converted into a pivoting motion (which is amplified by the joints length). The observable effect of this expansion is a closure of the gap (either full or partial) at the end of the joint furthest from the weld. Once the completed weld begins to cool, the volumetric weld shrinkage closes the gap slightly at the weld site, cancelling-out most of the initial thermal expansion. However, the shrinkage only appears to affect the area local to the weld, and does not reopen the closed portion of the joint. The length of the weld is critical to the size of the effect, with a shorter weld producing a more pronounced closure effect, as a longer weld looks to cancel-out the pivoting effect. Previous

scientific interest on welding has been primarily focused on seam welding, so this effect has gone unnoticed, by previous studies.

- Because of the inter-component interfaces restricting the component's movement, the distortion mechanism in a fixtured ring appears driven primarily by weld shrinkage, rather than the thermal expansion model observed in the free-state study. This shrinkage driven distortion was observed initially with the fixtured two-plate welding trials, but also later in the studies of full ring assemblies.
- Previous chapters have determined the inevitable existence of V-shaped angular breaking errors within the geometry of a segmented ring assembly. The V-shaped format of these errors dictates that one end of the inter-component joint be a point contact between adjacent assembly components. Furthermore, it is this point contact that then determines the rigid-body interaction between neighbouring components during the assembly process. However, during the welding trial of two fixtured plates separated by a v-gap, it was noted that the generation of the weldpool saw these point contacts being melted. The melting of the point contact geometry was then shown to generate room for the components to move under the influence of volumetric weld shrinkage. This mechanism was first identified in the results of the DIC measurement system, used to study fixtured plates during welding, however the mechanism also manifested as a diametric shrinkage in the full welded ring trials. The implication of this melting is that an

assembly's geometry is not fixed and can change during the welding process. As a consequence, if precise control of an assembly's diameter is required, the loss due to melting of an assembly's base material must be accounted for. As a side note; the melting of component base material due to welding, implies that a full ring assembly will always shrink in diameter between the assembled and welded states. Consequently, this post-weld reduction in diameter may cause unloading difficulties of the finished structure. Especially, if fixed datum locators at the assembly's inner diameter are used to fixture the assembly. Finally, it should be noted that these findings relate to a shallow 3mm thick assembly conjoined via an autogenous welding process. Yet, an assembly constructed from a thicker material may not be subject to the same melting mechanism, especially if the thickness of the base material is much greater than the length of the tack weld used. Similarly, the melting of the base material might be partially negated if a filler material is used during welding, rather than an autogenous weld process.

- The placement of the initial weld relative to the gaps created by the angular breaking errors is critical in controlling PWP distortion when welding ring structures. The experimental and FEA welding trials showed that welding the contact point of the V-shaped angular breaking errors first, will result in a flatter geometry in the completed weldment. Therefore, the PWP should be performed at the outer edge first, when the angular sum of the assembly's

components is greater than 2π radians. Conversely, should the sum of the component angles be less than 2π radians, the PWP should be performed at the inner edge first. The welding trials also showed that once the PWP weld has been performed at the contact point of the joint, the gap-end can then be welded with little effect on the assembly's resultant geometry. This is because, the stiffness of the first weld stabilises the assembly's geometry, resisting the volumetric shrinkage of the second weld which is trying to pull the gap closed.

- When constructing annular assemblies from wedge shaped segments, two fundamental geometric distortions exist, both of which are due to manufacturing variance within the angular wedge faces of the assembly's components. The fundamental geometric distortions are: (1) the geometrically stable quantised conic, found in assemblies where the sum of the component angles is less than 2π radians; (2) the geometrically unstable (and thus less predictable) quantised saddle, found in assemblies where the sum of the angles is greater than 2π radians. However, although closing a ring assembly's angular breaking error gaps fully (and instantaneously) will generate these geometries, in reality these geometries in their pure form are unlikely to occur; due to the transient nature of a typical welding process and the limited shrinkage generated by the small PWP welds. Therefore, typical ring weldment geometries are likely to be a flattened variant of the identified fundamental

geometric distortions. This was demonstrated in experimental and the FEA weld studies, where the transient weld cycle meant that each weld in the assembly had cooled and solidified before the latter welds were begun. This creates an asymmetry in the distortion, and thus diverts the generation of the identified fundamental forms.

8 Conclusions

8.1 Introduction

The aim of this project was the creation of a design framework for the construction of large welded annular assemblies. Geometrically, the primary focus of the project was in the enhancement of the assembly's key characteristics (KC) - being circularity and the profile of gas-wash face. However, other geometric qualities (i.e. out-of-plane error) have also been investigated. Component manufacturing variance, the stack-up of component variance during assembly, the impact of fixture location and the PWP weld distortions have all been studied. It was discovered that the key characteristics for the component was the effective component chord length and the true wedge angle. Moreover, it is an understanding of these fundamental input uncertainties that have acted as the foundation on which the proposed framework is based. Using the framework, "variation conscious" approaches to assembly fixturing have been developed. These novel approaches offer manufacturers an opportunity to produce large ring assemblies at levels of accuracy beyond the reach of traditional fixturing approaches.

8.1.1 Summary of approach

To develop a design framework for the assembly of large high accuracy annular assemblies a multi-staged research process was used. The main research stages of the project were:

- The analysis of an existing build process (chapter 4): An illustrative industrial test-piece and its build process were critically assessed as an exemplar high accuracy annular weldment.

- Modelling of component variance (chapter 5): As the components form the fundamental building blocks of the assembly, so a model was developed to capture the likely manufacturing variance within each assembled part.

- The modelling of assembly/fixturing approaches (chapter 5): Traditional and novel "variation conscious" fixturing methods for assembling annular ring structures were modelled mathematically.

- An experimental validation of assembly/fixturing approaches (chapter 6): The modelled assembly approaches were experimentally validated using a specially designed flexible assembly fixture.

- A study of the influence of gaps upon the PWP (chapter 7): The modelling and experimental work identified that angular breaking errors were an inevitable part of an assembled ring structure. On that basis, this body of work examined how these gaps may affect the quality of the tack welded assembly.

8.2 Key academic outcomes

Looking at the research presented within this thesis a number of key academic outputs can be identified, these being:

- A critical understanding of the fundamental shortcomings of the current fixed datum approaches to fixturing annular assemblies - Current industrial fixturing approaches would appear to pay little consideration to manufacturing variation within the assembled components. Moreover, as an annular assembly generates a closed loop geometry, so each component must properly interface the components either side to ensure a completely closed ring is created. Therefore, at least one degree-of-freedom from each component must be controlled by the neighbouring components rather than the fixture. As a consequence it has been shown that the diametric size of the assembled ring is based primarily on the stacked chord-length variance of the assembled parts, rather than the location diameter of the fixture. Over and above this, the research has also shown that the reliance of each part on its neighbours prevents the traditional 3-2-1 location strategy from being used in this type of fixture.
- A geometric model to describe the manufacturing variance of a typical annular assembly component part - Analysing the build of the illustrative industrial test-piece, it became apparent that the effective inner chord length and true angle are KC for the

component when considering the quality of the final assembly; circularity and profile being KCs for the assembly. The model has shown that the component chord lengths are KC geometric parameters for two main reasons: firstly, The chord lengths stack to define the diametric size of the assembly; secondly, the chords also define the angle between the component's wedge faces, and it is the accuracy of this wedge angle which ultimately determines the quality of the interface between assembled components (impacting the profile KC of the assembly). Therefore, a geometric model based around the chord lengths and "true" wedge angle has been developed.

- A model mapping the propagation of chord and angular error within a closed loop annular assembly - Based upon the modelling of component chord and wedge angle variance; a model was generated which describes their stacking to form a closed ring. This modelling showed that because the sum of the component wedge angles could never equal exactly 2π radians, so the assembled components will never have a true face-face contact between them. The model further showed that only a point contact is possible. However, it is the relative sum of the components wedge angles which influences the global position of these point contacts. If the sum of the assembled wedge angles is greater than 2π radians, then these point contacts will occur at the outer edge of the assembly. While, should the sum of the angles be less than 2π radians, then

the point contacts will occur at the assembly's inner edge. This has important implications for both the positions of fixture locator blocks and the positions of the tack welds, especially at the non-contact, gap-end of the joint - referred to as the "angular breaking error".

- The creation of three novel "Variation Conscious" Assembly Fixturing (VCAF) approaches have been presented, based on the need of the assembly and component KCs. These innovative "Variation Conscious" approaches improve the fixture's set-up for the variance present within an assembly's components; an approach which fundamentally differs from traditional fixturing methods of forcing a set of components to adhere to a fixed nominal build diameter. Three VCAF build methods were proposed: the Geometric Circumscribed (CG), which generates a theoretical build circle and places a polygon constructed from the component chord lengths inside the theoretical circle; the Geometric Inscribed (IG), which places the chord length polygon externally tangential to the theoretical build circle; and the Translation Build (TB), which slides each component out to the ideal radial position based on its chord length.
- An experimental validation of the VCAF build approaches and an evaluation of their performance against traditional fixed build methodologies - The CG and TB approaches where both tested experimentally against traditional fixed diameter fixturing

methods. This testing was performed using an innovative flexible fixturing platform and a test-bed assembly which contained both implicit and explicit errors. In terms of circularity, the new CG method has been shown to substantially outperform the traditional fixturing methodologies, showing a 5x improvement. Although, the TB method performed badly in terms of pure circularity, it was demonstrated to be a most robust assembly approach, capable of constructing close annular structures even in the face of assembly builds containing exaggerated amounts of implicit error.

- An evaluation of the per-joint weld distortion generated due to the presence of assembly gaps during autogenous tack-welding - The per-joint influence of small assembly gaps on the thermal-mechanical distortions of the PWP have been modelled (in FEA software) and examined experimentally. This study has identified that a single point weld performed on a pair of unconstrained plates separated by a small gap, will cause partial closure of the gap as a result of the thermo-mechanical weld cycle. Furthermore, it has been identified that this closure occurs at the point along the joint's length which is furthest from the weld. Experimentally, the per-joint weld distortion trials were also extended to include a pair of fixtured plates separated by a small V-shaped gap. In this instance it was shown that the presence (simulated by a fixture) of the neighbouring components caused the V-shaped gap between the components to open-out during welding. This study has been

of importance, as the current focus of welding research appears to be primarily interested in seam welding operations, so this tack welding study has offered insight into a little studied area of welding technology.

- An in-depth understanding (with experimental validation) of the distortion mechanisms of a full ring assembly containing angular breaking errors during an autogenous PWP - Building upon the study of the per-joint welding distortion model, a FEA model of a full six segment ring which contained angular breaking errors was created and validated experimentally. This modelling and experimental work demonstrated why the positioning of the first tack weld is critical when welding a full ring assembly.

Based on the highlighted academic outcomes, the aim and objectives established at the beginning of the project would appear to be fulfilled. That is to say that, embodied within the innovative VACF approaches is a framework which understands the fundamental science of constructing large annular structures. This framework equips an understanding of the variance present within each wedge shaped component and offers an insight into the stacking of these variances during assembly operations. Furthermore, the successful experimental demonstration of the VCAF approaches shows the in-depth understanding of the variances within annual assemblies is based upon a sound mathematic model.

8.2.1 Industrial relevance

Although the presented research has been first and foremost an academic endeavour, being a manufacturing project this research intrinsically has a wider practical relevance to an industrial audience. The VCAF methods outlined in this thesis offer manufacturers a robust framework for the fixturing and creation of large near net-shape ring structures. Moreover, these new assembly methodologies offer manufacturers a “right-first-time” production ethos, saving cost, as the number and severity of finishing operations is reduced. Beyond the improved quality of the final assembly, this research has also highlighted the importance of component chord length and wedge angle when constructing annular assemblies. Consequently, this enables manufacturers the opportunity to intelligently control component tolerancing schemes, focusing production effort only where it is most needed. Finally, insights into the PWP distortions and the influence of assembly gaps, offers industry scope to adjust welding processes and improve the quality of ring shaped weldments.

9 Future work

This project has achieved a great deal in terms of addressing the issues surrounding the geometric improvement of large welded annular structures. Rolls-Royce themselves have seen the relevance of the research and are currently using a variant of the CG VCAF approach in a production fixture. Despite being in use industrially, this is not the end of the story as this research has opened new avenues for possible future study, these being:

Assembly and fixturing further research

- This project modelled and built only undersized annular structures (where the sum of the wedge angles is < 2π radians), with locators placed at the inner edge of the assembly. It is most likely that these undersized builds offer the best build quality, however it might not always be technically feasible to fixture internally in this way. Therefore, the implications of building oversized ring assemblies (sum of the wedge angles is > 2π radians) requires further examination.

- The current study constructs its ring structures using truncated wedge shaped components. An interesting future study may be to look at assembling complex cylindrical assemblies (without an internal diameter) which are based on triangular wedge shaped "pie" slices.

- Although the current variance modelling has been shown to be effective, it is somewhat two-dimensional in its approach. This could be problematic for taller or deeper ring structures. Therefore, a further study be may needed to create a more three-dimensional model of the component manufacturing variance and assembly build methodologies.

- Due to its extended flexibility, the current flexible test-bench fixture is a very manual process which requires a great deal of operator precision. This type of fixturing may be acceptable within a research setting, but it is not well suited to an industrial production environment. Consequently, to truly productionise a variation conscious fixture an automated tooling approach would be the best option. An automated fixture would set the locator positions automatically without human intervention prior to part loading.

- An assumption for this project was that each component in the assembly was unique and cannot be swapped for another component within the assembly. However, for many typical ring assemblies this may not be true. In this situation a “best fit” approach may be possible, where for example; placing an undersized component next to an oversized component may cancel out at least some of the manufacturing variance with in the

assembly. Therefore, a further body of research may be required to create this sort of algorithm.

- The build approaches described within this project assumes that the components are perfectly rigid, non-deformable bodies. However, there may be instances where the assembled parts are thin and compliant (e.g. steel pressings). This would potentially offer an opportunity to deform the component slightly in order to obtain the best assembly fit. This would require modelling the possible component deformations and understanding how these could be utilised during assembly.

<u>Welding and the PWP process further research</u>

- The presented research has focused upon the PWP, colloquially known as tack welding. However, the PWP is generally used as a precursive operation, which stabilises an assembly's geometry prior to seam welding. Further research is required to understand the thermal-mechanical distortion generated by seam welding the tack welded ring assembly.

- Beyond the tack and seam welding operations some assemblies require a finish process known as a "wash weld". Although these are not as industrially ubiquitous as tack or seam welding, they are of great importance to industries which require high integrity welds (i.e. aerospace and nuclear). Wash welds are both a cosmetic

and a structural process, as they smooth the transition between the brittle weld and the base material, to improve the overall fatigue life of the fused joint. A downside to this type of weld is that its wide profile and shallow depth makes for a steep temperature gradient across the weld; making this process prone to generating large amounts of distortion in the ultimate weldment. However, like the PWP there is little scientific literature examining the application of this weld type, making it suitable for further study.

- The weld operations studied in this project were autogenous (without filler), which is only possible with relatively few welding processes. However, most welding processes use some form of filler material (normally using it as an electrode) to replace the base material lost through spatter and vaporisation. Consequently, adding filler should reduce solidification shrinkage of the weldpool and assist the bridging of gaps. Therefore, it is suggested that further research be undertaken to examine the use of filler when welding annular assemblies.

References

1. Wang, H., et al., *Computer aided fixture design: Recent research and trends.* Computer-Aided Design, 2010. **42**(12): p. 1085-1094.
2. Bi, Z.M. and W.J. Zhang, *Flexible fixture design and automation: Review, issues and future directions.* International Journal of Production Research, 2001. **39**(13): p. 2867-2894.
3. Ramesh, R., M.A. Mannan, and A.N. Poo, *Error compensation in machine tools — a review: Part I: geometric, cutting-force induced and fixture-dependent errors.* International Journal of Machine Tools and Manufacture, 2000. **40**(9): p. 1235-1256.
4. *Image of Trent 900 Turbofan Aeroengine*. [cited 2013 16/12/2013]; Available from: http://www.rolls-royce.com/civil/products/largeaircraft/trent_900/.
5. Boeing *Current Market Outlook 2013-2032*. 2013. 42.
6. Airbus *Global Market Forecast (GMF) – "Future Journeys" – 2013-2032*. 2013. 124.
7. Stuppy, J. and H. Meerkamm, *Tolerance analysis of mechanisms taking into account joints with clearance and elastic deformations*, in *Proceedings of the 17th International Conference on Engineering Design, ICED'09*. 2009: Stanford, CA, USA p. 489-500.
8. Walter, M., et al., *Simulation based generation of an initial design taking into account geometric deviations and deformations*, in *18th International Conference on Engineering Design (ICED 11), Impacting Society through Engineering Design, Vol. 10: Design Methods and Tools pt. 2*. 2011: Lyngby/Copenhagen, Denmark. p. 78-90.
9. Taguchi, G. and D. Clausing, *Robust Quality*. Harvard Business Review, 1990(68): p. 67-75.
10. Roy, U., C.R. Liu, and T.C. Woo, *Review of dimensioning and tolerancing : representation and processi ng* Computer-Aided Design, 1991. **Vol 23 Num 7**: p. 466-483.
11. Islam, M.N., *Functional dimensioning and tolerancing software for concurrent engineering applications.* Computers in Industry, 2004. **54**(2): p. 169-190.
12. Anselmetti, B., *Generation of functional tolerancing based on positioning features.* Computer-Aided Design, 2006. **38**(8): p. 902-919.
13. Mathieu, L. and B. Marguet, *Integrated Design Method to Improve Producibility based on Product Key Characteristics and Assembly Sequences.* CIRP Annals - Manufacturing Technology, 2001. **50**(1): p. 85-88.
14. Zheng, L., et al., *A Novel Algorithm of Posture Best Fit based on Key Characteristics for Large Components Assembly.* Procedia CIRP, 2013. **10**(0): p. 162-168.
15. plc, R.-R., *SABRe : Supplier Management System Requirements Definitions*. 2014.
16. Mantripragada, R. and D.E. Whitney, *The Datum Flow Chain: A systematic approach to assembly design and modeling.* Research in Engineering Design, 1998. **10**(3): p. 150-165.
17. Whitney, D.E., *The role of key characteristics in the design of mechanical assemblies.* Assembly Automation, 2006. **26**(4): p. 315-322.
18. Lee, D.J. and A.C. Thornton. *The Identification And Use Of Key Characteristics In The Product Development Process*. in *Proceedings of The 1996 ASME Design Engineering Technical Conferences and Computers in Engineering Conference* 1996. Irvine, California.

19. Engineers, S.o.A., *AS9100C - Quality Management Systems - Requirements for Aviation, Space and Defense Organizations*. 2009.
20. Li, W.D. and Z.M. Qiu, *State-of-the-art technologies and methodologies for collaborative product development systems.* International Journal of Production Research, 2006. **44**(13): p. 2525-2559.
21. Thornton, C.A., *A Mathematical Framework for the Key Characteristic Process.* Research in Engineering Design, 1999. **11**(3): p. 145-157.
22. Hong, Y.S. and T.C. Chang, *A comprehensive review of tolerancing research.* International Journal of Production Research, 2002. **40**(11): p. 2425-2459.
23. Henzold, G., *Geometrical Dimensioning and Tolerancing for Design, Manufacturing and Inspection*. 2nd ed. 2006: Elsevier.
24. Simmons, C.H., N. Phelps, and T.L.D.E. Maguire, *Chapter 29 - The Duality Principle – the Essential Link Between the Design Intent and the Verification of the End Product*, in *Manual of Engineering Drawing (Fourth Edition)*. 2012, Butterworth-Heinemann: Oxford. p. 243-245.
25. International Organization for Standardization, *ISO 14660-1:2000 : Geometrical Product Specifications (GPS) - Geometrical features - Part 1: General terms and definitions*. 2000.
26. International Organization for Standardization, *ISO 17450-1:2011: Geometrical product specifications (GPS) — General concepts Part 1: Model for geometrical specification and verification*. 2011.
27. International Organization for Standardization, *ISO 8015:2011(E) : Geometrical product specifications (GPS) -- Fundamentals -- Concepts, principles and rules*. 2011.
28. Trabelsi, A. and A. Delchambre, *Assessment on Tolerance Representation and Tolerance Analysis in Assemblies.* Concurrent Engineering, 2000. **8**(4): p. 244-262.
29. Armillotta, A. and Q. Semeraro, *Geometric Tolerances - Impact on Product Design, Qaulity Inspection and Statisical Process Monitoring*, B.M. Colosimo and N. Senin, Editors. 2011, Springer-Verlag.
30. Riveire A, Clement A, and Valade C, *The TTRS: 13 Oriented constraints for dimensioning, tolerancing and inspection.* Advanced in Mathematics for Applied Sciences, 1997. **45**: p. 24-42.
31. Creveling, C.M., *Tolerancing Design : A handbook for developing optimal specifications*. 1997: Addison-Wesley.
32. International Organization for Standardization, *ISO 129-1:2004 :Technical drawings — Indication of dimensions and tolerances — Part 1: General principles*. 2004.
33. The British Standards Institute, *BS 8888:2013 - Technical product documentation and specification*. 2013.
34. International Organization for Standardization, *ISO 2768-1:1989 : General tolerance - Part 1: Tolerance and angualr dimensions without individual tolerance indications*. 1989.
35. Herbert, B.V., *The current state of affairs in dimensional tolerancing.* Integrated Manufacturing Systems, 1998. **9**(4): p. 205-217.
36. Sahani, A.K., P.K. Jain, and S. S.C., *Geometrical Tolerance Stack-Up Techniques, Chapter 52*. 2013: DAAAM International Scientic Book 2013.
37. International Organization for Standardization, *ISO 1101:2004(E) : Geometrical Product Specifications (GPS) — Geometrical tolerancing — Tolerances of form, orientation, location and run-out*. 2004.
38. The American Society Of Mechanical Engineers (ASME), *Y14.5 : Dimensioning and Tolerancing (2009)*.

39. International Organization for Standardization, *ISO 2768-2:1989 Part 2: Geometrical tolerances for features without individual tolerance indications*. 1989.
40. International Organization for Standardization, *ISO 12781-1:2011 : Geometric Product Specifications (GPS) - Flatness - Part 1: Vocabulary and parameters of flatness*. 2011.
41. International Organization for Standardization, *ISO 12181-1:2011(E) : Geometric Product Specifications (GPS) - Roundness - Part 1: Vocabulary and parameters of roundess*. 2011.
42. Huang, J., *An exact solution for the roundness evaluation problems.* Precision Engineering, 1999. **23**(1): p. 2-8.
43. Wen-Yuh, J., L. Chein-Hong, and C. Cha'o-Kuang, *The min-max problem for evaluating the form error of a circle.* Measurement, 1999. **26**: p. 273-282.
44. Dhanish, P.B., *A simple algorithm for evaluation of minimum zone circularity error from coordinate data.* Machine Tools and Manufacture, 2002. **42**: p. 1589-1594.
45. Samuel, G.L. and M.S. Shunmugan, *Evaluation of circularity from coordinate and form data using computational geometric techniques.* Precision Engineering, 2000. **24**: p. 251-263.
46. Anthony, G.T., et al., *Reference software for finding Chebyshev best-fit geometric elements.* Precision Engineering, 1996. **19**(1): p. 28-36.
47. Nam-Hyun, K. and K. Seung-Woo, *Geometrical tolerances; Improved linear approximation of least squares evaluation of circularity by minimum variance.* International Journal Tools and Manufacture, 1996. **36**(3): p. 355-366.
48. Murthy, T.S.R., *A comparison of different algorithms for circularity evaluation.* Precision Engineering, 1986. **8**(1): p. 19-23.
49. International Organization for Standardization, *ISO 14660-2:1999 : Geometric Product Specifications (GPS) - Geometrical features - Part 2: Extracted median line of a cylinder and a cone, extracted media surface, local size of an extracted feature*. 1999.
50. Bui, M.H., F. Villeneuve, and A. Sergent, *Manufacturing tolerance analysis based on the model of manufactured part and experimental data.* Proceedings of the Institution of Mechanical Engineers, Part B: Journal of Engineering Manufacture, 2013. **227**(5): p. 690-701.
51. Nigam, S.D. and J.U. Turner, *Review of statistical approaches to tolerance analysis.* Computer-Aided Design, 1995. **27**(1): p. 6-15.
52. Mansuy, M., M. Giordano, and P. Hernandez, *A new calculation method for the worst case tolerance analysis and synthesis in stack-type assemblies.* Computer-Aided Design, 2011. **43**(9): p. 1118-1125.
53. Bryan R. Fischer, *Mechanical Tolerance Stackup and Analysis.* . 2004, New York: Marcel Dekker Inc.
54. Singh, P.K., P.K. Jain, and S.C. Jain, *Important issues in tolerance design of mechanical assemblies. Part 1: Tolerance analysis.* Proceedings of the Institution of Mechanical Engineers, Part B: Journal of Engineering Manufacture, 2009. **223**(10): p. 1225-1247.
55. Mansoor, E.M., *The Application of Probability to Tolerances Used in Engineering Designs.* Proceedings of the Institution of Mechanical Engineers, 1963. **178**(1): p. 29-39.
56. A. Bender, *Statisical tolerancing as it relates to quality control and the designer.* SAE Trans, 1968. **Vol. 77**(May 1968): p. 1965–1971.
57. Gladman, C.A., *Applying probability in tolerance technology.* Trans. Instn Engr Austral. Mech. Engng, 1980. **MES 2**: p. 82-90.

58. Shen, Y.L. and N.A. Duffie, *Comparison of Combinatorial Rules For Machine Error Budgets.* Annals of the CIRP, 1993. **42**(1): p. 619-622.
59. Spotts M. F., *Dimensioning stacked assemblies.* Machine Design, 1978. **50**(9): p. 60-63.
60. Greenwood, W.H. and K.W. Chase, *Worst Case Tolerance Analysis with Nonlinear Problems.* Journal of Manufacturing Science and Engineering, 1988. **Vol 110**(Issue 3): p. 4.
61. Gao J, K.W. Chase, and Magleby S. P. *Comparsion of Assembly Tolerance by the Direct Linearization and Modified Monte Carlo Simualtion Methods*. in *Proceedings of the ASME Design Engineering Techincal Conferences*. 1995. Boston MA.
62. Anselmetti, B. and H. Louati, *Generation of manufacturing tolerancing with ISO standards.* International Journal of Machine Tools and Manufacture, 2005. **45**(10): p. 1124-1131.
63. Polini, W., *Taxonomy of models for tolerance analysis in assembling.* International Journal of Production Research, 2012. **50**(7): p. 2014-2029.
64. Fortini, E.T., *Dimensioning for Interchangeable Manufacturing*. 1967: Industrial Press.
65. Chase, K.W., J. Gao, and S.P. Magleby, *General 2-D tolerance analysis of mechanical assemblies with small kinematic adjustments.* 1995.
66. Leishman, R.C. and K.W. Chase, *Direct Linearization Method Kinematic Variation Analysis.* Journal of Mechanical Design, 2010. **132**(7): p. 071003-071003.
67. Chase, K.W., et al., *Including geometric feature variations in tolerance analysis of mechanical assemblies.* IIE transactions, 1996. **28**(10): p. 795-808.
68. Polini, W., *Geometric Tolerances - Impact on Product Design, Qaulity Inspection and Statisical Process Monitoring*, B.M. Colosimo and N. Senin, Editors. 2011, Springer-Verlag.
69. Chen, H., et al., *A comprehensive study of three dimensional tolerance analysis methods.* Computer-Aided Design, 2014. **53**: p. 1-13.
70. Glancy C. G. and Chase K. W, *A second-order method for assembly tolerance analysis*, in *Proceedings of the 1999 ASME Design Engineering Technical Conferences*. 1999, ASME: Las Vegas, Nevada.
71. Bo, C., et al., *A comparison of tolerance analysis models for assembly.* The International Journal of Advanced Manufacturing Technology, 2013. **68**(1): p. 739-754.
72. Marziale, M. and W. Polini, *A review of two models for tolerance analysis of an assembly: vector loop and matrix.* The International Journal of Advanced Manufacturing Technology, 2008. **43**(11): p. 1106-1123.
73. Hillyard, R.C. and I.C. Braid, *Analysis of dimensions and tolerances in computer-aided mechanical design.* Computer-Aided Design, 1978. **10**(3): p. 161-166.
74. Bing, L. and U. Roy, *Positioning of toleranced parts in a 2D polygonal assembly and its use in tolerance analysis.* Robotics and Automation, IEEE Transactions on, 2001. **17**(3): p. 357-360.
75. Gupta, S. and J.U. Turner, *Variational solid modeling for tolerance analysis.* Computer Graphics and Applications, IEEE, 1993. **13**(3): p. 64-74.
76. Whitney, D.E., O.L. Gilbert, and M. Jastrzebski, *Representation of geometric variations using matrix transforms for statistical tolerance analysis in assemblies.* Research in Engineering Design, 1994. **6**(4): p. 191-210.
77. Marziale, M. and W. Polini, *Review of variational models for tolerance analysis of an assembly.* Proceedings of the Institution of Mechanical

Engineers, Part B: Journal of Engineering Manufacture, 2011. **225**(3): p. 305-318.
78. Polini, W., *To model joints with clearance for tolerance analysis.* Proceedings of the Institution of Mechanical Engineers, Part B: Journal of Engineering Manufacture, 2014.
79. Sodhi, R. and J.U. Turner, *Relative positioning of variational part models for design analysis.* Computer-Aided Design, 1994. **26**(5): p. 366-378.
80. Wang, N. and T.M. Ozsoy, *Representation of assemblies for automatic tolerance chain generation.* Engineering with Computers, 1990. **6**(2): p. 121-126.
81. Anantha, R., G.A. Kramer, and R.H. Crawford, *Assembly modelling by geometric constraint satisfaction.* Computer-Aided Design, 1996. **28**(9): p. 707-722.
82. Whitney, E.D., et al., *Designing Assemblies.* Research in Engineering Design, 1999. **11**(4): p. 229-253.
83. Whitney, D.E., et al., *Toward a Theory for Design of Kinematically Constrained Mechanical Assemblies.* The International Journal of Robotics Research, 1999. **18**(12): p. 1235-1248.
84. Wu, C.H. and M.G. Kim, *Modeling of part-mating strategies for automating assembly operations for robots.* Systems, Man and Cybernetics, IEEE Transactions on, 1994. **24**(7): p. 1065-1074.
85. Desrochers, A. and A. Rivière, *A matrix approach to the representation of tolerance zones and clearances.* The International Journal of Advanced Manufacturing Technology, 1997. **13**(9): p. 630-636.
86. Laperrière, L. and P. Lafond, *Modeling Dispersions Affecting Pre-Defined Functional Requirements of Mechanical Assemblies Using Jacobian Transforms*, in *Integrated Design and Manufacturing in Mechanical Engineering '98: Proceedings of the 2nd IDMME Conference held in Compiègne, France, 27–29 May 1998*, J.-L. Batoz, et al., Editors. 1999, Springer Netherlands: Dordrecht. p. 381-388.
87. Laperrière, L. and H.A. ElMaraghy, *Tolerance Analysis and Synthesis Using Jacobian Transforms.* CIRP Annals - Manufacturing Technology, 2000. **49**(1): p. 359-362.
88. Wilma, P. and C. Andrea, *Geometric tolerance analysis through Jacobian model for rigid assemblies with translational deviations.* Assembly Automation, 2016. **36**(1): p. 72-79.
89. Waldron, K.J., *The constraint analysis of mechanisms.* Journal of Mechanisms, 1966. **1**(2): p. 101-114.
90. Gao, J., K.W. Chase, and S.P. Magleby, *Generalized 3-D tolerance analysis of mechanical assemblies with small kinematic adjustments.* IIE Transactions, 1998. **30**(4): p. 367-377.
91. Villeneuve, F., O. Legoff, and Y. Landon, *Tolerancing for manufacturing: A three-dimensional model.* International Journal of Production Research, 2001. **39**(8): p. 1625-1648.
92. Sergent, A., et al., *Identification of machining defects by Small Displacement Torsor and form parameterization method*, in *IDMME - Virtual Concept 2010 International conference*. 2010: Bordeaux, France, October 20 – 22, 2010.
93. Kang, Y., Y. Rong, and J.C. Yang, *Computer-Aided Fixture Design Verification. Part 2. Tolerance Analysis.* International Journal of Advanced Manufacturing Tecnology, 2003. **21**: p. 836–841.
94. Hu, J. and Y. Peng, *Development of a function oriented computer aided tolerancing (FOCAT) system.* Proceedings of the Institution of Mechanical

Engineers, Part B: Journal of Engineering Manufacture, 2011. **225**(7): p. 1189-1203.
95. Changhong, G., et al. *The research and realization on computer-aided aircraft tolerance design based on UG*. in *Mechanic Automation and Control Engineering (MACE), 2010 International Conference on*. 2010.
96. Lowth, S., D. Axinte, and S. Wei, *An investigation into the infulence of inter-component assembly gaps upon the geometry of tack welded annualr structures.* CIRP Annals - Manufacturing Technology, 2015.
97. Armillotta, A., G. Moroni, and W. Polini, *To Analytically Estimate the 3D Position Deviation of a Holes Pattern due to Fixturing.* Procedia CIRP, 2013. **10**: p. 186-193.
98. LLC, S., *Datasheet - Sigmetrix*. 2010.
99. Byungwoo, L., et al., *Variation Analysis of Three Dimensional non-rigid Assemblies*, in *Assembly and Manufacturing, 2007. ISAM '07. IEEE International Symposium on*. 2007. p. 13-18.
100. Ngoi, B.K.A. and C.T. Ong, *Product and process dimensioning and tolerancing techniques. A state-of-the-art review.* The International Journal of Advanced Manufacturing Technology, 1998. **14**(12): p. 910-917.
101. Spotts, M.F., *Allocation of Tolerances to Minimize Cost of Assembly.* Journal of Engineering for Industry, 1973. **95**(3): p. 762-764.
102. Speckhart, F.H., *Calculation of Tolerance Based on a Minimum Cost Approach.* Journal of Engineering for Industry, 1972. **94**(2): p. 447-453.
103. Chase, K.W., et al., *Least cost tolerance allocation for mechanical assemblies with automated process selection.* Manufacturing review, 1990. **3**(1): p. 49-59.
104. Smathers E. W. and P.F. Ostwald, *Optimization of Component Functional Dimension and Tolerances.* American Society of Mechanical Engineers, 1972(72-DE-18).
105. Ostwald, P.F. and J. Huang, *A Method for Optimal Tolerance Selection.* Journal of Engineering for Industry, 1977. **99**(3): p. 558-565.
106. Kim, S.H. and K. Knott, *A pseudo-boolean approach to determining least cost tolerances.* International Journal of Production Research, 1988. **26**(1): p. 157-167.
107. Monte, M. and Dateris E., *Optimum Tolerance Selection for Minimum Manufacturing Costs and Other Design Criteria.* Technical Paper, 1982. **82-DET-35**: p. 1-9.
108. Lee, W.J. and T.C. Woo, *Optimum Selection of Discrete Tolerances.* Journal of Mechanisms, Transmissions, and Automation in Design, 1989. **111**(2): p. 243-251.
109. Michael, W. and J.N. Siddall, *The Optimization Problem With Optimal Tolerance Assignment and Full Acceptance.* Journal of Mechanical Design, 1981. **103**(4): p. 842-848.
110. Michael, W. and J.N. Siddall, *The Optimal Tolerance Assignment With Less Than Full Acceptance.* Journal of Mechanical Design, 1982. **104**(4): p. 855-860.
111. Zhang, C., H.P. Wang, and J.K. Li, *Simultaneous Optimization of Design and Manufacturing — Tolerances with Process (Machine) Selection.* CIRP Annals - Manufacturing Technology, 1992. **41**(1): p. 569-572.
112. Cheng, B.-W. and S. Maghsoodloo, *Optimization of mechanical assembly tolerances by incorporating Taguchi's quality loss function.* Journal of Manufacturing Systems, 1995. **14**(4): p. 264-276.
113. Altan, M., *Reducing shrinkage in injection moldings via the Taguchi, ANOVA and neural network methods.* Materials & Design, 2010. **31**(1): p. 599-604.

114. Kusiak, A. and C.-X. Feng, *Deterministic tolerance synthesis: a comparative study.* Computer-Aided Design, 1995. **27**(10): p. 759-768.
115. Feng, C.-X. and A. Kusiak, *Robust Tolerance Synthesis With the Design of Experiments Approach.* Journal of Manufacturing Science and Engineering, 1999. **122**(3): p. 520-528.
116. Montgomery, D.C., *The Use of Statistical Process Control and Design of Experiments in Product and Process Improvement.* IIE Transactions, 1992. **24**(5): p. 4-17.
117. Lee, J. and G.E. Johnson, *Special Issue Uncertainties in geometric design: Optimal tolerance allotment using a genetic algorithm and truncated Monte Carlo simulation.* Computer-Aided Design, 1993. **25**(9): p. 601-611.
118. Al-Ansary, M.D. and I.M. Deiab, *Concurrent optimization of design and machining tolerances using the genetic algorithms method.* International Journal of Machine Tools and Manufacture, 1997. **37**(12): p. 1721-1731.
119. Singh, P.K., S.C. Jain, and P.K. Jain, *Advanced optimal tolerance design of mechanical assemblies with interrelated dimension chains and process precision limits.* Computers in Industry, 2005. **56**(2): p. 179-194.
120. Rao, R.V. and K.C. More, *Advanced optimal tolerance design of machine elements using teaching-learning-based optimization algorithm.* Production & Manufacturing Research, 2014. **2**(1): p. 71-94.
121. Sivakumar, K., C. Balamurugan, and S. Ramabalan, *Simultaneous optimal selection of design and manufacturing tolerances with alternative manufacturing process selection.* Computer-Aided Design, 2011. **43**(2): p. 207-218.
122. Ji, S. and X. Li, *Tolerance synthesis using second-order fuzzy comprehensive evaluation and genetic algorithm.* International Journal of Production Research, 2000. **38**(15): p. 3471-3483.
123. Kopardekar, P. and S. Anand, *Tolerance allocation using neural networks.* The International Journal of Advanced Manufacturing Technology, 1995. **10**(4): p. 269-276.
124. Zhang, H.C. and S.H. Huang, *Applications of neural networks in manufacturing: a state-of-the-art survey.* International Journal of Production Research, 1995. **33**(3): p. 705-728.
125. D. H. Besterfiled, *Quality Control*. 6th ed. 2001: Pearson Education. 471.
126. Powell, T.C., *Total quality management as competitive advantage: A review and empirical study.* Strategic Management Journal, 1995. **16**: p. 15–37.
127. Godecke, W. and B. Peter, *Six sigma for small and medium-sized enterprises.* The TQM Magazine, 2004. **16**(4): p. 264-272.
128. Jiju, A., K. Maneesh, and N.M. Christian, *Six sigma in small- and medium-sized UK manufacturing enterprises: Some empirical observations.* International Journal of Quality & Reliability Management, 2005. **22**(8): p. 860-874.
129. Kanji, G.K., *Total quality management: the second industrial revolution.* Total Quality Management, 1990. **1**(1): p. 3-12.
130. Caulcutt, R., *Why is Six Sigma so successful?* Journal of Applied Statistics, 2001. **28**(3-4): p. 301-306.
131. D. C. Montgomery, *Statistical Quality Control: A modern Introduction*. 7th ed. 2013: John Wiley & sons.
132. Linderman, K., et al., *Six Sigma: a goal-theoretic perspective.* Journal of Operations Management, 2003. **21**(2): p. 193-203.
133. Schroeder, R.G., et al., *Six Sigma: Definition and underlying theory.* Journal of Operations Management, 2008. **26**(4): p. 536-554.

134. General Electric. *What is six sigma: the roadmap to customer impact.* 2004 [cited 2016 7th July].
135. S. Dalglesish, *Six Sigma? No thnks.* Quality, 2003. **42**(4).
136. Clifford, L., *Why you can safely ignore Six Sigma* Fortune, 2001(140).
137. Zu, X., L.D. Fredendall, and T.J. Douglas, *The evolving theory of quality management: The role of Six Sigma.* Journal of Operations Management, 2008. **26**(5): p. 630-650.
138. Mahesh, S.R., et al., *Six Sigma: concepts, tools, and applications.* Industrial Management & Data Systems, 2005. **105**(4): p. 491-505.
139. R. A. Fisher, *The design of experiments*. 1935: Oliver and Boyd
140. Nee, A.Y.C., A.S. Kumar, and Z.J. Tao, *Advanced Treatise on Fixture Design and Planning*. 2004, River Edge, NJ, USA: World Scientific Publishing Co.
141. Camelio, J., S. Jack Hu, and W. Zhong, *Diagnosis of multiple fixture faults in machining processes using designated component analysis.* Journal of Manufacturing Systems, 2004. **23**(4): p. 309-315.
142. Song, H. and Y. Rong, *Locating completeness evaluation and revision in fixture plan.* Robotics and Computer-Integrated Manufacturing, 2005. **21**(4–5): p. 368-378.
143. Ratchev, S., K. Phuah, and S. Liu, *FEA-based methodology for the prediction of part–fixture behaviour and its applications.* Journal of Materials Processing Technology, 2007. **191**(1–3): p. 260-264.
144. Raghu, A. and S.N. Melkote, *Modeling of workpiece location error due to fixture geometric error and fixture-workpiece compliance,*. Journal of Manufacturing Science and Engineering, 2005. **127**: p. 75-83.
145. Siebenaler, S.P. and S.N. Melkote, *Prediction of workpiece deformation in a fixture system using the finite element method.* International Journal of Machine Tools and Manufacture, 2006. **46**(1): p. 51-58.
146. Abellan-Nebot, J.V., J. Liu, and F. Romero Subirón, *Quality prediction and compensation in multi-station machining processes using sensor-based fixtures.* Robotics and Computer-Integrated Manufacturing, 2012. **28**(2): p. 208-219.
147. Nee, A.Y.C., A.S. Kumar, and Z.J. Tao, *An intelligent fixture with a dynamic clamping scheme.* Proceedings of the Institution of Mechanical Engineers, Part B: Journal of Engineering Manufacture, 2000. **214** (3): p. 183-196.
148. Bakker, O.J., et al., *Model-Based Control of An Active Fixture for Advanced Aerospace Components.* Proceedings of the Institution of Mechanical Engineers, Part B: Journal of Engineering Manufacture, 2011. **225**(1): p. 35-51.
149. Bukowski, A., W. Kwasny, and J. Jedrzejewski, *Mechatronic approach to the development of an intelligent fixturing system test bed*, in *AFFIX Workshop on New Assembly Alignment and Fixturing Technology*. 2008: Wroclaw, Poland.
150. Hussain, T., et al., *Straight-Build Assembly Optimization: A Method to Minimize Stage-by-Stage Eccentricity Error in the Assembly of Axisymmetric Rigid Components (Two-Dimensional Case Study).* Journal of Manufacturing Science and Engineering, 2011. **133**.
151. Yang, Z., A.A. Popov, and S. McWilliam, *Variation propagation control in mechanical assembly of cylindrical components.* Journal of Manufacturing Systems, 2012. **31**(2): p. 162-176.
152. Schenk, T., et al., *A study on the influence of clamping on welding distortion.* Computational Materials Science, 2009. **49**: p. 999-1005.

153. Ceglarek, D., et al., *Time-Based Competition in Multistage Manufacturing: Stream-of-Variation Analysis (SOVA) Methodology—Review.* International Journal of Flexible Manufacturing Systems, 2004. **16**(1): p. 11-44.
154. Ceglarek, D., J. Shi, and S.M. Wu, *A Knowledge-Based Diagnostic Approach for the Launch of the Auto-Body Assembly Process.* Journal of Engineering for Industry, 1994. **116**(4): p. 491-499.
155. Hu, S.J. and Y. Koren, *Stream-of-Variation Theory for Automotive Body Assembly.* CIRP Annals - Manufacturing Technology, 1997. **46**(1): p. 1-6.
156. Abellan-Nebot, J.V., J. Liu, and F.R. Subiron, *Design of Multi-station manufaturing processes by intergating stream-of-varation model and shop-floor data.* Journal of Manufacturing Systems, 2011. **30**: p. 70-82.
157. Ding, Y., D. Ceglarek, and J. Shi. *Modeling and diagnosis of multistage manufacturing processes: part I: state space model*. in *Proceedings of the 2000 Japan/USA symposium on flexible automation*. 2000.
158. Jin, J. and J. Shi, *State Space Modeling of Sheet Metal Assembly for Dimensional Control.* Journal of Manufacturing Science and Engineering, 1999. **121**(4): p. 756-762.
159. Camelio, J., S.J. Hu, and D. Ceglarek, *Modeling Variation Propagation of Multi-Station Assembly Systems With Compliant Parts.* Journal of Mechanical Design, 2004. **125**(4): p. 673-681.
160. Xie, K., J.A. Camelio, and L.E. Izquierdo, *Part-by-part dimensional error compensation in compliant sheet metal assembly processes.* Journal of Manufacturing Systems, 2012. **31**(2): p. 152-161.
161. Shi, J., *Stream of variation modeling and analysis for multistage manufacturing processes*. 2007: CRC/Taylor & Francis.
162. Ding, Y., D. Ceglarek, and J. Shi, *Design Evaluation of Multi-station Assembly Processes by Using State Space Approach.* Journal of Mechanical Design, 2002. **124**(3): p. 408-418.
163. Mantripragada, R. and D.E. Whitney, *Modeling and controlling variation propagation in mechanical assemblies using state transition models.* IEEE Transactions on Robotics and Automation, 1999. **15**(1): p. 124-140.
164. Haixia, W. and C. Dariusz, *Variation propagation modeling and analysis at preliminary design phase of multi-station assembly systems.* Assembly Automation, 2009. **29**(2): p. 154-166.
165. Huang, W., et al., *Stream-of-Variation Modeling—Part I: A Generic Three-Dimensional Variation Model for Rigid-Body Assembly in Single Station Assembly Processes.* Journal of Manufacturing Science and Engineering, 2007. **129**(4): p. 821-831.
166. Huang, W., et al., *Stream-of-Variation Modeling—Part II: A Generic 3D Variation Model for Rigid Body Assembly in Multistation Assembly Processes.* Journal of Manufacturing Science and Engineering, 2007. **129**(4): p. 832-842.
167. Loose, J.-P., et al., *Integrating GD&T into dimensional variation models for multistage machining processes.* International Journal of Production Research, 2010. **48**(11): p. 3129-3149.
168. Djurdjanovic, D. and N. Jun, *Stream-of-Variation (SoV)-Based Measurement Scheme Analysis in Multistation Machining Systems.* Automation Science and Engineering, IEEE Transactions on, 2006. **3**(4): p. 407-422.
169. Ceglarek, D. and J. Shi, *Dimensional variation reduction for automotive body assembly.* Manufacturing Review, 1995. **8**(2): p. 139-154.

170. Carlson, J.S. and R. Söderberg, *Assembly Root Cause Analysis: A Way to Reduce Dimensional Variation in Assembled Products.* International Journal of Flexible Manufacturing Systems, 2003. **15**(2): p. 113-150.
171. Maropoulos, P.G., et al., *A new paradigm in large-scale assembly—research priorities in measurement assisted assembly.* The International Journal of Advanced Manufacturing Technology, 2013. **70**(1): p. 621-633.
172. Muelaner, J.E., O.C. Martin, and P.G. Maropoulos, *Achieving Low Cost and High Quality Aero Structure Assembly through Integrated Digital Metrology Systems.* Procedia CIRP, 2013. **7**(0): p. 688-693.
173. Webb, P., et al., *Automated aerostructure assembly.* Industrial Robot: An International Journal, 2005. **32**(5): p. 383-387.
174. Jamshidi, J., et al., *Manufacturing and assembly automation by integrated metrology systems for aircraft wing fabrication.* Proceedings of the Institution of Mechanical Engineers, Part B: Journal of Engineering Manufacture, 2010. **224**(1): p. 25-36.
175. Mei, Z. and P.G. Maropoulos, *Review of the application of flexible, measurement-assisted assembly technology in aircraft manufacturing.* Proceedings of the Institution of Mechanical Engineers, Part B: Journal of Engineering Manufacture, 2014. **228**(10): p. 1185-1197.
176. Maisano, D.A., et al., *A comparison of two distributed large-volume measurement systems: The mobile spatial co-ordinate measuring system and the indoor global positioning system.* Proceedings of the Institution of Mechanical Engineers, Part B: Journal of Engineering Manufacture, 2009. **223**(5): p. 511-521.
177. Morey B., *Metrology Technologies Elevating Aircraft Manufacturing*, in *Manufacturing Engineering magazine*. 2013, SME.
178. Peggs, G.N., et al., *Recent developments in large-scale dimensional metrology.* Proceedings of the Institution of Mechanical Engineers, Part B: Journal of Engineering Manufacture, 2009. **223**(6): p. 571-595.
179. Jayaweera, N., P. Webb, and C. Johnson, *Measurement assisted robotic assembly of fabricated aero-engine components.* Assembly Automation, 2010. **30**(1): p. 56-65.
180. European Co-operation for Accreditation, *EA-4/02 Expression of the uncertainty of measurement in calibration*. 1999.
181. Bell, S., *A Beginner's Guide to Uncertainty of Measurement*, Nataional Physical Laboratory, Editor. 2001, HMSO.
182. Birch, K., *Esitmating Uncertainties in Testing*, Natioal Physcial Laboratory, Editor. 2003: HMSO. p. 40.
183. Taylor, B.N. and C.E. Kuyatt, *Guideliines for Evaluating and Expressing the Unertainty of NIST Measurement Results*, N.I.o.S. Technology, Editor. 1994: Giatherburg.
184. International Organization for Standardization - *ISO/IEC Guide 98-3:2008 : Uncertainty of measurement -- Part 3: Guide to the expression of uncertainty in measurement (GUM:1995).*
185. Kessel, W., *Measurement uncertainty according to ISO/BIPM-GUM.* Thermochimica Acta, 2002. **382**(1–2): p. 1-16.
186. International Organization for Standardization, *ISO/IEC Guide 99:2007 · International vocabulary of metrology -- Basic and general concepts and associated terms (VIM).* 2007.

187. International Organization for Standardization, *ISO/IEC Guide 98-1:2009 · Uncertainty of measurement -- Part 1: Introduction to the expression of uncertainty in measurement.* 2008.
188. Martins, M.A.F., R. Requião, and R.A. Kalid, *Generalized expressions of second and third order for the evaluation of standard measurement uncertainty.* Measurement, 2011. **44**(9): p. 1526-1530.
189. International Organization for Standardization, *ISO 10360-1:2000 -- Geometrical Product Specifications (GPS) -- Acceptance and reverification tests for coordinate measuring machines (CMM) -- Part 1: Vocabulary*. 2000.
190. International Organization for Standardization, *ISO/TS 23165:2006 - Geometrical product specifications (GPS) -- Guidelines for the evaluation of coordinate measuring machine (CMM) test uncertainty*. 2000.
191. Wilhelm, R.G., R. Hocken, and H. Schwenke, *Task Specific Uncertainty in Coordinate Measurement.* CIRP Annals - Manufacturing Technology, 2001. **50**(2): p. 553-563.
192. Savio, E., *Uncertainty in testing the metrological performances of coordinate measuring machines.* CIRP Annals - Manufacturing Technology, 2006. **55**(1): p. 535-538.
193. Weckenmann, A., M. Knauer, and H. Kunzmann, *The Influence of Measurement Strategy on the Uncertainty of CMM-Measurements.* CIRP Annals - Manufacturing Technology, 1998. **47**(1): p. 451-454.
194. Sprauel, J.M., et al., *Uncertainties in CMM Measurements, Control of ISO Specifications.* CIRP Annals - Manufacturing Technology, 2003. **52**(1): p. 423-426.
195. Choi, W., T.R. Kurfess, and J. Cagan, *Sampling uncertainty in coordinate measurement data analysis.* Precision Engineering, 1998. **22**(3): p. 153-163.
196. Flack, D., *Good Practicse Guide No. 42 : CMM Verification*. 2011: National Physical Laboratory.
197. Dhanish, P.B. and J. Mathew, *Effect of CMM point coordinate uncertainty on uncertainties in determination of circular features.* Measurement, 2006. **39**(6): p. 522-531.
198. Luo, P.F., et al., *Accurate measurement of three-dimensional deformations in deformable and rigid bodies using computer vision.* Experimental Mechanics, 1993. **33**(2): p. 123-132.
199. Peters, W.H. and W.F. Ranson, *DIGITAL IMAGING TECHNIQUES IN EXPERIMENTAL STRESS ANALYSIS.* Optical Engineering, 1982. **21**(3): p. 427-431.
200. Basehore, M.L. and D. Post, *Moiré method for in-plane and out-of-plane displacement measurements.* Experimental Mechanics, 1981. **21**(9): p. 321-328.
201. Chu, T.C., W.F. Ranson, and M.A. Sutton, *Applications of digital-image-correlation techniques to experimental mechanics.* Experimental Mechanics, 1985. **25**(3): p. 232-244.
202. Su, X. and Q. Zhang, *Dynamic 3-D shape measurement method: A review.* Optics and Lasers in Engineering, 2010. **48**(2): p. 191-204.
203. Li, K., et al., *Calibration error for dual-camera digital image correlation at microscale.* Optics and Lasers in Engineering, 2012. **50**(7): p. 971-975.
204. Toutin, T., *Review article: Geometric processing of remote sensing images: models, algorithms and methods.* International Journal of Remote Sensing, 2004. **25**(10): p. 1893-1924.
205. Blaschke, T., *Object based image analysis for remote sensing.* ISPRS Journal of Photogrammetry and Remote Sensing, 2010. **65**(1): p. 2-16.

206. Brajlih, T., et al., *Possibilities of Using Three-Dimensional Optical Scanning in Complex Geometrical Inspection.* Strojniški vestnik - Journal of Mechanical Engineering; Vol 57, No 11 (2011): Strojniški Vestnik - Journal of Mechanical Engineering, 2011.
207. Luhmann, T., *Close range photogrammetry for industrial applications.* ISPRS Journal of Photogrammetry and Remote Sensing, 2010. **65**(6): p. 558-569.
208. Savio, E., L. De Chiffre, and R. Schmitt, *Metrology of freeform shaped parts.* CIRP Annals - Manufacturing Technology, 2007. **56**(2): p. 810-835.
209. Bing, P., et al., *Two-dimensional digital image correlation for in-plane displacement and strain measurement: a review.* Measurement Science and Technology, 2009. **20**(6): p. 062001.
210. Sutton, M.A., et al., *The effect of out-of-plane motion on 2D and 3D digital image correlation measurements.* Optics and Lasers in Engineering, 2008. **46**(10): p. 746-757.
211. Garcia, D., J.J. Orteu, and L. Penazzi, *A combined temporal tracking and stereo-correlation technique for accurate measurement of 3D displacements: application to sheet metal forming.* Journal of Materials Processing Technology, 2002. **125–126**: p. 736-742.
212. Orteu, J.-J., *3-D computer vision in experimental mechanics.* Optics and Lasers in Engineering, 2009. **47**(3–4): p. 282-291.
213. Su, Y., et al., *Quality assessment of speckle patterns for DIC by consideration of both systematic errors and random errors.* Optics and Lasers in Engineering, 2016. **86**: p. 132-142.
214. Dantec Dynamics, *Technical note - T-Q-400-Accuacy-3DCORR-003-EN : Error Estimation of 3D Digital Image Correlation Measuremants*. 2006.
215. Dantec Dynamics, *3D Measuring System Q-400 TCT*. 2011: http://www.dantecdynamics.com/docs/products-and-services/dic/F-Q-400TCT.pdf.
216. Chen, F., G.M. Brown, and M. Song, *Overview of three-dimensional shape measurement using optical methods.* Optical Engineering, 2000. **39**(1): p. 10-22.
217. Reich, C., R. Ritter, and J. Thesing, *3-D shape measurement of complex objects by combining photogrammetry and fringe projection.* Optical Engineering, 2000. **39**(1): p. 224-231.
218. GOM. *ATOS 3D Digitizer*. 2016 09/07/2016].
219. Blais, F., *Review of 20 Years of Range Sensor Development.* Journal of Electronic Imaging, 2004. **13**(1).
220. Schwenke, H., et al., *Optical Methods for Dimensional Metrology in Production Engineering.* CIRP Annals - Manufacturing Technology, 2002. **51**(2): p. 685-699.
221. Short, A.B., *Gas Tungsten Arc Welding of α+β Titanium Alloys: A Review.* Materails Science and Technology, 2009. **25**(3): p. 309-324.
222. Deng, D., H. Murakawa, and W. Liang, *Numerical simulation of welding distortion in large structures.* Computer Methods in Applied Mechanics and Engineering, 2007. **196**(45–48): p. 4613-4627.
223. American Weld Soceity, *AWS Welding Handbook, Fundamentals of welding*. 7th ed, ed. C. Wiseman. Vol. 1. 1975. 373.
224. Messler, R.W., *Pinciples of Welding: Process, Physic, Chemistry and Metrology*. 1999: Wiley-Interscience. 662.
225. Xu, Y.L., et al., *Marangoni convection and weld shape variation in A-TIG welding process.* Theoretical and Applied Fracture Mechanics, 2007. **48**(2): p. 178-186.

226. Egry, I., et al., *Surface tension of liquid metals and alloys — Recent developments.* Advances in Colloid and Interface Science, 2010. **159**(2): p. 198-212.
227. Mollicone, P., D. Camilleri, and T. Gray, *Procedural influences on non-linear distortions in welded thin-plate fabrication.* Thin-Walled Structures, 2008. **46**(7–9): p. 1021-1034.
228. Deng, D., H. Murakawa, and W. Liang, *Prediction of welding distortion in a curved plate structure by means of elastic finite element method.* Journal of Materials Processing Technology, 2008. **203**(1–3): p. 252-266.
229. Guirao, J., et al., *Use of a new methodology for prediction of weld distortion and residual stresses using FE simulation applied to ITER vacuum vessel manufacture.* Fusion Engineering and Design, 2009. **84**(2009): p. 2187-2196.
230. Barsoum, Z. and A. Lundbäck, *Simplified FE welding simulation of fillet welds – 3D effects on the formation residual stresses.* Engineering Failure Analysis, 2009. **16**(7): p. 2281-2289.
231. Smith, M.C. and A.C. Smith, *NeT bead-on-plate round robin: Comparison of residual stress predictions and measurements.* International Journal of Pressure Vessels and Piping, 2009. **86**(1): p. 79-95.
232. Zhang, J., et al., *Modeling of weld residual stresses in core shroud structures.* Nuclear Engineering and Design, 2000. **195**(2): p. 171-187.
233. Long, H., et al., *Prediction of welding distortion in butt joint of thin plates.* Materials & Design, 2009. **30**(10): p. 4126-4135.
234. Zeng, Z., et al., *Determination of welding stress and distortion in discontinuous welding by means of numerical simulation and comparison with experimental measurements.* Computational Materials Science, 2010. **49**(3): p. 535-543.
235. Jarnstroem, P., et al., *MicroTack technology; Revolution in tack welding of thin walled structures.* Welding International, 2011. **Vol. 25 Issue 4**(4): p. 323-235.
236. Jonsson, M., L. Karlsson, and L. Lindgren, *Simulation of Tack Welding Procedures in Butt Joint Welding of Plates.* Welding Journal, 1985. **Vol. 64**(10): p. s296-s301.
237. Heinze, C., C. Schwenk, and M. Rethmeier, *The effct of tack welding on numerically calculated welding-induced distrotions.* Journal of Materials Processing Technology, 2012. **212**: p. 308-314.
238. Abid, M. and M. Siddique, *Numerical simulation to study the effect of tack welds and root gap on welding deformations and residual stresses of a pipe-flange joint.* International Journal of Pressure Vessels and Piping, 2005. **82**(11): p. 860-871.
239. Rong, Y., S.H. Huang, and Z. Hou, *Advanced Computer-aided Fixture Design*. 2005: Elsevier Academic Press.
240. Mahapatra, M.M., et al., *Modelling the effects of constraints and single axis welding process parameters on angular distortions in one-sided fillet welds.* Proceedings of the Institution of Mechanical Engineers, Part B: Journal of Engineering Manufacture, 2007. **220**: p. 397-407.
241. Sun, Z. and M. Kuo, *Bridging the joint gap with wire feed laser welding.* Journal of Materials Processing Technology, 1999. **87**(1–3): p. 213-222.
242. Agricola, I. and T. Friedrich, *Elementary Geometry*. Vol. Student Marthmatical Library Vol.43. 2005: American Mathmatical Society. 243.
243. ESI Group, *Visual-Weld user documentation; "Modelling Filler Material"*. 2011.
244. Pichot, F., et al., *Numerical definition of an equivalent GTAW heat source.* Journal of Materials Processing Technology, 2013. **213**(7): p. 1241-1248.

245. Raj, B., V. Shankar, and A.K. Bhaduri, eds. *Welding Tecnology For Engineers*. 1st ed. 2006, Alpha Science International. 411.

Appendix 1 – Engineering Drawings

List of engineering drawings:

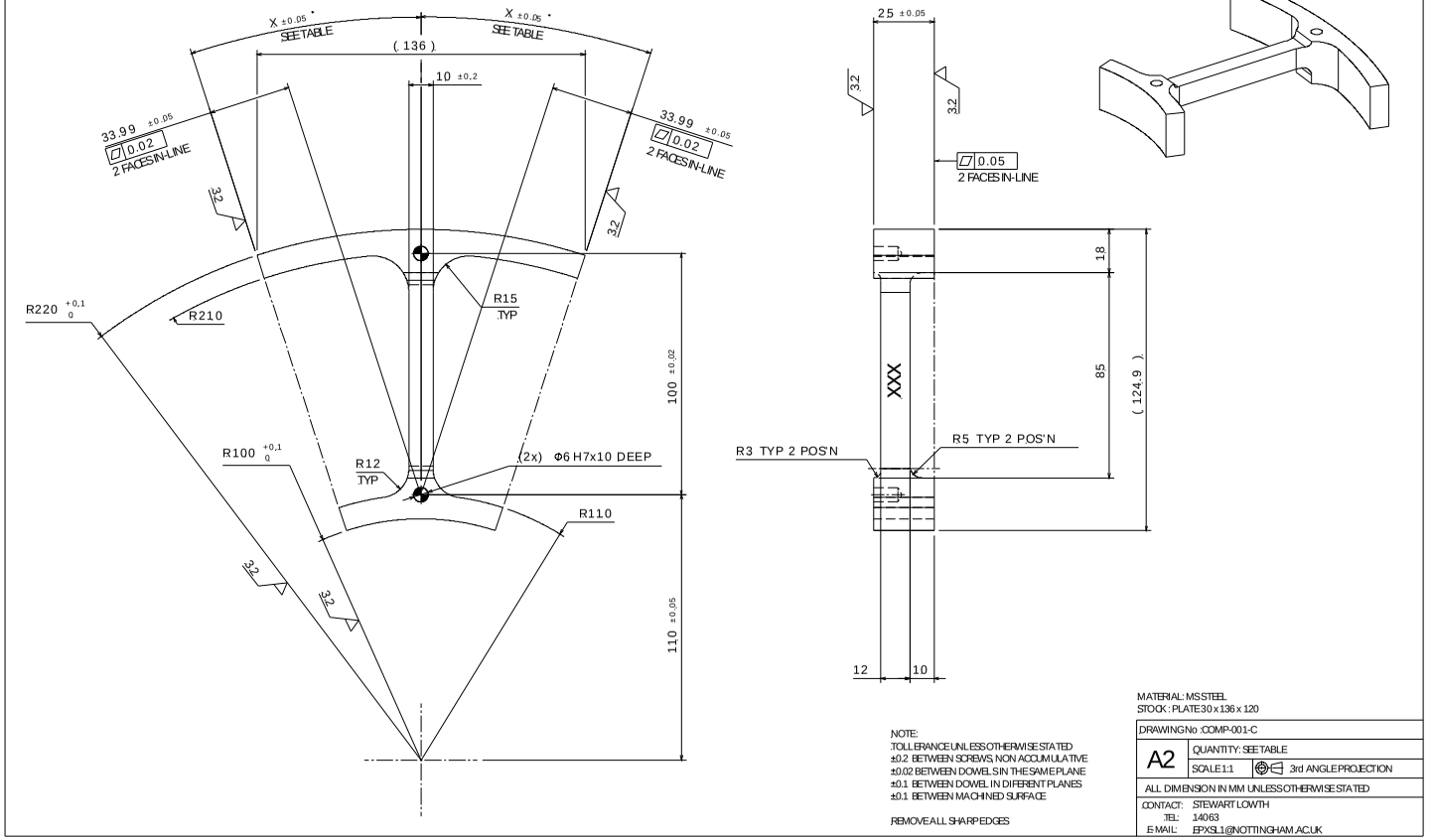
- Assembly components for testing VCAF build methods (Page 345)
- General assembly of flexible test-bench fixture (Pages 346 & 347)
- Base (unit 01) for flexible test-bench fixture (Pages 348-352)
- LaCCU (unit 02) for flexible test-bench fixture (Pages 353-361)
- Free-state weld trial assembly (Page 362)
- V-gap weld trial fixture and components (Pages 363-366)
- Welded ring fixture and components (Pages 367-369)

DIMENSION X	QTY PARTS
18°	10-OFF
19°	4-OFF
17°	4-OFF

MARK DIMENSION "X" ON COMPONENT
AT POSITION INDICATED "XXX"

JOB NUMBER XXX-XXX

REV-C - 22/04/12
QTY CHANGED
DRAWING RELEASED FOR MANUFACTURE
REV-D - 27/04/12
ANGLES IN TABLE CHANGED WAS 17.5°
& 18.5°, NOW 17° & 19°



NOTE:
TOLLERANCE UNLESS OTHERWISE STATED
±0.2 BETWEEN SCREWS, NON ACCUMULATIVE
±0.02 BETWEEN DOWELS IN THE SAME PLANE
±0.1 BETWEEN DOWEL IN DIFERENT PLANES
±0.1 BETWEEN MACHINED SURFACE

REMOVE ALL SHARP EDGES

MATERIAL: MS STEEL
STOCK : PLATE 30 x 136 x 120

DRAWING No :COMP-001-C	
A2	QUANTITY: SEE TABLE
	SCALE 1:1 — 3rd ANGLE PROJECTION
ALL DIMENSION IN MM UNLESS OTHERWISE STATED	

CONTACT: STEWART LOWTH
TEL: 14063
E-MAIL: EPXSL1@NOTTINGHAM.AC.UK

STOCKLIST - TEST FIXTURE - UNIT 000

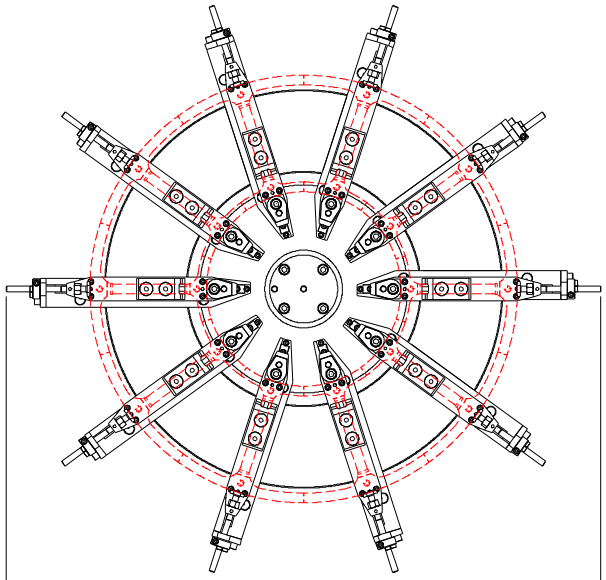
REVISION C

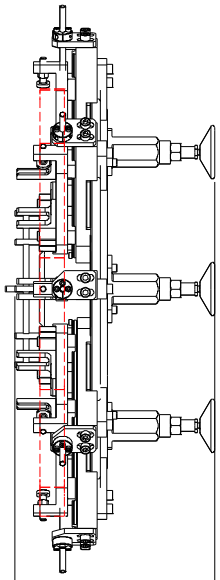
05/03/2012

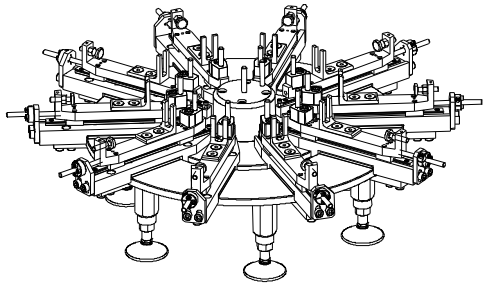
ITEM	DESCRIPTION	MATL / MANUF	STOCK / ORDER CODE	QTY.	TYPE
001	BASE UNIT			1	
002	CLAMPING UNIT			10	

JOB NUMBER XXX-XXX

REV C - 22/04/12
DRAWING RELEASED FOR MANUFACTURE





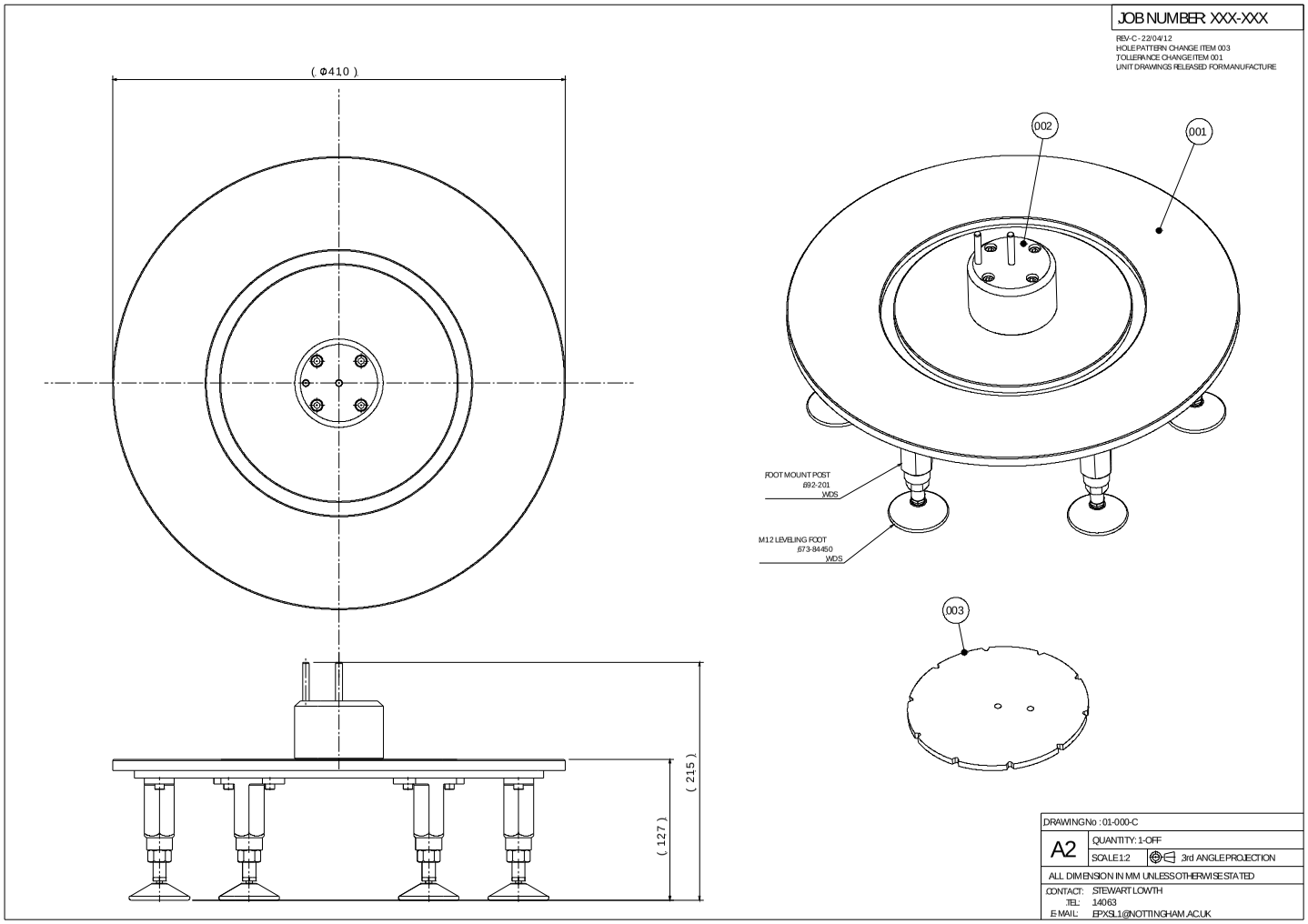


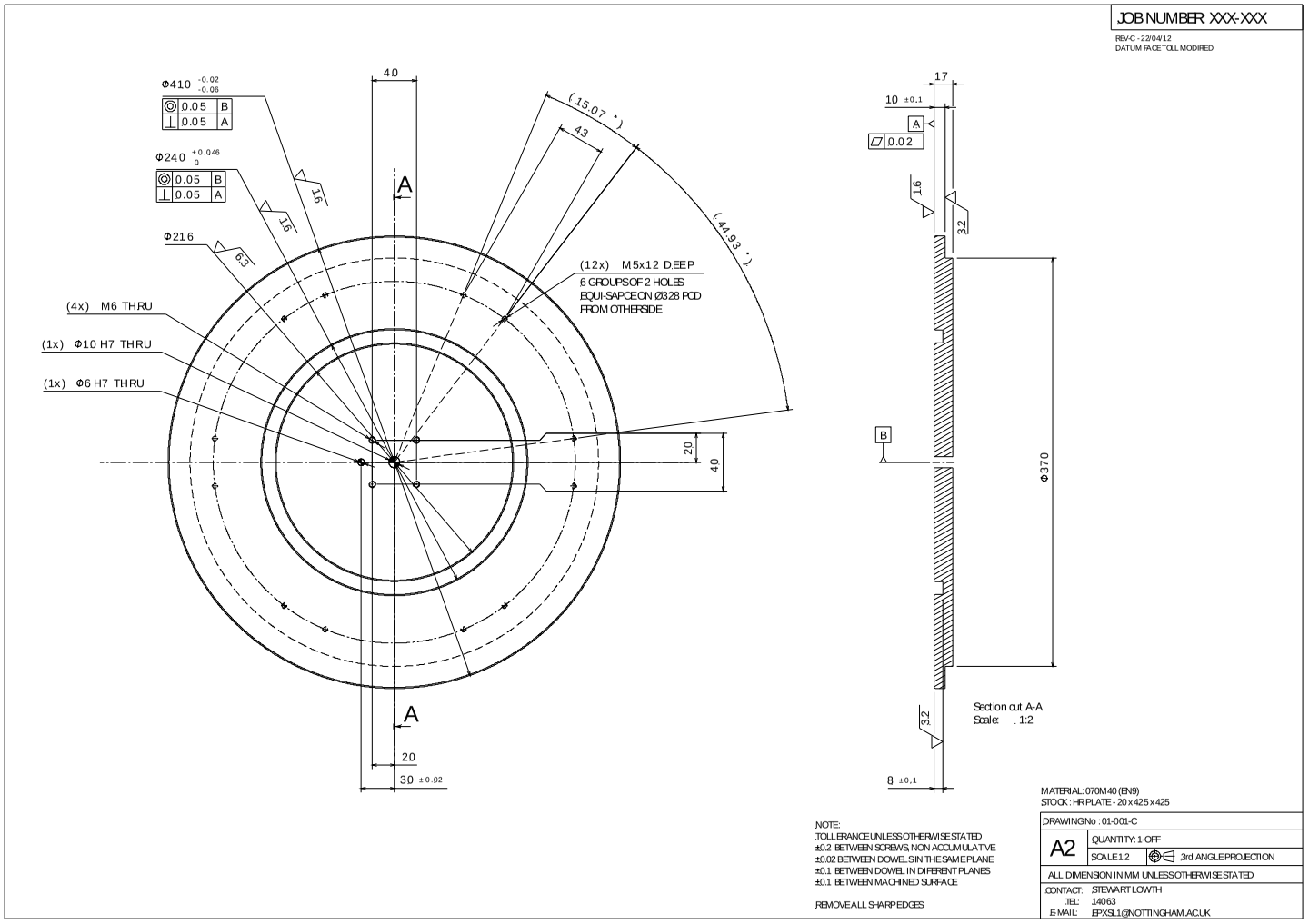
(612)

(205)

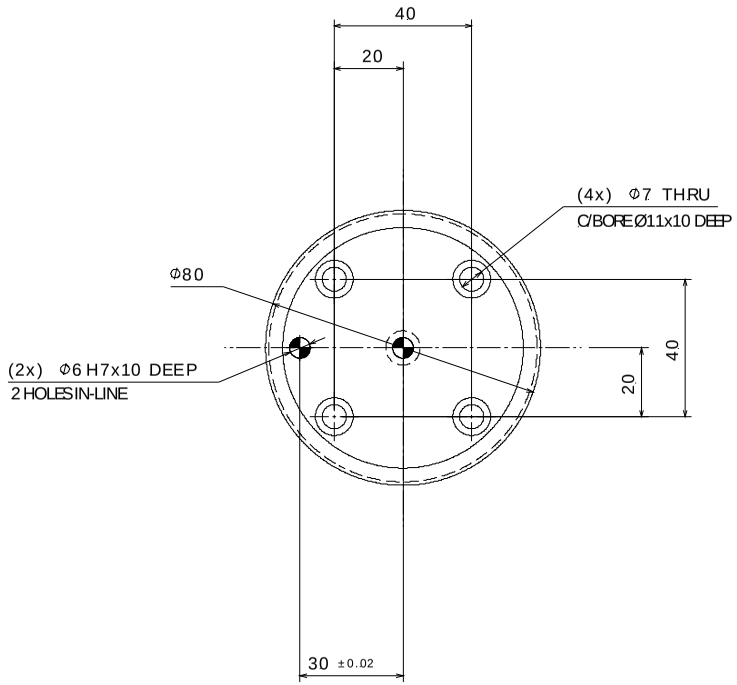
DRAWING No : 00-000-C		
A2	QUANTITY: 1-OFF	
	SCALE 1:2.5	3rd ANGLE PROJECTION
ALL DIMENSION IN MM UNLESS OTHERWISE STATED		
CONTACT:	STEWART LOWTH	
TEL:	14063	
E-MAIL:	EPXSL1@NOTTINGHAM.AC.UK	

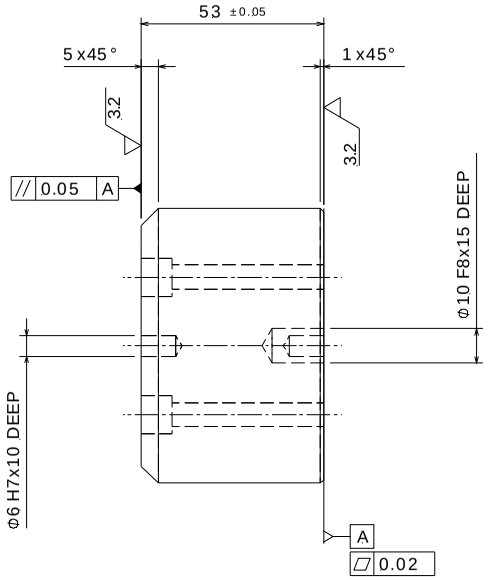
STOCKLIST - TEST FIXTURE - UNIT 001				REVISION A 05/03/2012	
ITEM	DESCRIPTION	MATL / MANUF	STOCK / ORDER CODE	QTY.	TYPE
001	BASE PLATE	070M40 (EN9)	PLATE 20 x 425 x 425	1	M
002	CENTRE DATUM	BMS	ROUND Ø80 x 60	1	M
003	SETTING PLATE	MS	PLATE 10 x 170 x 170	1	M
	M12 LEVELING FOOT	WDS	673-84450	6	P
	FOOT MOUNT POST	WDS	692-201	6	P


JOB NUMBER XXX-XXX
REV-C - 22/04/12
HOLE PATTERN CHANGE ITEM 003
TOLLERANCE CHANGE ITEM 001
UNIT DRAWINGS RELEASED FOR MANUFACTURE
(Φ410)
002
001
003
FOOT MOUNT POST
692-201
WDS
M12 LEVELING FOOT
673-84450
WDS
(215)
(127)
DRAWING No : 01-000-C
A2
QUANTITY: 1-OFF
SCALE 1:2
3rd ANGLE PROJECTION
ALL DIMENSION IN MM UNLESS OTHERWISE STATED
CONTACT: STEWART LOWTH
TEL: 14063
E-MAIL: EPXSL1@NOTTINGHAM.AC.UK


JOB NUMBER XXX-XXX
REV-C - 22/04/12
DATUM FACE TOLL MODIRED
Φ410 -0.02 -0.06
0.05 B
0.05 A
Φ240 +0.046 0
0.05 B
0.05 A
Φ216
1.6
1.6
6.3
40
(15.07 °)
43
(44.93 °)
(12x) M5x12 DEEP
6 GROUPS OF 2 HOLES
EQUI-SAPCE ON Ø328 PCD
FROM OTHERSIDE
(4x) M6 THRU
(1x) Φ10 H7 THRU
(1x) Φ6 H7 THRU
20
40
A
A
20
30 ±0.02
17
10 ±0.1
A
0.02
1.6
3.2
B
Φ37.0
3.2
8 ±0.1
Section cut A-A
Scale: 1:2
NOTE:
TOLLERANCE UNLESS OTHERWISE STATED
±0.2 BETWEEN SCREWS, NON ACCUMULATIVE
±0.02 BETWEEN DOWELS IN THE SAME PLANE
±0.1 BETWEEN DOWEL IN DIFERENT PLANES
±0.1 BETWEEN MACHINED SURFACE
REMOVE ALL SHARP EDGES
MATERIAL: 070M40 (EN9)
STOCK : HR PLATE - 20 x 425 x 425
DRAWING No : 01-001-C
A2
QUANTITY: 1-OFF
SCALE 1:2
3rd ANGLE PROJECTION
ALL DIMENSION IN MM UNLESS OTHERWISE STATED
CONTACT: STEWART LOWTH
TEL: 14063
E-MAIL: EPXSL1@NOTTINGHAM.AC.UK

JOB NUMBER: ***,***





NOTE:
TOLLERANCE UNLESS OTHERWISE STATED
±0.2 BETWEEN SCREWS, NON ACCUMULATIVE
±0.02 BETWEEN DOWELS IN THE SAME PLANE
±0.1 BETWEEN DOWEL IN DIFERENT PLANES
±0.1 BETWEEN MACHINED SURFACE

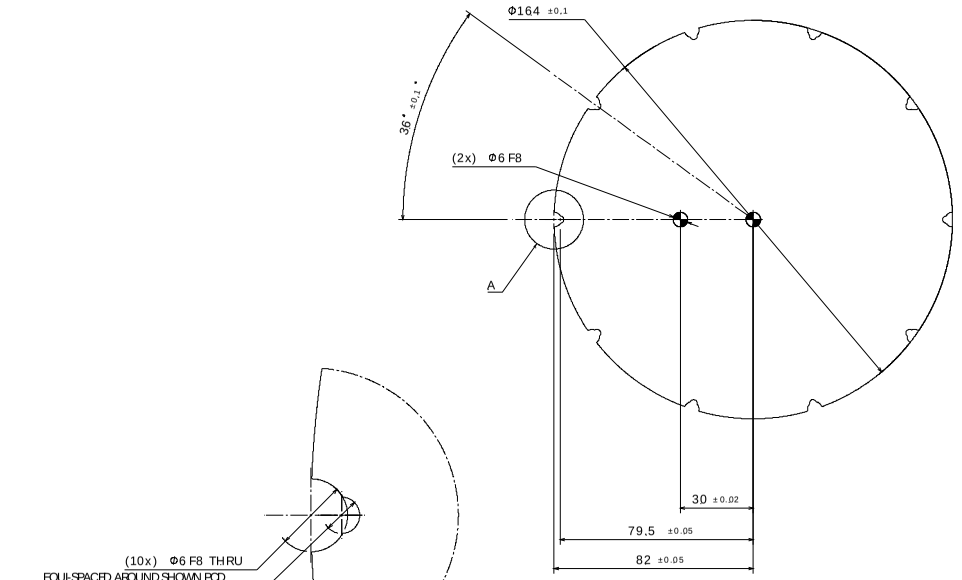
REMOVE ALL SHARP EDGES

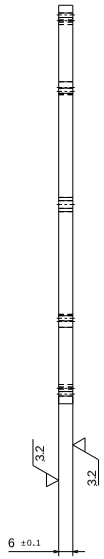
MATERIAL: 070M20 (EN3A)
STOCK : HR RD BAR - Ø80 x 60

DRAWING No : 01-002-A		
A3	QUANTITY: 1-OFF	
	SCALE 1:1	3rd ANGLE PROJECTION
ALL DIMENSION IN MM UNLESS OTHERWISE STATED		
CONTACT: STEWART LOWTH 14063 EPXSL1@NOTTINGHAM.AC.UK		

JOB NUMBER XXX-XXX

REV-C - 22/04/12
HOLE PATTERN WAS 12-OFF NOW 10-OFF
TOLLERANCE ADDED TO 36° DIMENSION





Detail A
Scale: 5:1

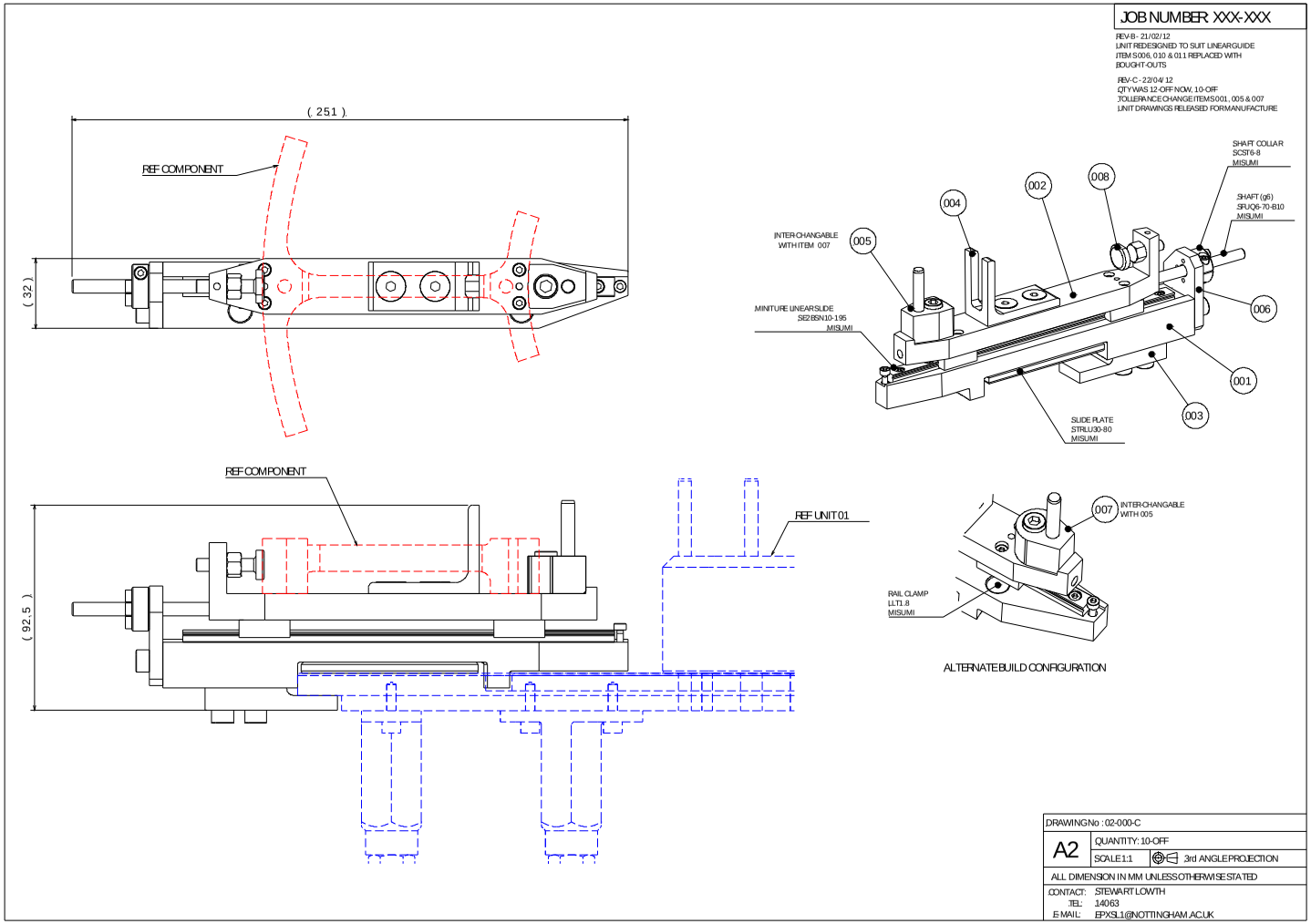
NOTE:
TOLLERANCE UNLESS OTHERWISE STATED
±0.2 BETWEEN SCREWS, NON ACCUMULATIVE
±0.02 BETWEEN DOWELS IN THE SAME PLANE
±0.1 BETWEEN DOWEL IN DIFERENT PLANES
±0.1 BETWEEN MACHINED SURFACE

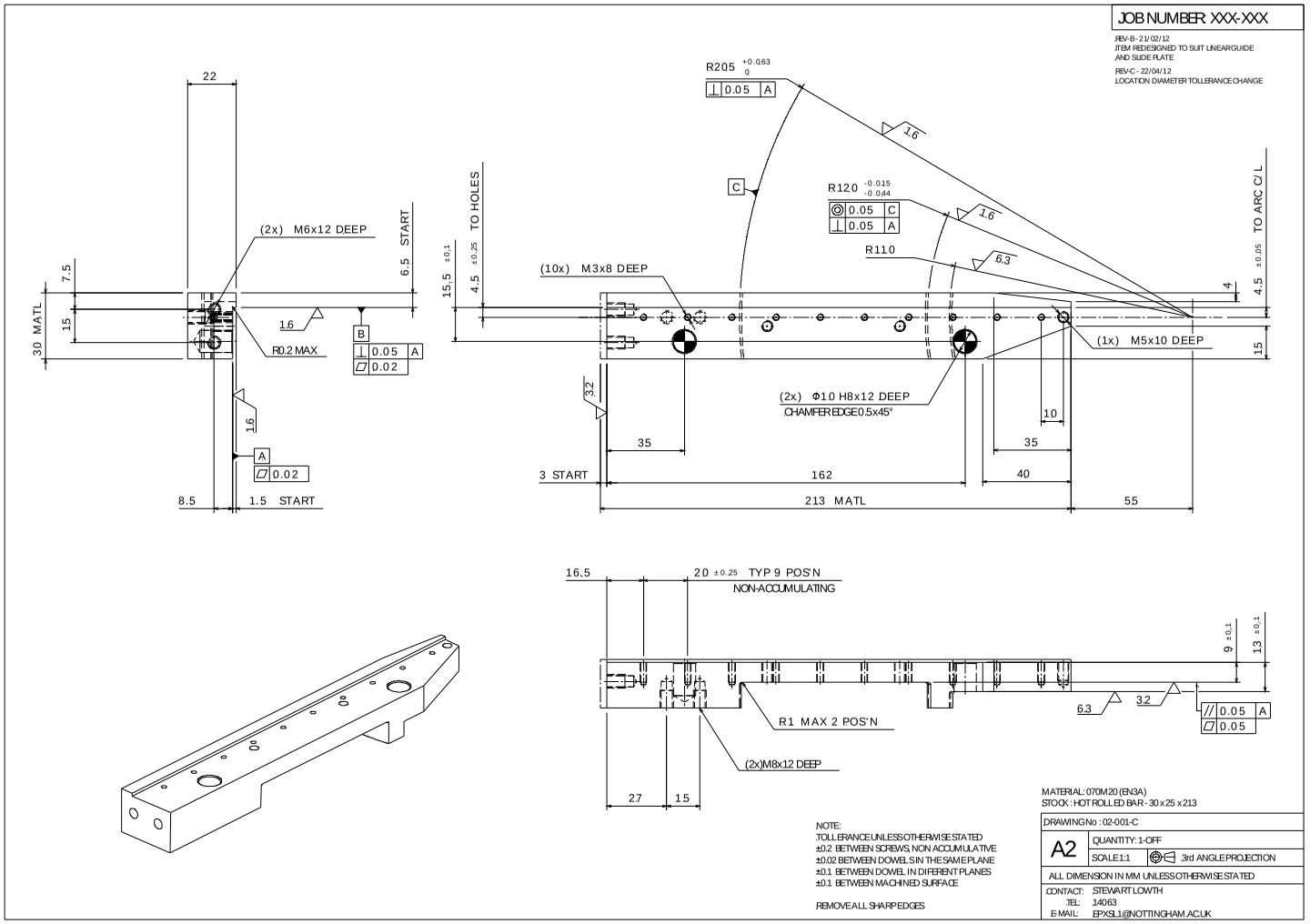
REMOVE ALL SHARP EDGES

MATERIAL: 070M20 (EN3A)
STOCK : HR PLATE - 10 x 170 x 170

DRAWING No : 01-003-C	
A2	QUANTITY: 1-OFF
	SCALE 1:1 — 3rd ANGLE PROJECTION
ALL DIMENSION IN MM UNLESS OTHERWISE STATED	
CONTACT: STEWART LOWTH	
TEL: 14063	
E-MAIL: EPXSL1@NOTTINGHAM.AC.UK	

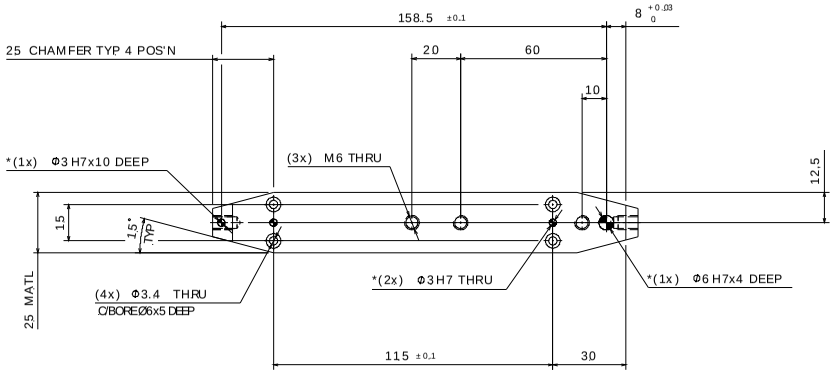
STOCKLIST - TEST FIXTURE - UNIT 002				REVISION C 23/04/2012	
ITEM	DESCRIPTION	MATL / MANUF	STOCK / ORDER CODE	QTY.	TYPE
001	RUNNER	MS	PLATE 25 x 30 x 213	1	M
002	SLIDE	MS	FLAT 40 x 25 x 175	1	M
003	UNIT CLAMP	BMS	FLAT 20 x 10 x 60	1	M
004	ROUGH LOCATOR	MS	ANGLE 50 x 40 x 5 x 22 LONG	1	M
005	DATUM BLOCK	MS	SQUARE 20 x 32 LONG	1	M
006	END PLATE	BMS	FLAT 30 x 6 x 45	1	M
007	DATUM BLOCK	MS	SQUARE 20 x 32 LONG	1	M
008	COMPONENT CLAMP	MS	ROUND Ø15 x 40	1	M
	MINITURE LINEAR SLIDE	MISUMI	SE2BSN10-195	1	P
	SLIDE PLATE	MISUMI	STRLU30-80	1	P
	SHAFT (g6)	MISUMI	SFAQ6-70-B10	1	P
	SHAFT COLLAR	MISUMI	SCST6-8	1	P
	UNDERSIZE DOWLE	MISUMI	MSGB3-12	2	P
	RAIL CLAMP	MISUMI	LLT1.8	2	P

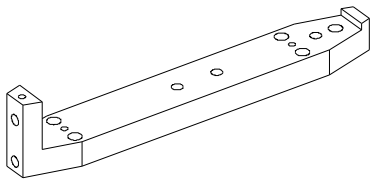

JOB NUMBER XXX-XXX
REV-B - 21/02/12
UNIT REDESIGNED TO SUIT LINEAR GUIDE
ITEM S 006, 010 & 011 REPLACED WITH
BOUGHT-OUTS
REV-C - 22/04/12
QTY WAS 12-OFF NOW, 10-OFF
TOLLERANCE CHANGE ITEMS 001, 005 & 007
UNIT DRAWINGS RELEASED FOR MANUFACTURE
(251)
REF COMPONENT
(32)
SHAFT COLLAR
SCST6-8
MISUMI
SHAFT (g6)
SFUQ6-70-B10
MISUMI
002
008
004
INTER-CHANGABLE
WITH ITEM 007
005
006
MINITURE LINEAR SLIDE
SIZE BSN10-195
MISUMI
001
003
SLIDE PLATE
STRLU30-80
MISUMI
REF COMPONENT
REF UNIT 01
(92.5)
007
INTER-CHANGABLE
WITH 005
RAIL CLAMP
LLT1.8
MISUMI
ALTERNATE BUILD CONFIGURATION
DRAWING No : 02-000-C
A2
QUANTITY: 10-OFF
SCALE 1:1
3rd ANGLE PROJECTION
ALL DIMENSION IN MM UNLESS OTHERWISE STATED
CONTACT: STEWART LOWTH
TEL: 14063
E-MAIL: EPXSL1@NOTTINGHAM.AC.UK

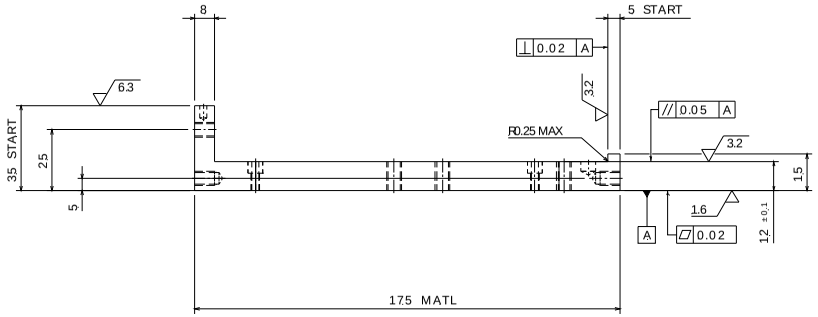

JOB NUMBER XXX-XXX
REV-B - 21/02/12
ITEM REDESIGNED TO SUIT LINEARGUIDE AND SLIDE PLATE
REV-C - 22/04/12
LOCATION DIAMETER TOLLERANCE CHANGE
22
(2x) M6x12 DEEP
6.5 START
7.5
30 MATL
15
1.6
R0.2 MAX
B
0.05 A
0.02
16
A
0.02
8.5
1.5 START
R205 +0.063 0
0.05 A
1.6
C
R120 -0.015 -0.044
0.05 C
0.05 A
R110
6.3
15.5 ±0.1
4.5 ±0.25 TO HOLES
(10x) M3x8 DEEP
4
4.5 ±0.05 TO ARC C/L
15
(1x) M5x10 DEEP
3.2
(2x) Φ10 H8x12 DEEP
CHAMFER EDGE 0.5x45°
10
35
35
3 START
162
40
213 MATL
55
16.5
20 ±0.25 TYP 9 POS'N
NON-ACCUMULATING
9 ±0.1
13 ±0.1
R1 MAX 2 POS'N
6.3
3.2
0.05 A
0.05
(2x)M8x12 DEEP
27
15
NOTE:
TOLLERANCE UNLESS OTHERWISE STATED
±0.2 BETWEEN SCREWS, NON ACCUMULATIVE
±0.02 BETWEEN DOWEL S IN THE SAME PLANE
±0.1 BETWEEN DOWEL IN DIFERENT PLANES
±0.1 BETWEEN MACHINED SURFACE
REMOVE ALL SHARP EDGES
MATERIAL: 070M20 (EN3A)
STOCK : HOT ROLLED BAR - 30 x 25 x 213
DRAWING No : 02-001-C
A2
QUANTITY: 1-OFF
SCALE 1:1
3rd ANGLE PROJECTION
ALL DIMENSION IN MM UNLESS OTHERWISE STATED
CONTACT: STEWART LOWTH
TEL: 14063
E-MAIL: EPXSL1@NOTTINGHAM.AC.UK

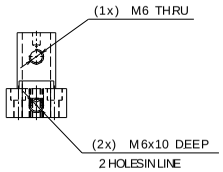
JOB NUMBER XXX-XXX

REV-B - 21/02/12
ITEM REDESIGNED TO SUIT LINEARGUIDE









NOTE:
TOLLERANCE UNLESS OTHERWISE STATED
±0.2 BETWEEN SCREWS, NON ACCUMULATIVE
±0.02 BETWEEN DOWELS IN THE SAME PLANE
±0.1 BETWEEN DOWEL IN DIFERENT PLANES
±0.1 BETWEEN MACHINED SURFACE

REMOVE ALL SHARP EDGES

MATERIAL: 070M20 (EN3A)
STOCK : HOT ROLLED BAR - 40 x 25 x 175

DRAWING No : 02-002-B

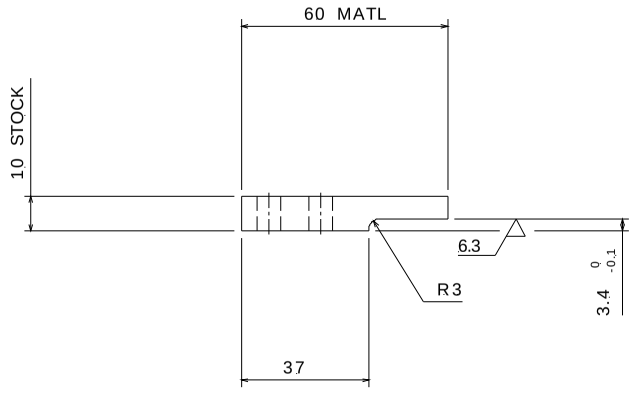
A2 | QUANTITY: 1-OFF | SCALE 1:1 | 3rd ANGLE PROJECTION

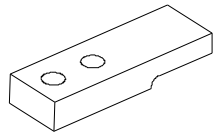
ALL DIMENSION IN MM UNLESS OTHERWISE STATED

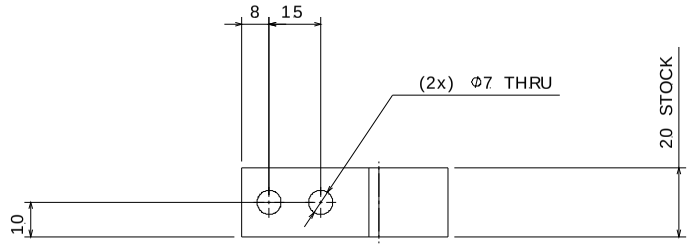
CONTACT: STEWART LOWTH
TEL: 14063
E-MAIL: EPXSL1@NOTTINGHAM.AC.UK

* ENSURE ALL DOWELS ARE IN-LINE ±0.02

JOB NUMBER: ***,***







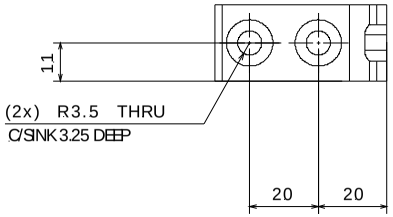
NOTE:
.TOLLERANCE UNLESS OTHERWISE STATED
±0.2 BETWEEN SCREWS, NON ACCUMULATIVE
±0.02 BETWEEN DOWELS IN THE SAME PLANE
±0.1 BETWEEN DOWEL IN DIFERENT PLANES
±0.1 BETWEEN MACHINED SURFACE

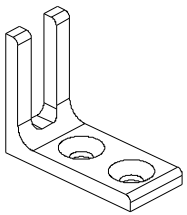
REMOVE ALL SHARP EDGES

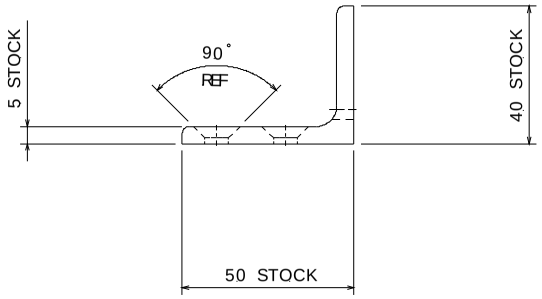
MATERIAL: 070M20 (EN3A)
. STOCK : BRIGHT BAR - 20 x 10 x 60

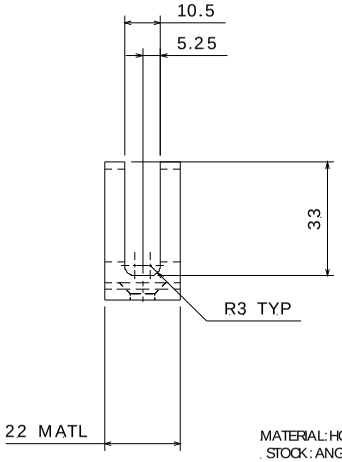
DRAWING No : 02-003-A		
A3	QUANTITY: 1-OFF	
	SCALE 1:1	3rd ANGLE PROJECTION
ALL DIMENSION IN MM UNLESS OTHERWISE STATED		
CONTACT: STEWART LOWTH 14063 EPXSL1@NOTTINGHAM.AC.UK		

JOB NUMBER: ***,***









NOTE:
TOLLERANCE UNLESS OTHERWISE STATED
±0.2 BETWEEN SCREWS, NON ACCUMULATIVE
±0.02 BETWEEN DOWELS IN THE SAME PLANE
±0.1 BETWEEN DOWEL IN DIFERENT PLANES
±0.1 BETWEEN MACHINED SURFACE

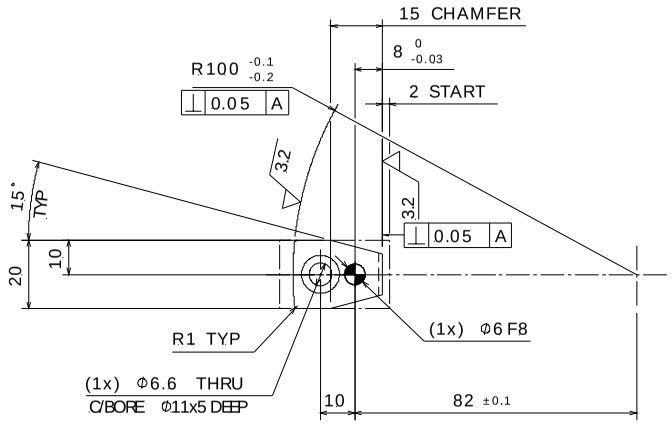
REMOVE ALL SHARP EDGES

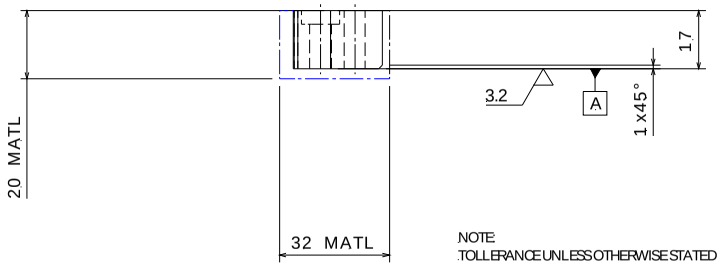
MATERIAL: HOT ROLLED MS
. STOCK : ANGLE - 40 x 50 x 5 x 22

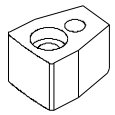
DRAWING No : 02-004-A		
A3	QUANTITY: 1-OFF	
	SCALE 1:1	3rd ANGLE PROJECTION
ALL DIMENSION IN MM UNLESS OTHERWISE STATED		
CONTACT: STEWART LOWTH 14063 EPXSL1@NOTTINGHAM.AC.UK		

JOB NUMBER: ***,***

REV-C - 22/04/12
HOLE TOLL WAS H7 NOW F8







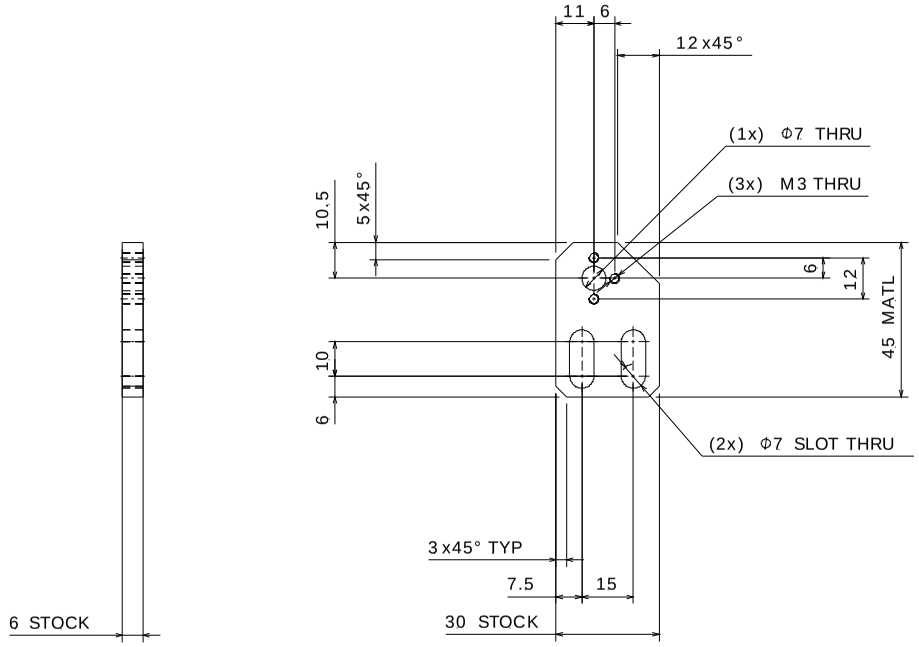
NOTE:
TOLLERANCE UNLESS OTHERWISE STATED
±0.2 BETWEEN SCREWS, NON ACCUMULATIVE
±0.02 BETWEEN DOWELS IN THE SAME PLANE
±0.1 BETWEEN DOWEL IN DIFERENT PLANES
±0.1 BETWEEN MACHINED SURFACE

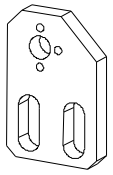
REMOVE ALL SHARP EDGES

MATERIAL: 070M20 (EN3A)
STOCK : SQR BAR - 20 x 20 x 32

DRAWING No : 02-005-C		
A3	QUANTITY: 1-OFF	
	SCALE 1:1	3rd ANGLE PROJECTION
ALL DIMENSION IN MM UNLESS OTHERWISE STATED		
CONTACT: STEWART LOWTH 14063 EPXSL1@NOTTINGHAM.AC.UK		

JOB NUMBER: ***,***





NOTE:
TOLLERANCE UNLESS OTHERWISE STATED
±0.2 BETWEEN SCREWS, NON ACCUMULATIVE
±0.02 BETWEEN DOWELS IN THE SAME PLANE
±0.1 BETWEEN DOWEL IN DIFERENT PLANES
±0.1 BETWEEN MACHINED SURFACE

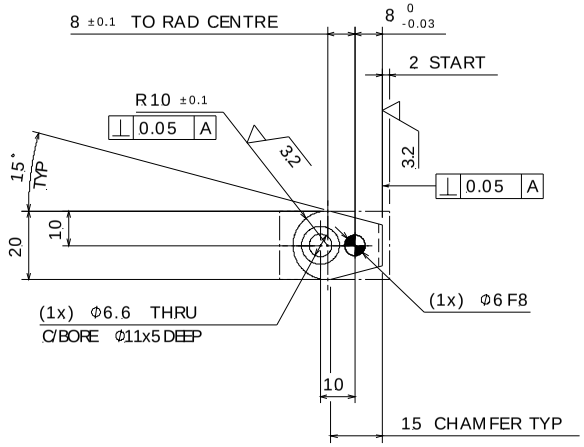
REMOVE ALL SHARP EDGES

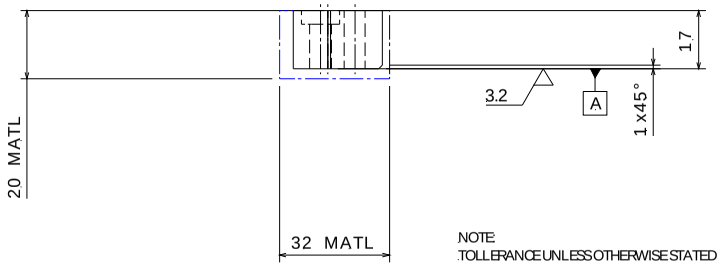
MATERIAL: 070M20 (EN3A)
. STOCK: BRIGHT FLAT - 6 x 30 x 45

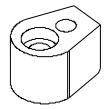
DRAWING No : 02-006-A		
A3	QUANTITY: 1-OFF	
	SCALE 1:1	3rd ANGLE PROJECTION
ALL DIMENSION IN MM UNLESS OTHERWISE STATED		
CONTACT: STEWART LOWTH 14063 EPXSL1@NOTTINGHAM.AC.UK		

JOB NUMBER: ***,***

REV-C - 22/04/12
HOLE TOLL WAS H7 NOW F8







NOTE:
TOLLERANCE UNLESS OTHERWISE STATED
±0.2 BETWEEN SCREWS, NON ACCUMULATIVE
±0.02 BETWEEN DOWELS IN THE SAME PLANE
±0.1 BETWEEN DOWEL IN DIFERENT PLANES
±0.1 BETWEEN MACHINED SURFACE

REMOVE ALL SHARP EDGES

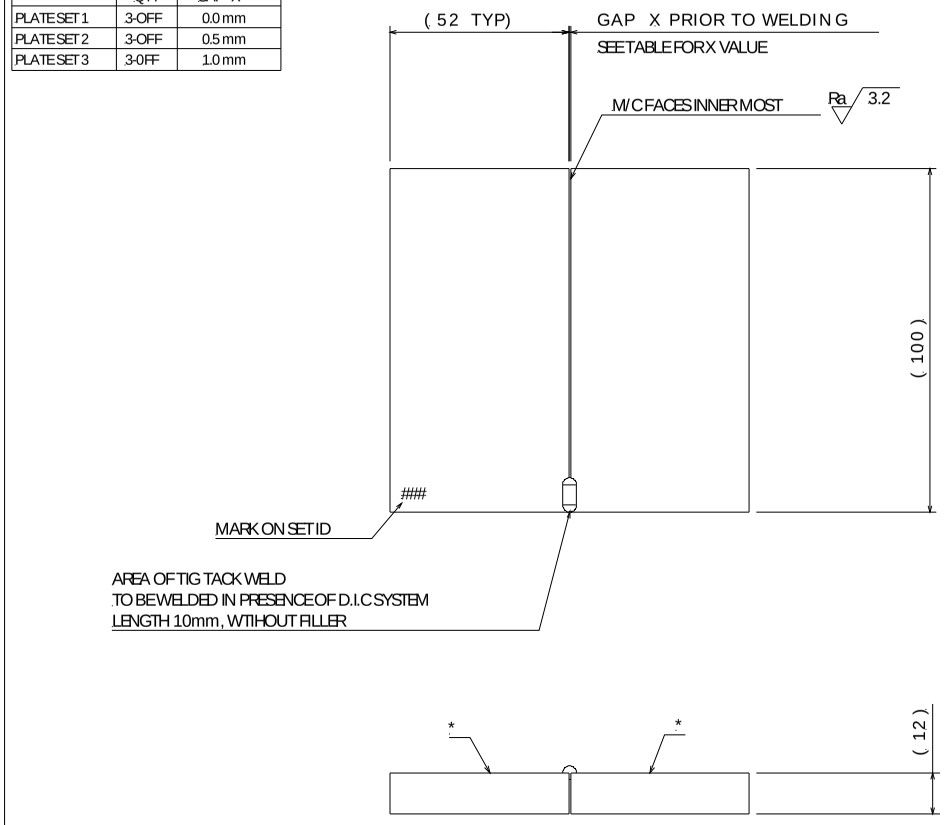
MATERIAL: 070M20 (EN3A)
. STOCK : SQR BAR - 20 x 20 x 32

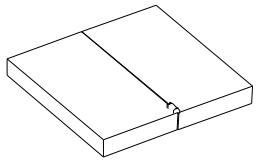
DRAWING No : 02-007-C		
A3	QUANTITY: 1-OFF	
	SCALE 1:1	3rd ANGLE PROJECTION
ALL DIMENSION IN MM UNLESS OTHERWISE STATED		

CONTACT: STEWART LOWTH
14063
EPXSL1@NOTTINGHAM.AC.UK

	QTY	GAP "X"
PLATE SET 1	3-OFF	0.0 mm
PLATE SET 2	3-OFF	0.5 mm
PLATE SET 3	3-OFF	1.0 mm

JOB NUMBER: 111-999





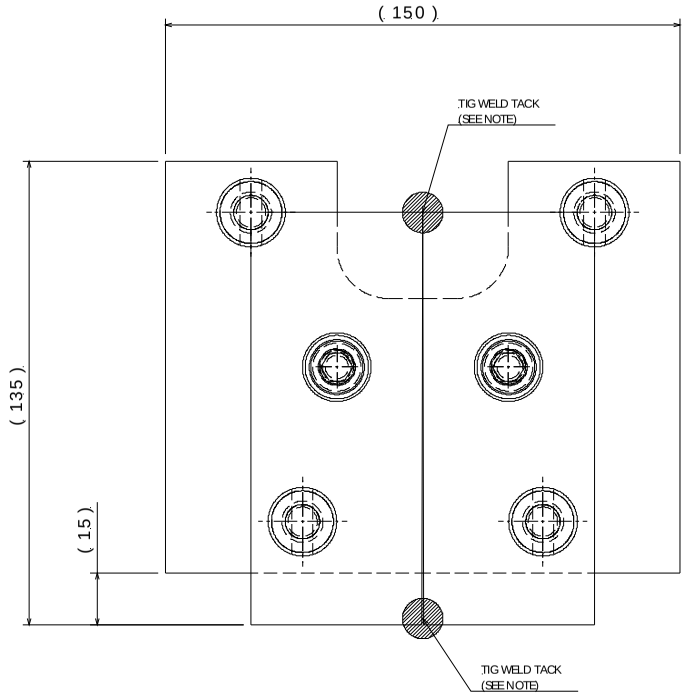
MATERIAL: TI-6/4 - 100 x 52 x 12
REQUIRED MATERIAL WILL BE SUPPLIED

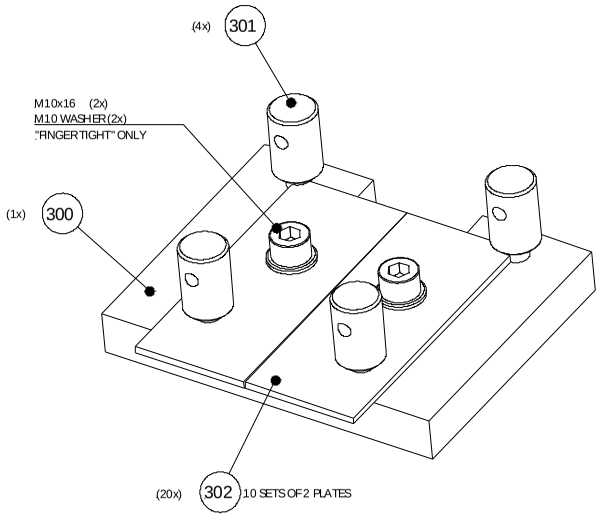
ALL SURFACES MARKED " * " TO BE FREE FROM
SCALE AND SUITABLE FOR PAINT PRIOR TO WELDING

ENSURE PLANAR FACES MARKED "*" ARE ALIGNED PIOR TO WELDING

A3	QUANTITY: 9-OFF WELDED SETS	
	SCALE 1:1	3rd ANGLE PROJECTION
ALL DIMENSION IN MM UNLESS OTHERWISE STATED		
CONTACT: STEWART LOWTH 14063 EPXSL1@NOTTINGHAM.AC.UK		

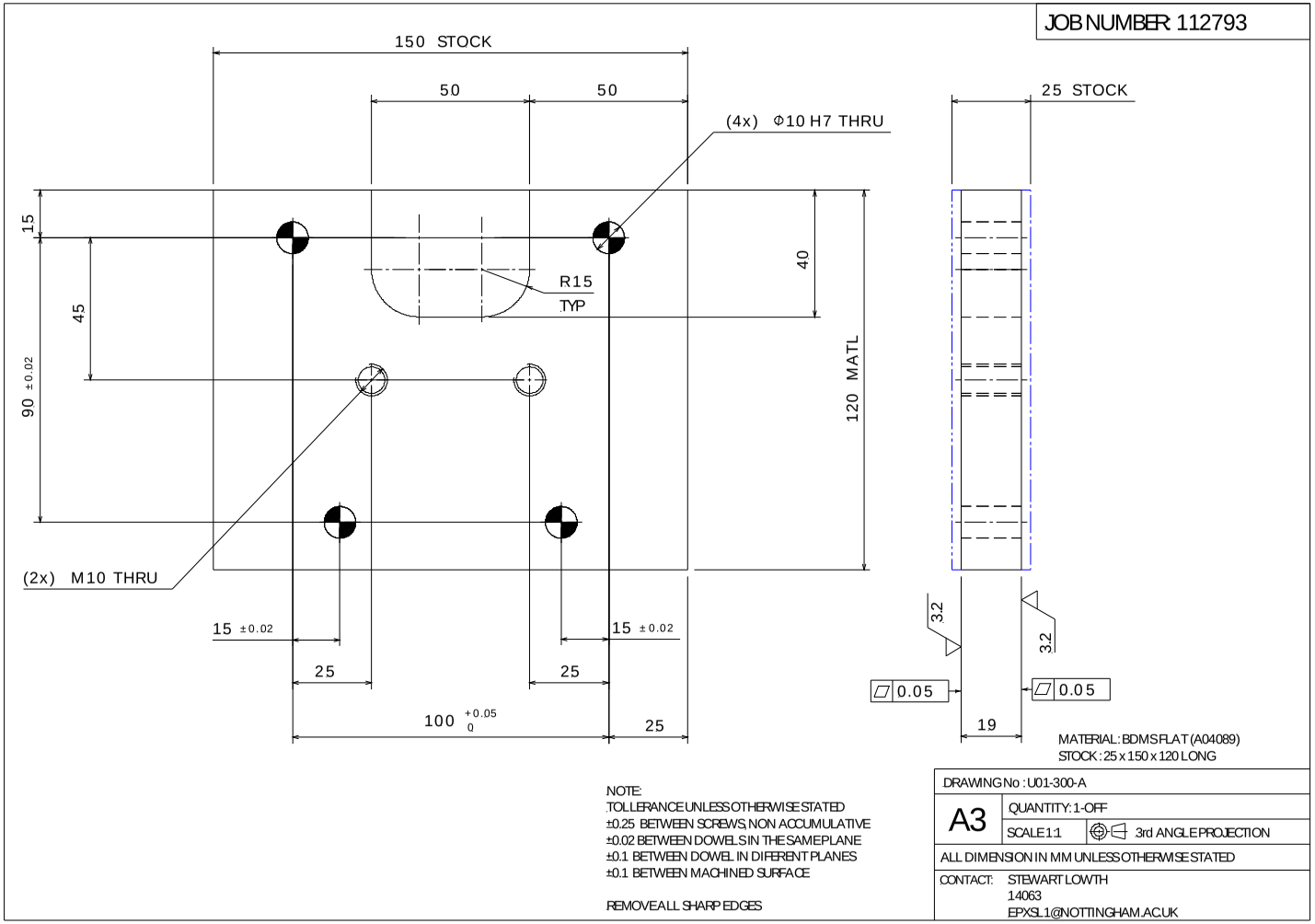
JOB NUMBER: 112793



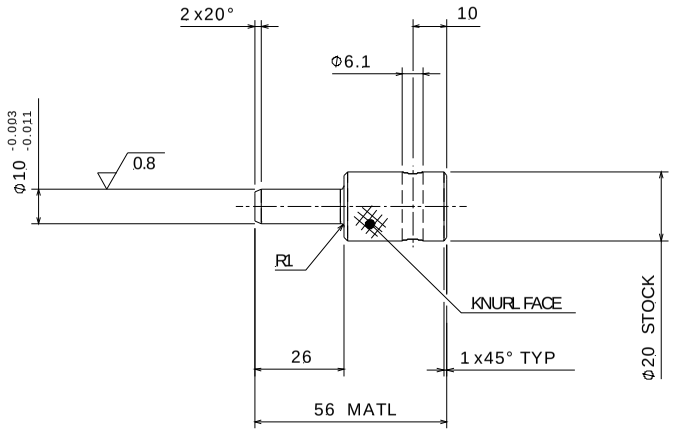


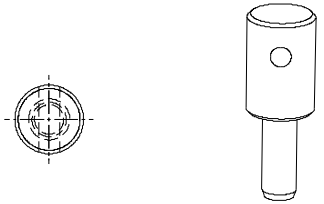
NOTE: EXPERIMENTAL TIG WELDING FIXTURE. WELDING TO BE PERFORMED IN PRESENCE OF DIC CAMERA SYSTEM

DRAWING No : U01-100-A		
A3	QUANTITY: 1-OFF	
	SCALE 1:1	3rd ANGLE PROJECTION
ALL DIMENSION IN MM UNLESS OTHERWISE STATED		
CONTACT: STEWART LOWTH 14063 EPXSL1@NOTTINGHAM.AC.UK		


JOB NUMBER: 112793
150 STOCK
50
50
(4x) Φ10 H7 THRU
25 STOCK
15
45
90 ±0.02
40
R15
TYP
120 MATL
(2x) M10 THRU
15 ±0.02
15 ±0.02
25
25
100 +0.05 0
25
3.2
3.2
0.05
0.05
19
MATERIAL: BDMS FLAT (A04089)
STOCK : 25 x 150 x 120 LONG
NOTE:
TOLLERANCE UNLESS OTHERWISE STATED
±0.25 BETWEEN SCREWS, NON ACCUMULATIVE
±0.02 BETWEEN DOWELS IN THE SAME PLANE
±0.1 BETWEEN DOWEL IN DIFERENT PLANES
±0.1 BETWEEN MACHINED SURFACE
REMOVE ALL SHARP EDGES
DRAWING No : U01-300-A
A3
QUANTITY: 1-OFF
SCALE 1:1
3rd ANGLE PROJECTION
ALL DIMENSION IN MM UNLESS OTHERWISE STATED
CONTACT: STEWART LOWTH
14063
EPXSL1@NOTTINGHAM.AC.UK

JOB NUMBER: 112793





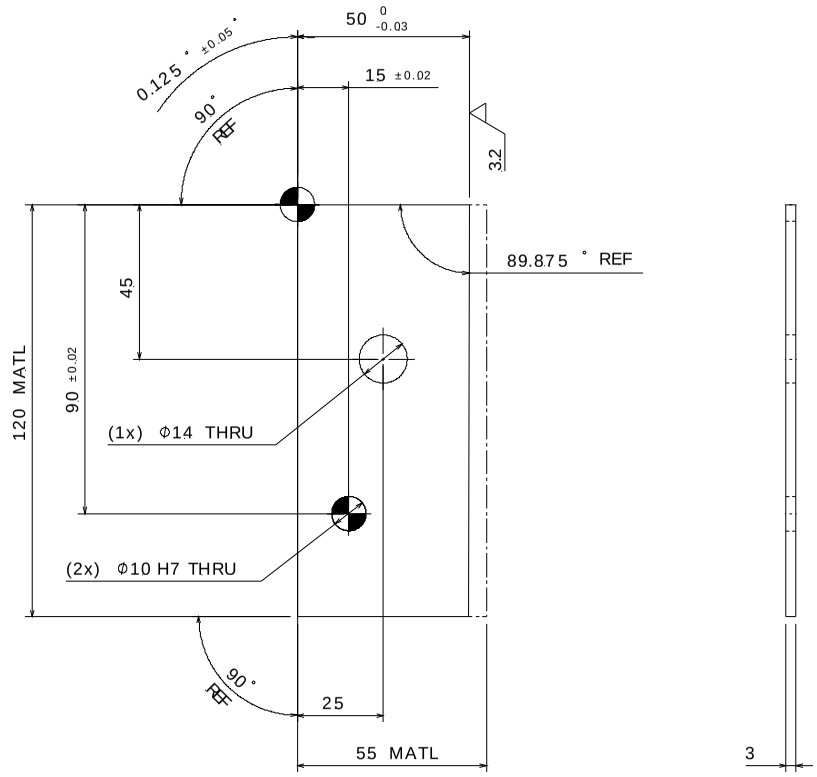
NOTE:
.TOLLERANCE UNLESS OTHERWISE STATED
±0.25 BETWEEN SCREWS, NON ACCUMULATIVE
±0.02 BETWEEN DOWELS IN THE SAME PLANE
±0.1 BETWEEN DOWEL IN DIFERENT PLANES
±0.1 BETWEEN MACHINED SURFACE

REMOVE ALL SHARP EDGES

MATERIAL: BDMS ROUND (A02011)
STOCK : Ø25 x 70 LONG

DRAWING No : U01-301-A		
A3	QUANTITY: 4-OFF	
	SCALE 1:1	3rd ANGLE PROJECTION
ALL DIMENSION IN MM UNLESS OTHERWISE STATED		
CONTACT: STEWART LOWTH 14063 EPXSL1@NOTTINGHAM.AC.UK		

JOB NUMBER: 112793



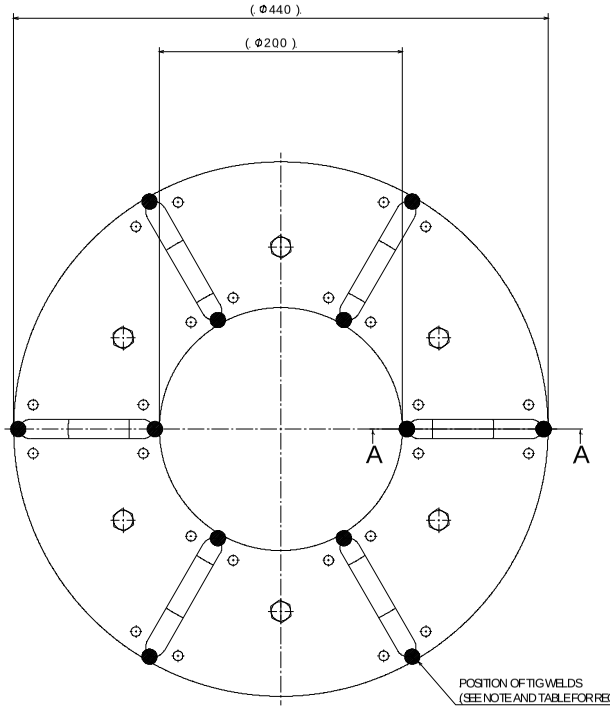
NOTE:
TOLLERANCE UNLESS OTHERWISE STATED
±0.25 BETWEEN SCREWS, NON ACCUMULATIVE
±0.02 BETWEEN DOWELS IN THE SAME PLANE
±0.1 BETWEEN DOWEL IN DIFERENT PLANES
±0.1 BETWEEN MACHINED SURFACE

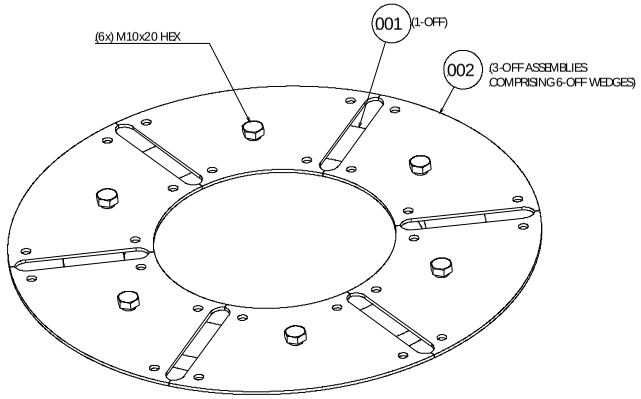
REMOVE ALL SHARP EDGES

MATERIAL: MS SHEET (A01014)
STOCK: 3 x 120 x 55

DRAWING No : U01-302-A		
A3	QUANTITY: 20-OFF	
	SCALE 1:1	3rd ANGLE PROJECTION
ALL DIMENSION IN MM UNLESS OTHERWISE STATED		
CONTACT: STEWART LOWTH 14063 EPXSL1@NOTTINGHAM.AC.UK		

JOB NUMBER 112-641



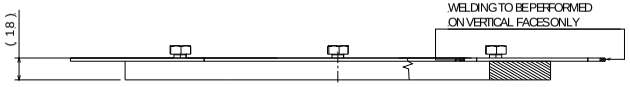


POSITION OF TIG WELDS
(SEE NOTE AND TABLE FOR REQUIREMENTS)

NOTE: A TOTAL OF 3 ASSEMBLIES ARE TO BE BUILT, EACH WITH DIFFERING REQUIREMENTS FOR THE POSITION OF THE WELDS. THE TABLE BELOW SPECIFIES THE REQUIRED POSITION OF THE WELDS TO BE PERFORMED AND FOR WHICH BUILD.

WELDING IS TO BE PERFORMED ON VERTICAL SURFACE ONLY, SEE BREAK-OUT SECTION

WELD / BUILD TABLE			
BUILD	NUMBER REQ'D	INNER DIAMETER WELDS	OUTER DIAMETER WELDS
INNER	1-OFF	YES	NO
OUTER	1-OFF	NO	YES
BOTH	1-OFF	YES	YES



BREAK-OUT SECTION A-A

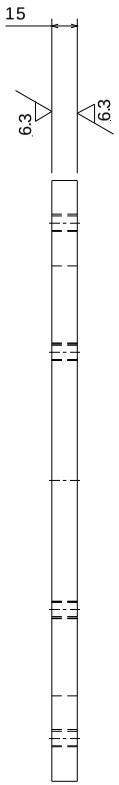
DRAWING No : RING DRW_000

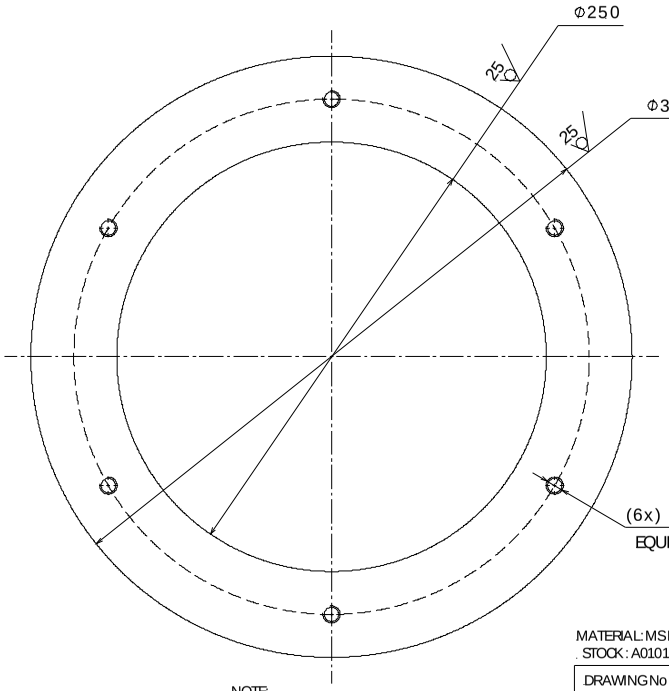
A2 | QUANTITY: 1-OFF | SCALE 1:2 | 3rd ANGLE PROJECTION

ALL DIMENSION IN MM UNLESS OTHERWISE STATED

CONTACT: STEWART LOWTH
TEL: 14063
E-MAIL: EPXSL1@NOTTINGHAM.AC.UK

JOB NUMBER: 112-641





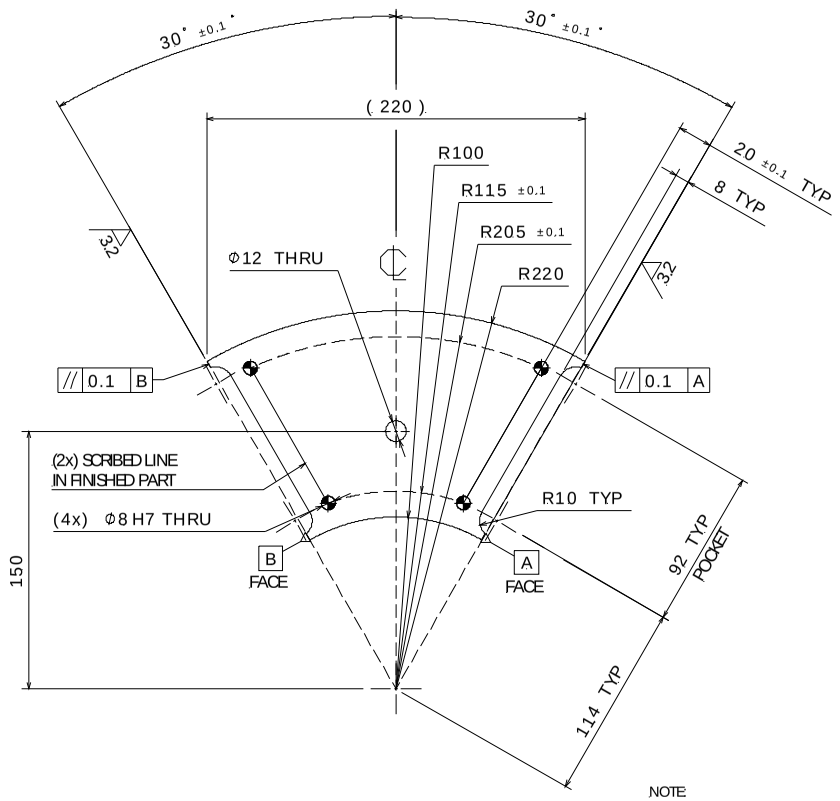
NOTE:
TOLLERANCE UNLESS OTHERWISE STATED
±0.2 BETWEEN SCREWS, NON ACCUMULATIVE
±0.02 BETWEEN DOWELS IN THE SAME PLANE
±0.1 BETWEEN DOWEL IN DIFERENT PLANES
±0.1 BETWEEN MACHINED SURFACE

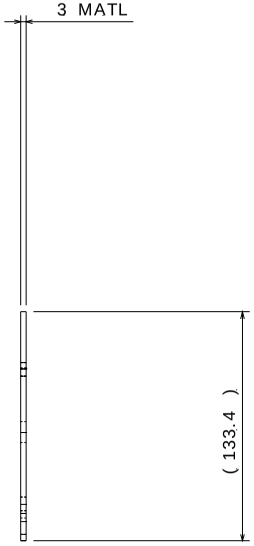
REMOVE ALL SHARP EDGES

MATERIAL: MS PLATE
STOCK : A01019 - 20 x 375 x 375

DRAWING No : RING DRW_001		
A3	QUANTITY: 1-OFF	
	SCALE 1:2	3rd ANGLE PROJECTION
ALL DIMENSION IN MM UNLESS OTHERWISE STATED		
CONTACT: STEWART LOWTH 14063 EPXSL1@NOTTINGHAM.AC.UK		

JOB NUMBER 112-641





NOTE:
TOLLERANCE UNLESS OTHERWISE STATED
±0.2 BETWEEN SCREWS, NON ACCUMULATIVE
±0.02 BETWEEN DOWELS IN THE SAME PLANE
±0.1 BETWEEN DOWEL IN DIFFERENT PLANES
±0.1 BETWEEN MACHINED SURFACE

REMOVE ALL SHARP EDGES

MATERIAL: MS PLATE
. STOCK : A01014 - 3 x 200 x 134

NOTE : SHOULD AN ALTERNATIVE FLAT BAR STOCK MATRIAL BE USED, IT MUST NOT BE COLD ROLLED OR "BRIGHT"

DRAWING No : RING_DRW_002		
A3	QUANTITY: 18-OFF	
	SCALE 1:2	3rd ANGLE PROJECTION
ALL DIMENSION IN MM UNLESS OTHERWISE STATED		

CONTACT: STEWART LOWTH
14063
EPXSL1@NOTTINGHAM.AC.UK

Appendix 2 – CMM Uncertainty calculations

This appendix outlines the uncertainty measurements performed on the Mitutoyo Euro C-A-121210 CMM which was used for the experimental portion of this thesis. Type A uncertainties were obtained using multiple measurements (n=50) of either the component (36-8) or the A1 build assembly. The fixture was not used for measurement the components were placed directly onto the bed of the CMM. For each repeat measurement set the mean and standard deviation ($\boldsymbol{s}$) was derived, which was then used (via Apx Eq.1) to calculate the standard uncertainty ($\boldsymbol{u}$) for that measurement on the assumption of a Gaussian distribution.

$$u = \frac{s}{\sqrt{n}} \qquad \text{Apx Eq.1}$$

Once the standard uncertainty is calculated a coverage factor (k in standard deviations) can be applied to give the expanded uncertainty (U) for at given confidence level. Coverage factors for a normal/Gaussian distribution are:

k = 1 a confidence level of ≈ 68%

k = 2 a confidence level of ≈ 95%

k = 2.58 a confidence level of ≈ 99%

k = 3 a confidence level of ≈ 99.7%

To apply the confidence level to the calculated standard uncertainties and generate the expanded uncertainty Apx Eq.2 is use

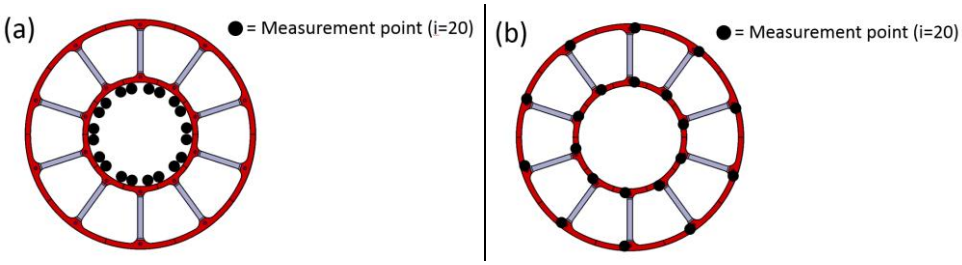
$$U = k \cdot u \qquad \text{Apx Eq.2}$$

The measurements

The measurements were split in to three families: axis, assembly and part:

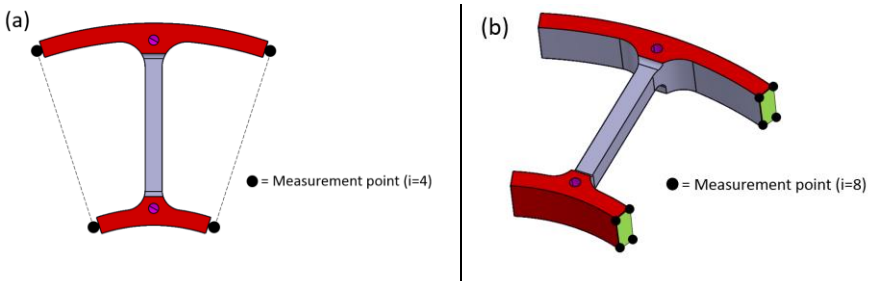
Axis: A point measurements for each axis (X, Y, and Z).

Assembly: The assembly's inner diameter was measured with 20 points (see Apx Fig. 1(a)). The flatness across the upper face of the assembly was measured with 20 points (see Apx Fig. 1(b)).



Apx Fig. 1: (a) inner diameter & (b) flatness measurements

Part: Two Two-point lines were measured between the upper and lower contact surfaces and the angle calculated (see Apx Fig. 2(a)). Two four-point planes were used to measure the parallelism between the part contact faces (see Apx Fig. 2(b)).



Apx Fig. 1: (a) angular & (b) parallelism measurements

Results

The individual measurements are shown in the table Apx 1, while a summary of the calculated uncertainties are shown in table Apx 2,

X only (mm) i=1	Y only (mm) i=1	Z only (mm) i=1	Diameter (mm) i=20	Flatness (mm) i=20	Angular (°) i=4	Parallelism (mm) i=8
746.9620	243.5150	99.9900	200.6805	0.03	36.0038	0.11
746.9640	243.5490	99.9910	200.6491	0.05	36.0034	0.12
746.9610	243.5160	99.9900	200.6786	0.03	36.0035	0.11
746.9630	243.5340	99.9910	200.6641	0.04	36.0034	0.12
746.9640	243.5440	99.9900	200.6550	0.03	36.0034	0.12
746.9650	243.5180	99.9900	200.6773	0.06	36.0038	0.10
746.9630	243.5230	99.9900	200.6723	0.03	36.0033	0.12
746.9610	243.5180	99.9900	200.6782	0.03	36.0038	0.13
746.9630	243.5210	99.9900	200.6750	0.03	36.0035	0.11
746.9650	243.5340	99.9900	200.6627	0.02	36.0036	0.12
746.9610	243.4920	99.9900	200.7000	0.03	36.0034	0.11
746.9620	243.5190	99.9900	200.6777	0.05	36.0033	0.11
746.9620	243.5010	99.9900	200.6941	0.03	36.0034	0.11
746.9640	243.5020	99.9900	200.6932	0.03	36.0034	0.11
746.9640	243.4800	99.9900	200.7114	0.04	36.0033	0.10
746.9620	243.5010	99.9900	200.6927	0.03	36.0038	0.10
746.9610	243.4850	99.9910	200.7073	0.03	36.0035	0.12
746.9620	243.5040	99.9900	200.6909	0.04	36.0034	0.12
746.9620	243.4940	99.9900	200.6991	0.03	36.0034	0.12
746.9600	243.4600	99.9900	200.7291	0.05	36.0031	0.12
746.9590	243.4700	99.9900	200.7209	0.03	36.0033	0.11
746.9600	243.4680	99.9900	200.7227	0.04	36.0036	0.10
746.9620	243.4810	99.9900	200.7105	0.04	36.0035	0.10
746.9600	243.4510	99.9900	200.7364	0.04	36.0035	0.11
746.9600	243.4510	99.9900	200.7373	0.03	36.0036	0.11
746.9580	243.4290	99.9900	200.7568	0.03	36.0034	0.12
746.9610	243.4350	99.9900	200.7514	0.06	36.0035	0.10
746.9620	243.4340	99.9900	200.7518	0.03	36.0034	0.10
746.9610	243.4270	99.9900	200.7582	0.03	36.0034	0.10
746.9600	243.4350	99.9900	200.7518	0.03	36.0036	0.11
746.9610	243.4270	99.9900	200.7591	0.05	36.0033	0.10
746.9620	243.4270	99.9900	200.7577	0.03	36.0035	0.09
746.9620	243.4170	99.9900	200.7664	0.03	36.0036	0.12
746.9610	243.4120	99.9900	200.7718	0.03	36.0034	0.11
746.9610	243.4290	99.9900	200.7577	0.05	36.0035	0.11
746.9630	243.4350	99.9910	200.7514	0.03	36.0036	0.12
746.9650	243.4350	99.9900	200.7509	0.03	36.0035	0.11
746.9630	243.4360	99.9900	200.7505	0.05	36.0038	0.10
746.9610	243.4190	99.9900	200.7659	0.03	36.0039	0.12
746.9630	243.4440	99.9900	200.7445	0.03	36.0038	0.12
746.9650	243.4340	99.9900	200.7518	0.02	36.0035	0.11
746.9650	243.4290	99.9900	200.7559	0.05	36.0035	0.11
746.9650	243.4310	99.9910	200.7550	0.03	36.0036	0.11
746.9640	243.4620	99.9900	200.7277	0.03	36.0034	0.11
746.9650	243.4320	99.9900	200.7532	0.03	36.0035	0.11
746.9670	243.4260	99.9900	200.7582	0.04	36.0036	0.11
746.9640	243.4540	99.9900	200.7350	0.03	36.0034	0.12
746.9630	243.4470	99.9900	200.7414	0.05	36.0034	0.13
746.9640	243.4610	99.9900	200.7286	0.03	36.0031	0.11
746.9660	243.4660	99.9900	200.7232	0.03	36.0035	0.117

Table Apx 1. The measurements

X only (mm) i=1	Y only (mm) i=1	Z only (mm) i-1	Diameter (mm) i=20	Flatness (mm) i=20	Angular (°) i=4	Parallelism (mm) i=8	
50	50	50	50	50	50	50	***n***
746.96248	243.46828	99.99010	200.72184	0.03540	36.00352	0.11108	***Mean***
0.00191	0.03932	0.00030	0.03486	0.00943	0.00015	0.00782	***s***
0.00027017	0.00556022	0.00004243	0.00492957	0.00133297	0.00002145	0.00110629	***u***
2	2	2	2	2	2	2	***k***
0.00054034	0.01112044	0.00008485	0.00985914	0.00266593	0.00004290	0.00221257	***U***

Table Apx 2. Calculated uncertainties at 95% (k=2)